

COMPUTER ASSISTED CHARACTERIZATION  
OF A FILAMENT ELECTROTHERMAL ATOMIZER

By

David Norman Baxter

A DISSERTATION

Submitted to

Michigan State University

in partial fulfillment of the requirements

for the degree of

DOCTOR OF PHILOSOPHY

Department of Chemistry

1977

## ABSTRACT

### COMPUTER ASSISTED CHARACTERIZATION OF A FILAMENT ELECTROTHERMAL ATOMIZER

By

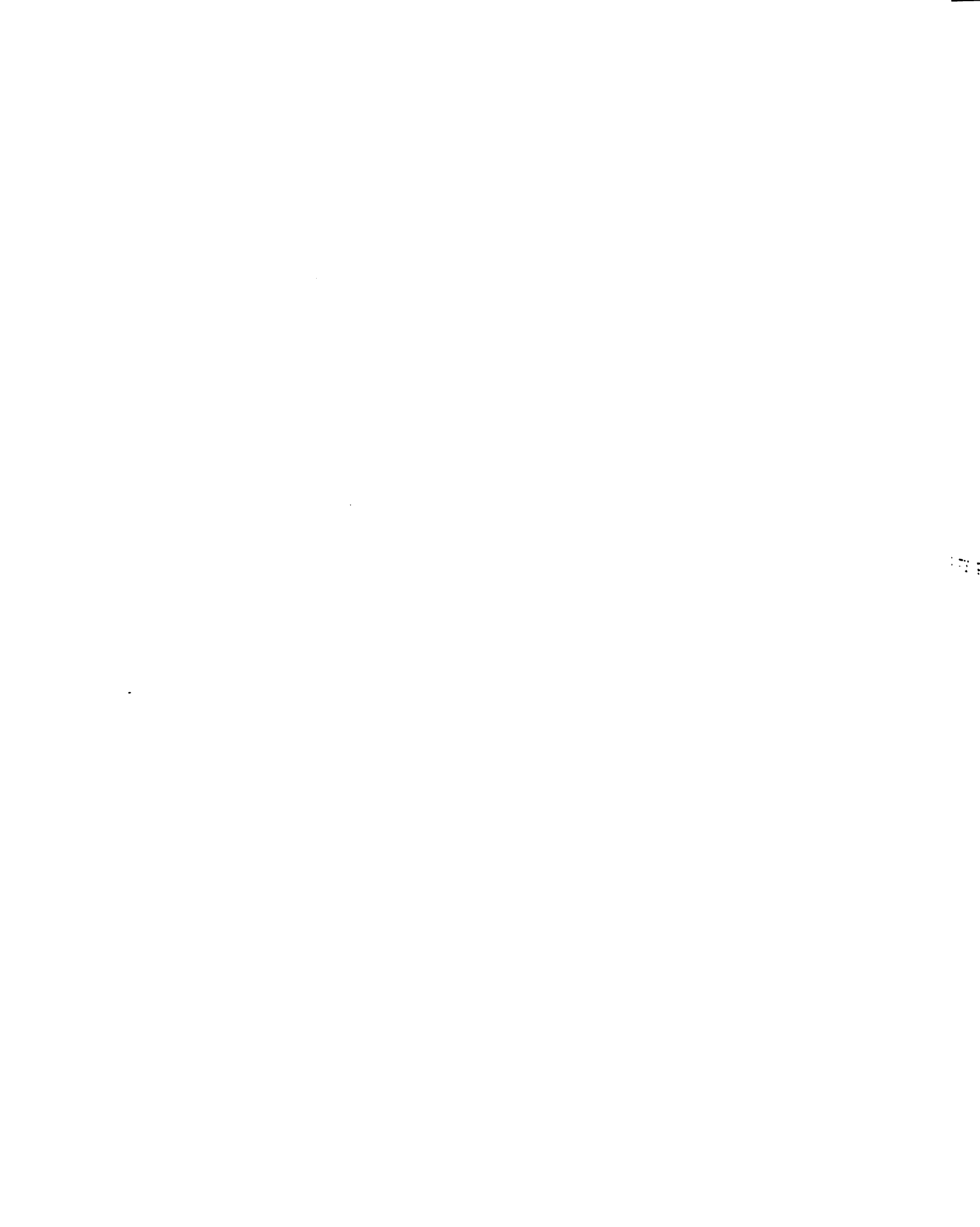
David Norman Baxter

The influence of modern solid state electronic instrumentation and computers upon analytical chemistry is profound. The continuing decrease in cost and increase in capabilities of laboratory minicomputers, particularly with the advent of the microprocessor, have combined to make sophisticated computer supervision of scientific instrumentation highly beneficial. Electrothermal atomizers are also becoming increasingly important in atomic spectrometric research. Many devices have been proposed in the literature, but considerable research remains to be done in further characterizing them.

Three specific investigations, all of which employ versatile, computer-controlled instrumentation, have been performed with one such atomizer, the graphite braid. Scanning electron microscopy with x-ray microprobe fluorescence has been used to examine the physical appearance and evolution of graphite braids as they receive and atomize analytical samples. Changes which occur in

trials as  
emitted  
The condi  
theory  
various  
and, a  
the inte  
rescent  
second o  
is shown  
theory t  
proved a  
lower de  
Temperat  
In cond  
atomizat  
of space  
atomized  
with the  
of origi  
atomizat  
and a "s  
solution  
atomic c  
ticks w  
the des

braids as they are in service, and some of the behavior exhibited by deposited samples are observed and discussed. The control of temperature in electrothermal atomic spectrometry is an extremely important parameter. Of the various feedback signals which can be used for this control, a method known as radiation programming, in which the intensity of the blackbody emission from the incandescent atomizer is the control signal, is a superior method of temperature regulation. Radiation programming is shown to provide lengthened atomizer lifetimes, insensitivity to changes in certain system parameters, and improved atomization characteristics with implications for lower detection limits and freedom from sample matrices. Temperature calibration of the atomizer is also illustrated. In conclusion, to learn more about the mechanisms of atomization and the behavior of free atoms, two dimensional spatial profiles of atomic concentrations above the atomizer have been acquired. This work was carried out with the assistance of two computer-controlled instruments of original design: a "positioner" which translates the atomization cell with respect to a fixed optical axis, and a "sampler" which automatically deposits aliquots of solution on the atomizer. The general shapes of the free atomic clouds of various elements are shown, and observations which concern the effects of some sample matrices are described.



## DEDICATION

To my parents and family:

for so much support through so many years

I am  
work po  
practice  
I w  
Lesson  
for one  
Profess  
and Pro  
also we  
I o  
Dr. Ed  
of comp  
at orde  
to my C  
softwa  
have g  
pation  
To  
such a  
teachi  
sizee  
alent  
ware a  
I  
netce

## ACKNOWLEDGMENTS

I am indebted to many people for making much of this work possible, and I wish to express to them my deepest gratitude.

I wish at first to thank my research preceptor, Professor Stanley R. Crouch, for his support and guidance for the past four and a half years. Thanks are also due Professor Chris Enke, who served as my second reader, and Professors James Dye and Richard Schwendeman, who also were on my guidance committee.

I owe much to our postdoctoral fellow of 1974-1976, Dr. Eric Johnson. He personally increased my knowledge of computers and electronic instrumentation by at least an order of magnitude. Similar credit should be given to my coworker, Gene Pals, without whose comprehensive software and instrumental contributions this work would have gone nowhere, and who always was a valuable second opinion and source of ideas.

To Professor Andrew Timnick goes my thanks for being such a good friend and coworker through many terms of teaching. To Dr. Tom Atkinson I extend my gratitude for three pleasant terms of employment, and for formidable talents and assistance in all facets of computer hardware and software.

I have drawn heavily upon the services of our departmental support facilities in constructing the instrumentation,

and I owe much to the men who work in them for putting up with my unreasonable demands and periodic raids on their stock. Included in this category are Ron Haas and the staff of the electronics shop, Russ Geyer and the staff of the machine shop, and Marty Rabb of the instrumentation consulting service.

I have had much material assistance from sources outside the university as well. Thanks are due Dr. Paul Beckwith and the BASF Corporation of Wyandotte, Michigan for their generous donation of both time and supplies on their scanning electron microscopy facility. I acknowledge also five terms of research support in the form of both a summer and a full year ACS Analytical Fellowship under the kind sponsorship of the Procter and Gamble Company of Cincinnati, Ohio. My thanks also go to Peri-Anne Warstler for typing the original manuscript.

Finally, I wish to thank all of my fellow graduate students in the analytical division who either contributed in some way to this work, no matter how small, or who simply were good friends throughout my stay here. To name everyone would take up another page in this already oversized mound of ink, paper, and finely divided silver. May I simply say that losing your daily companionship is the most sincere regret I have in leaving MSU.

Chapter

LIST OF

LIST OF

INTRODUCTION

CHAPTER

A.

B.

C.

D.

E.

F.

G.

CHAPTER

A.

B.

## TABLE OF CONTENTS

Chapter	Page
LIST OF TABLES. . . . .	ix
LIST OF FIGURES . . . . .	xii
INTRODUCTION. . . . .	1
HISTORICAL. . . . .	6
A. Early Observations and Developments of Atomic Spectrometric Techniques. . . . .	6
B. Comparison of Flame and Electrothermal Methods . . . . .	9
C. Furnace Electrothermal Atomizers. . . . .	13
D. Filament Electrothermal Atomizers . . . . .	18
E. Sampling Boat and Probe Techniques. . . . .	22
F. Chemical Atomization Techniques . . . . .	24
G. Specific Literature Background of the Present Work . . . . .	25
COMPUTER CONTROLLED INSTRUMENTATION . . . . .	28
A. Introduction. . . . .	28
B. The Positioner. . . . .	29
1. General Introduction and Overview. . . . .	29
2. Sequence Structure and the Flow of States. . . . .	36
3. Detailed Logic. . . . .	43
a. Dual Synchronous Clock Source. . . . .	43
b. Sequence Initiation Circuitry . . . . .	45
c. Destination Preparation Circuitry . . . . .	47
d. Destination Seeking Circuitry . . . . .	52
e. Overcount Circuitry . . . . .	57



Chapter	Page
f. Motor Driving Circuitry . . . . .	61
4. Interface . . . . .	67
5. Power Supplies and Physical Structure . . . . .	67
6. Testing and Performance . . . . .	69
7. Operating Software. . . . .	74
C. The Autosampler . . . . .	75
1. History and Introduction. . . . .	75
2. Device Description. . . . .	80
3. Detailed Logic. . . . .	87
a. Registers . . . . .	87
b. Vertical Motor. . . . .	98
c. Turret Motor. . . . .	99
d. Rotation Motor. . . . .	102
e. Syringe Motor . . . . .	103
4. Interface . . . . .	110
5. Power Supplies and Physical Structure . . . . .	114
6. Testing and Performance . . . . .	115
7. Operating Software. . . . .	116
D. Data Acquisition System . . . . .	118
1. Multifrequency Real Time Clock . . . . .	118
2. A/D Converter . . . . .	126
3. Power Supplies and Physical Structure . . . . .	127
4. Testing and Performance . . . . .	130
5. Operating Software. . . . .	130
E. Perspectives. . . . .	131
1. Positioner. . . . .	132
2. Autosampler . . . . .	136
3. Data Acquisition System . . . . .	138
F. Miscellaneous Instrumentation . . . . .	139
1. Braid Heating Level Converter . . . . .	139

Chapter	Page
2. General Purpose Flags.....	142
3. Computer Conveniences.....	143
G. Remote Terminal Facility . . . . .	145
<b>MECHANICAL AND OPTICAL INSTRUMENTATION AND BASIC SYSTEM PERFORMANCE . . . . .</b>	<b>147</b>
A. The Atomization Cell . . . . .	147
B. The Optical System . . . . .	152
C. Atomic Absorption Instrumentation. . . . .	155
D. Braid Power Supply and Controller. . . . .	156
E. Operating Software . . . . .	157
F. Summary of Events for a Single Sample . . . . .	159
G. Calculation of Absorbance. . . . .	161
H. Perpendicular Versus Parallel Braid Orientation. . . . .	165
I. Effect of Entrance Slit Geometry . . . . .	167
J. Nature of Instrumental Noise . . . . .	169
K. Importance of Background Correction. . . . .	176
L. Alternate Methods of Data Reduction. . . . .	179
<b>SCANNING ELECTRON MICROSCOPY STUDIES OF GRAPHITE BRAIDS. . . . .</b>	<b>183</b>
<b>AN EVALUATION OF THE RADIATION METHOD FOR ATOMIZER TEMPERATURE CONTROL . . . . .</b>	<b>203</b>
A. Introduction . . . . .	203
B. Qualitative Comparison of the Techniques . . . . .	205
C. Temperature Calibration of the Graphite Braid . . . . .	207
D. Long Term Temperature Drifts of Graphite Braid . . . . .	217
E. Sheath Gas Flow and Contact Resistance Effects . . . . .	227
F. Performance of Methods During Atomizations . . . . .	230
G. Summary and Conclusions. . . . .	247

Chapter	Page
ATOMIC CONCENTRATION PROFILES OVER GRAPHITE BRAIDS. . . . .	251
A. Introduction . . . . .	251
B. Vertical Appearance of Concentration Profiles . . . . .	254
C. Horizontal Appearance of Concen- tration Profiles . . . . .	261
D. Effect of Temperature Upon Silver Integrated Absorbance. . . . .	271
E. A Discussion of Some Problems of Interpretation . . . . .	279
F. Effect of Oxygen Upon Free Atom Populations. . . . .	281
G. Effects of Matrices Upon Concen- tration Profiles . . . . .	286
SUMMARY AND CONCLUSIONS. . . . .	304
APPENDIX A: SIMPLE HARDWARE CONTROL APPROACH FOR SEQUENCING CHEMICAL INSTRUMENTATION. . . . .	308
APPENDIX B: SOURCES OF COMMERCIAL INSTRUMENTATION. . . . .	332
REFERENCES . . . . .	335

## LIST OF TABLES

Table		Page
1	Command set for positioner interface. . . . .	66
2	Precision of location of the reset point: vertical. . . . .	71
3	Precision of location of the reset point: horizontal. . . . .	73
4	Bit assignments of the autosampler registers. . . . .	89
5	Ballast resistor values for the autosampler motors . . . . .	109
6	Command set for autosampler interface. . . . .	113
7	Frequencies available from the data acquisition system. . . . .	124
8	Command set for the data acquisi- tion system interface. . . . .	129
9	Command set for the final instru- mental sections. . . . .	144
10	Improvement of signal and precision for parallel versus perpendicular braid orientation. . . . .	166
11	Effect of monochromator orientation upon results . . . . .	168



Table	Page
12	Significance of the need for background correction. . . . . 177
13	Comparison of algorithms for the calculation of absorbance. . . . . 181
14	Comparison of pyrometrically observed temperatures with the present method . . . . . 216
15	Instrumental parameters for the comparison of radiation and power programming. . . . . 232
16	Analysis of the cadmium-copper mixture. . . . . 248
17	Common instrumental parameters for atomic concentration profile work . . . . . 255
18	Change in integrated absorbance of silver samples with temperature . . . 273
19	Transit times for silver samples at different temperatures. . . . . 276
20	Effect of sheath flow rate upon cadmium spatial data . . . . . 278
21	Effect of sulfate ion from sulfuric acid upon integrated absorbance of cadmium. . . . . 287
22	Effect of chloride ion from potassium chloride upon integrated

Table	Page
	absorbance of cadmium. . . . . 292
23	Matrix effects of zinc and cadmium at lowered total salt concentrations . . . . . 296
24	Effects of matrices upon inte- grated absorbance for copper and magnesium. . . . . 297

## LIST OF FIGURES

Figure		Page
1	Block diagram of computer-controlled atomic spectrometric instrumentation. . . .	5
2	Assignment of atomizer cell locations . . .	32
3	Block diagram of positioner control logic . . . . .	34
4	Flow of states and functions in a GO cycle. . . . .	37
5	Flow of states and functions in a RESET cycle . . . . .	40
6	Schematic diagram of a sequencer. . . . .	42
7	Schematic diagram of the dual, synchronous clock source. . . . .	44
8	Schematic diagram of the sequence initiation circuitry. . . . .	46
9	Schematic diagram of the decimal registers . . . . .	48
10	Schematic diagram of the principal positioner registers. . . . .	49
11	Schematic diagram of the gates and direction control circuitry . . . . .	53
12	Schematic diagram of the condition 4 detect logic. . . . .	54
13	Schematic diagram of the overcount circuitry . . . . .	59

Figure	Page
14	Schematic diagram of the stepper motor waveform generator. . . . . 62
15	Schematic diagram of the stepper motor drivers . . . . . 63
16	Normal rest position of the auto- sampler . . . . . 83
17	Sample depositing position of the autosampler . . . . . 83
18	Turret addressing position of the autosampler . . . . . 84
19	Sample filling or emptying position of the autosampler. . . . . 84
20	Schematic diagram of the gate, direction control, and error detect circuitry for the vertical motor. . . . . 91
21	Schematic diagram of the fine positioning circuitry for the vertical motor. . . . . 94
22	Schematic diagram of the stop circuitry for the vertical motor. . . . . 97
23	Schematic diagram of the circuitry for the turret motor. . . . . 100
24	Schematic diagram of the circuitry for the rotation motor. . . . . 104

Figure	Page
25	Schematic diagram of the gate, error detect, and stop circuitry for the syringe motor . . . . . 106
26	Schematic diagram of the sample size control circuitry for the syringe motor . . . . . 107
27	Schematic diagram of the autosampler interface flag and clock sources. . . . . 111
28	Schematic diagram of the clock source and frequency select circuitry for the data acquisition system. . . . . 120
29	Schematic diagram of the frequency dividing and gating circuitry for the data acquisition system . . . . . 121
30	Schematic diagram of the data ac- quisition system interface flag and data reading circuitry. . . . . 128
31	Improved flow of states and func- tions for a RESET cycle . . . . . 135
32	Schematic diagram of an improved gate circuit for the autosampler motors. . . . . 137
33	Schematic diagram of the braid heating level control circuitry . . . . . 140

80

81

82

83

84

85

86

87

Figure	Page
34	Illustration of the atomization cell. . . . . 148
35	Optical system for the atomic absorption experiments. . . . . 153
36	Illustration of the effect of readout time constants upon integrated absorbance . . . . . 164
37	Noise characteristics of the instrumentation over various periods of observation: silver hollow cathode. . . . . 172
38	Noise characteristics of the instrumentation over various periods of observation: lead hollow cathode . . . . 173
39	Virgin graphite braid at 50 diameters . . . . . 186
40	Degassed virgin braid at 50 diameters . . . . . 186
41	Virgin braid at 500 diameters . . . . . 188
42	Individual fiber of braid at 20,000 diameters. . . . . 188
43	Individual fiber of a used braid at 20,000 diameters: electrode holder region . . . . . 190

Figure

44

100

at

ex

45

20

at

20

46

20

20

47

20

a

48

20

20

49

20

20

20

20

20

20

20

20

20

20

20

20

Figure	Page
44 Individual fiber of a used braid at 20,000 diameters, with apparent extensive damage. . . . .	190
45 Individual fiber of a used braid at 10,000 diameters, with deposited particulates. . . . .	192
46 Individual fiber of an old braid at 20,000 diameters: central region. . . . .	192
47 Braid intentionally damaged through atmospheric exposure, 500 diameters . . . . .	193
48 Braid used in high temperature work, 100 diameters . . . . .	193
49 Copper nitrate salt particle on braid, 10,000 diameters. . . . .	196
50 Nickel nitrate salt particle on braid, 10,000 diameters . . . . .	196
51 Glass bead on braid, 10,000 diameters . . . . .	198
52 Combined cadmium and zinc nitrate salt particle on braid, 10,000 diameters . . . . .	198
53 Exploded silver nitrate salt particle on braid, 10,000 diameters . . . . .	200
54 Copper nitrate salt particle on braid, 10,000 diameters . . . . .	200

Figure

55 C

s

a

56 m

i

v

57

58

59

60

61

62

Figure	Page
55	Oscilloscope photographs of power supply responses under radiation and power programming . . . . . 206
56	Temperature calibration of graphite braid with respect to reference voltage: low temperature region . . . . . 212
57	Temperature calibration of graphite braid with respect to reference voltage: high temperature region. . . . . 214
58	Temperature calibration of graphite braid with respect to phototransistor output: low temperature region. . . . . 218
59	Temperature calibration of graphite braid with respect to phototransistor output: high temperature region . . . . . 219
60	Temperature decay of graphite braid under radiation and power programming: low temperature . . . . . 220
61	Temperature decay of graphite braid under radiation and power programming: moderate temperature. . . . . 224
62	Temperature decay of graphite braid under radiation and power programming: high temperature. . . . . 226

Figure	Page
63	Cadmium transients under ratiation
	programming . . . . . 234
64	Cadmium transients under power
	programming . . . . . 235
65	Lead transients under radiation
	programming . . . . . 236
66	Lead transients under power
	programming . . . . . 237
67	Silver transients under radiation
	programming . . . . . 238
68	Silver transients under power
	programming . . . . . 239
69	Copper transients under radiation
	programming . . . . . 240
70	Copper transients under power
	programming . . . . . 241
71	Nickel transients under radiation
	programming . . . . . 242
72	Nickel transients under power
	programming . . . . . 243
73	Distortion of transients under
	radiation programming by readout
	time constants. . . . . 245

Figure	Page
74	Normalized concentration profiles with vertical height for silver, cadmium, and lead . . . . . 257
75	Normalized concentration profiles with vertical height for zinc, mercury, and thallium . . . . . 258
76	Normalized concentration profiles with vertical height for copper and magnesium. . . . . 259
77	Normalized concentration profiles with horizontal displacement at a vertical height of 0 mm . . . . . 262
78	Normalized concentration profiles with horizontal displacement at a vertical height of 6 mm. . . . . 263
79	Normalized concentration profiles with horizontal displacement for silver at various vertical heights . . . . 266
80	Normalized concentration profiles with horizontal displacement at a vertical height of 0 mm and a perpendicular braid . . . . . 268
81	Normalized concentration profiles with horizontal displacement at a vertical height of 6 mm and a perpendicular braid.. . . . 269



Figure	Page
82	Normalized concentration profiles with horizontal displacement at a vertical height of 12 mm and a perpendicular braid. . . . . 270
83	Normalized concentration profiles with horizontal displacement for silver at various atomizer temperatures. . . . . 274
84	Effect of oxygen upon the vertical concentration profile of cadmium . . . . . 283
85	Effect of oxygen upon the vertical concentration profile of zinc. . . . . 284
86	Effect of oxygen upon the vertical concentration profile of lead. . . . . 285
87	Effect of added chloride ion as ammonium chloride upon the vertical concentration profile of cadmium . . . . . 289
88	Effect of added chloride ion as potassium chloride upon the high resolution vertical concentration profile of cadmium . . . . . 293
89	Effect of sulfate ion as potassium sulfate upon the vertical concentration profile of copper . . . . . 298

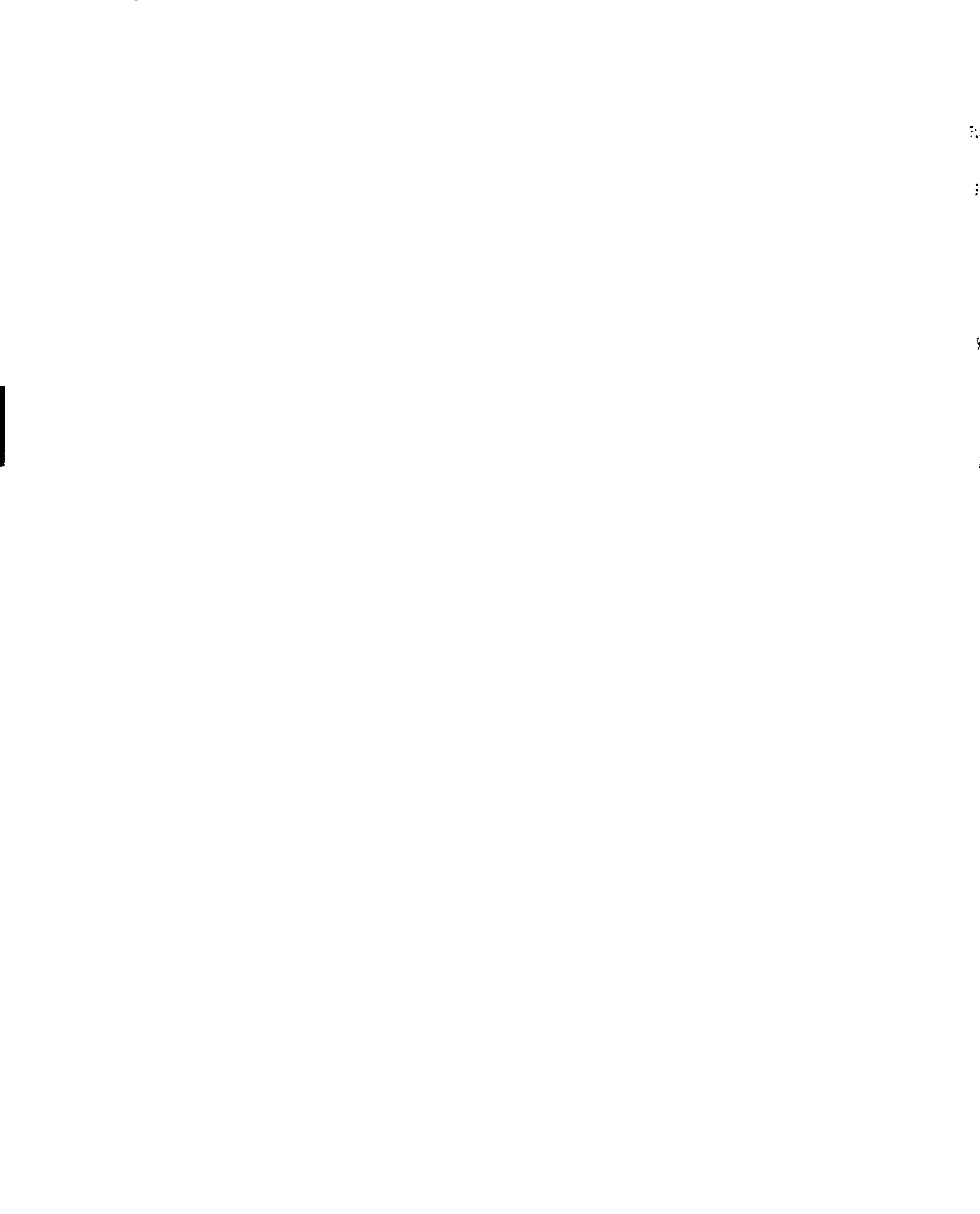
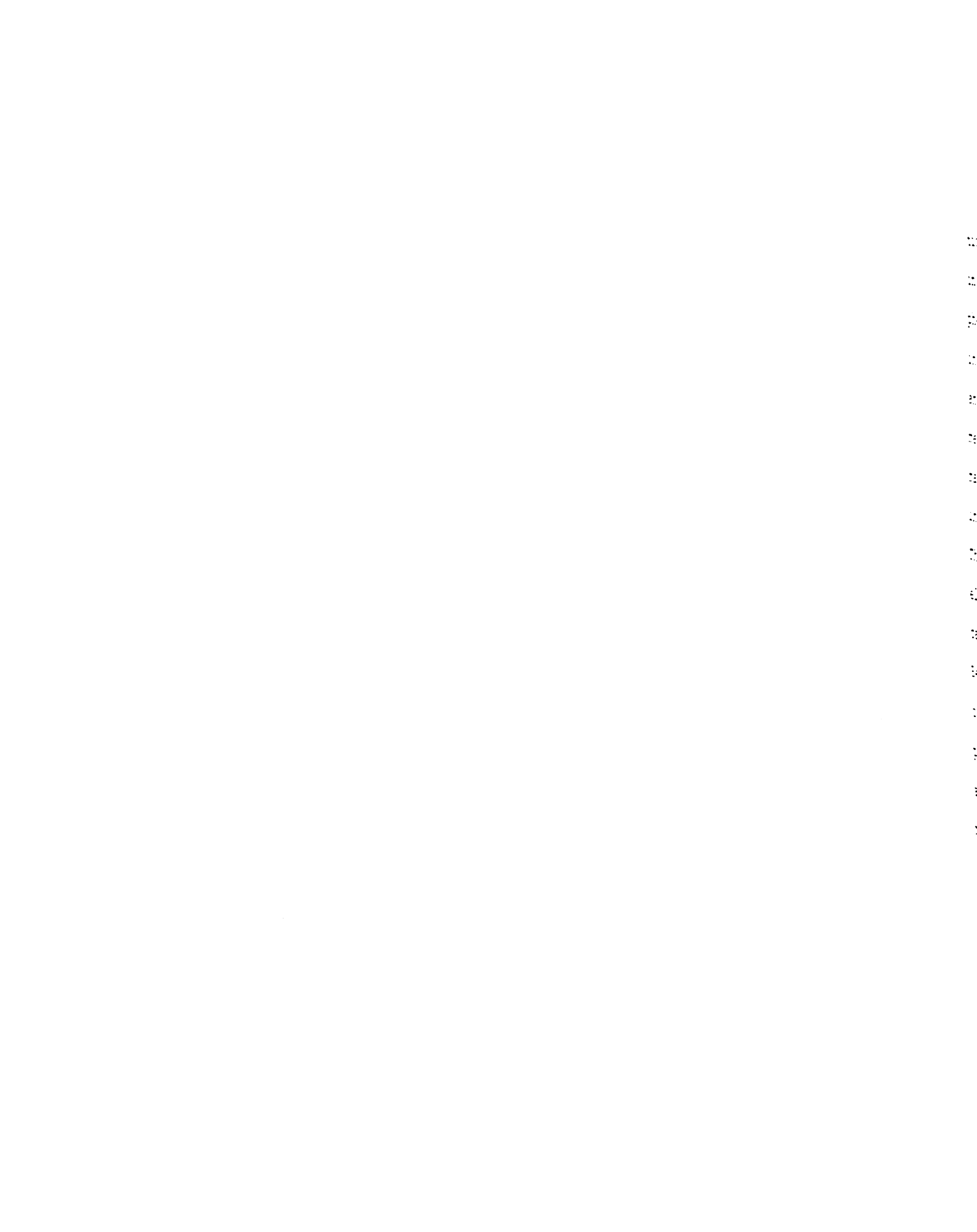


Figure	Page
90	Concentration dependence of the effect of added fluoride ion upon the vertical concentration profile of magnesium . . . . . 301
91	Effect of added fluoride ion upon the high resolution vertical concen- tration profile of magnesium . . . . . 302
A1	Basic flowchart units for transfer conditions and transfer functions. . . . . 314
A2	Sequencer flowchart for the example of a bath thermostat . . . . . 316
A3	General schematic diagram of a controller . . . . . 317
A4	Sequencer flowchart for the example of an automatic fraction collector . . . . . 320
A5	Schematic diagram of the controller for the example of the automatic fraction collector . . . . . 322
A6	Sequencer flowchart for the filament positioning instrument . . . . . 326
A7	Schematic diagram of the controller for the filament positioning instrument. . . 328



## INTRODUCTION

The practice of analytical chemistry has been revolutionized in recent years by the tremendous advances made in scientific instrumentation. The variety of physical phenomena of analytical importance for which precision instrumentation is available has expanded dramatically, and the sophistication of both new and familiar instruments increases annually. Much of this progress has been made possible by a parallel and equally burgeoning growth in the technology of computers and solid state electronics. The size, cost, and power consumption of computers and electronic instruments have steadily dropped, whereas their capabilities, speed, and performance have continually risen. Because of these trends, modern analytical instrumentation can not only perform determinations or observe phenomena previously unobtainable, but can also guide its own activities, monitor and correct drifts in its performance, and relieve the user of many necessary but routine duties. When coupled to a computer, an analytical instrument becomes a particularly powerful tool for scientific investigations, in which the complex capabilities of the computer can serve to provide detailed and flexible control over the instrumental functions, as well as comprehensive treatment and presentation of the acquired data. In recent years, the attainment of such goals has been

made

provid

proce

in a

been

they

The

that

then

more

that

the

and

the

the

in

in

the

made particularly possible through the introduction and growth of microprocessors, in which the entire central processing unit of a modern minicomputer can be placed on a single solid state device. Their impact has already been felt in existing instrumentation, and the promise they hold for future instruments is virtually limitless. The research described in this thesis has as its central goal the use of such modern, custom-designed instrumentation in conjunction with computer-controlled operation to investigate various facets of an analytical technique that would be prohibitively difficult to study without the benefits such control can provide. The technique under study is filament-type electrothermal atomic absorption spectrometry, with an atomizer known as the graphite braid.

Atomic spectrometry is an analytical technique rich in both instrumental requirements and chemical complexity. Studies of variables in these categories have been performed for some time by many workers. Most of these have been with the traditional flame atomizer. The nonflame, or electrothermal atomizers are more recent developments; the oldest of them has existed less than twenty years. In the past decade, a great many such devices have been described in the literature. Much work remains to be done, however, in better characterizing atomizers that already exist.

If a device is to serve effectively as an electrothermal

atomizer, it follows that studies of the device itself can be of great potential benefit in learning what physical and chemical processes occur as it is used. In the present work, scanning electron microscopy and x-ray microprobe fluorescence have been employed to observe the appearance of graphite braid and the changes which it undergoes while in service as an atomizer.

The control of temperature in electrothermal atomizers is an extremely important parameter. Because an atomizer will age with continued use, it is a serious matter to assure that the power supply which heats the device can be effectively and sensitively regulated to preserve as nearly consistent temperatures from atomization to atomization as possible. If an electrical parameter such as the voltage developed across the atomizer is the control signal, the drift of atomizer temperature with continued use can be considerable, because control is based upon an input to the atomizer rather than an output from it. The radiation method of atomizer control, which follows the blackbody emission from the device, is such an output parameter. It will be shown in the present work that this method is an excellent control signal for electrothermal atomic spectrometry, and that it provides superior consistency in atomizer temperatures, increased atomizer lifetime, and the promise of improved detection limits and ability to deal with complex sample matrices.

Although computer control and powerful instrumentation

plays a significant role in the above studies, their full capabilities are realized in the final field of investigation, which is a study of the spatial profiles of free atom concentrations above the atomizer. To perform such studies, repeated atomizations of a constant sample are taken while the atomization cell is systematically translated in two dimensions with respect to a fixed optical axis. This work is extremely time consuming because of the discrete nature of electrothermal atomic spectrometric sampling. It is also very tedious to perform manually. In the present work, two sophisticated, computer-controlled instruments are described which make these studies practical. One of these is a positioning device which is capable of performing the orderly movement of the atomization cell. The second is a versatile and precise autosampling unit. With these two instruments, and additional instrumentation which includes a dedicated data collection system, a complete, computer-controlled atomic absorption spectrometer is described which is able to run itself virtually unassisted by the user. As an aid and convenient reference for the descriptions to follow, Figure 1 shows a block diagram of the entire operating system.

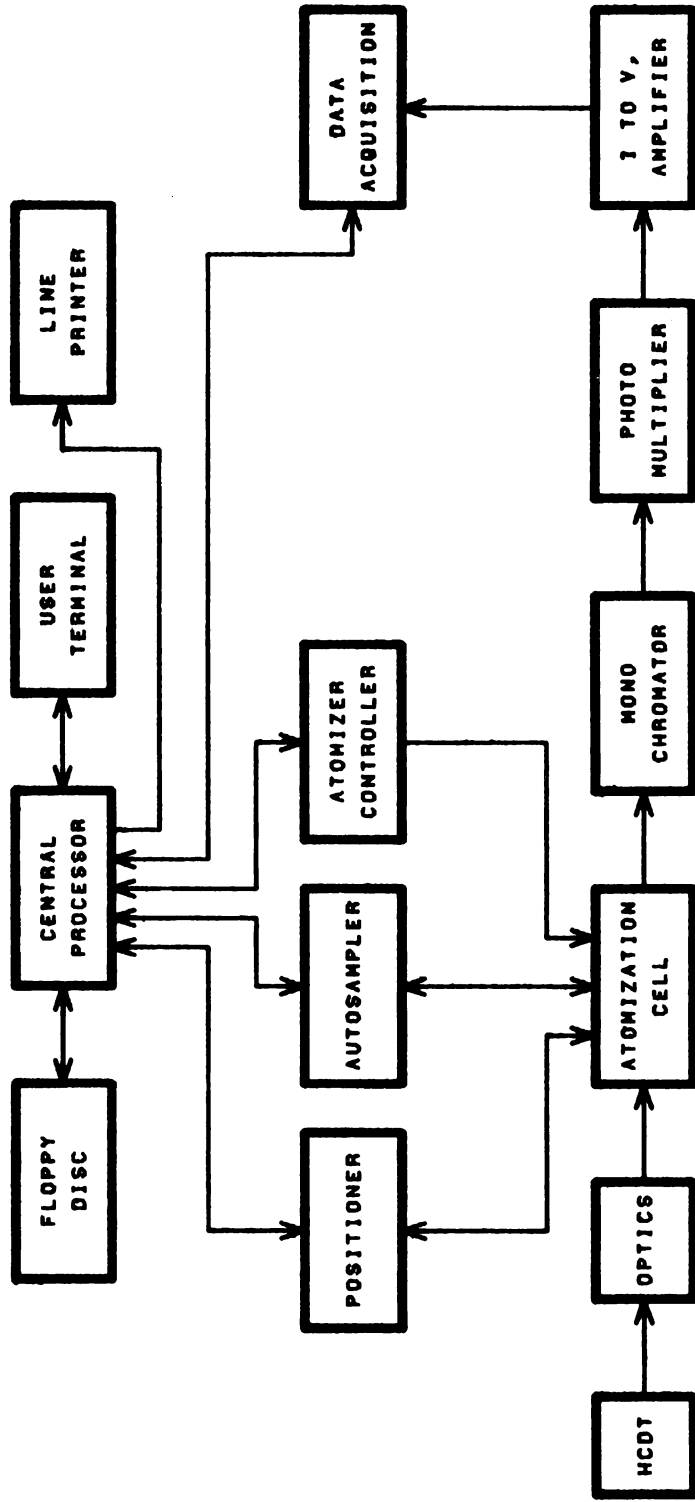


Figure 1. Block diagram of computer-controlled atomic spectrometric instrumentation.

2

v

t

t

t

A

e

t

t

t

s

D

t

T

S

B

W

R

t

## HISTORICAL

Atomic spectrometry is today a well established laboratory technique. It is capable of performing a wide variety of both qualitative and quantitative determinations, and finds a place in laboratories which do everything from the most current and speculative research to the most routine and common repetitive sample analysis. Atomic spectrometric methods are applicable to nearly every metallic and metalloidal element of the periodic table, and are frequently the techniques of choice for the determination of trace quantities of sample constituents, or for multielement determinations of several species within the sample.<sup>1-4</sup>

### A. EARLY OBSERVATIONS AND DEVELOPMENTS OF ATOMIC SPECTROMETRIC TECHNIQUES

Initial observations of atomic spectrometric phenomena probably date from pre-Lavoisierian chemistry in the form of the familiar colored flame tests for qualitative analysis. These early discoveries were given a more systematic and scientific chemical treatment in the pioneering work of Bunsen and Kirchhoff over one hundred years ago,<sup>5</sup> at which time the observation of prism sorted emission spectra represented one of the prime experimental techniques for the discovery and confirmation of additional known elements.

With the growth of technological skills in optics and electrical power generation, the study of emission spectra and their permanent recording on photographic plates came to be established as one of the earliest instrumental techniques. In the years since, electrical arc and spark atomic emission spectrography have developed a literature rich in both theory and practice for a great many chemical systems.<sup>6-8</sup> In fact, emission methods remain today as the workhorse techniques for the analysis of materials having metallurgical or geological significance, or for studies in specialized fields such as astronomy. Applications and advances in flame emission and radiofrequency emission techniques have enjoyed a parallel growth no less impressive.<sup>9-11</sup>

A satisfactory theoretical and mathematical explanation of atomic spectra was not possible until the development of quantum mechanics in the early part of this century, after which a full rationalization of atomic spectra was rapidly developed. By the early thirties, a very complete body of knowledge had been acquired, which could effectively and consistently explain all of the basic atomic spectrometric phenomena, as well as a considerable number of the more common deviations from ideal model behavior.<sup>12</sup> In return, atomic spectrometry served as one of the principal techniques for the experimental confirmation of early quantum mechanical predictions, the Bohr atom being a particularly prominent and well known example. Inherent

in the theoretical treatment, and in some experimental observations at the time, was the realization of the existence of the other two atomic spectrometric techniques, atomic absorption and atomic fluorescence.

Although atomic absorption had been known since 1802 with Wollaston's discovery of the Fraunhofer lines in the sun's spectrum, true chemical applications of the method did not occur until the early 1950's, partly because of instrumental limitations imposed by the lack of a practical, stable, narrow line source.<sup>13</sup> With the adoption of the hollow cathode discharge tube, and the groundbreaking work of Alan Walsh in Australia, atomic absorption moved into the realm of viable analytical chemical techniques.<sup>14,15</sup> After a somewhat slow start during the remainder of the fifties, atomic absorption grew rapidly during the mid-sixties. Several lines of competitive instrumentation appeared in the marketplace, and an intensive though at times overly idealistic sales program got underway. By the end of the sixties, an atomic absorption instrument of some sort was likely to be found in nearly every major academic and industrial lab, and the growth of the method has been prodigious ever since.<sup>16,17</sup>

Atomic fluorescence is an even more recent development than atomic absorption. Although it too had been recognized theoretically and experimentally for some years,<sup>18,19</sup> it was not until 1962 that Alkemade proposed its application to chemical analysis,<sup>20</sup> and not until

1964 that the first modern paper on the subject appeared by Winefordner and Vickers.<sup>21</sup> In the short time since, it too has enjoyed a significant growth,<sup>22,23</sup> although it remains at this writing primarily a research method only, chiefly because of the lack of commercial instrumentation, and some reluctance by instrument builders to accept it as a companion to atomic absorption rather than a duplication or a competitor.

#### B. COMPARISON OF FLAME AND ELECTROTHERMAL METHODS

With the exception of the electrical arc and spark techniques, most experimentation in atomic spectrometry has been performed using a flame as the medium with which to produce free atomic vapor. This is historically the natural development of the discipline, and a flame supporting instrument is still the standard configuration for commercial atomic spectrometric systems. This is not to imply, however, that the flame is an outmoded or fundamentally unsuitable atomization device. Flames do possess a number of characteristics that recommend their use.<sup>24</sup> Burners and auxiliary apparatus to ignite and sustain a flame are common and readily available in a variety of modifications. They are capable of producing a flame of high stability and reproducibility. The number of different fuel and oxidant combinations available, as well as the ability to adjust fuel-to-oxidant ratios, allows flames

to be used over a wide range of temperatures. Flames offer very good levels of detectability and sensitivity for many elements with resonance lines in the common region of 200 to 400 nm. Finally, the sample in a flame system may be continually aspirated, which gives rise to a DC signal that may be detected as such or modulated with an AC component for phase-locked detection, and improvement of signal-to-noise qualities.

Yet, in spite of their popularity and capabilities, flame atomizers do suffer from numerous disadvantages that detract from their usefulness. The flame itself is an extraordinarily complex chemical environment, rich in molecular, atomic, and radical species which can seriously plague an analysis. This is true both from the chemical standpoint of depopulating the supply of free atomic species through formation of stable analyte compounds such as hydroxides or oxides, and from the physical standpoint through such effects as molecular quenching of fluorescence. The high rates of flow and the expansion effects of the combusting gases act to dilute the atomic concentration of analyte in the flame. Flames can often contribute significantly to the background emission or absorption character of the system, especially for those elements with analysis wavelengths near the vacuum ultraviolet. The overall efficiencies of aspiration, desolvation, and vaporization are rather low for flame systems. Finally, the amount of sample solution required may be excessive,

if not impossibly large, for critical samples such as are found in clinical work. It may certainly be counter-argued that much modern research has been directed towards alleviating these problems. The use of ultrasonic nebulization to improve sample transport efficiencies is a case in point.<sup>25</sup> Nonetheless, because of effects such as these, alternative methods of atomization in atomic spectrometry have found increasing use in recent years.

The alternative practical energy source for atomic spectrometric atomization is electrical power. Over the past fifteen to twenty years, many researchers have proposed and characterized such "flameless", or more properly stated, electrothermal atomizers, which are generally fashioned out of some substance which is sufficiently refractory to withstand sudden and repetitive heating to temperatures as high as 3000° K.<sup>26</sup> Perhaps the most fundamental contrast between these methods and the more classical flame approaches is that in electrothermal techniques, the sample is not usually continuously aspirated by some sort of nebulizer, but is rather deposited as a discrete sample of typically only a few microliters total volume directly onto the atomizer. In a similar manner, the atomizer itself is not usually continuously at the atomization temperature, but is instead stepped through a heating sequence. First, gentle heating is employed to remove the solvent, followed by strong heating to affect atomization, with an optional intermediate

heating level for the ashing of organic matrices. From these differences arise many of the comparative advantages and disadvantages of the electrothermal techniques. Electrothermal atomizers lack the complex chemical environment of a burning flame, as well as much of the expanding gas dilution effect. They also possess considerably less spectral background interference. These effects all combine favorably to give electrothermal atomizers a general advantage over flames in terms of detectability and sensitivity for many elements. The very small sample sizes are beneficial to those analyses where sample conservation is essential. Furthermore, the fact that the entire sample may be discretely placed directly upon the atomizer surface substantially improves the overall efficiency in making the transitions from a dilute solution to an atomic vapor.

At the same time the electrothermal methods suffer difficulties as well. One of the most vexing, at least for those devices employing discrete sampling, is the transitory nature of the analytical signal. In place of the DC level or AC waveform that can be observed and processed over tens of seconds, many electrothermal atomizers produce an absorbance spike of duration as short as one quarter second. In addition, sampling cannot be repeated much faster than one sample per minute. The instrumental readout must consequently be prepared to follow transients, and integration of the transient is advisable for quantitation of results over a reasonable

dynamic range. Furthermore, the same atomizer must be used over and over for each successive sample, which inevitably leads to drifts due to aging, and often requires the eventual discarding of a spent device. A final problem is the difficulty in reproducibly drawing and depositing sample quantities on the order of only a few microliters. Electrothermal atomizers can be divided into either the "furnace" or "filament" categories. They are discussed here in that order.

### C. FURNACE ELECTROTHERMAL ATOMIZERS

The concept of using a furnace-like device for atomic spectrometric studies dates back to the early part of this century, when King proposed the use of a furnace manufactured from graphite for studies in atomic spectrophysics.<sup>27-29</sup> The first such device intended specifically for analytical chemical work was that proposed by L'vov about 1961.<sup>30</sup> His atomizer consisted of a graphite tube 30 to 50 mm long and 2.5 to 5 mm in inner diameter. The sample was placed onto a treated graphite electrode which was inserted into an opening in the side of the furnace. To atomize the sample, an arc was struck from this electrode, while simultaneously another power source heated the main furnace body to temperatures as high as 3000° K. To protect the device from atmospheric attack, it was enclosed in an argon-filled container fitted with quartz windows

to

L

st

st

Fi

fi

fi

de

pe

es

is

wa

wa

di

a

di

di

in

fi

z

a

t

a

f

M

to permit passage of the source beam down the furnace axis. L'vov and Lebedev improved upon the original design with such additions as two channel operation with an internal standard, a simpler means of heating samples, use of pyrolytic graphite in the furnace to retard sample diffusion into the walls, and the ability to function at greater than atmospheric pressure.<sup>31,32</sup> Some forty elements were examined and detection limits on the order of picograms of material were realized.

In the late sixties, Woodriff and coworkers constructed a furnace atomizer 150 mm long and 7 mm in diameter.<sup>33-39</sup> It was continuously heated by a high wattage supply, and was enclosed in an insulated, steel container provided with a continuous flow of argon. Samples were either discretely deposited, or nebulized into the furnace through a side arm. A number of elements were examined with this device, as were some matrix effects.

About the same time as Woodriff's work, Massmann devised another furnace similar to L'vov's, but simpler in construction.<sup>40,41</sup> The tube measured 55 mm long and 6.5 mm in diameter. It was resistively heated up to 2600° K by a high wattage supply. Samples were deposited through a small hole bored in the side of the furnace. Both solution and solid samples were examined, and the device was also redesigned in an alternate shape specifically intended for atomic fluorescence. A further modification of the Massmann device was marketed in 1970 by the Perkin-Elmer

C

A

e

2

3

C

E

S

3

C

V

7

3

W

G

1

C

7

S

7

B

B

B

A

B

Corporation, and named the HGA-2000 ("Heated Graphite Atomizer").<sup>42-44</sup> It was the first of several commercial electrothermal devices, and is in increasingly widespread use.

A furnace atomizer for use in atomic fluorescence was designed by Wineforder.<sup>45</sup> It featured observation slits cut in the graphite so as to prevent observation of black-body radiation by the detector, as well as a septum and syringe method of sample injection. Robinson and coworkers described an induction heated atomizer for the determination of air pollutants.<sup>46-48</sup> Air is drawn through a tube filled with carbon chunks and heated to about 1400° C. The carbon monoxide produced acts with additional hot carbon to reduce metallic ion vapors to the elemental state, after which they are analyzed in a second heated tube made of quartz. The system was capable of detecting cadmium at levels as low as 0.005 microgram per cubic meter of air.<sup>49</sup> Other inductively heated graphite tube furnaces were proposed by Headridge and Smith,<sup>50</sup> and by Langmyhr and Thomasen.<sup>51</sup>

The advantage of continuous sample introduction first realized by Woodriff has also been retained in several additional devices. Veillon and coworkers have described a vertically oriented graphite tube furnace, useful in atomic fluorescence, which receives sample continuously in the form of an argon carried aerosol.<sup>52</sup> Wineforder and his students have explored techniques for continuous

sample introduction into furnaces through the use of a pneumatic nebulizer and steel desolvation chamber.<sup>53,54</sup>

Papers have also appeared in which already existing atomizers have been modified to improve their performance. Chapman, Dale, and Kelly reduced the diameter of a furnace on either side of the sample deposition region to produce regions of greater heat that would retard the diffusion of atomic vapor out of the observation window.<sup>55</sup> Robinson and coworkers have described techniques in which a sample in a complex matrix is placed into the side arm of Woodriff-type furnaces for extensive pretreatment designed to destroy and flush out the matrix. The analyte of interest can then be atomized relatively matrix free.<sup>56,57</sup> Successful direct analyses for trace metals in such difficult matrices as blood, urine, and sea water were reported. Church et al. have designed a low temperature Woodriff-type furnace for mercury determinations in which oxygen is actually drawn through the furnace to assist in sample matrix combustion.<sup>58</sup>

Several authors have performed investigations designed to improve and extend furnace methodology. Veillon and his students have experimented with techniques to deposit and maintain pyrolytic graphite coatings upon atomizers, through use of a constant supply of methane gas at trickle flow rates.<sup>59,60</sup> Similar studies have been reported by Molnar and Winefordner,<sup>61</sup> and by Sturgeon and Chakrabarti.<sup>62</sup> Runnels and his associates have proposed a related process

in which the coating is a refractory metal carbide. Improved performance of the furnace in analyses of metals prone to carbide formation was observed.<sup>63</sup> Fuller and Thompson have evaluated some concepts of solid sampling techniques.<sup>64</sup> Thomassen et al. have proposed analyses in which the trace metals of interest are electrodeposited on graphite sticks, which are then scraped, and the resulting powder analyzed in a cup-like device.<sup>65</sup> Extensive exploratory work has been performed by Ottaway and coworkers to extend the applications of furnaces to atomic emission analysis of elements such as the alkali metals and alkaline earths.<sup>66</sup> DeGalan has published a critical study of some of the practical pitfalls and implications of furnace atomic spectrometric work.<sup>67</sup>

Applications of furnace type atomizers to specific analyses are extensive; dozens of references could be cited.<sup>1,2,26</sup> Some representative papers from only the past few years may be given here as examples. Among the clinical and biological methods may be listed analyses for aluminum,<sup>68</sup> cadmium,<sup>69</sup> chromium,<sup>70</sup> gold,<sup>71</sup> and lead<sup>72</sup> in blood, mercury,<sup>73</sup> and lead<sup>74</sup> in urine, or chromium<sup>75</sup> and selenium<sup>76</sup> in tissues. Many applications may be found for geological samples, including cadmium,<sup>77</sup> silver, lead, thallium, and zinc<sup>78</sup> in rocks. Environmental samples continue to be of interest, with methods reported for silver, beryllium, cadmium, and lead in air,<sup>79</sup> cadmium in seawater,<sup>80</sup> or selenium in industrial effluents.<sup>81</sup> Among the food

a  
a  
M  
t  
i  
a  
i  
  
a  
i  
d  
f  
c  
z  
a  
a  
a  
f  
s  
t  
c  
c  
7

analyses may be included aluminum, chromium, copper, lead, and zinc in mussels,<sup>82</sup> and cobalt in feed grains.<sup>83</sup> Metal and alloy analyses are well represented also, with techniques available for aluminum in steels,<sup>84</sup> silver, bismuth, and cobalt in tin,<sup>85</sup> iron in silver and gold,<sup>86</sup> and lead, bismuth, selenium, tellurium, thallium, and tin in metal chunks.<sup>87</sup>

#### D. FILAMENT ELECTROTHERMAL ATOMIZERS

The furnace devices were the first to be developed and are the most numerous among commercial instrumentation in the field. Aside from the comparative advantages and disadvantages with respect to flames previously mentioned, furnaces as electrothermal atomizers have the advantages of solid sample capabilities, and a more flamelike environment for the sample in that it is surrounded by the hot atomizer. Samples are thus more likely to be efficiently atomized and kept in the atomic state. Problems associated with their use include their bulkiness, a necessity for cooling facilities, and the requirement of a power supply of arc welder proportions to heat them rapidly to the requisite high temperatures. Because of these detractions, the alternative type of electrothermal device, known as the filament atomizer, was developed.

The first filament atomizer was that reported by T. S. West and his colleagues in 1969-1970.<sup>88-91</sup> It



consisted of a filament originally 25 mm long by 2 mm in diameter with a notch grooved in the center to take the sample. It was secured to stainless steel electrodes and enclosed in an argon purged chamber with quartz windows. Performance of this device in both atomic absorption and atomic fluorescence was reported for about twenty elements, with detection limits roughly comparable to the furnaces.

Belyaev and coworkers developed a solid sample graphite atomizer shaped like a miniature cup, and used to examine samples prepared in graphite powder. Representative determinations included cadmium and silver in rocks.<sup>92-95</sup> A commercial device based on the filament design was marketed by Varian Techtron.<sup>96,97</sup> It is actually a miniaturized Massmann furnace consisting of a rod 9 mm in diameter with a 3.5 mm transverse hole, supported by water cooled graphite electrodes. This atomizer has the provision for supplying hydrogen gas around the filament during analysis, allowing the user to suppress many matrix effects.

Several other authors have also reported filament type devices, most of which are not too dissimilar from the original West concept. Such atomizers would include the designs of Dipierro and Tessari,<sup>98</sup> as well as the atomizer used in this work which was reported by Crouch and Montaser.<sup>99-101</sup> Still another device was reported by Molnar and Winefordner,<sup>102</sup> which was surrounded



during use by a laminar hydrogen-argon-entrained air flame to assist in preserving the atomic population.

Among the filament devices, there are also a variety of atomizers which are made of materials other than graphite. Donega and Burgess developed an atomizer prepared from 25 micron thick tantalum or tungsten foil, and shaped into a boat structure 50 mm long by 6 mm wide, with a depression for containing the sample solution.<sup>103</sup> The device was provided with a quartz envelope, and operated at subatmospheric pressures. A simplified version of the Donega and Burgess device was developed by Hwang and coworkers, and eventually became the Flameless Sampler produced by Instrumentation Laboratory.<sup>104</sup> Other devices in this category include the tantalum strip of Takeuchi et al.<sup>105</sup> the tantalum filament of Maruta and Takeuchi,<sup>106</sup> and the tungsten filament of Cantle and West.<sup>107</sup>

A closely related class of nongraphite atomizers are the wire loop devices. Tungsten and platinum loops were investigated by Winefordner and coworkers.<sup>108-110</sup> Their loop had a diameter of 1/32 inch, and receives sample solution through a dipping process. Crouch et al. investigated automated analysis in atomic fluorescence using platinum wire loops.<sup>111</sup> A tungsten filament atomizer was proposed by Williams and Piepmeier using the tungsten element of an ordinary light bulb.<sup>112</sup> Chauvin and colleagues used loops prepared from an exceptionally high melting tungsten-rhenium alloy.<sup>113</sup> Other similar

atomizers would include the tungsten filament of McCullough and Vickers,<sup>114</sup> the molybdenum ribbon of Ohta and Suzuki,<sup>115</sup> the molybdenum filament of McIntyre, Cook, and Boase,<sup>116</sup> and the tungsten wire loop of Newton and Davis.<sup>117</sup>

Applications of the filament and loop type atomizers to real analysis problems are competitively numerous with the furnace methods. The nature of the matrices encountered are similar as well. Thus, reports have been offered on the determination of zinc,<sup>118</sup> copper,<sup>119</sup> and lithium<sup>120</sup> in blood or serum, zinc in saliva,<sup>121</sup> and cadmium in fish.<sup>122</sup> Arsenic, antimony, and tin have been examined in steel,<sup>123</sup> selenium in copper,<sup>124</sup> iridium in noble metals,<sup>125</sup> and selenium in copper and iron.<sup>126</sup> Filament techniques have been applied to the analysis of arsenic,<sup>127</sup> beryllium,<sup>128</sup> and manganese<sup>129</sup> in water. Cadmium has been examined in air particulates,<sup>130</sup> as has zinc in sediments.<sup>131</sup> Rock samples have been analyzed for gold, cobalt, lead, and vanadium,<sup>132</sup> and the cobalt levels of soils have received attention.<sup>133</sup> Additional successful analyses would include those of metals in jet engine oil,<sup>134</sup> gold in photographic film,<sup>135</sup> barium and antimony in gunshot residue,<sup>136</sup> chromium, copper, and iron in polymers,<sup>137</sup> and lead in canned milk.<sup>138</sup>

Compared to the furnaces, a filament atomizer enjoys the prime advantage of not needing nearly as much electrical power to reach the highest analysis temperatures,

which makes a corresponding reduction in the size of both the atomizer and its supporting facilities. The filament devices can also be more beneficial in atomic fluorescence because their smaller size cuts down on the amount of background radiation observed by the detector. On the negative side, the filament devices do not sustain the sample after atomization. Unlike flames and furnaces which surround the sample with a hot medium, the filament expels the sample into the sheath gas, where it is rapidly cooled and subject to condensation. As a result, it is often observed that analyses in difficult matrices can at times be better done in a furnace. Several workers have observed, however, that use of hydrogen in the sheath gas to ignite and sustain a hydrogen diffusion flame during atomization is greatly beneficial to preserving the atomic population.<sup>96,102,140</sup> Confining the optical field of view to the region immediately above the filament is also of merit.<sup>139</sup>

#### E. SAMPLING BOAT AND PROBE TECHNIQUES

Aside from the purely electrothermal techniques, there are also several other classes of atomizers which exploit chemical peculiarities of specific systems, or attempt to combine virtues of both the flame and electrothermal methods. Prudnikov has explored the enhancement of flame method sensitivities through introduction

of liquid or solid samples directly into the flame on the tip of a graphite microprobe, which may or may not be externally heated.<sup>141-143</sup> A technique employing a tantalum sampling boat was developed by Kahn and coworkers,<sup>144</sup> and by Ringhardt and Welz,<sup>145</sup> in which a sample is pipetted into a small tantalum trough, dried by gentle heating, and then pushed reproducibly into a conventional flame. A variety of clinical determinations such as cadmium in blood<sup>146</sup> or thallium in urine<sup>147</sup> have been performed with this technique, and the boats themselves are available commercially. Perhaps the best known of these combination approaches is the Delves cup, which combines the concepts of mechanical sample introduction with the use of an absorption tube resident in the flame. This tube serves as a containment chamber for the gases of the atomized sample during analysis.<sup>148</sup> Delves intended his method to address the problem of lead poisoning, through analysis of lead in blood. An air-acetylene flame is used, and the absorption tube is manufactured from nickel. A 10  $\mu\text{l}$  sample of blood is placed in a nickel cup, dried, and treated with peroxide. It is then inserted into the flame for analysis. For determinations of lead in blood, it is extremely successful, and has been developed into a rapid, mass screening clinical procedure.<sup>149-152</sup> Other researchers have extended its capabilities to elements other than lead, and to matrices other than blood.<sup>153-156</sup>

## F. CHEMICAL ATOMIZATION TECHNIQUES

A final field of atomic spectrometric techniques which do not employ flames for production of atomic vapor are the chemical vaporization processes for mercury, and for elements forming volatile hydrides. The latter class of elements includes arsenic, antimony, selenium, bismuth, germanium, tin, and tellurium. The concept of determining these elements by volatilizing them out of solution as an easily decomposed hydride was first proposed by Holak in a flame determination of arsenic.<sup>157</sup> The hydride was generated by the reaction which takes place in acidic solution in the presence of potassium iodide, stannous chloride, and granular zinc. At a later date, the method was modified by several workers to eliminate the flame and substitute an absorption tube heated to about 700° C.<sup>158-160</sup> Another improvement was the use of sodium borohydride to generate the hydride species,<sup>161-163</sup> which allows a significant reduction in the time required for hydride generation.

The cold vapor technique for mercury takes advantage of mercury's unusually high vapor pressure and ease of reduction to the atomic state. The cold vapor method was first proposed by Poluektov and coworkers,<sup>164</sup> and has since developed rapidly into a method of choice for determining mercury in just about every matrix encountered. The technique generally consists of reducing mercury

to the atomic state with stannous chloride solution, and sweeping the resulting atomic vapor out of solution and on to an absorption tube for analysis. Representative recent determinations would include mercury in sediments,<sup>165</sup> grain,<sup>166</sup> fish,<sup>167</sup> and oil.<sup>168</sup> The method has also received attention from a critical standpoint, and has been the subject of optimization studies.<sup>169</sup>

The popularity of the volatile hydride and mercury cold vapor techniques arises from their convenience, and from the fact that they provide an unusual opportunity to combine the actual analysis with an effective and highly quantitative separation of the analyte from even the most complex of matrices. Also appealing is the simplicity of the extra apparatus which must be assembled to convert existing instruments to such methods.

#### G. SPECIFIC LITERATURE BACKGROUND OF THE PRESENT WORK

There are some direct literature precedents for portions of the present work. The concept of using various electrical and optical parameters as a means by which to control the heating of an electrothermal atomizer was explored by Montaser and Crouch using the graphite braid.<sup>101</sup> A total of four possible parameters were explored as candidates for serving as the feedback control signal in atomizer temperature regulation. They are

the voltage across the atomizer, the current passing through it, the power dissipated by it, or the blackbody radiation emitted from it. The first two methods, although better than an unregulated system, were not very acceptable as control signals, due to their inability to correct for changes in atomizer characteristics with age. Combining both voltage and current into a signal representing electrical power improved the situation somewhat, but the greatest benefits were definitely seen using the blackbody emission technique for atomizer control. Similar observations were noted as well by Lundgren, Lundmark, and Johansson, who used a photodiode in combination with a triac-controlled switching regulator for governing the heating of a Massmann-type furnace.<sup>170</sup> These authors noted the superior precision of temperature control under the radiation method, and demonstrated how the improved rate of atomizer heating can be put to good advantage in real sample determinations, such as cadmium in sea water.

The exploration of atomic populations at various positions with respect to an electrothermal atomizer has been attempted by several workers. Winefordner and his students examined the decay of atomic populations up to 18 mm above their filament device through use of both atomic absorption and atomic fluorescence techniques.<sup>171,172</sup> A number of elements were investigated, including silver, cadmium, copper, mercury, lead, tin, thallium, and zinc.

The decay was generally observed to be exponential in shape. Dramatic improvements in both the initial concentration and the later preservation of free atoms were observed for most elements by including hydrogen in the sheath gas flow. This was attributed to the efficacy of hydrogen in breaking up metal oxide species and in serving as a general scavenger of oxygen.

West and coworkers have briefly examined the decay of atomic populations with vertical height for several elements above their filament.<sup>139,173-176</sup> The intent here was principally to locate an optimum height above the filament for analyses of the element in question. However, a few specific matrix studies were also performed. Finally, Torsi and Tessari have studied vertical concentration profiles in the experimental testing of their theoretical models for the production and dissipation of atomic vapors from filament atomizers.<sup>177</sup> In all of these systems, the ability to examine populations was limited to the vertical dimension only. In addition, the instrumentation was not automated under computer control.

The use of electron microscopy to examine electrothermal atomizer appearances appears to be rather unprecedented, except for an occasional reference in which the technique was applied to the examination of a specific point of interest.<sup>62</sup>

## COMPUTER CONTROLLED INSTRUMENTATION

### A. INTRODUCTION

As has been previously mentioned, the nature of much of this investigation is such that extensive computer control of many aspects of the necessary instrumentation, including mechanical devices as well as traditional real time data acquisition, is all but indispensable. The monotonous, time consuming tasks of depositing samples, locating the atomization cell, and cycling the atomizer itself constitute a great potential source of procedural errors if done manually. In addition, manual execution is subject to inconsistencies in the timing of various portions of a complete instrumental cycle, even if the cycle itself is performed error free. A computer, however, is well suited to the repetitive performance of a defined task, and furthermore will do so from cycle to cycle with a consistency as rigid as the executing software and instrumentation under control will permit.

For achieving such computer control in the present work, three sophisticated devices were designed and constructed. The first is what is commonly referred to as the "positioner", which controls the movement of the atomization cell in two dimensions with respect to a fixed optical axis, for the purpose of scanning the array of space to be included in an atomic concentration profile.

The second is the "sampler" which, through computer control, automatically deposits samples of a specified size and source on the atomizer. The third is a dedicated, multifrequency real time clock and data acquisition system for on-line observation of signals produced during atomizations. These instruments will be discussed in the following sections in the order just listed.

## B. THE POSITIONER

### 1. General Introduction and Overview

To develop two dimensional profiles of atomic populations above an atomizer, it is necessary to have some means by which a systematic scan of the two dimensional space may be performed as samples of the solution under investigation are repetitively atomized. This requirement is met in the present work by locating the optical axis of an atomic absorption instrument at a fixed position in space. The atomization cell is then mounted on two stacked, optical translation stages driven by leadscrews, which permits the cell to be independently displaced vertically and horizontally with respect to the optical beam. The motive force for the leadscrews is supplied by two stepper motors, chosen because of the ability of a stepper motor to rotate through a precisely defined angle in either direction, as well as the inherently digital nature of such motion.<sup>178</sup>

To control the orderly movement of this mounted cell, an instrument known as the positioner was designed and constructed. The positioner is a self-contained device which independently moves the atomization cell in the vertical and horizontal directions under the guidance of internal logic sequencers. The instrument in general is built under the philosophy of providing computer triggered, but not software controlled functions. In other words, the computer has only to give the appropriate command and supply the proper data, and the positioner will then internally assume all responsibility for executing that command properly. No further interaction with the computer is required until the done flag is signalled. Thus, the device's own logic governs such functions as the distance and the direction of the cell movement. Operation is either computer controlled or manual, as selected by a front panel switch.

The positioner performs two basic cycles of operation, known as GO and RESET. When a GO command is received, the positioner moves the atomization cell to the vertical and horizontal destinations specified. When requested to RESET, the cell is moved steadily in a fixed direction until the moving stages encounter mechanical boundaries defined by miniature optointerrupters. The optointerrupter and a piece of metal are mounted on appropriate structural surfaces of the assembly so that as movement in that respective direction occurs, the metal piece

and optointerrupter either approach or recede from each other. When a RESET is requested, the cell is moved until the metal piece intercepts the beam of the interrupter, and when this occurs, that location of the cell in that dimension is defined as location 0. In this way, the positioner is capable of calibrating the absolute location of the cell at any time. (This feature is chiefly of importance when the positioner is first powered up, and has no knowledge of where the cell might be.)

Because the computer used with these studies is a twelve-bit machine, and is thus capable of directly representing decimal integers between 0 and 4095, it was decided that the complete segment of distance over which the cell could be moved in either dimension would be divided up into 4096 equally spaced locations, numbered sequentially from 0 to 4095, with location 0 being the position of the reset boundary. The convention selected for assigning these locations is shown in Figure 2. When the cell is so positioned that the optical beam is directly above and centered over the atomizer, (the condition known as "grazing incidence") the vertical dimension is at location 0 and the horizontal is at the midpoint, or location 2048. Movement away from the interrupter (towards locations of higher number) is defined as being positive motion.

The translation stages upon which the cell is mounted have a total displacement of approximately one inch, and

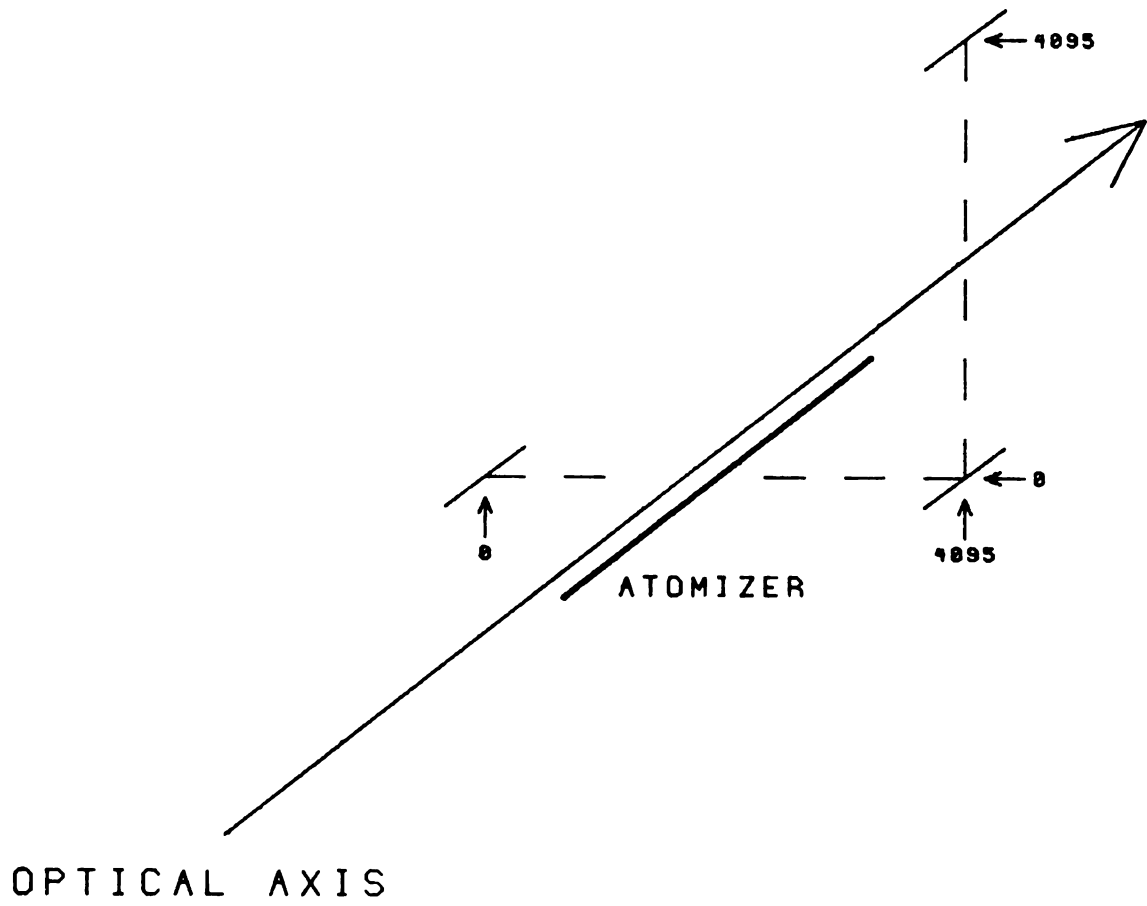


Figure 2. Assignment of atomizer cell locations.

are driven by forty-thread-per-inch leadscrews. The stepper motors turning the leadscrews take two hundred steps per revolution. Therefore, eight thousand motor steps are required to translate the cell one inch in the given dimension. With the highest location being numbered 4095, it was decided that adjacent locations would be two motor steps apart. Thus, the movement from one end of a dimension to the other requires 8192 motor steps, which results in a net actual displacement of 1.024 inch, and which permits a scan of an area slightly in excess of one square inch above and horizontally centered with respect to the atomizer itself.

Before discussing the detailed logic of the positioner, it would be helpful to gain some general insight into its operation with the aid of Figure 3, which illustrates in block form the basic interrelationships among the instrument's major register arrays, of which there are two identical such units, one for each motor.

When operated manually, the user enters the desired horizontal and vertical locations of the cell as numbers which range from 0 to 4095. The numerical locations are entered from separate, front panel, four decade thumb-wheel switch assemblies. These switches are coded in a BCD format. When a toggle switch is momentarily depressed to issue the GO command, these destinations are loaded into the sixteen-bit decimal register, after which

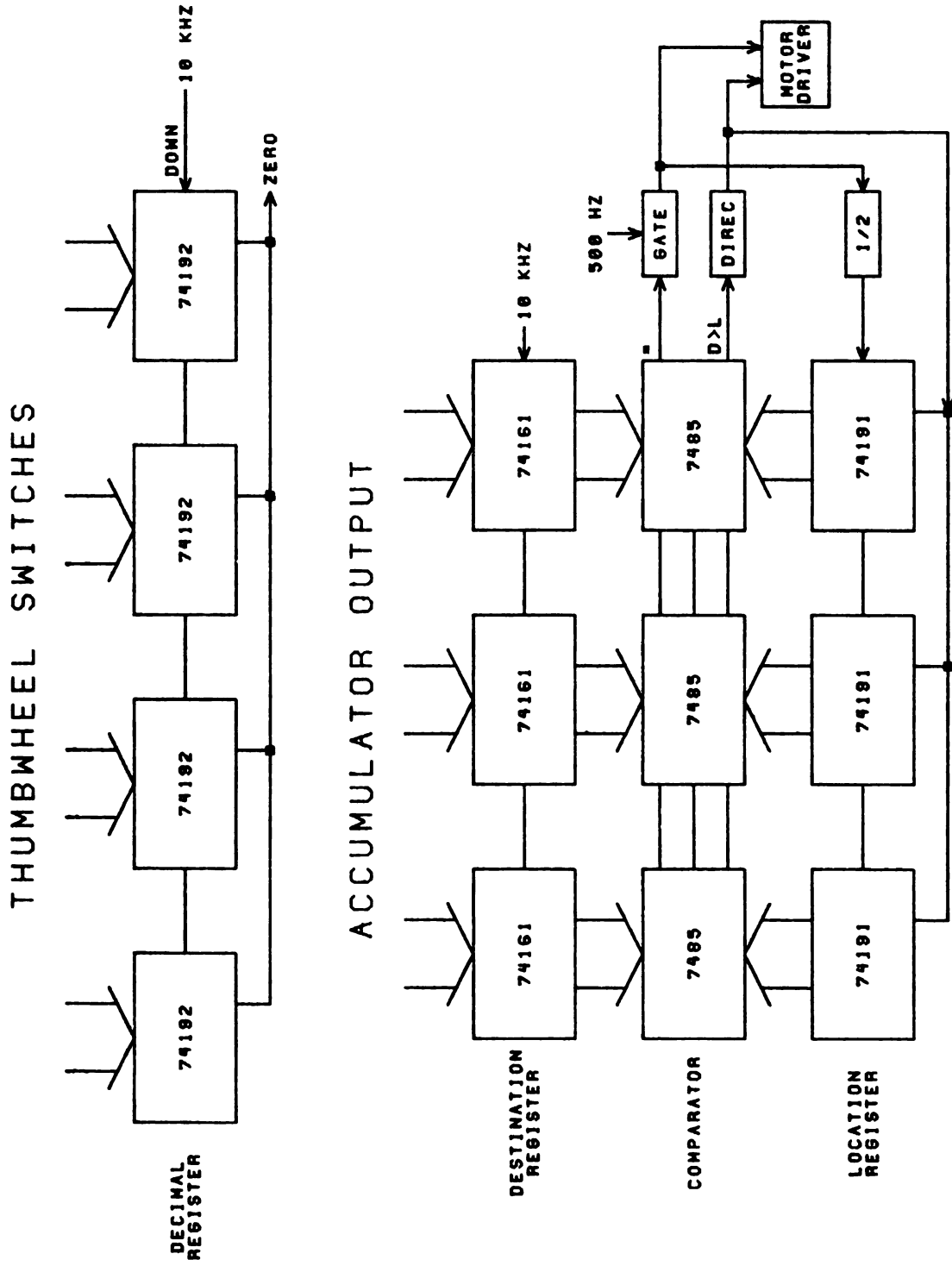


Figure 3. Block diagram of positioner control logic.

a BCD-to-binary conversion occurs by clearing the twelve-bit destination register, and then simultaneously decrementing the decimal and incrementing the destination registers until the former reaches zero. Should the user enter a value larger than 4095 from the thumbwheel switches, it is detected by the code-converting logic and causes the sequence to abort prior to motor movement, a condition known as "overflow". When operated from the computer, the destinations are loaded in binary format directly into the destination register.

The destination register is compared at all times through the use of cascaded four bit digital comparators with a third twelve-bit register, known as the location register, which contains at all times the actual location of the atomization cell. Once a valid destination has been either loaded or clocked into the destination register, the comparators detect whether or not this destination is different from the current location, and, if so, in what direction the new destination lies. The motors are then stepped toward this new destination, and, simultaneously, the location register is incremented or decremented at one half the motor stepping rate. This continues until the comparators once more detect a state of equality between the two registers. A final procedure designed to eliminate "lost" steps due to mechanical looseness in the translation stage leadscrews may then take place; it is described in detail in a subsequent section.

## 2. Sequence Structure and the Flow of States

The flow of logic in the positioner that executes all of the individual details of the two basic cycles in proper order is supervised by two identical, sophisticated, yet simple decision-making sequencers based on a design by C. L. Richards.<sup>179,180</sup> A basic understanding of the terminology and function of this sequencer, given in Appendix A, is essential in comprehending the details of the circuitry to follow.

The flow of states and functions involved in a GO cycle are illustrated in Figure 4. While idle, the sequencer holds in a wait loop formed by state 0, a condition indicated by a front panel "READY" LED. When a GO command is received, the overflow flag is cleared and the sequencer determines whether operation is under manual or computer control. If manual, a BCD-to-binary conversion of the destination is in order. The system checks for overflow, and if overflow is not present, it checks to see if the BCD-to-binary conversion is complete. If conversion is not complete, the two registers are clocked as previously described, and the checks for overflow and end of conversion are repeated. This cycle continues until conversion is complete, or until overflow occurs. Should overflow happen, the cycle is aborted with the overflow flag set, as shown by a front panel "OVERFLOW" LED. For legal destinations the end of the BCD-to-binary

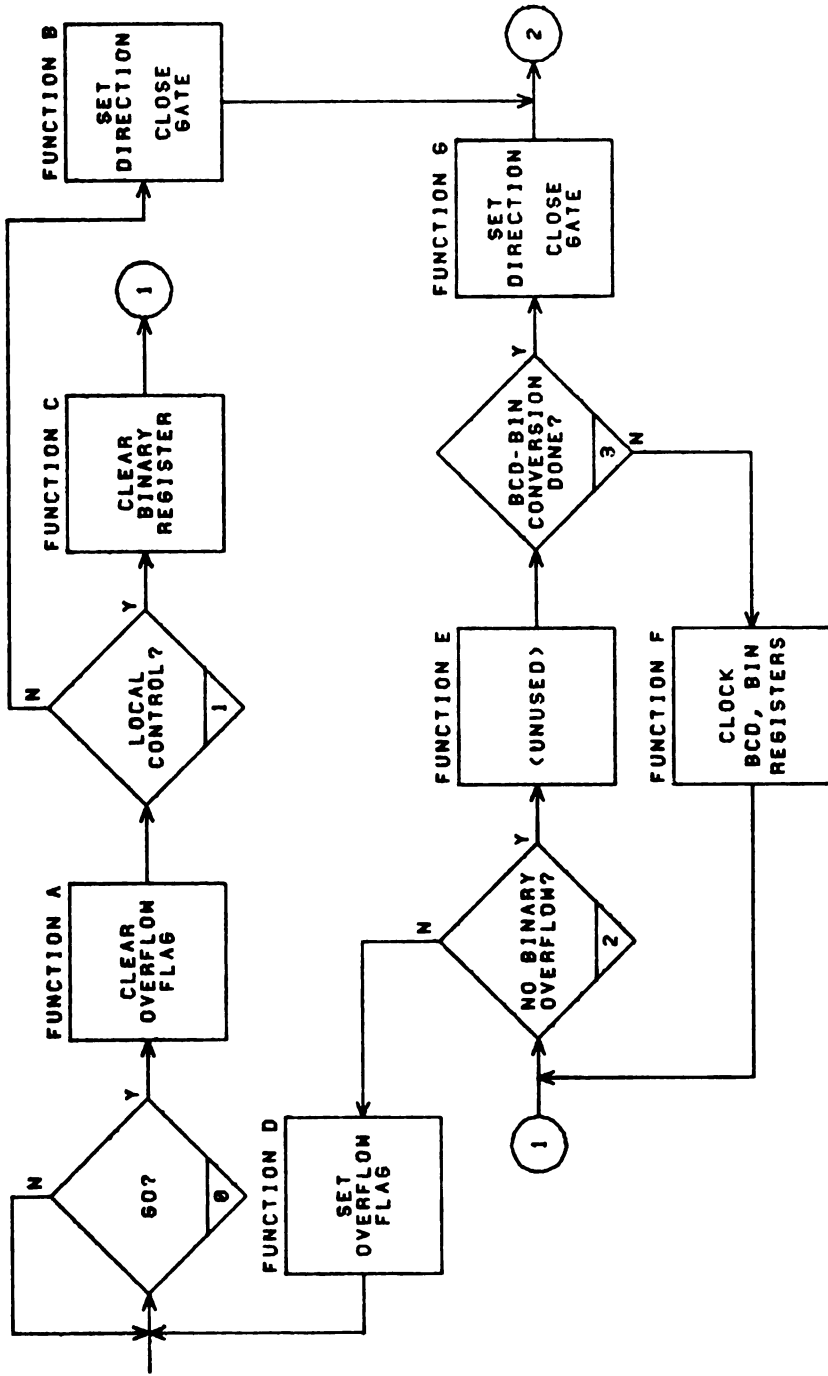


Figure 4. Flow of states and functions in a GO cycle.

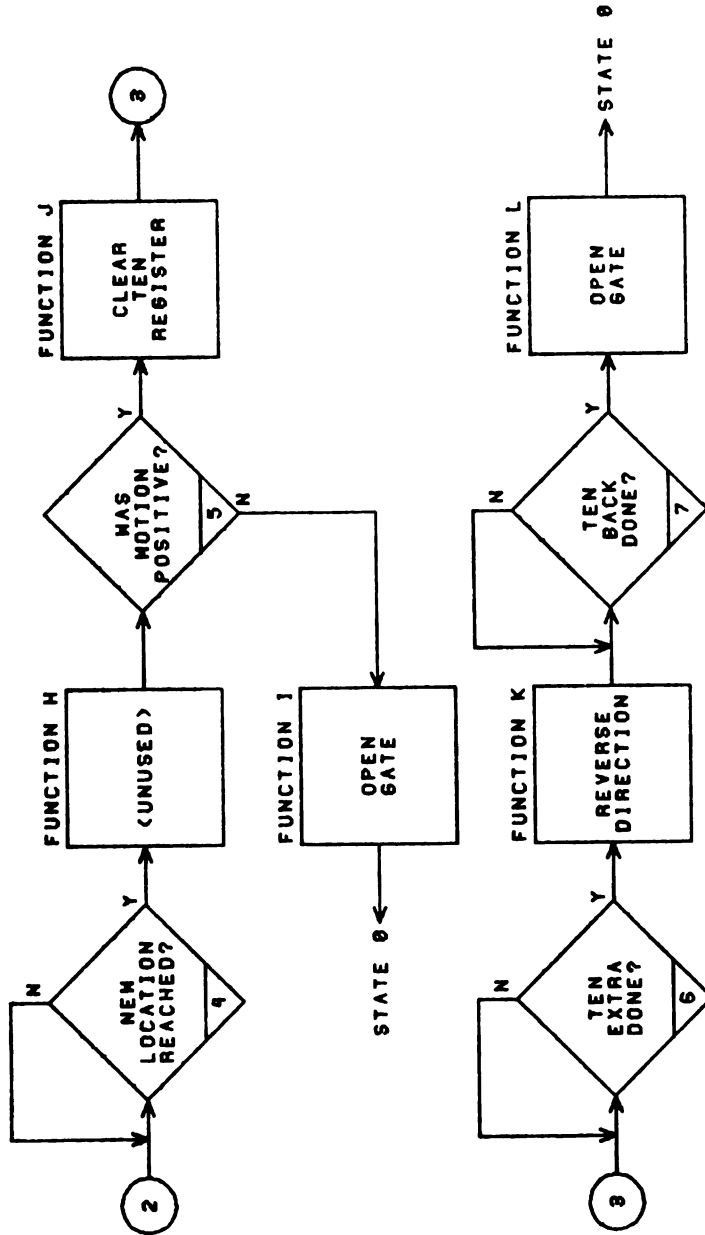


Figure 4. Continued.

conversion permits the sequence to advance beyond state three and start moving the motors in the direction indicated by the comparators. As previously mentioned, if the system is under computer control, no BCD-to-binary conversion is needed (and no overflow is possible). Thus, the sequence jumps directly from state one to state four and motor movement.

The motors move, and the location register is clocked until the new destination is reached. At that point, the sequencer reminds itself of whether the movement just performed was positive or negative. If negative, the GO cycle is complete, and the sequencer returns immediately to the state 0 wait loop with the READY LED lit once more. If motion was positive, however, the process of moving and counting locations continues upward ten extra locations beyond the nominal destination, at which point the motor direction and location register clocking are reversed, the ten extra locations are counted back, and the cycle concludes. In this manner, no matter whether the net movement was positive or negative, the cell is moved last in the negative direction, leaving the leadscrews tightly meshed in that direction of movement.

The flow of states and functions for a RESET cycle is basically that of an abbreviated GO cycle, as illustrated in Figure 5. The cycle begins in the same manner as a GO operation to a destination of zero would, except

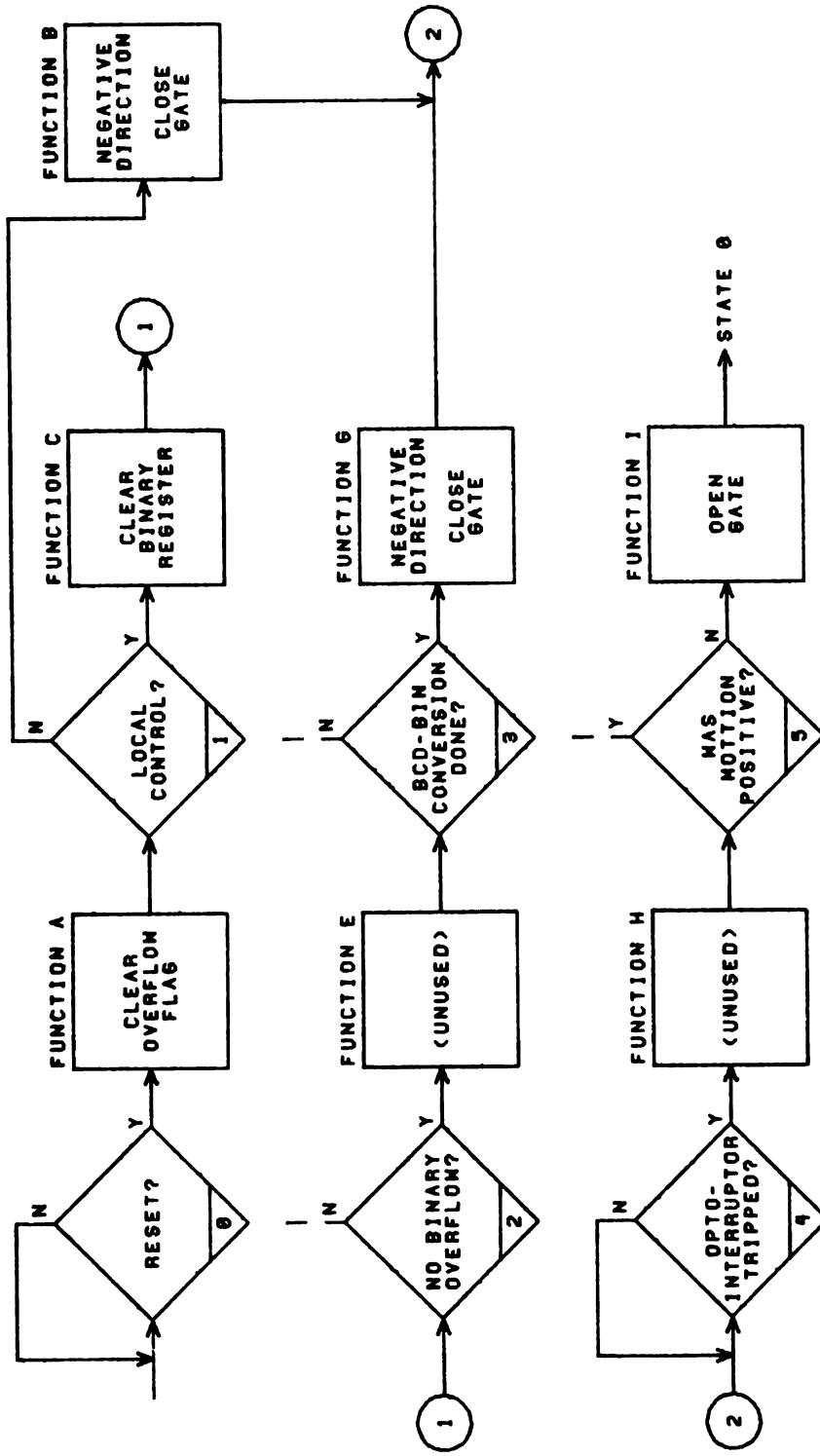


Figure 5. Flow of states and functions in a RESET cycle.

that the location register is cleared at the outset and held in the clear state throughout the cycle. If under manual operation, no BCD-to-binary conversion is needed nor is overflow possible, since by definition of RESET the destination is inherently zero. Thus, the branches of the cycle associated with these steps are missing as they will never be followed. Motor movement commences, and continues not until location zero is reached, but until the respective optointerrupter is tripped. At this point the cycle concludes with the location register defined equal to zero through its having been held clear. There is no possibility of positive motion overcounting, as again, the definition of a RESET automatically implies negative movement, so once more, this section of the flow is missing.

The specific implementation of a sequencer based on these cycles is shown in Figure 6. The structure of the sequencer is based squarely upon the suggested Richards design with the exception of the three gates which pass the state address lines to the function decoders. Addition of these gates was found necessary to assure that the total propagation delay involved in responding to a state change would be shorter for the multiplexer than for the decoders. Should the opposite be true, the possibility exists that false function pulses may be produced by the decoders until the multiplexer catches up with them.

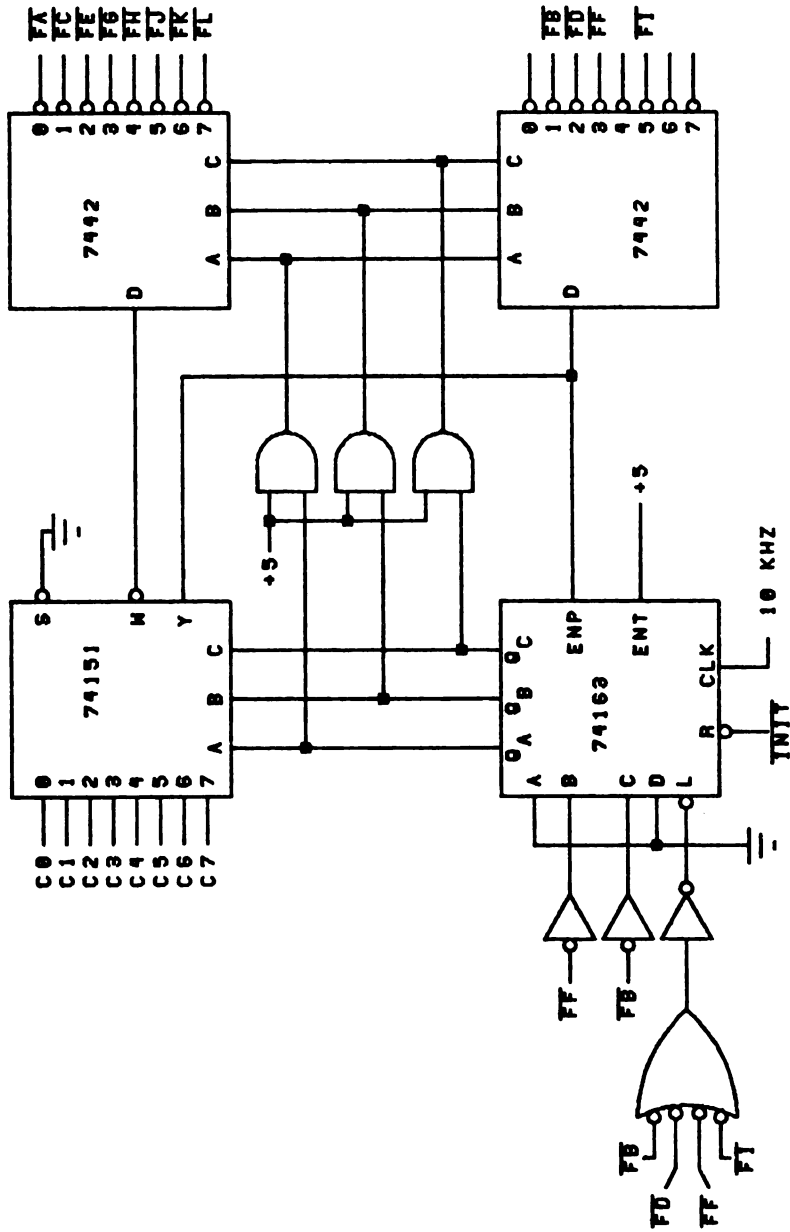


Figure 6. Schematic diagram of a sequencer.

(At the time, the preferred technique of solving this problem through use of, say, a Schottky multiplexer chip was not possible due to lack of the proper IC. The expedient solution shown here has thus survived in the present instrument.) Two identical such sequencers are present in the positioner, one for each motor. In fact, with the exception of the clock circuit discussed next, all circuitry of the following subheading, "Detailed Logic", is similarly duplicated in the instrument for each motor.

### 3. Detailed Logic

#### a. Dual Synchronous Clock Source

The instrument logic and motors are driven by a dual, synchronous clock source. This clock is shown in Figure 7 along with a representation of its output waveform. A base frequency of 10 kHz is supplied by a 555 timer configured for astable operation. This is divided to 10 KHz by two flipflops which are wired to toggle on opposite edges of the source. The output of one of these flops is used as the clock source for driving the logic sequencers. The output of the other flop is further divided by a factor of 20 to produce a frequency of 500 Hz, used for stepping the motors and clocking the location registers. (The remaining circuitry which acts as a gate upon the output of this 500 Hz clock is discussed later.)



The use of two flipflops to perform the first division of the source frequency, and the interwiring of these flops with each other's outputs and J-K inputs assures that the 10 KHz and 500 Hz clocks always bear the timing relationship to each other shown in the waveforms. When the instrument was first completed, the two clock frequencies were derived from separate, asynchronous 555 timers. This led to occasional anomolous instrumental behavior due, it is believed, to periodic, random synchronizing or near synchronizing of the clocks such that certain portions of circuitry required to respond at times to both clocks could not do so reliably. With the present clock, the relationship of the two frequencies is always rigid, and ample time between an edge of one and an edge of the other always exists for the satisfaction of propagation delays in the logic.

#### b. Sequence Initiation Circuitry

Circuitry involved in initiating the instrumental cycles is shown in Figure 8. The front panel switch, which selects manual or computer operation, controls a set of multiplexers which pass GO or RESET commands originating either from the computer or from debounced front panel switches. When given, either command from either source will cause the clearing of the READY flip-flop, which extinguishes the corresponding front panel

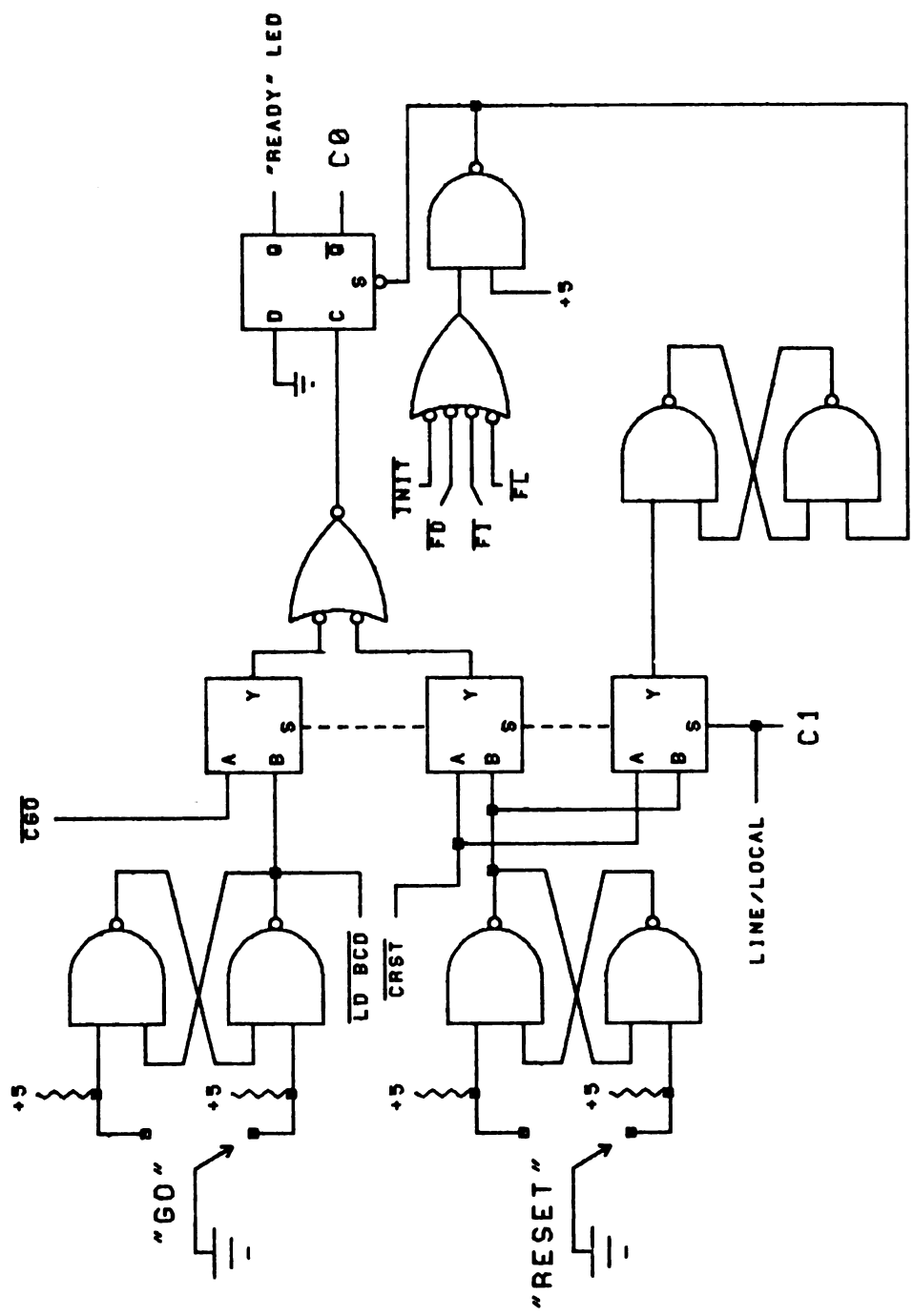


Figure 8. Schematic diagram of the sequence initiation circuitry.

LED and satisfies condition 0 of the logic sequence to begin the cycle. This flop may be reset to the ready state, indicating a completed or aborted cycle, by any of the sequence concluding function pulses or by the  $\overline{\text{INIT}}$  pulse. A second flipflop of the RS variety is used to distinguish the GO from the RESET command, being set by a RESET command and cleared by the same sources as the READY flop. The multiplexers' select line also serves as condition 1 to the sequencer.

The remaining three sections of logic to be discussed systematically follows the actions taken by the instrumental logic in executing the sequences.

#### c. Destination Preparation Circuitry

The first major task of the sequencer is to perform the BCD-to-binary conversion of the destination, should the positioner be under manual control. The circuitry associated with these steps of the sequence is illustrated in Figures 9 and 10, which show the decimal register, the OVERFLOW flipflop, and the actual wiring of the major registers shown previously in block form.

A manual GO command causes the loading of the destination from the thumbwheel switches by signal  $\overline{\text{LD}} \overline{\text{BCD}}$ . An example of one of the sixteen input lines to the decimal register is shown. The thumbwheel switches produce complementary BCD code. This is inverted and passed to

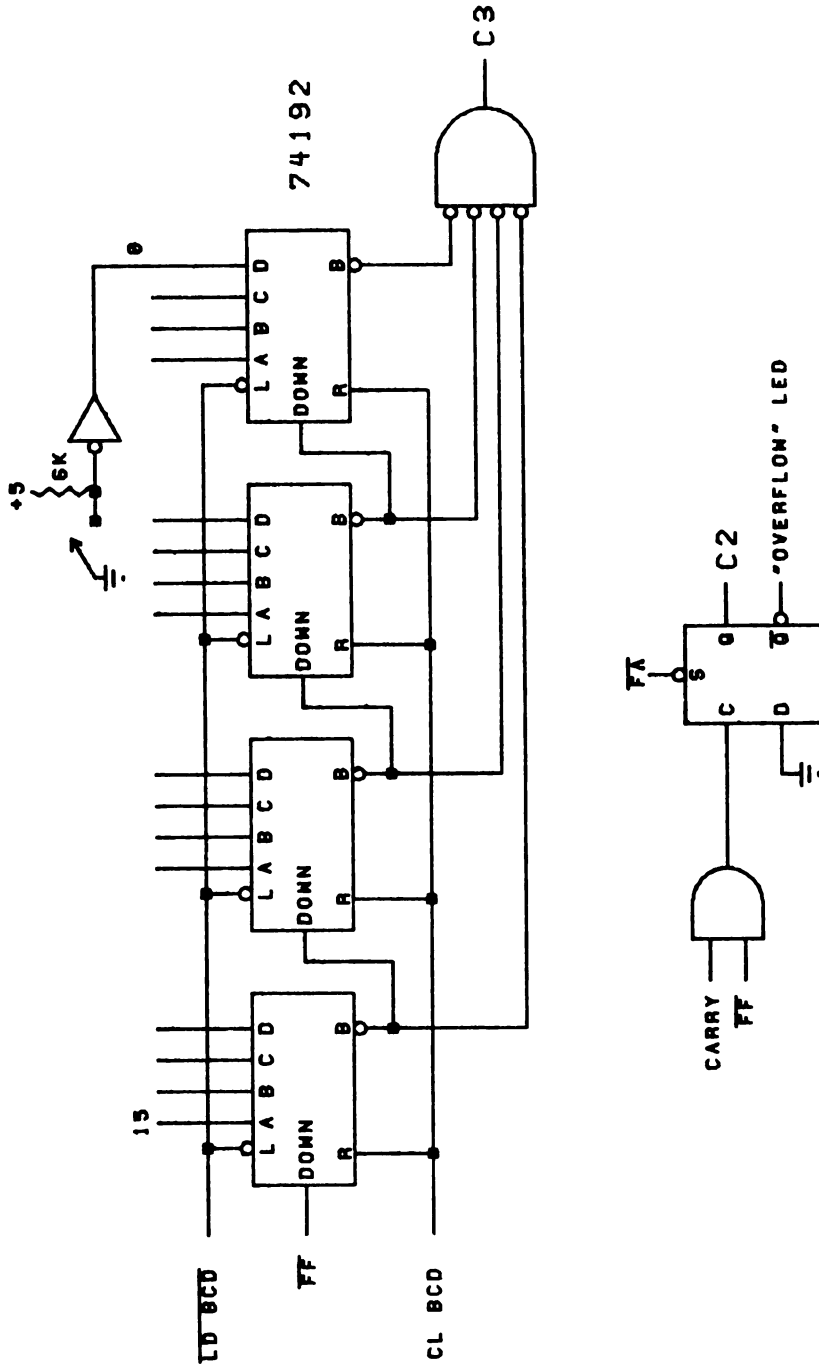


Figure 9. Schematic diagram of the decimal registers.

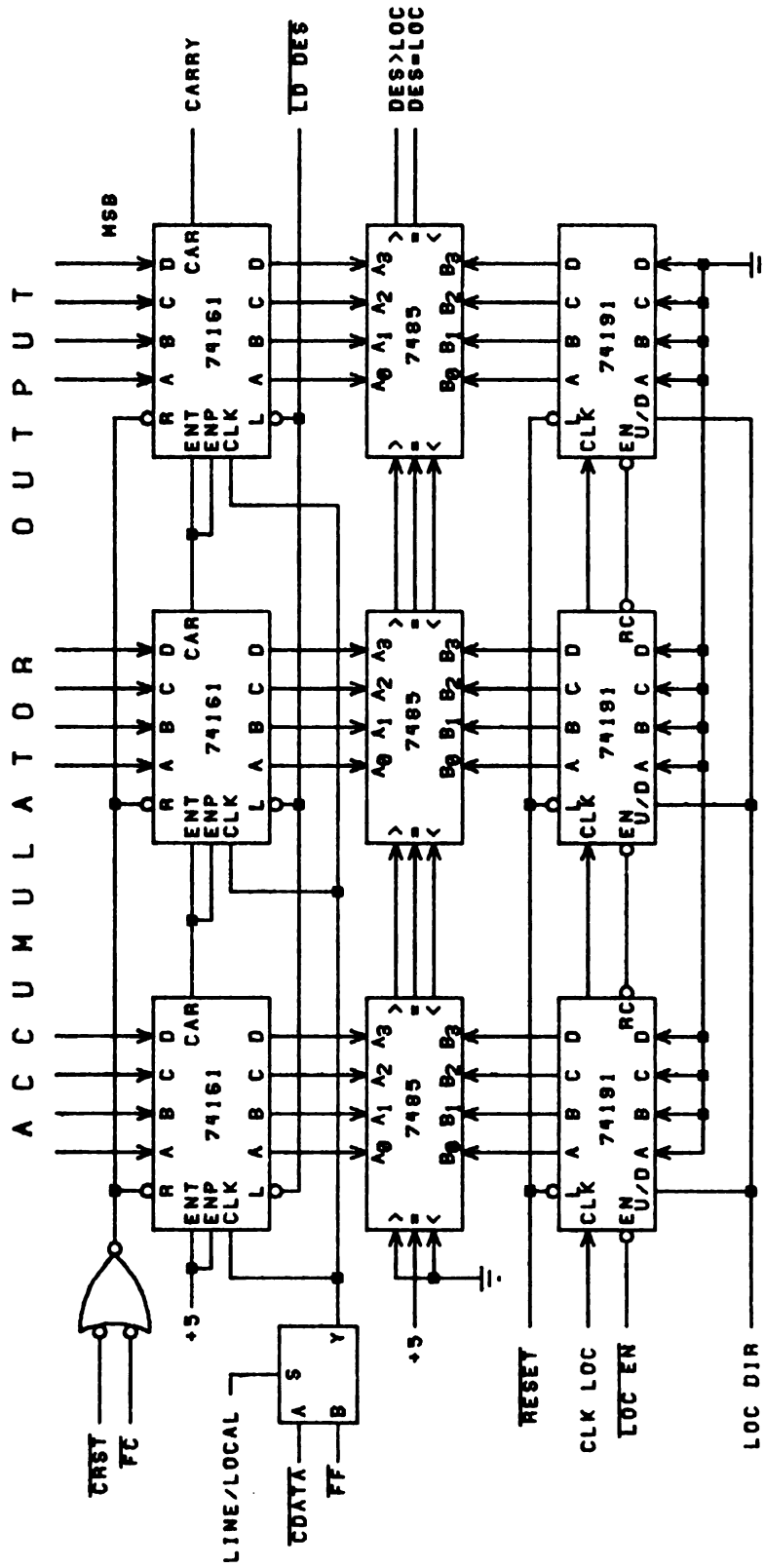


Figure 10. Schematic diagram of the principal positioner registers.

the register. The sequencer passes from state 0 to state 1, which generates pulse  $\overline{FA}$  and sets the OVERFLOW flip-flop. The test for manual operation is performed and, since at present manual operation is assumed, the test will be true, which causes pulse  $\overline{FC}$  to clear the destination register in preparation for the conversion of data. The test for absence of overflow takes place, and it will be initially true. Pulse  $\overline{FE}$  is generated, but not used anywhere. The test for complete conversion takes place next. The condition for complete conversion is derived from the NOR gate which monitors the  $\overline{BORROW}$  lines of the decimal register IC's. If the destination entered happened to be zero, the conversion would be "complete" since none is needed, and the logic would proceed to state 4. We will assume a nonzero destination however, so that conversion is not complete and condition 3 is false. Pulse  $\overline{FF}$  is then generated, thereby decrementing the decimal and incrementing the destination registers by one, and backing up the sequencer to state 2. The overflow test is performed again, followed by the conversion complete check, etc., until conversion is complete or overflow occurs.

An overflow is indicated by the destination register having reached 4095 with conversion still not complete. When the destination register reaches 4095, signal CARRY will be asserted, and if an additional  $\overline{FF}$  pulse occurs in an attempt to continue the conversion, these two

signals will together clear the OVERFLOW flipflop. The next test of condition 2 will then be false, and the cycle will abort through generation of pulse  $\overline{FD}$ , leaving the front panel OVERFLOW LED lit.

If conversion does complete itself at or before the assertion of CARRY however, the zero state of the decimal register will be sensed by the NOR gate already mentioned. Condition 3 is thus satisfied and the sequence is allowed to proceed.

The discussion has thus far assumed manual operation. If computer operation is in effect, the test for condition 1 will be false, and almost all elements of the sequence that deal with the above circuitry are skipped. Instead, prior to starting the sequence, the destination is loaded directly into the destination register with the signals  $\overline{LD}$   $\overline{DES}$  and CDATA (which are both required to defeat the synchronous loading characteristics of a 74161) after which the cycle is initiated by issuing  $\overline{CGO}$ . The actions of loading the destination and starting the sequence are separate under computer control, since the computer can supply destination data for only one dimension at a time. With manual operation, the loading and starting processes are simultaneous because of the separate thumb-wheel switch assemblies.

Most of the above circuitry is also unused if the given command is a RESET. A manual reset command asserts the signal CL BCD which puts a destination of zero in

the decimal register, satisfies the tests for no overflow and complete conversion in rapid succession as previously shown, and allows the sequence to proceed on to state 4. Similarly, a computer originated reset clears the destination register with signal  $\overline{\text{CRST}}$  (which unlike loading is an asynchronous event in a 74161) and proceeds directly from state 1 to state 4. Note that in the event of a reset sequence, the RESET RS flipflop asserts the signal RESET throughout the entire sequence, and, thus, holds the location register in the clear state.

#### d. Destination Seeking Circuitry

The next major section of circuitry is that which controls the movement of the motors in the proper direction to the desired destination and simultaneously clocks the location register. This circuitry is shown in Figures 11 and 12 and acts identically for either manual or computer controlled operation.

The gating of 500 Hz pulses into the motor driver and location register is governed by the RS flipflop formed by gates A and B. This flop is set by either  $\overline{\text{FB}}$  or  $\overline{\text{FG}}$ , the two pulses which advance the sequence into state 4 depending on the source of control. It is cleared by  $\overline{\text{INIT}}$  or either of the two pulses  $\overline{\text{FI}}$  and  $\overline{\text{FL}}$  which conclude a sequence after state 4. The JK flipflop accomplishes the task of clocking the location register at one half

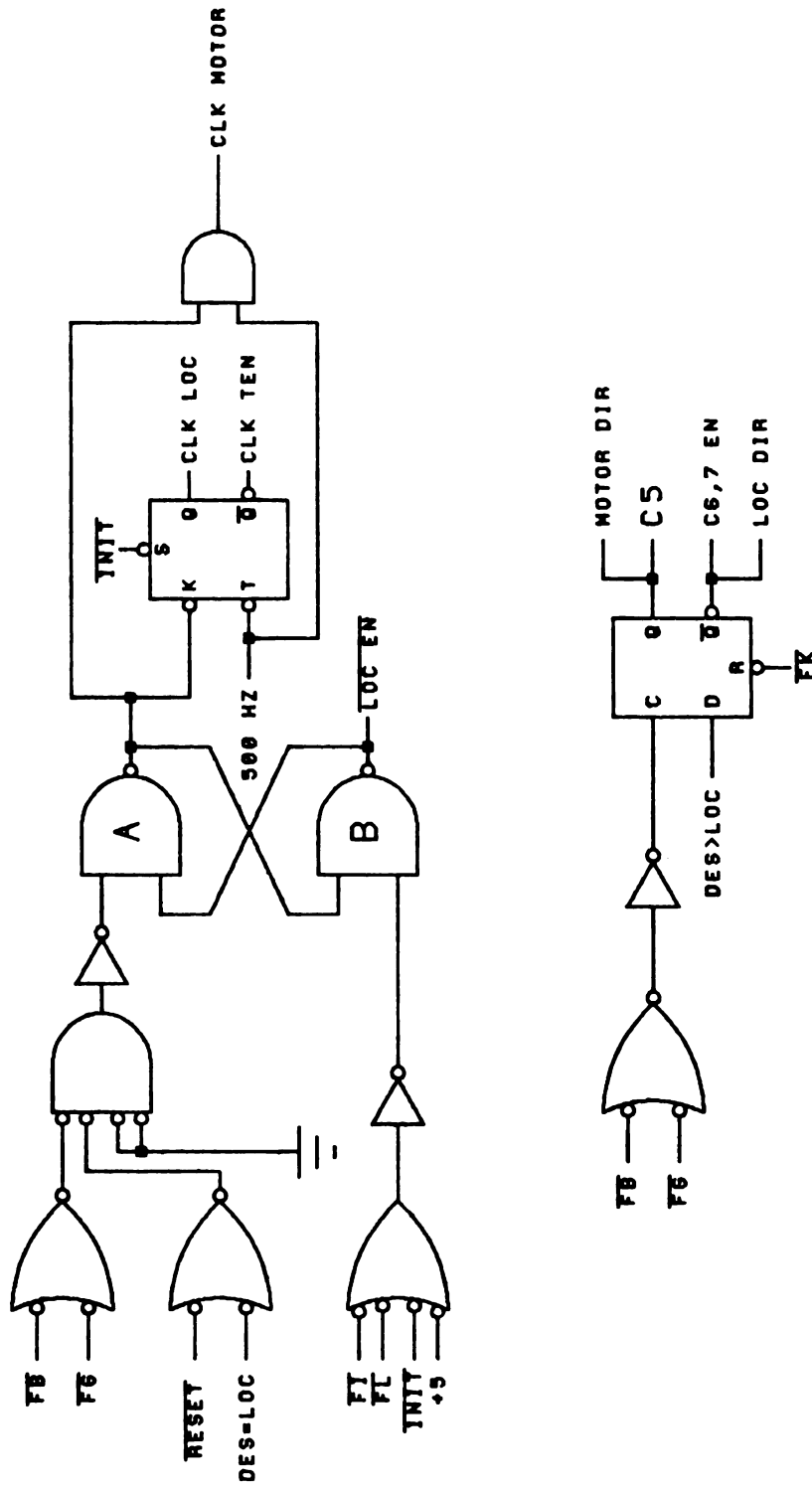


Figure 11. Schematic diagram of the gates and direction control circuitry.

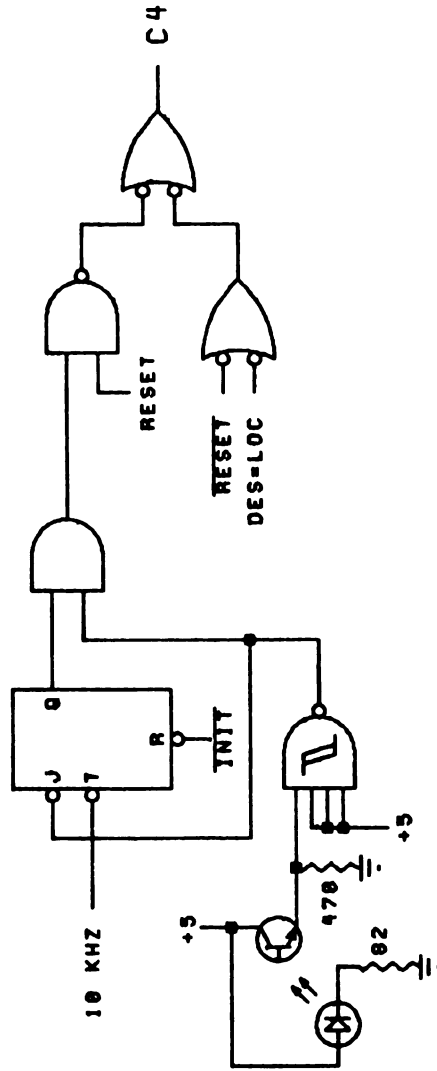


Figure 12. Schematic diagram of the condition 4 detect logic.

the motor stepping rate.

The direction of movement is indicated by the state of the signal  $DES > LOC$  produced by the cascaded comparators. If high or low, the same pulses which close the gate will set or clear, respectively, the direction flipflop, the complementary output of which controls the direction line on the location register.

The final section of circuitry shown in Figure 12 is a multiplexer for controlling the assertion of condition 4, which depends on whether the cycle in progress is a GO or a RESET.

To understand this circuitry, consider first a GO command. As state 4 is entered and motor movement is to begin, the pulse  $\overline{FB}$  or  $\overline{FG}$  closes the gate and properly prepares the state of the direction flipflop in light of signal  $DES > LOC$ . The action of the gate is very carefully designed to assure that the stepping of the motors and the clocking of the location register at half that rate is done without ambiguity. (The success of this precise operation depends in large measure on the rigid relationship between the two clocks, as previously discussed.) Until the gate closes, the location register is disabled by signal  $\overline{LOC} \overline{EN}$ , and the JK flipflop is in the set state by virtue of the low level at its K input. The fact that this flop is set assures that the clock line of the location register is high when idle, a condition

required by the 74191 IC if its clock direction line is to be unambiguously assigned, as is the case here. When the gate closes, the register is enabled, and the next 500 Hz falling edge toggles the flop and steps the motor. The next falling edge does the same, and in addition, through the flop, clocks the location register. Thus, the stepping of the motor and clocking of the register are in phase, and the divide by two process on the register clock line is conducted properly.

When eventually the gate opens again, the divide by two flipflop will have just toggled into the set state, and clocked the location register the final time, which causes the comparators to once more assert DES=LOC. This signal, in combination with  $\overline{\text{RESET}}$  (which in effect means GO), then satisfies condition 4 of the sequence. Pulse  $\overline{\text{FH}}$  is generated but not used, and the test for positive or negative motion is performed, with the output of the direction flipflop tested for condition 5. If the motion just performed was negative, condition 5 will be false, and pulse  $\overline{\text{FI}}$  will open the gate and conclude the sequence.

A special case occurs if the destination called for happens to be the location at which the cell already is. In such an instance, as state 4 is entered, the DES=LOC line will still be asserted, and the combination of that signal with  $\overline{\text{RESET}}$  will prevent  $\overline{\text{FB}}$  or  $\overline{\text{FG}}$  from closing the gate. Simultaneously, DES > LOC will be low, allowing  $\overline{\text{FB}}$  or  $\overline{\text{FG}}$  to put the direction flipflop into the clear

state, and causing the sequence to conclude with pulse  $\overline{FI}$ , thereby "arriving" at the new destination without having to move. This special case occurs quite often in actual use of the positioner, as one dimension is scanned while the other is held at a constant location.

In the event of a RESET command, the action of the gate is similar to that of a GO, except that the pulses which attempt to decrement the location register are disregarded, since that register is held clear from the outset during a reset cycle. The direction flipflop is inherently cleared, and the sequence always concludes with condition 5 false and pulse  $\overline{FI}$  generated. The one distinctive aspect of the reset cycle is in the circuitry used to control the assertion of condition 4. During a reset, satisfying condition 4 means tripping the opto-interrupter. When this occurs, the tripping of the interrupter is squared up by a Schmitt trigger. Then, because this tripping is independent of the sequencer, it is synchronized with the sequencer clock by a flipflop, and used in combination with signal RESET to assert condition 4.

#### e. Overcount Circuitry

The final circuitry of the sequencer is that which governs the correction for mechanical hysteresis by counting upward ten extra locations past the proper destination

and then back again whenever a positive motion GO command is executed. This circuitry performs identically under either manual or computer control, and is never used at all during RESET commands because of the inherently negative motion of a reset operation.

Figure 13 shows the logic involved. The ten register is a single decade counter clocked from the same flipflop that clocks the location register. While the motor is moving to its desired destination, this register counts redundantly and without effect. When the destination is reached however, and the test of condition 5 shows positive movement, the sequence does not conclude as before with pulse  $\overline{FI}$ . Instead, pulse  $\overline{FJ}$  is produced, which clears the ten register to zero and sets the D flipflop. Movement continues, and ten extra locations are counted. As the tenth extra location is reached, the ten register rolls over from a nine to a zero, causing the flop to load the state of the signal C6,7 EN. This signal, derived from the direction flipflop, will inherently be low at this time because of the positive motion, so the net effect is the clearing of the flop, and the satisfaction of condition 6. In response to this, the sequencer produces  $\overline{FK}$ , which clears the direction flipflop, and causes the motor movement and location counting to reverse. Another ten pulses are then counted as the cell returns to the proper destination, and at the end of the tenth pulse, the flop again loads C6,7 EN, which will now be

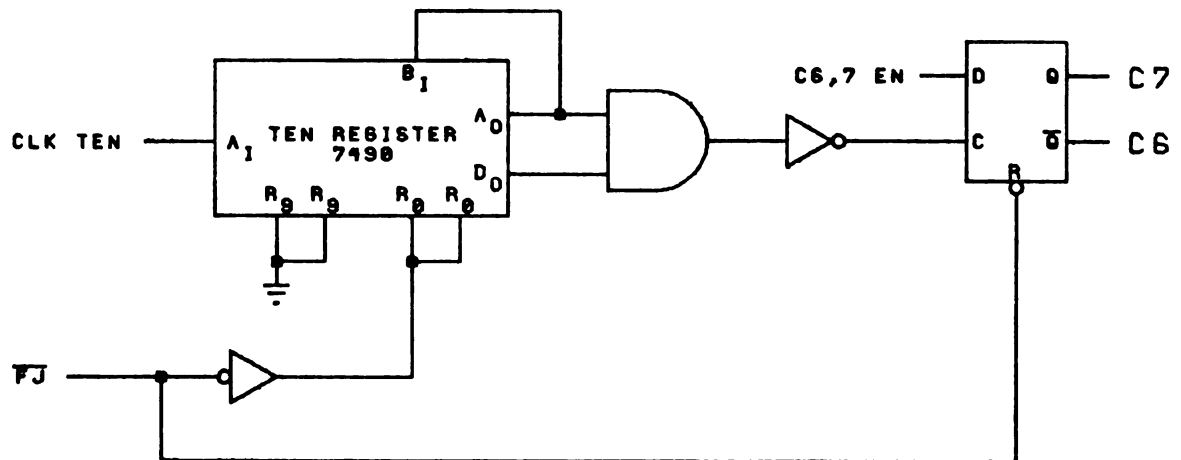


Figure 13. Schematic diagram of the overcount circuitry.

high. This causes condition 7 to be satisfied, and the sequence to conclude by assertion of pulse  $\overline{FL}$ .

There is one complication to this action. It was discovered when the positioner was first tested that the sudden reversal of motor movement during this correction sequence would not work at motor stepping speeds much in excess of 100 Hz, due to the inability of the motors to overcome their mechanical inertia of movement with such a sudden change. The net result was that the motors stuttered, and lost steps. However, because a stepping speed of 500 Hz was desired, it was decided to correct the problem by inserting a pause into the sequence before reversing direction, to allow the motors to truly stop before reversing. This pause is accomplished with the circuitry previously postponed from the discussion of the clock circuit of Figure 7.

Normally, flipflop A of Figure 7 is clear, which holds flipflop B and counter C in the clear state as well. Under these conditions, 500 Hz pulses are passed without interruption to the two sequencers. If, however, either sequencer should generate a  $\overline{FK}$ , which indicates that it is about to reverse direction in an overcount correction, that  $\overline{FK}$  will set flop A, and gate off the 500 Hz pulses to the motors. At the same time, flop B and counter C, acting together as a divide by 32 counter, will begin counting pulses of frequency 62.5 Hz. As the thirty second such pulse is counted, the falling edge at the

output of C returns flop A to the clear state, and gates on the 500 Hz pulses once more. The net effect is that assertion of a  $\overline{FK}$  pulse from either sequencer suspends the motor stepping pulses for about one half second; adequate time for the motor to dissipate its inertia and reverse without difficulty. Note that with the same clock line running both motors, it often happens that one sequencer, in calling for this half-second pause, stops the other motor from moving as well for no reason. The effect is harmless however, as the sequencers have no concern for how long it takes the system to reach a given destination; they will wait patiently in the proper state until the destination is indeed finally reached.

#### f. Motor Driving Circuitry

Figure 14 shows the circuitry used to control the stepper motor drivers. It is a full-wave, four-phase waveform generator of commercial origin.<sup>181</sup>

The schematic of the drivers themselves is illustrated in Figure 15, the set for each motor being composed of four identical units of the type illustrated. If the input signal to the diode is low, the current passed by the 1 k $\Omega$  resistor is sunk to ground through the diode by the low TTL output. The specific use of a germanium diode assures that the base of T1 is at a low enough voltage to hold T1 fully off. If the input signal is high, the diode

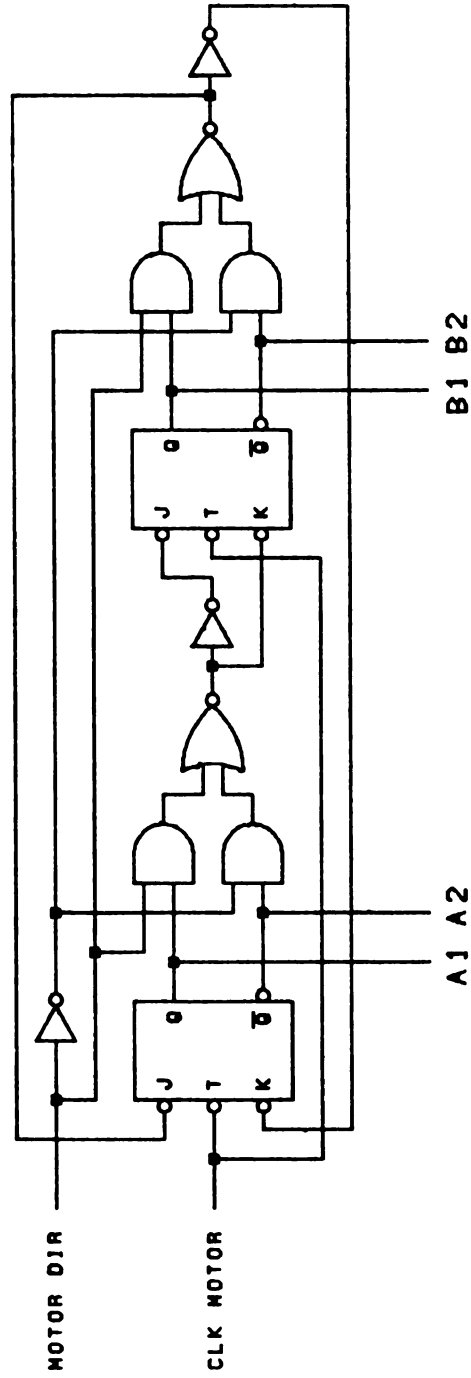


Figure 14. Schematic diagram of the stepper motor waveform generator.

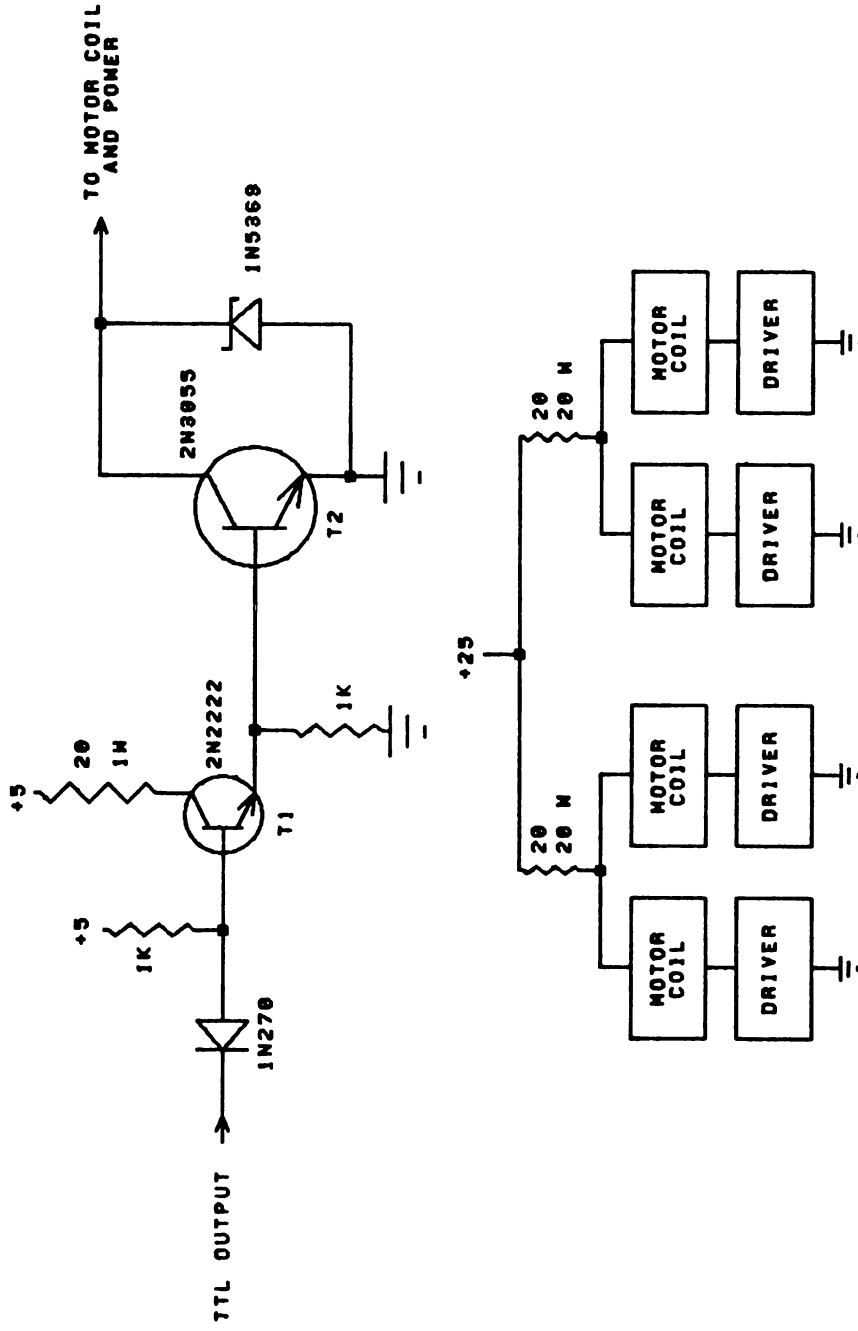


Figure 15. Schematic diagram of the stepper motor drivers.

is reverse biased and T1 is switched on. T1 forms the first stage of a Darlington pair. Its emitter current switches on the high power transistor T2, which passes current from the +25 volt supply through the motor coil and ballast resistor to ground. The value of the ballast resistor is that recommended by the manufacturer of the motors to provide the proper coil current of 1 A. (The other components of the circuit are such that T2 is driven into near saturation, able to conduct as much as 4 A if needed.) The zener diode on the collector of T2 serves to clip the peaks of inductive voltage spikes generated by the motor coils as they turn off. Without such clipping, these spikes could potentially damage T2 by exceeding its maximum collector-to-emitter voltage rating.

#### 4. Interface

The computer interface to the positioner need not be illustrated, as it is a rather simple circuit of the programmed I/O type very common for DEC 8/e computers using the KL8A Positive I/O Bus Interface.<sup>182</sup> It consists basically of the familiar circuitry used to interpret device codes and IOP pulses, coupled with an instrument flag which is set by the ANDed combination of the READY signals from both sequencers, and cleared by the start of a new sequencer cycle or by a separate command. This flag is usually checked by computer software

on a skip test basis, but provision is present for an interrupt driven facility as well. The complete command set of the interface is given in Table 1, along with the names of the digital signals they represent. In addition to these signals, a signal representing device code 34 is also decoded and passed to the sequencers to serve as signal CDATA, previously mentioned in the discussion of the sequencer logic as necessary to defeat the synchronous loading of a 74161 IC. The device codes selected for the positioner are arbitrary, and were chosen at the time of construction so as not to interfere with any other known peripherals. Alteration of the codes is easily accomplished if desired by the relocating of jumper wires on the interface circuit board, with the restriction that all three codes must share the same more significant octal digit.

The interface is also the source of the signal  $\overline{\text{INIT}}$ , frequently seen in the schematics of the sequencer logic. This signal is composed of a ORed combination of the computer's  $\overline{\text{INIT}}$  line with a local initialize pulse which is generated by the positioner interface logic at power-up time.

Table 1. Command Set for Positioner Interface

6341	Load AC into destination register of horizontal dimension sequencer ( $\overline{\text{LD}}$ $\overline{\text{DES}}$ )
6342	Load AC into destination register of vertical dimension sequencer ( $\overline{\text{LD}}$ $\overline{\text{DES}}$ )
6344	Reserved for future use
6351	RESET ( $\overline{\text{CRST}}$ )
6352	GO ( $\overline{\text{CGO}}$ )
6354	Skip on Flag
6361	Clear Flag
6362	Enable interrupt facility from positioner
6364	Disable interrupt facility from positioner

## 5. Power Supplies and Physical Structure

The entire instrument is housed within a commercially produced enclosure. Power for the device is provided by separate +5 and +25 V supplies. The +5 V regulated supply used to power the digital logic is of original, but highly conventional design, and need not be illustrated in detail. It is based upon the familiar 723 IC voltage regulator, employing two parallel, external pass transistors, and is capable of delivering in excess of 6 A of current. The +25 V supply, used for the stepper motors, is a very basic, filtered but unregulated DC supply capable of delivering 12 A. As presently constructed, the existing circuitry consumes approximately 67 and 33 percent, respectively of the ratings of these supplies. Adequate cooling of such parts as the +5 V supply pass transistors or the motor ballast resistors is assured by the presence of a blower fan.

The bulk of the instrumental circuitry is assembled on six printed circuit boards. Two of these contain the digital logic of the two sequencers. These boards are of commercial origin, with provisions for thirty six chips, and accompanying power and ground buses. The chips are socket mounted and interconnected with wire wrap technology. Two additional boards of original design and layout contain the components of the associated stepper motor drivers. The final two boards contain the

circuitry of the clock sources and the computer interface. They are also of original layout and design and employ wire wrapping for signal connections. These six boards stand vertically in a horizontal row within the instrument and are inserted into standard edge connectors which are mounted in a printed circuit backplane board which lies along the bottom of the chassis and serves as a signal bus for all necessary interconnections among the six boards. A final printed circuit board is located at the front panel, and contains the inverters associated with the thumbwheel switches as well as TTL drivers for the front panel LED's. Connections of this board with the bus board are made with simple cable bundles, with the exception of the data from the thumbwheel switches, which is passed to the appropriate sequencer logic board directly through use of bundled wires terminated by an IC header cap which inserts into one of the IC sockets on the logic board. Connection of the computer interface terminal to the positioner is made via a ribbon cable patch which inserts into an edge connector in the rear of the chassis. Similarly, three multiple conductor cables leaving the rear of the instrument serve to make electrical connection to the horizontal motor, vertical motor, and optointerrupters, respectively.

There is sufficient physical room on the front panel and signal bus for the addition of a complete, third sequencer and driver should future applications of the

instrument require a third motor. Similarly, the computer interface is already configured to recognize a third motor, and the power supplies have ample reserve capacity to handle a third load.

## 6. Testing and Performance

Most of the initial work involved in testing the positioner consisted of the inevitable task of debugging the digital logic. (Indeed, the schematic diagrams of the sequencer logic given in the figures are, in some cases quite different from their original design concepts.) This work was done with oscilloscopes and test probes and with one very advantageous technique involving the sequencer clocks. Many individual problems in the logic, particularly the verification of correct action of the gate and overcount circuitry, were solved by using an external clock source running at only a few Hz. This slow source enabled the individual states of the sequencer to be followed with test probes, as well as permitting a direct count of pulses received by the stepper motors at critical stages of a sequence by simply holding the motor shaft and feeling the pulses one by one. So useful was this external clock in proving out the instrument that provisions for using it have been kept in the final device: the output of the 555 timer that provides the basic clock frequency is passed to the remaining circuitry via a long, looping jumper wire which stands off the clock

circuit board. By removing the timer chip and connecting an external TTL source to the loop, the sequencer and motors can be run at one half and one fortieth, respectively, of most any reasonable frequency desired.

Of more direct concern to the intended use of the positioner was an examination of the optointerrupter reset. If the optointerrupter is to serve as the absolute calibrator of location zero, then it must act in a highly reproducible manner. That is, the exact instant at which the interrupt occurs must always happen with interrupter and metal occluder at precisely the same consistent orientation with respect to each other.

To test the quality of this action, the following experiment was conducted. An events counter was temporarily connected to the sequencer signal CLK MOTOR, so that the counter could register the total number of pulses sent to the motor during a given instrument cycle. The cell was then displaced to a known location. Finally, a reset was commanded, and during the reset operation, the number of pulses sent to the motor was counted. If the optointerrupter defines location zero consistently, then the number of pulses required to reach the reset point should always be simply twice the value of the location from which the reset was performed. Repetitive counts were taken for both motors from locations 1000, 2000, 3000, and 4000, thus covering the total range of displacement. The results are shown in Tables 2 and 3.



Table 3. Precision of Location of the Reset Point -  
Horizontal Number of Counts Accumulated

From Location 1000	From Location 2000
2001	4001
2001	4001
2001	4001
2001	4001
2001	4001
2001	4001
2001	4001
2001	4001
2001	4001
2002	4001
2001	4001
From Location 3000	From Location 4000
6001	8001
6001	8001
6001	8001
6001	8001
5999	8001
6001	7999
6001	8001
6001	8001
6001	8001
6001	8001

The results are amazingly precise. No deviation is seen at all for the vertical motor at any location, any slight errors being rounded off by the inherently quantized motion of the cell. (The consistent extra count arises from an inherent gating artifact in the events counter.) Only a few scattered, minor deviations are seen for the horizontal motor, (due perhaps to the fact that the horizontal motor must move not only the cell but the vertical motor and its stage and support as well) but even here the deviations are not significant with respect to this work. Eight motor steps are required to displace the cell one milliinch. Conservatively rated, the location of the reset points is equally as good. But one milliinch is far more precise than the atomic absorption work performed here. The resolution of the optics alone is at least an order of magnitude larger, and even if the resolution of the optics matched that of the cell location, it is doubtful whether transients of atomic vapor violently ejected from a hot atomizer into a gently flowing stream of sheath gas would be equally as precise. It may be concluded therefore, that the calibration of the cell by the reset operation is as good as the mechanical rigidity with which the translation stages and optointerrupters are assembled.

## 7. Operating Software

The basic package of three assembly language sub-routines are employed to operate the positioner. These routines were written and are maintained by Mr. Eugene Pals, to whose thesis the reader is directed for details of their operation. A short commentary on the use of these routines will be given here for completeness of the instrumental discussion.

The first routine receives two arguments from the calling routine which represent the desired horizontal and vertical destinations of the cell. These destinations are entered in units of millimeters to the calling routine by the user, with 0.0 mm vertical being at grazing incidence, and 0.0 mm horizontal being centered. In these units the vertical locations may range between 0.0 and 26.0 mm above the braid, and the horizontal locations may vary out to  $\pm 12.7$  mm on either side of the braid. When passed to the assembler subroutines, the necessary conversion from millimeters to twelve bit format is performed. The positioner flag is cleared, after which the arguments are converted into machine code and sent out successively to the horizontal and vertical destination registers. In conclusion, the cycle command GO is issued. The second routine clears the flag and issues the cycle command RESET. The final routine performs a skip test of the positioner flag. With these three routines the

full scope of positioner operations can be accessed, with the exception of the interrupt facility, which is not presently in use. The divorcing of the skip test from the cycle commands is particularly convenient in that it permits the computer to start the positioner on a task and then direct its attention elsewhere, only returning to check the positioner flag when truly necessary.

### C. THE AUTOSAMPLER

#### 1. History and Introduction

One of the principal reasons for constructing the positioner was to provide a sophisticated instrument that would relieve the user of all responsibility for correctly placing and translating the atomization cell. Indeed, the general goal was to achieve this degree of independence in the entire AA system. Ideally, once the user had specified to the computer the tasks to be performed, the instrumentation would automatically take care of executing them without the need for further user intervention; the system would be able to run itself for hours on end. In order to truly reach this goal, it was necessary to have along with the positioner a companion instrument to perform a mechanical task even more mundane and common than locating the atomization cell: namely, the deposition of samples. There is considerable precedent in these

laboratories for the construction and use of automatic samplers. Two such devices have in fact been employed with the graphite braid.<sup>183,184</sup>

The first autosampler was a simple device designed to deliver repetitively a fixed amount of a single sample. This was accomplished by forcing the sample in question out of a delivery tip manufactured from a metallic syringe needle. This needle was mounted in an aluminum arm, which in turn was mounted in a pivot on a main chassis. At the time of sample deposition, the arm and needle were pivoted forward through an angle of 90 degrees by a small pneumatic cylinder, thereby bringing the tip of the needle to the top edge of the braid. As the tip reached the braid, a microswitch would be tripped by the moving arm that would engage a motor and cams combination, which would then dispense the sample by momentarily compressing a short length of the tygon tubing through which sample was drawn from the source cup. The cams were used not only to compress the tubing, but also to block reverse flow, so that the sample would be forced out of the needle onto the braid. Upon concluding this action, the pneumatic cylinder would release, and the arm would return to its rest position.

The precision of this sampler was quite acceptable, about 2-3%. It had the advantages of a reasonably small physical size and rapid sampling rate; the entire sampling operation took about five seconds. For repetitive sampling,

it was in fact fairly servicable. However, it lacked many features of a truly versatile automatic sampler. The sample size was variable from about one-half to five microliters (by controlling how much tubing was compressed by the cam), but it was not computer controllable, being governed instead by a manual screw assembly. The source of the sample was fixed by what the network of tubing happened to contain at the moment, and changing the sample was very tedious, as it involved continuously pumping old sample through the tip five microliters at a time until the system was drained, and then following this up with more pumping of first rinse water and then new sample solution. Because of the fairly large dead volume of tubing involved, this process could take as much as a half hour. The need for both electrical and pneumatic power was inconvenient, and the metal delivery tip was prone to often severe scavenging of solutions through electrochemical deposition of the trace metals present.

Many of the limitations of the first autosampler were recognized soon after its completion and a second device was constructed to attempt to overcome them. The new autosampler retained the concept of pivoting an arm and delivery system through 90 degrees with a pneumatic cylinder at the time of sample deposition, but the sampling device itself was changed to a stepper motor driven micrometer syringe mounted in a housing which could be finely translated and rotated with screw adjustments to

allow precise positioning of the delivery tip over the graphite braid. A rotating sample turret driven by a DC motor was provided which contained room for as many as six sample cups. The pneumatic cylinder which pivoted the arm and syringe forward was accompanied by an additional cylinder which could rotate the arm about 45 degrees horizontally so that the syringe, when thus rotated, could address either the atomizer or the sample turret. Operation of the device was controlled by an ingeniously constructed series of cams turned by slow speed appliance motors. Upon receiving the command to deposit a sample, one such series of cams would be turned through a complete revolution, bearing upon a series of microswitches that would automatically sequence the pneumatic cylinders properly to pivot the syringe to the braid, wait for sample deposition, and then return. Similar cam systems could, upon receipt of a single command, move the syringe over to the sample turret and refill it, or even perform a discarding of old sample and double rinsing of the syringe assuming that one sample cup would be reserved for waste and another for deionized water.

This sampler was a great improvement over the previous one in that it provided computer-selectable sample size and sample source, and employed a delivery system of greater potential resolution which could be cleaned or changed more readily and had far less dead volume. The precision of delivery was again on the order of a

few percent. Unfortunately, these advantages were gained at some cost. The size of the sampler was tremendously increased. It literally enveloped the old atomization cell used with it, and was inherently physically incompatible with the new positionable cell. The requirement of pneumatic power was still present, as was the use of a metal needle on the syringe. The new device was ponderously slow. The intricate cams which could automatically execute the complicated mechanical sequences had no extensive means of detecting the completion of various stages of the cycles, and thus had to operate on a basis of allowing generous times for the completion of individual steps. The time for sample deposition was on the order of thirty seconds, and the more complicated refilling or purging operations required times on the order of minutes. Finally, certain desirable automatic features were missing; for example, the computer had to provide the pulse train of proper length and frequency to step the syringe motor instead of having this task done externally.

Thus, neither sampler was truly acceptable as a general purpose device. It was therefore decided to construct a third system which would combine as best as possible the small size and rapidity of the first sampler with the versatility of the second, and place it all under the control of a sophisticated external controller.

## 2. Device Description

The basic principles of the new sampler's construction may be most easily conveyed with the assistance of the photographs on the following pages. The main framework of the device consists of a small baseplate bolted to the spectrometer optical rail behind the atomization cell which, with the aid of triangular braces, supports two bar shaped vertical members. These members resemble a block letter U in cross section, and are oriented so that the "U's" face each other, thereby forming a vertical channel. Located in this channel and able to move up and down in it is a metal plate, to the rear of which is bolted a large stepper motor. The shaft of this motor protrudes through the plate and is fitted with a  $\frac{1}{2}$ " gear. This gear bears against the larger member of a  $2\frac{1}{2}$ "- $\frac{1}{2}$ " combination gear, the smaller member of which in turn bears against a length of rack bolted to the right hand vertical bar. Thus, by rotating the stepper motor, the motor, plate, and anything secured to the plate will ride up and down in the vertical track. The gears provide a fivefold mechanical torque advantage for the lifting of considerable weight. The plate is lined with strips of teflon along those edges which contact the vertical bars to minimize friction when moving.

On top of the vertically moving plate is secured another, horizontally oriented plate. Under the rear

half of this plate is mounted a second, smaller stepper motor, having a protruding shaft and  $\frac{1}{2}$ " gear similar to the first. This gear bears against a single  $2\frac{1}{2}$ " gear which is mounted on a teflon disc centered directly over the vertical plate, and fitted with a shaft and bearing so that rotation of the small stepper motor will cause the large gear and anything secured to it to also rotate in the horizontal plane. To this gear is affixed an open, rectangular, box-shaped structure, upon one end of which is bolted the stepper motor driven syringe assembly. This syringe was salvaged virtually intact from the older autosampler previously described. It consists of a 200  $\mu$ l micrometer syringe driven by a 200 step per revolution motor. One revolution of the micrometer will dispense or draw 10.0  $\mu$ l of solution, thus giving a theoretical resolution of 0.05  $\mu$ l per step. The structures in which this syringe is mounted include screw driven fine positioning adjustments which allow the precise locating of the delivery tip in both the X and Y dimensions, defining the Z dimension as vertical.

Associated with the main unit is a second, physically separate piece which serves as the source of samples. It consists basically of a flat metal disc with sixteen equally spaced holes around its outer perimeter. These holes are of proper size to accommodate 2 ml disposable Autoanalyzer sample cups. This disc is mounted with a

shaft and bearings to a simple framework chassis. Also mounted on the shaft is a third  $2\frac{1}{2}$ " gear, which again is turned by a stepper motor and  $\frac{1}{2}$ " gear combination. The motor used here is small, owing to the minimal torque requirements.

The four photographs illustrate the basic movements performed by the sampler when in operation. The usual rest position of the device is shown in Figure 16, with the moving assemblies located at the top of the vertical track. Figure 17 illustrates the position taken during sampling. When the commands to deposit a sample on the braid are received, the large motor (vertical motor) lowers the entire assembly to the braid. Upon arriving, the syringe dispenses the sample, after which the vertical motor returns the apparatus to the top of the track, out of the way of the atomization cell and optics.

If replenishing or changing the contents of the syringe is necessary, the syringe must be moved over to address the sample turret. The first step in this process is shown in Figure 18, in which the small motor (rotation motor) has rotated the box structure and syringe assembly 90 degrees counter-clockwise so that the delivery tip is now over the sample turret instead of the braid. Finally, Figure 19 shows the assembly lowered by the vertical motor to the turret. Notice how the open structure of the rectangular box permits the principal vertical members to pass actually through the box as the assembly

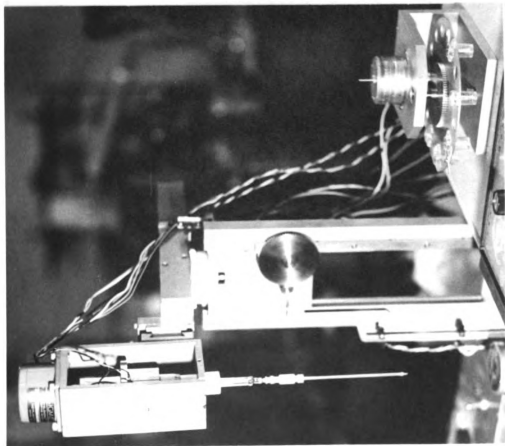


Figure 16. Normal rest position of the autosampler.

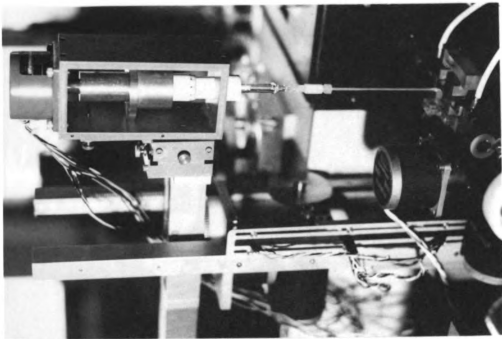


Figure 17. Sample depositing position of the autosampler.

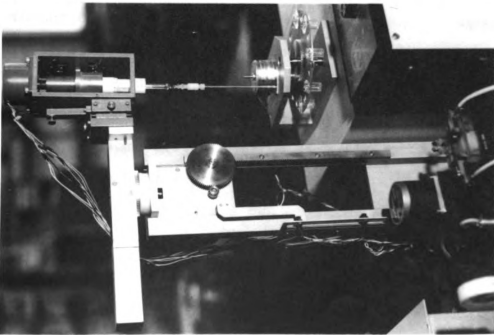


Figure 18. Turret addressing position of the autosampler.

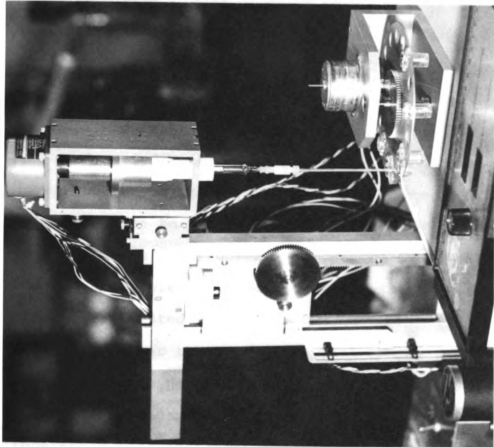


Figure 19. Sample filling or emptying position of the autosampler.

is lowered.

The proper places at which each motor is to stop moving are indicated by optointerrupters identical to those used in constructing the translatable atomization cell. Three such devices define the locations of "top", "braid", and "turret" to the vertical motor; two of them are used to indicate "left" (over the braid) and "right" (over the turret) to the rotation motor; and a single device is used to indicate sample cup "zero" to the sample turret. These interrupters are tripped by appropriately mounted small pieces of metal. Similarly, two micro-switches activated by a structure on the syringe plunger indicate whether the syringe is full or empty.

Unlike the positioner, the sampler is designed to operate only under computer control; manual sampling is inherently more efficient using a simple hand-held syringe. Though operable by computer only, the sampler control logic still retains the philosophy employed with the positioner of requiring only minimum attention from the computer. However, considered as computer-controlled devices, there are some differences between the two instruments. Each of the nine separate requests responded to by the positioner was given its own computer command. It was thought, however, that this was a rather wasteful procedure, as only two (potentially three) of the commands have data transfer associated with them. The other six are bare instructions. A similar situation exists for the sampler.

Only movements of the sample turret and syringe require data transfer of any appreciable sort. The vertical and rotation movements are essentially data free, as are again such commands as flag checks and interrupt statuses. It was thus concluded that two commands could serve all possible mechanical movements of the sampler. One of these would direct the actions of the syringe, using eleven bits of the accumulator for data, and the remaining bit as a sign bit to signal filling or emptying. The other command would control all motions of the other three motors, using four bits for data to the sample turret, and leaving the remaining eight free for assignment as a sort of enable register whose exact contents would indicate a particular set of motions.

Another basic difference between the two instruments is also well served by this combination-of-commands concept. Unlike the positioner, whose two motors and stages are completely independent physically and able to move back and forth at will oblivious to each other, there are several constraints imposed in the sampler with respect to simultaneous movement by more than one motor. For example, if the sampler is in the positions of Figures 17 or 19, simultaneous movement by both the vertical and rotation motors will cause the rotating assembly to strike and labor against the vertical members long before they are cleared in ascending. Thus, precautions against this and other forbidden movement combinations must be taken

to avoid damage to the unit. This too is facilitated by use of a single command and enable register concept, in that illegal requests can be detected as forbidden combinations of register bits by the control logic, which can then act to block the disallowed command from actually starting the motors moving.

A final difference between the two is that in the sampler, there is, along with the enable register, a status register which can be used to input information to the computer regarding the sampler's physical location. By reading this register, the computer can determine, for example, that the sampler might be vertically at the top and rotated over turret sample cup zero with the syringe empty. Such ability to check orientations facilitates initializing the device upon power up.

### 3. Detailed Logic

#### a. Registers

None of the four motors of the sampler executes a function which is excessively complicated. Thus, the logic of the device consists of four independent groups custom designed to the needs of each motor, all serviced by a common interface and signalling a combined flag. A sequencer such as the Richards unit of the positioner is not needed either, as the logic sequencing is direct enough to be of the self guiding, "fall through" type.

The logic of the four motors will be considered one by one, after which the flag and interface will be treated.

First, it will be helpful to list the bit assignments of the enable and status registers to make the logic easier to coordinate. These assignments are given in Table 4. The enable register, as previously mentioned, is an output register containing four bits of data for the turret and potentially eight bits to determine which motors are to move and to what destinations. The status register is an input register which uses four bits to signal attempts at illegal commands for each motor, and eight bits for informing the computer of the physical orientation of the instrument. With these assignments available for reference, an examination of the four logic networks of the motors can begin.

#### b. Vertical Motor

The logic of the vertical motor is easily the most complicated of the four, due to the existence of some specialized manual controls associated with the precise positioning of the syringe tip over the graphite braid. There are three basic positions of the vertical motor. The first is at the top of the track, which is the normal rest position and the position at which rotation takes place. The others are the braid and turret positions, being respectively the proper heights at which to address

Table 4  
Autosampler Registers

Enable Register		Status Register	
EN 0	: Unassigned	ST 0	: Vertical Error
EN 1	: Unassigned	ST 1	: Rotation Error
EN 2	: Vertical Up/Down	ST 2	: Syringe Error
EN 3	: Vertical Enable	ST 3	: Turret Error
EN 4	: Rotation Left/Right	ST 4	: Syringe Full
EN 5	: Rotation Enable	ST 5	: Syringe Empty
EN 6	: Turret MSB	ST 6	: Rotation at Left
EN 7	: Turret Bit	ST 7	: Rotation at Right
EN 8	: Turret Bit	ST 8	: Vertical at Top
EN 9	: Turret LSB	ST 9	: Vertical in Turret
EN 10	: Turret Enable	ST 10	: Turret at Zero
EN 11	: Unassigned	ST 11	: All Motors Idle

either the sample turret cups or the braid itself. These latter two positions are easily set up as necessary by simply moving their optical interrupters up or down on the mounting bracket. The logic also contains the ability to recognize yet a fourth position, which is not currently in use, but which will be explained anyway.

Three basic sections of the vertical logic are shown in Figure 20. Certain aspects of the first two of these are used repeatedly with the other three motors. The first section is the gate used to start or stop motor movement. It is closed by setting flipflop A. This takes place when the computer gives the combined motor command (CMD 1), provided that movement of this motor is requested by bit 3 of the enable register (EN 3), and that the command is not blocked by an error condition preventing it (VERR is not low). The following AND gate, inverter, and flipflop B serve to synchronize the computer request with the 600 Hz clock which actually steps the motor. With flipflop A set, the next falling clock edge sets flipflop B, which in turn gates the clock to the motor via a final OR gate whose use will be explained later. In essence, this circuitry is thus a synchronous gate which provides a "clean" waveform to the vertical stepper motor driver whenever a legal movement of this motor is requested by the computer.

The second logic section, shown at the lower right, is used to detect illegal movements of the vertical motor.



An illegal motion is requested, and must be prevented, through any mechanism which asserts  $\overline{\text{VERR}}$ . From the gates preceeding the origin of this signal, it can be seen that illegal vertical motion is requested if simultaneous rotation is also requested (EN 5), if rotation from a previous legal command is still in progress ( $\overline{\text{DONE R}}$ ), or if the syringe is over the turret and turret motion is requested (EN 10 · LEFT), or in progress ( $\overline{\text{DONE T}} \cdot \text{LEFT}$ ). Any one or more of these conditions will assert  $\overline{\text{VERR}}$  and block the setting of flipflop A by CMD 1. But, in addition, flipflop C will be set by the same CMD 1, producing signal ERR V, which is passed forward to the sampler flag to signal the computer that the requested action was aborted. The computer can then respond by detecting ERR V as bit 0 of the status register with the command STATUS. Similar error detect networks will be seen later in the other motors.

The final section of logic merely determines the direction of motion of the motor by preparing flipflop D in light of the state of EN 2 at CMD 1 time. The outputs of this flop control not only the direction of the vertical motor waveform generator, but also provide the signals UP and DOWN, used in a future section of logic to detect when motor movement is to cease through generation of the signal  $\overline{\text{STOP}}$ . The gates associated with the R and S inputs of this flop are concerned with the previously mentioned manual controls, which will now be explained.

Although the framework upon which the syringe is mounted contains provisions for fine screw adjustments of the exact positioning of the delivery tip, one aspect of this positioning available to the control logic is the precise point at which the vertical motor stops in descending to the braid. The optical interrupter nominally known as the Braid OI is in fact actually located a quarter inch or so above the level of the braid, with the remaining distance covered through guidance of the circuitry shown in Figure 21. The circuit is centered around two eight bit registers, known as the reference and working registers. Clock pulses of one tenth the normal stepping frequency can be gated into the reference register from the debounced front panel switch "TUNE". These pulses cause this register to either increment or decrement according to the setting of the panel switch "UP-DOWN". These same pulses also cause the vertical motor to move synchronously up or down through use of the signals  $\overline{\text{TUNE}}$ , which is passed to the motor through the OR gate postponed from the discussion of the gate circuit, and UP/DOWN, which forces the state of flipflop D through the circuitry on its R and S inputs. Gate A detects overflow or underflow of the reference register and cuts off the 60 Hz pulses at a count of 255 or 0, respectively, should either event threaten to occur. Gate A also stops the motor motion. The contents of the reference register may be cleared by either the signal  $\overline{\text{INIT}}$ , or front panel

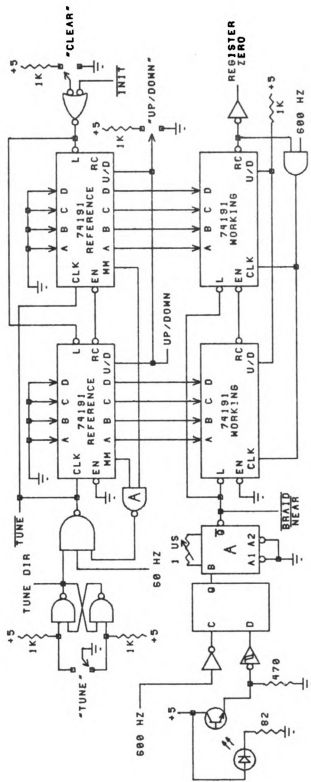


Figure 21. Schematic diagram of the fine positioning circuitry for the vertical motor.

switch "CLEAR".

When the vertical motor is sent down to the braid, it continues down until the Braid OI is reached. When this happens, the event is latched and monostable A is triggered which loads the contents of the reference register into the working register. Motor movement then continues synchronously with decrementation of the working register until this register reaches zero, at which point the signal REGISTER ZERO stops the motor, as will be seen in the next figure.

Typically then, the user, upon turning the sampler on or pushing the "CLEAR" switch, executes a computer routine which causes the syringe to descend to the braid. The reference register will be initially clear at this point, so the motor stops at the Braid OI, since the working register will load a zero and assert REGISTER ZERO immediately when the OI is struck. Using the "TUNE" and "UP-DOWN" switches, the user then positions the tip of the syringe precisely to his satisfaction, and signals the computer to return the syringe to the top rest position. Whenever told to descend after that, the net number of pulses entered into the reference register are used to bring the syringe past the Braid OI to exactly the tuned position in the manner just described. In this way, slight differences in positioning of successive braids can be accommodated without having to move interrupters or adjust syringe mounts.

When the gate circuit was discussed, only the means for closing the gate were outlined. Figure 22 shows the circuitry which detects, for each destination of the vertical motor, when to open the gate again to stop motion. All of this circuitry is dedicated to generating, by one means or another, the signal  $\overline{\text{STOP}}$ , which causes the clearing of both flipflops A and B of the gate circuit (A directly, and B as a result of A). The AOI gate A divides this circuitry into two basic branches, namely that which controls stopping motion for descending movements and that which controls it for ascending movements. The signals UP and DOWN at two inputs of A activate one branch or the other as necessary.

Let us consider first the branch which stops ascending motions. As of this writing, the only possible destination when ascending is the top. Thus, when the Top OI is reached, its signal in combination with UP asserts  $\overline{\text{STOP}}$  through all of the gating. (Note that to conserve space in the diagrams, the interrupter producing signal  $\overline{\text{Top OI}}$  is not shown, nor will be those of any further interrupter signals. They are all identical to the one illustrated in full for the Braid OI in the previous figure.) Flipflop E and gate B are presently not used, and have to do with the possibility of a fourth vertical destination previously mentioned. When the sampler was designed, it was foreseen that when rinsing between sample types, the syringe would be quite busy at the turret

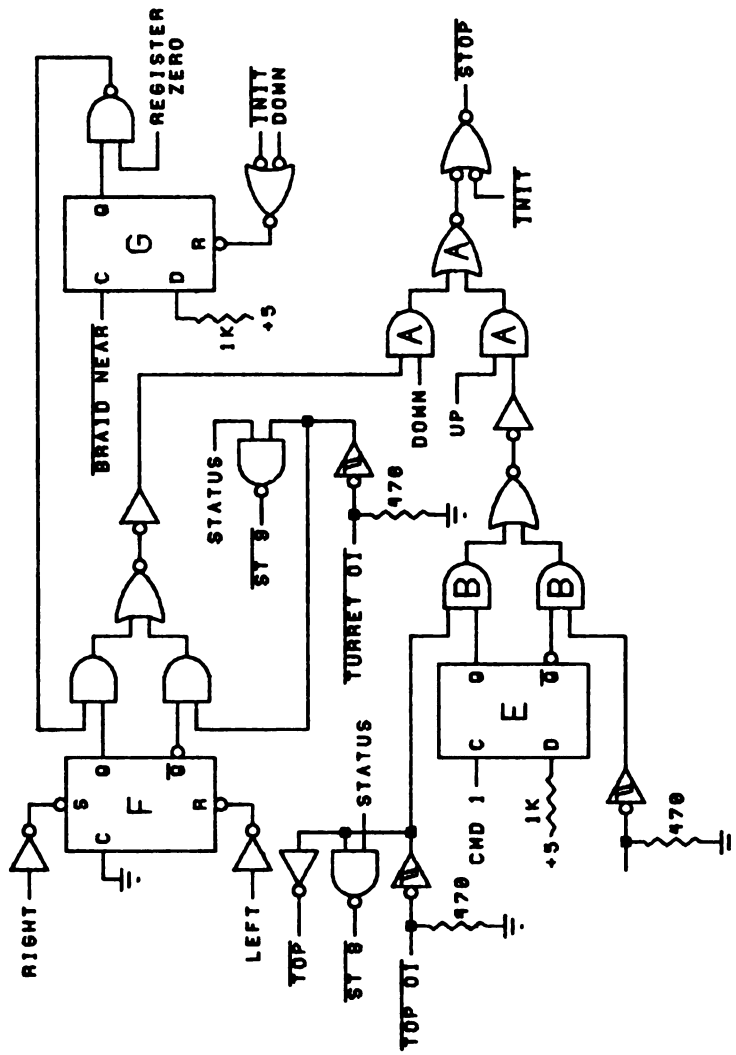


Figure 22. Schematic diagram of the stop circuitry for the vertical motor.

drawing and dispensing rinse water and solutions. It was thought that in such cases, forcing the syringe to return all the way to the top while rotating the turret would be wasteful of time. It would be better to have an alternate ascending destination which would allow the syringe tip to just clear the turret, and only go all the way up to the top when ready to rotate over to the braid. It turns out however that the best place to put the sample turret at present is on top of the monochromator, which already puts it very close to the top anyway. Thus, the extra destination was left out as being only marginally useful now. Should future applications require, however, it can be installed, and its OI connected to the available Schmitt trigger shown. The D input of flipflop E could then be connected to one of the remaining available enable register bits instead of to +5 volts, and then each occurrence of CMD 1 for ascending motions would prepare the flop to recognize either the Top or the new OI as necessary for generating  $\overline{\text{STOP}}$  through AOI gate B. Note that the vertical position "top" is available to the status register as bit 8.

The other branch of gate A controls stopping in the downward direction. Such stopping is to take place at either the Turret or vicinity of the Braid OI's. The stopping point depends on whether the syringe is rotated right or left. Flipflop F keeps track of the current position

of rotation. If at the left, F is clear, and  $\overline{STOP}$  will be generated during descending movements by the signal from the Turret OI in combination with DOWN. If at the right, F is set, and  $\overline{STOP}$  is derived from the network around flipflop G, which properly responds to the manual tuning circuitry previously described. When descending over the braid, as the Braid OI is passed, the same monostable which loads the working register sets flipflop F with the signal  $\overline{BRAID NEAR}$ . When, in addition, the signal REGISTER ZERO is asserted (either immediately or after decrementing a nonzero working register), these two combine with DOWN to assert  $\overline{STOP}$ . Flipflop G is cleared for the next such occurrence by the absence of signal DOWN when the inevitable ascention after sampling takes place. Note that the vertical position "turret" is present in the status register as bit 9, and that the signal  $\overline{INIT}$  assures that the vertical motor is halted when the sampler is first powered up.

#### c. Turret Motor

The circuitry of the turret motor logic is shown in Figure 23. The lower section is the illegal command detect section, which is structured in a manner almost identical to that of the vertical motor. The error conditions possible are either turret movement attempted simultaneous with or during movement of the vertical motor,

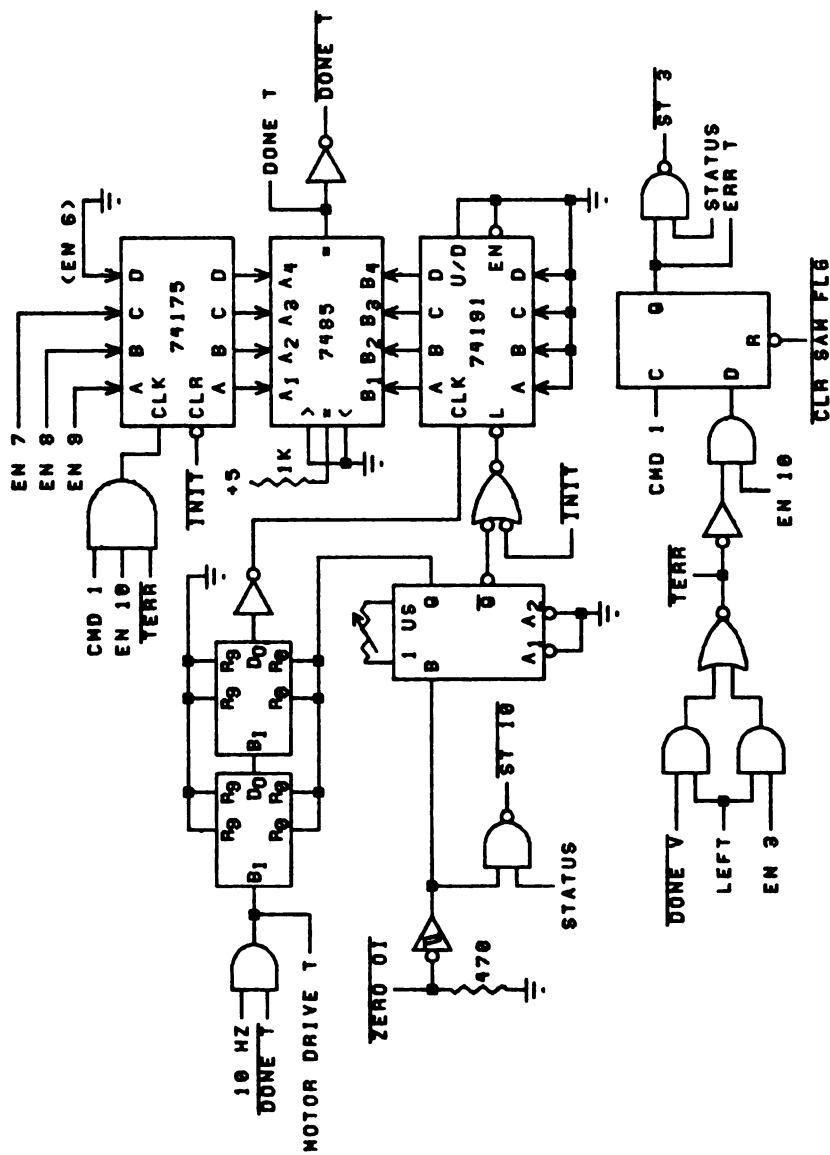


Figure 23. Schematic diagram of the circuitry for the turret motor.

should the syringe be located at the left over the turret. If an error occurs, it is detectable as status register bit 3.

The upper section is the gate for motor movement and the counting circuit for seeking the proper sample cup. The method used is suggested by the techniques employed in the positioner. If CMD 1 is given along with EN 10, and the signal is not blocked by an error, the identity of the sample cup to be rotated into position under the syringe is loaded into a four bit latch from enable register bits 6 through 9. The contents of this latch is compared by a four bit comparator with a counter which contains the actual identity of the current sample cup. Removing the condition of equality between the latch and counter by specifying a different cup asserts  $\overline{\text{DONE T}}$ , which allows clock pulses of 10 Hz to pass to the turret motor driver. For every twenty five pulses passed to the driver (as counted by two successive divide by five sections of decade counters), the cup counter is increased in value by one unit, twenty five being presently the proper number of pulses at the motor shaft between adjacent sample cups. When the condition of equality is reestablished between latch and counter, the assertion of  $\overline{\text{DONE T}}$  is lost, and pulses are cut off. (Note that the turret motor moves in one direction only.) At present, the stepper motor used with the turret is a rather large angle device ( $9^\circ$  per step) that was conveniently available.

Because of the large step size, only eight of the potential sixteen cup positions are currently in use, spaced two positions apart, and numbered 0 through 7. It is for this reason that EN 6 is not actually connected where it belongs, which causes the latch and counter to function as three-bit devices.

The final few gates assure the proper initialization of the turret. An optical interrupter and piece of trip metal are situated so as to define sample cup zero. Every time the OI is struck by the revolving metal piece, the monostable is triggered, which resets both the cup counter and divide by twenty five network to zero. This reset is also accomplished by the  $\overline{\text{INIT}}$  pulse, so that when first powered up, the turret will think it is at position zero no matter where it might really be. Two successive commands to send it first to some nonzero, and then to the zero location will assure that the turret makes a complete revolution. Sooner or later during that process, the interrupter will be struck, and the true position of zero will thus be established. Predictably, this important turret interrupter is available to the computer as a status register bit, bit 10.

#### d. Rotation Motor

The circuitry associated with the rotation motor is even simpler, as this motor has only the humble task of moving back and forth through (at present) 90 degrees

between the interrupter defined limits of left or right. Figure 24 illustrates the logic. The gate for starting and stopping the motor is all but a direct copy of that used with the vertical motor, and the illegal movement detect circuit is once more very similar. Here the illegal movements consist of rotation attempted simultaneous with or during vertical movement, or rotation under any circumstances whatsoever if the syringe is not vertically at the top. The opening of the motor gate is also equally direct. Simply put, the motor is stopped when the Left OI is struck if moving left, or when the Right OI is found when moving right. The assertion of the proper signal LEFT or RIGHT is governed directly by a flipflop prepared according to the state of EN 4 at CMD 1 time. Again, the  $\overline{\text{INIT}}$  signal assures that motion is halted when power is first applied. Both the left and right interrupter signals are open to computer query as status register bits 6 and 7 respectively.

e. Syringe Motor

The three motors discussed thus far are all serviced by the same command to begin movement, to sort out the proper duties through use of the enable register, and to respond to the computer with the status register. The final motor, namely that of the syringe itself, has its own separate command since it needs the full twelve

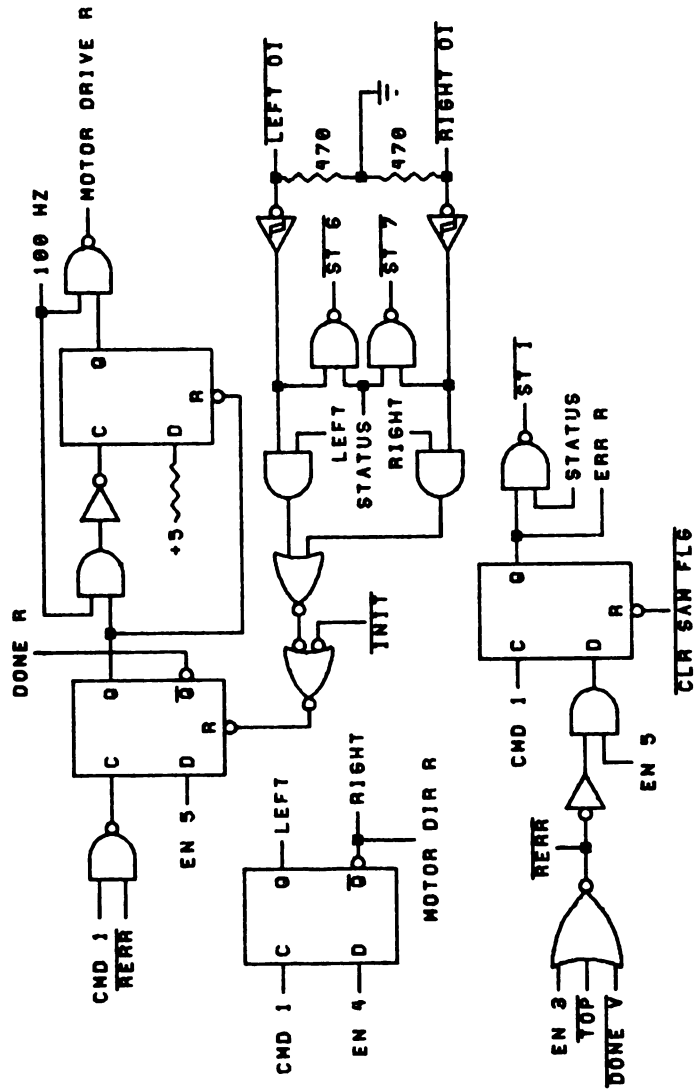


Figure 24. Schematic diagram of the circuitry for the rotation motor.

accumulator bits for data. It does, however, still use the same status register and device flag.

Figure 25 shows the gate, error detect, and stop circuitry for the syringe. Once more, the gate is very similar to those of the vertical and rotation motors, except for lack of an enable bit at the D input of the first flipflop. The syringe motor is halted as usual by  $\overline{\text{INIT}}$ , by two mechanical limit microswitches similar in action to the two interrupters of the rotation motor should the syringe reach the end of its micrometer travel when filling (UP) or emptying (DOWN), or by the signal ZERO which will be explained with the sample quantity computing circuitry of the next figure. The full and empty limit conditions are available respectively as bits 4 and 5 to the status register. The error conditions are attempted movement of the syringe if the vertical motor is moving or if the vertical motor is at the top. Technically, these errors are mechanically harmless, as the syringe can theoretically be moved whenever desired. The restrictions were incorporated though as the syringe has no business being used at any position other than at the braid or in a sample cup. A syringe error is detectable as status register bit 2.

The logic drawn in Figure 26 controls the all important functions of filling or of emptying, and of determining how much in either case. The twelve bits of the accumulator are structured as a twelve bit two's complement



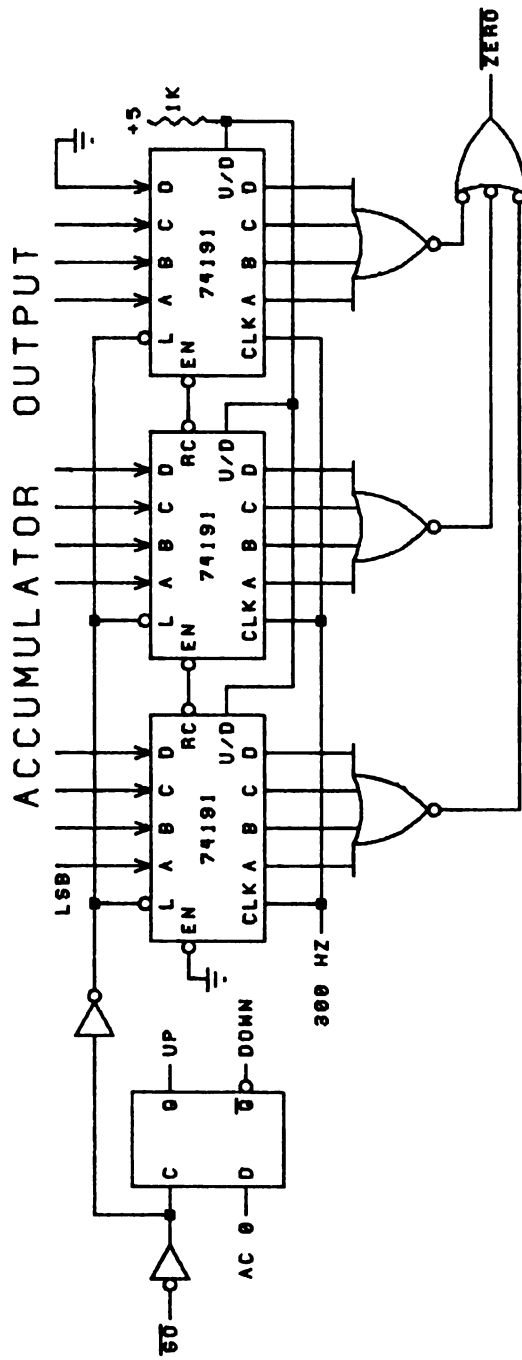


Figure 26. Schematic diagram of the sample size control circuitry for the syringe motor.

number with bit 0 being the sign bit used to signify fill or empty. The remaining eleven bits are used for data to a synchronous, down counting register. Three NOR gates and a NAND gate provide a zero detect for this register, the resulting signal being  $\overline{\text{ZERO}}$ , seen previously as one of the motor gate opening signals of Figure 25.

Both the sign and data bits are loaded into a flip-flop and the register, respectively, by the signal  $\overline{\text{GO}}$ , which is merely the combination of CMD 2 and the consent of the error detect logic. Upon loading, the motor direction is set, and movement begins, with the data register down counting synchronously with motor movement. When the register reaches zero, the requested amount of solution has been either drawn up or dispensed, and the resulting signal  $\overline{\text{ZERO}}$  stops the motor.

#### f. Motor Drivers, and Clock Sources

The pulse trains directed from the gates to the motors, as well as the motor direction control lines, are used to run four full-wave stepper motor sequencers of the exact same construction as that presented with the positioner as Figure 14. Similarly, the outputs of these sequencers in turn are used to control four sets (sixteen total units) of motor coil drivers identical to those of positioner Figure 15, except that the ballast resistors are different for each motor as listed in Table 5. (The

Table 5

## Ballast Resistor Values for Sampler Motors

---

---

Vertical Motor	7 $\Omega$
Syringe Motor	16 $\Omega$
Rotation Motor	20 $\Omega$
Turret Motor	42 $\Omega$

---

---

use of identical drivers for each motor simplified construction of the electronics of the sampler, even though the large vertical motor is the only motor truly requiring the full current switching capability they possess.)

#### 4. Interface

The flag circuit used for the entire sampler is illustrated in Figure 27. As can be seen, the flag may signal the computer through either the skip test or program interrupt modes, as was the case with the positioner. The interrupt facility is enabled or disabled with the command SAM INT and associated accumulator output bit 0. Operation of the flag itself is centered around flipflop A and gate B. When first powered up, or after the computer responds to a previous raising of the flag with the  $\overline{\text{CLR}} \overline{\text{SAM}} \overline{\text{FLG}}$  command, flipflop A is clear, which keeps gate B low and the  $\overline{\text{SKP}}$  and  $\overline{\text{PI}}$  lines inactive. If either CMD 1 or CMD 2 is given to start an operation, flipflop A will be set. The action of gate B then depends on what happened when the CMD instruction was given. If the attempted command was legal, all of the ERR i signals will be low, as will be at least one of the DONE i signals. This causes the other input of gate B to be low as well. Once all motors are finished moving and all DONE i signals are again asserted, gate B will assert the flag. If the command given was illegal, it will have been

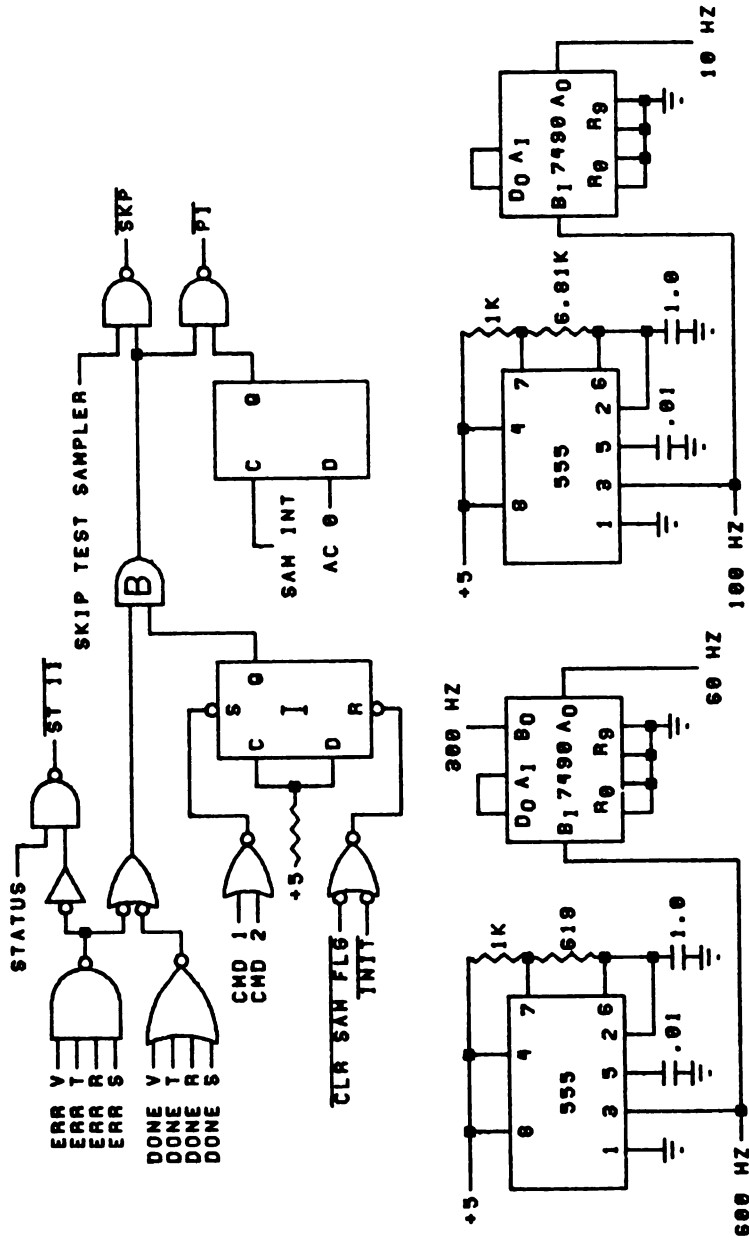


Figure 27. Schematic diagram of the autosampler interface flag and clock sources.

blocked by some error detect logic network. As a result, at least one of the ERR i lines will be high, which causes gate B to signal the flag immediately to notify the computer that something was wrong. Finally, if the command given was legal, but redundant in that what it requested was already true anyway, none of the DONE i signals will leave the high state, and again the flag will be signalled immediately. The fact that all four motors are done with their tasks is available to the computer as status register bit 11. This facility is provided so that the computer can test for a stable state of the sampler without having to wait for the skip test or risk pulling an interrupt which may not be opportune. The complete command set is shown in Table 6.

Also shown in Figure 27 are the two 555 astable multivibrators and their associated frequency dividers which are used as the sources of the clock frequencies for the various motors.

The remainder of the sampler interface need not be illustrated. As was the case with the positioner, it consists of the usual circuitry for decoding device identities and commands from the computer, circuitry for transferring data of the various registers into or out of the accumulator, and circuitry for managing the skip and interrupt lines. The INIT signal is again derived from the interface as a combination of the computer initialize pulse or a local pulse generated at power up time.

Table 6

## Computer Command Set for Autosampler

---

---

6301:CMD 1 - Combined motor command for vertical, rotation, and turret motors

6302:STATUS - Input status word of sampler to computer

6304:CMD 2 - Motor command for syringe motor

6311:CLR SAM FLG - Clear sampler flag

6312:SKIP TEST SAMPLER - Skip test of sampler flag

6314:SAM INT - Enable or disable sampler interrupt facility

---

---

## 5. Power Supplies and Physical Structure

The electronics for the autosampler are assembled on printed circuit cards of original design and construction mounted in a commercially produced card cage. The logic of the vertical and syringe motors are contained on one board, and that of the rotation and turret motors and the sampler flag on a second. These boards are general purpose integrated circuit cards having room to accommodate as many as 42 fourteen or sixteen pin devices, with power and ground buses. Signals are brought to the boards via double sided edge connectors of 58 contacts per side on tenth inch spacing. All chips on these boards are socket mounted and interconnected with wire wrapping. Decoupling capacitors are provided at each package. The three front panel controls associated with the vertical motor are mounted on a simple aluminum bracket secured to the circuit board.

The sixteen motor coil drivers for the sampler motors are mounted on a third board. A fourth board similar to the logic boards is used to contain the computer interface, with connections to the computer terminal being made via the usual ribbon cable and paddle board system. The four boards communicate with each other through a backplane bus wire wrapped among the terminals of the various edge connectors. Signals taken out to the sampler for powering the interrupters and microswitches are routed

with bundled groups of ordinary hookup wire, which are demountable at the wall of the card cage through use of a nylon connector.

The power supply used for the sampler logic is a commercial device capable of supplying as much as 12 A of regulated +5 V. The large supply is used because the card cage contains the circuitry of the data acquisition system as well as that of the sampler, and even then is only half full. The supply used for the stepper motors is a +25 V filtered, but unregulated, device of original, but ordinary design. It contains the elements of the power supply, a cooling fan, and the motor ballast resistors. Connections from the supply to the motors are made with a socket demountable multiple conductor cable. Return lines from the motors to the motor driver board are similarly joined, and a single ground wire of heavy gage completes the circuit back to the motor supply.

## 6. Testing and Performance

All facets of operation of the autosampler were tested with appropriate computer routines, and changes were made in the original logic design until proper performance was realized. This process was simpler than that encountered with the positioner because of the separable nature of the sampler motor movements and the use of self-guiding logic rather than control sequencers in executing

the operations. It was at this time that the proper frequencies of motor stepping were selected and permanently hardwired.

A very extensive characterization of the sampler as an instrument for use in electrothermal atomic spectroscopy was undertaken by Mr. Pals, to whose thesis the reader is referred for evaluations of performance under a variety of conditions.

## 7. Operating Software

Two assembly language routines written by Mr. Pals are used to control the sampler, both of which operate on the principle of storing in memory a series of words whose values represent the proper combinations of bits to direct various motor motions. The simple act of sampling, for example, involves a descent to the braid, a deposition of the sample, and a return to the top. The bit patterns for a vertical descent, delivery of an amount of sample specified by a passed argument, and vertical ascent are stored in sequential memory locations. When the controlling routine calls for sample deposition therefore, it will call the sampler subroutine in such a manner as to summon these three words from memory one by one and output them to the sampler along with the proper motor command. Skip tests occur between each such word to allow completion of the task. Status register checks occur

after each step for an illegal command or malfunction. Should an error be detected, the computer will halt to prevent possible damage to the sampler through further commands.

One of the two subroutines operating in this manner is used to initialize the sampler. When called it directs the sampler, via the self indexing word system described above, to execute the following series of motions: ascend to top, rotate over turret, send turret to cup one, send turret to cup zero, descend to turret, empty syringe, ascend to top. This sequence of operations assures that the sampler will legally "find" all of the optical interrupters properly, and leave itself in a well defined position: over turret cup zero (reserved for waste) with an empty syringe. (The double turret command initialization was previously explained in the turret logic, and total emptying of the syringe to strike the lower limit microswitch is assured by two successive deposit sample commands of maximum quantity.) This routine may be called whenever desired, and contains a built in check to assure that it is called before regular use of the sampler is attempted.

The second subroutine manages routine use of the sampler. When first called to load the initial sample, or whenever called afterwards to change to a different sample, it directs the sampler to the turret to empty its contents into cup 0, twice fill (cup 1) and empty (cup 0)

itself completely in a rinsing process with deionized water, fill completely with the proper sample, and finally deposit the same in an argument specified amount on the braid. The routine then keeps track of what the syringe contains, as well as a running tally of how much so that in successive sampling operations, it is able to choose among three possible sequences of code words either to deposit another sample, return to the turret to refill with more of the same sample solution before depositing it, or change samples entirely by executing the full rinsing operation described above. It is obvious that creation of new or modification of existing code word sequences can be used to alter the sampler's activities as desired.

At present the sampler is not interrupt driven, and so no interrupt facility is in use in the software.

#### D. DATA ACQUISITION SYSTEM

##### 1. Multifrequency Real Time Clock

Data acquisition for the graphite braid system consists of performing repetitive analog-to-digital conversions at specified rates upon the appropriately amplified spectrometer photomultiplier signal. The final major piece of instrumentation to be discussed is a computer-controlled, dedicated, multifrequency real-time clock for providing the necessary timing and signalling for such

conversions. It consists basically of a crystal clock source whose frequency is divided in orders of magnitude by a LSI device, the Mostek 5009 divider, and then further divided by smaller amounts with familiar logic to produce an output frequency which is passed to the convert input of an analog to digital converter. The logic associated with the device is illustrated in Figures 28 and 29.

Figure 28 shows the clock source and the latch circuitry used to receive the desired frequency of operation from the computer. The clock source is a 1.000 MHz quartz crystal which is activated and maintained by a simple series resonant circuit. The output of this circuit is squared up by an RS latch and symmetrically divided to 100 kHz by a decade counter. As shown in Figure 29, the 100 kHz line is passed into the external input of the 5009 divider, where it is divided by orders of magnitude according to the data present at the control inputs of the chip. The output from the 5009 is in turn passed into a second decade counter and a flipflop configured to toggle. The counter  $A_0$ , counter  $D_0$ , and flipflop Q outputs represent divisions, respectively, by 10, 5, and 2 upon the output of the 5009. These three lines are fed into three inputs of a four-to-one multiplexer, whose fourth input is grounded, being unused. The output of this carries the selected frequency clock train to the A/D converter via some concluding circuitry which will be dealt with later.

At this time, it will be best to discuss how the

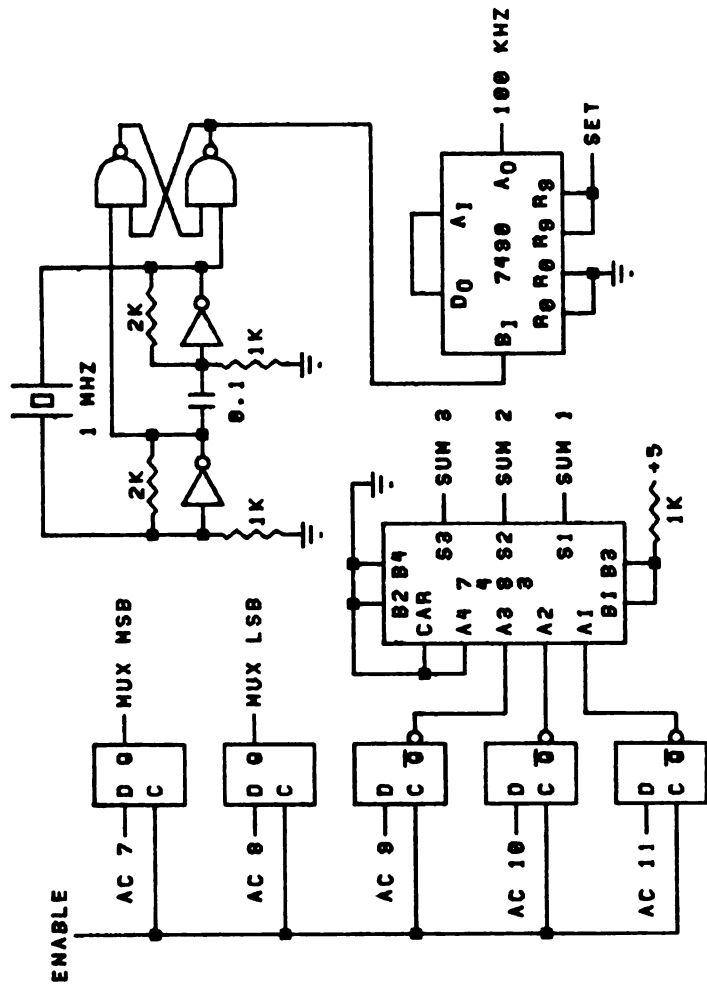


Figure 28. Schematic diagram of the clock source and frequency select circuitry for the data acquisition system.



control lines of the 5009 and MUX are used to determine the A/D conversion frequency. Refer back to the remaining section of Figure 28. Bits 7-11 of the accumulator are used to control the frequency of the clock. These bits are latched out into the clock circuit when the computer command ENABLE is given. Bits 9-11 are used to address the 5009, and thus control the exponent of the output frequency, whereas bits 7-8 address the MUX and govern the mantissa. The complement of the latched bits 9-11 is sent to a four-bit full adder, where a constant binary five is added to them. The outputs of this adder are then used to address the 5009. (This seemingly strange series of events provides a convenient code for remembering what frequency the clock is producing, as will be shortly seen by example.) Bits 7-8 are latched and sent directly to the MUX as its control lines.

To give an example of how the system functions, consider what frequency would be produced if bits 7-11 of the accumulator contained the binary pattern 10010 at the time ENABLE was asserted. Let us first deal with bits 9-11. They will be latched out as binary 010. The complement of this, or 101 will be sent to the four bit adder. There, a constant of five, or 101 will be added to them, producing the result 010, with the carry into the fourth adder bit being discarded. Thus, the  $2^2$ ,  $2^1$ , and  $2^0$  lines of the 5009 will be addressed by 0, 1, and 0 respectively. From the manufacturer's truth table, this combination of address

bits will cause the 5009 to divide by 100, producing a frequency at the 5009 output of 1 kHz. Bits 7-8 control the MUX, and with the pattern 10 in these bits, the selected channel will be that of the 2 input, which is the divide by five output of the second decade counter. Thus, the frequency at the output of the MUX will be one-fifth of 1 kHz or 200 Hz, and it is this frequency at which the A/D converter will function. The use of the circuitry employed to achieve this is now more reasonably seen. The original binary word used to produce this frequency was 10010. If a space is put between bits 8 and 9 in this word, it reads 10 010. In this manner, bits 7 and 8 are in binary the mantissa of the frequency, or two, and bits 9-11 give in binary the exponent, also two:  $2 \times 10^2$  Hz. With this arrangement, it is easier to remember how to construct computer software to decode and request frequencies of the desired value. The complete list of frequencies available from the clock is shown in Table 7. Addressing both lines of the MUX with 0 selects the grounded channel, making the device inactive. Also, addressing both lines with 1 selects a mantissa of five, not three. It can also be seen that the three bits used with the 5009 actually function as a three bit two's complement word for selecting the exponent, with the one notable exception that bit pattern 100, which in strict two's complement should be negative four, is in fact positive four in this application. The total range of frequencies selectable runs from

Table 7  
Frequencies Available from the A/D Clock

Bits 7-8: Mantissa	Bits 9-11: Exponent
00 - inactive	011 - $10^3$ Hz
01 - 1	010 - $10^2$
10 - 2	001 - $10^1$
11 - 5	000 - $10^0$
	111 - $10^{-1}$
	110 - $10^{-2}$
	101 - $10^{-3}$
	100 - $10^4$

50 kHz to 1 MHz, values which are respectively too fast for the computer to handle, and orders of magnitude slower than typical atomization times from the braid.

The remaining circuitry of Figure 29 may now be covered. It consists of a system used to start the clock at any desired frequency with minimum time jitter. A final accumulator bit, bit 6, is used as an enable bit to start the clock. If bit 6 is present when ENABLE is given, a monostable is fired, which sets all portions of the frequency division chain to their maximum count values. This assures that when the monostable pulse concludes, there will be a maximum time jitter of only 1  $\mu$ s between the conclusion of the pulse and the first rising (converting) edge out of the MUX no matter what the selected clock frequency may be. This circuit in effect assures a nearly exact synchronization between the crystal clock and the computer to within a margin of error insignificant with respect to the operating clock frequencies.

Whenever the ENABLE command is given, flipflop A is cleared. If bit 6 is present also at the time, A will be reset again after 10  $\mu$ s, and its outputs will permit the clock frequency coming from the MUX to be passed on to the A/D converter as the signal CONVERT. If bit 6 is not present when ENABLE is given, however, A will remain clear as the monostable is never fired, and clock frequencies coming from the MUX will not be passed to the converter. Instead, the line MAN CONV, or "manual convert"

will be active, and allow conversions to be requested from a source other than this clock if so desired. (The main reason this seemingly cumbersome flipflop arrangement is used is that it prevents spurious edges from passing down the CONVERT line as the clock frequency is being set up, a potentially important service if data acquisition should ever be incorporated into an interrupt driven facility.) Typically then, when this clock is used, it is activated at the start of a data acquisition interval by issuing ENABLE to latch the frequency data along with bit 6 to start the clock. At the conclusion of acquisition, ENABLE is again given with at least bit 6 low to turn the clock off.

## 2. A/D Converter

The signal CONVERT is passed directly to the start convert input of the A/D converter, which is a 12 bit, 8  $\mu$ s device. This converter is wired for unipolar, 0 to +10 volt operation, with trimpots provided for the adjustment of gain and offset as recommended by the manufacturer's data sheet. The digital output is complementary straight binary.

Figure 30 shows the flag and data reading circuitry associated with the converter. The flag is a straightforward device signalled by the conclusion of the converter's BUSY line. Upon being set, the flag may be queried by the

computer as usual either by the command SKIP TEST A/D or by pulling an interrupt if this facility has been enabled with the computer command A/D INT and bit 11 of the accumulator. The computer may also assert  $\overline{\text{CLR A/D FLAG}}$  to prepare for the next conversion.

The digital data from the converter is inverted back to straight binary and strobed onto the accumulator input lines with the command READ A/D. Table 8 gives a summary of all computer commands for the data acquisition system.

### 3. Power Supplies and Physical Structure

The circuitry of the data acquisition system is housed in the same card cage used to contain that of the auto-sampler. The logic of the clock and flag is contained on a general purpose logic board of the type previously described for the sampler, and is physically assembled with an identical philosophy as well. The A/D converter itself as well as the twenty four gates immediately associated with its digital outputs are contained on a second board. All unused space on this board is left covered with copper laminate to serve as a ground plane for the converter. Manufacturer's recommendations for suppression of noise and routing of grounds are observed. The analog input is a length of coaxial cable terminated with a BNC connector.

The data acquisition system is serviced by the same

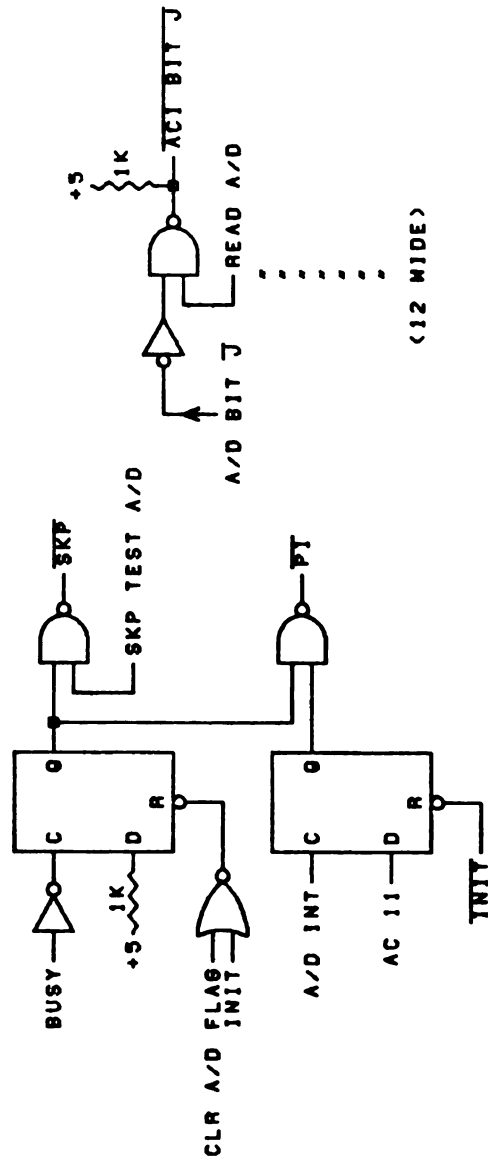


Figure 30. Schematic diagram of the data acquisition system interface flag and data reading circuitry.

Table 8

## Computer Command Set for A/D Converter and Clock

---

---

6521:ENABLE	- Start or stop clock and prepare desired frequency of same
6522:A/D INT	- Enable or disable A/D interrupt facility
6524:CLR A/D FLG	- Clear A/D Flag
6531:MAN CONVT	- Do an A/D conversion without using the clock
6532:SKIP TEST A/D	- Skip test A/D flag
6534:READ A/D	- Input digital output from A/D converter to computer

---

---

computer interface used for the autosampler, as well as by the same wire-wrapped backplane for distribution of signals.

The +5 V power requirements of the circuitry are met by the same supply which provides +5 V to the autosampler logic. The  $\pm 15$  V demands of the A/D converter are met by a separate supply of commercial origin. (The -15 V side of this supply is also used to provide the -12 V required by the Mostek 5009 chip through the expedient of a simple two resistor voltage divider.

#### 4. Testing and Performance

The logic of the data acquisition system was debugged as usual with computer test routines. In addition, the A/D converter was calibrated to zero offset and exact 0 to +10 volt (really 0 to +9.9976 volt) operation by adjusting the gain and offset potentiometers with the assistance of a voltage reference source.

#### 5. Operating Software

The data acquisition system and its dedicated clock are controlled by a sophisticated series of subroutines written by Mr. Pals which control the frequency of the clock as specified by the user and arrange to acquire and store in a buffer region of memory the results of

analog to digital conversions. These routines process the converted data in real time directly into OS/8 Fortran IV compatible floating point numbers through machine code techniques too complicated to warrant discussion here. Because of this real-time processing, it is possible to acquire data at rates as high as 1 kHz or more, which is far beyond the frequency attainable by acquiring and processing the data through the traditional method of subroutine calls managed by the Fortran IV run time system.

#### E. PERSPECTIVES

A distinct disadvantage to most academic instrument building is that the complex instruments built as one of a kind devices often suffer a lack of the benefits of prototyping. A system too complicated to check out by bread-boarding must simply be built with as much foresight as possible and then corrected or modified as necessary within the confines available. So it is with these instruments. Having built them, I have several thoughts on how they could have been better built. I mean by this various conceptual matters that if observed would have produced or could now improve an instrument having more capable, convenient, or reliable function than that which it now possesses.

For all three devices it may be immediately noted that if their design were begun from scratch tomorrow,

they would almost certainly be configured around microprocessors dedicated to managing each individual instrument's tasks, probably from a basis of local subroutines held in read only memory. All requirements of the instrument would be handled by its micro, which in turn would receive its assignments and data from the central minicomputer. Microprocessor control would provide a reduction in the amount of hardware logic required by the instruments. It would also give them the flexibility to customize their sequences of operations to accommodate virtually any reasonable task without the necessity to reconfigure electronic hardware. Finally, the software burden borne at present by the minicomputer could be substantially lowered. Even if microprocessor-based instruments were not possible, however, there are still a number of improvements which could be made in the units as they are currently built.

#### 1. Positioner

A modest but useful addition to the positioner would be the use of seven segment decoders and displays to present visually the contents of the location register. When under computer control, the user can only estimate the location of the atomization cell by observing its physical position, and even under local control, the thumbwheel switches only illustrate where the cell might be, not where it necessarily is. A straightforward LED display of this

information would be an appreciable convenience.

A more significant change would be the substitution of a static for a dynamic method of performing the front panel BCD-to-binary conversion of destination data. The present method, while logically sound, is cumbersome. Fully three states of the GO cycle, numbers 1-3, are dedicated to managing this system. Alternative methods of performing the conversion, such as using the 74184 BCD-to-binary converter or the 7483 four bit adder<sup>185</sup> would help to simplify the instrument. Because these methods would perform the conversion directly from the state of the thumbwheel switches on a constant basis, the three states of the GO cycle mentioned above could be eliminated altogether, which would compress the cycle to only five states, and would simplify the GO sequence from a branching to a nonbranching one. The distinction between local or computer-controlled operation would be removed from the sequence as well, and a possible saving in chips might result, although this is questionable because of the greater-than-unity relation between the number of converter packages required and the number of BCD decades being converted.

A third change would be a major restructuring of the RESET cycle. At present, when a RESET is performed, the positioner assumes that the action was not redundant; that is, the cell was not already reset when the command was given to do so. This is not necessarily the case in

practice. Consecutive RESET commands can be given, and each such extra command will move the cell one motor pulse farther past the true reset point into regions of hypothetical negative position. In addition, if the cell is physically moved so that the metal piece which signals the reset is screwed far down into the interrupter slot, the positioner cannot recognize the difference between this "reset" and the true reset achieved when the photoelectric beam is just barely cut off. To combat this problem, I would reconfigure the instrument to perform resets via the sequence illustrated in Figure 31. The sequence begins by moving the cell in the positive direction, away from the reset point, until the interrupter is definitely seen to be not tripped. Then an extra series of steps in the positive direction is taken, perhaps ten locations worth, to eliminate gear hysteresis, and then finally motion in the negative direction is begun and continued as is done presently until the true reset point is found. This new sequence would guarantee the validity of resets with respect to the above problems, and would yield a sequence shorter than the old one, nonbranching, and transparent to manual or computer-originated requests.

Mechanically the positioner has always performed well. As presently constructed, it lacks very little that is either essential or convenient to its intended purpose.

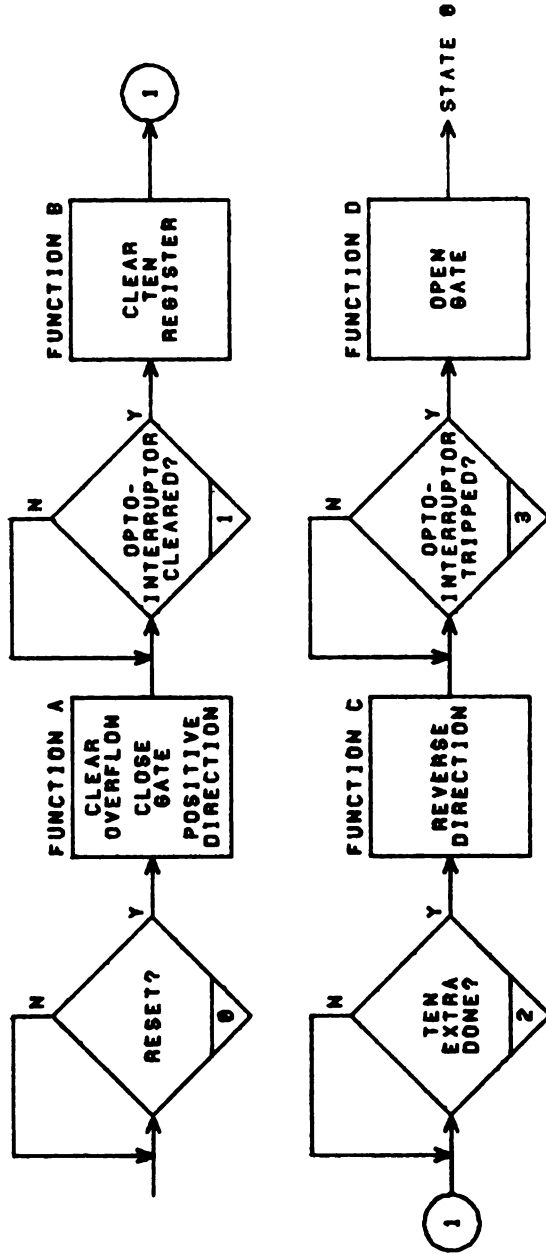


Figure 31. Improved flow of states and functions for a RESET cycle.

## 2. Autosampler

The electronics of the sampler have served well. Generally speaking, they control the movements of the device as thoroughly and properly as desired. Two small points might be mentioned with respect to them though. It would be convenient to have the turret capable of moving in both directions, so that it could back up from say, cup 1 to cup 0, instead of having to rotate all the way around as it now does. A direction control, perhaps best handled in the operating software, could productively extend the sophistication of the turret. In addition, the gate circuit used to start or stop three of the motors could be replaced with the edge triggered Jk gate circuit of Figure 32, which accomplishes the same task of producing a synchronized, clean waveform with elegant simplicity.<sup>185</sup> (Figure 32 illustrates how this gate would be connected with the rotation motor signals, for example.)

Mechanically the sampler could stand some improvement. The movement of the turret by a stepper motor, particularly a large angle stepper, is rather jerky, and causes solution splashing at times. The turret might well be better turned by a small DC motor or DC servo and position indicator system in order to provide smoother motion. Another problem is the drive of the rotation system. At present it is also rather jerky and somewhat under torqued. A fivefold gear reduction added to the drive train should

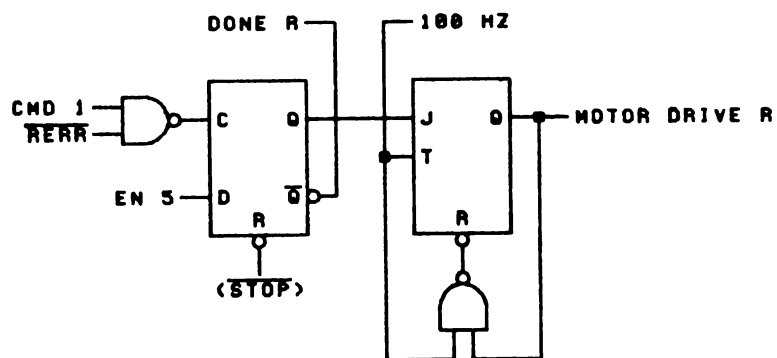


Figure 32. Schematic diagram of an improved gate circuit for the autosampler motors.

be of great benefit in correcting these problems.

There is also the question of having the sampler delivery system be only a multi-sample capacity device. Many commercial analogs of this instrument employ a simple tube delivery system that picks up and deposits samples one by one from the sample tray instead of filling a reservoir for multiple sampling. In much of the work done here, multiple sampling is desirable, but in most real sample situations, frequent sample changing is far more common. The possibility of another autosampler device, either commercial or self designed, to provide the capability for handling such situations, is one worthy of consideration. Some problems also exist in the sampler due to air space in the syringe barrel which acts like a cushion when the plunger is moved, and can prevent the deposition of reproducible sample volumes. Designs of new syringes that minimize this problem are of potential merit.

### 3. Data Acquisition System

The analog-to-digital conversion system and dedicated clock are rather simple devices. Any appreciable changes in them would result only from significant changes in either the manner or type of data collected, such as synchronization of the clock to an alternating pulsed hollow cathode source lamp system for purposes of

correcting nonspecific background absorption. It may be pointed out, however, that future extensions in the sophistication of this atomic absorption system might well extend into just such cases of multichannel data acquisition, or entirely alternate data acquisition systems such as multichannel detectors.

#### F. MISCELLANEOUS INSTRUMENTATION

A few small pieces of instrumentation remain to be mentioned which are not part of the three major instruments, but yet are of essential importance to the entire operating system.

##### 1. Braid Heating Level Converter

The most significant of these small pieces is the digital-to-analog converter used to set the heating levels of the graphite braid. It is a straightforward device illustrated in Figure 33. Digital data representing the desired heating level of the braid are latched out to the D/A converter with the computer command BURN. This data is supplied from a subroutine written by Mr. Pals which receives the desired level as an argument between 0 and 10 V from the calling routine and scales it accordingly as a binary number between 0 and 4095. Like the A/D converter of the data acquisition system, the D/A is a

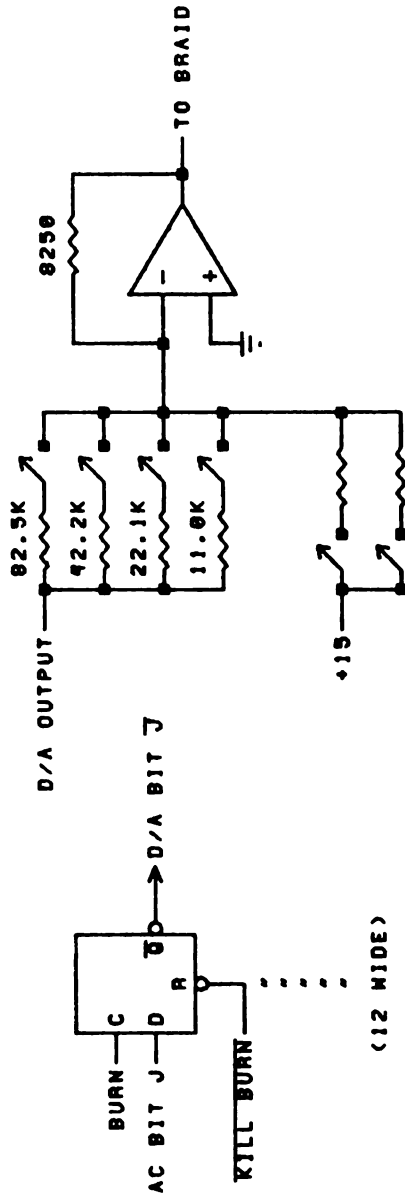


Figure 33. Schematic diagram of the braid heating level control circuitry.

complementary device, and so it is addressed by the  $\bar{Q}$  outputs of the latches. These latches may be cleared, turning off the braid, either by latching out all zeros with the BRAID command, or by simply giving the command KILL BURN, which is an ORed combination of a computer command and a front panel push button switch.

The D/A converter is wired and calibrated for unipolar, 0 to +10 volt output from complementary straight binary input as recommended by the manufacturer. The output of this converter is fed to a low noise, low drift operational amplifier, where it is amplified by factors of anywhere from 0.1 to 1.5 in steps of approximately 0.1, as selected by a binary combination of switch closures from a miniature switch array. This facility is used to scale the output of the converter to levels appropriate with respect to the atomization temperature of the element under study. In addition, current may be supplied directly to the summing point of the OA from either of two push-button front panel switches. Their heating levels of the braid correspond roughly to a few hundred degrees and to about 1500 degrees, for purposes of conveniently degassing newly mounted braids.

These facilities are contained on the same circuit board used to hold the A/D converter of the data acquisition system, and are powered from the same supplies. The final voltage output to the graphite braid power supply controller is provided by a length of coaxial cable

terminated with a BNC connector. This circuit board should be redone to replace the miniature mechanical switches with latches and FET switches so as to put the range scaling facility under the scope of the computer's control.

## 2. General Purpose Flags

The most common technique for regulating the heating of the braid is radiation programming, in which the blackbody radiation of the braid is monitored. Radiation programming is only possible if the braid is incandescent within the spectral response curve of the sensing phototransistor, which is not the case at the low levels of desolvation. When desolvating, the braid heating is regulated by monitoring the electrical power dissipated in it, and radiation programming is only activated at the onset of atomization. A flag is necessary to signal this transition. Similarly, there are other events which may conceivably be triggered at the onset of atomization, such as scope sweeps or chart paper tracings, which also require controlling flags. The interface board of the sampler-acquisition card cage contains provisions for three such flags. They are merely individual D flipflops set by a computer command FLAG if an accumulator bit at the D input is high, and cleared with FLAG if that bit is low. The outputs of these flags are available to accomplish whatever task is desired.

A subroutine written by Mr. Pals governs their activities. One such flag is presently in service to control the switching from power to radiation programming at the onset of atomizations.

### 3. Computer Conveniences

Finally, because the entire atomic absorption system is operated through use of a remote interface facility which communicates with the minicomputer over a distance of some 100 feet, it is valuable to have certain conveniences available to minimize trips back and forth from the instrument to the computer. Three such conveniences are present on the card cage interface board. One of them is a simple LED indicator which informs the user of whether or not the computer is running. A second is a debounced momentary action switch which when depressed fires a several  $\mu$ s monostable which forces the computer to perform a skip. This is convenient if the computer has become stalled in skip testing a flag which cannot be accessed due to, say, oversight in hooking up the instrument in question to the interface terminal. The final device is a set of six miniature switches, which can be read with a computer command to simulate options called for by settings in the computer's front panel switch register.

Table 9 gives the computer command summary for these final instrumental sections.

Table 9

## Command Summary for Final Instrumental Sections

- 
- 
- 6111: Latch digital data out to heating level D/A  
converter (BURN)
- 6112: Address control flags (FLAG)
- 6114: Clear braid D/A converter to zero (KILL BURN)
- 6121: Read miniature switch array
- 
-

## G. REMOTE TERMINAL FACILITY

The complete atomic absorption instrument in use here occupies a goodly portion of an entire lab bench, and cannot physically fit around the laboratory mini-computer. To allow for computerization of the instrument without sacrifice of physical room or permanence of location, a remote terminal facility was designed and constructed which transports all fifty three computer signals available to the outside world through the DEC Positive I/O Bus Interface Option back and forth between the computer and the instrument, a distance of some 100 feet.

The Bus Interface Option is traditionally accessed by the user through the Heath Computer Interface Buffer, commonly known as the "buffer box". For the remote facility, a terminal is provided which sits adjacent to the buffer box and connects to it with three short patches of paddle board terminated ribbon cable. Thirty seven of the signals from the computer travel from it to the instrumentation being interfaced. Each such signal is sent to an integrated circuit differential line driver which, with proper impedance matching and termination, places it onto the leads of a shielded, twisted pair wire group. These differential, paired signals are carried through two large cable bundles across the laboratory false ceiling to a central location in the atomic spectroscopy lab, where they are brought down to a second terminal which

contains identically matched and terminated differential line receivers for each of the signals. The restored TTL output of these receivers is presented to the user on edge connectors physically identical in number and pattern to those of the commercial buffer box. The remaining sixteen signals travelling from the instrumentation to the computer simply duplicate the process along the reverse route.

With this facility, the full interfacing capabilities of the computer are available in the alternate laboratory. Tests of the facility reveal that it can routinely transport the various signals with excellent noise immunity and at frequencies even exceeding those at which they are normally produced by the computer.

Two additional cables are also laid across the false ceiling which provide for remote connection of a CRT terminal and line printer for user-computer communications. The nature of these devices' interfaces is that, unlike the interface signals, they do not require special driving and receiving techniques for reliable data transmission.

MECHANICAL AND OPTICAL INSTRUMENTATION  
AND BASIC SYSTEM PERFORMANCE

A. THE ATOMIZATION CELL

A considerable amount has already been described about the graphite braid atomization cell in the discussion of the positioner. There remain, however, several points of significance which may now be dealt with.

The atomization cell is pictured in Figure 34. It is constructed around an aluminum base and support which secures to the side of the optical rail. Upon this structure is mounted the horizontally moving translation stage and its motor. To that stage is bolted the vertically moving stage, and to that in turn, the vertical motor and atomization cell proper. In addition, both of the lenses of the optical system are supported from the baseplate as well.

The cell itself is structured around a hollow, rectangular aluminum chamber which holds the components of the sheath gas flow system and serves to prevent air from getting into the cell through the bottom. A shelf is cut around the entire upper perimeter of the inside of this chamber, upon which rests the atomizer block. This block consists of two fixed, aircooled brass electrodes for holding the graphite braid, and machined plexiglas for

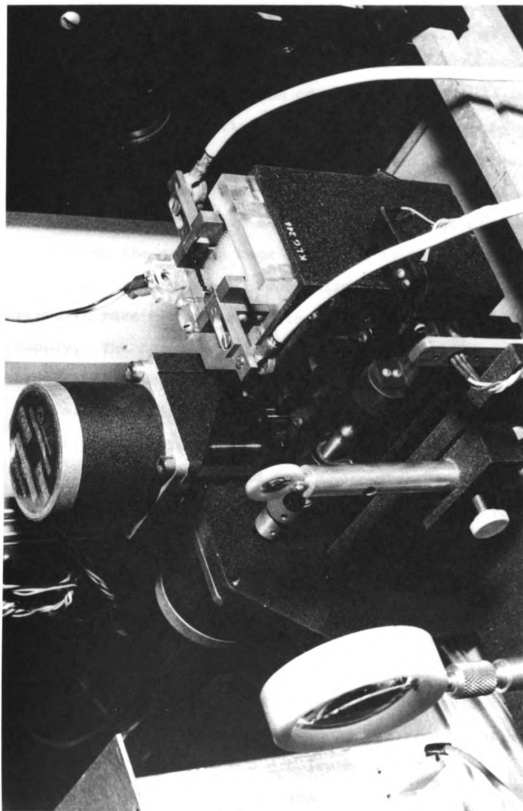


Figure 34. Illustration of the atomization cell.

securing the electrodes and supplying necessary mass where needed to complete the structure. The interior of this block, slightly over one square inch in area, is open, from which a continuous flow of sheath gas passes the braid at all times during use. The electrodes grip graphite braids by simple pinching. By loosening a screw, a section of the electrode may be slid back, exposing an open space into which an end of a braid may be placed. By pushing the section back again and tightening the screw, the mount is completed. Two simple knurled screws also serve to make connection of the electrodes to the power supply. The design of the electrodes is such that the braid itself is the highest object in the entire cell. This makes possible the passage of a source lamp beam directly at grazing incidence over the braid even if the braid is parallel with and just under the optical axis. The braid can be used in this position, or it may be turned perpendicular to the optical axis by a simple changeover operation amounting in essence to a ninety degree rotation of the atomizer block.

On one side of the block, aimed at  $45^\circ$  with respect to the braid, is a phototransistor housed in a short plastic tube which monitors the braid blackbody emission. During burns, the signal produced by the transistor may be used as a sensitive and precise means of regulating the heating of a braid to constant temperature.

The atomizer is protected from damage due to

atmospheric attack with a rectangular chimney fashioned from glued pieces of eighth-inch thick supracil quartz plates. This chimney sits in recesses cut into the plexiglas of the atomizer block, and extends upwards from the atomizer to a height of about two inches. The interior of this enclosed space defines the region available to the positioner for the scanning of atomic concentrations.

Electrothermal atomizers require a flow of sheath gas to carry atomized products through the optical beam for analysis and to protect the atomizer from damage by the atmosphere. In many devices, a simple flow of gas such as argon is sufficient to accomplish these purposes. In the present system however, a laminar sheath gas flow of high uniformity is desired so that the profiles of atomic concentrations reflect as little as possible the eddy and swirl patterns of the sheath. It is not possible to treat this problem too rigorously, as even the best laminar flow of gas designable cannot be expected to maintain its integrity when an object in its path is suddenly heated to as high as  $2500^{\circ}\text{K}$ ; nevertheless, the establishment of a good laminar flow is of high importance in obtaining meaningful profiles. In the present system this was accomplished by supplying the sheath gas through capillaries. Ordinary glass melting point tubes about three quarters of an inch long were held together with household glue in a honeycomb-like array about one inch square in cross section. This array is located in the

interior, open area of the atomizer block, directly underneath the braid. It is held by a closed, rectangular chamber made of plexiglas, which is mounted inside the principal aluminum chamber of the cell. Sheath gas whose flow rate is regulated by a rotometer is brought in through the bottom of the plexiglas holder using tubing. It disperses in the holder, and rises uniformly through the capillaries past the braid. Once beyond the capillaries, there is nothing to disturb the laminar flow except the braid itself, and the short sections of the electrodes which must be included within the chimney. A second, slow trickle of argon is allowed to flow into the aluminum body of the cell during use to keep the cell interior flushed free of oxygen.

The quality of flow provided by the capillaries may be appreciated from the behavior of freshly mounted braids. When a braid is first mounted, it must be heated once or twice to drive off contaminants. They are given off as smoke, which can be seen to rise in a steady and smooth pattern straight up from the braid all the way to the chimney top, where it scatters in the atmosphere. Some further observations along these lines were also done using a smoke generator. In a humid atmosphere, titanium tetrachloride hydrolyzes to the oxide, which fumes in a dense, white smoke. Observations were made in which argon gas was passed over water and then through the cell, in which was mounted a braid upon which drops of titanium

tetrachloride were introduced with a stirring rod. A streamer of smoke was observed to rise directly upwards from the braid without dispersion over the entire height of the chimney, although a slight wavering in the stream, amounting to about one or two millimeters, was frequently in evidence. It was also observed that unless the flow rate of gas was on the order of 2.5 to 3.0 liters per minute, a steady flow up the entire chimney height could not be sustained; rather, the gas would stagnate and lose its flowing qualities somewhere below the chimney top.

#### B. THE OPTICAL SYSTEM

The optics for a typical atomic absorption system often consist of a simple lens to collimate light from the source lamp and direct it through the atomization cell to the entrance slit of the monochromator. In the present system however, because of the desire to be able to isolate small regions of space above the atomizer for analysis, and to permit having the braid parallel to the optical axis, a somewhat more elaborate arrangement was required. The system used is illustrated in Figure 35. A large quartz lens, having both diameter and focal length equal to two inches, is used to collect light from a hollow cathode source. This lens is located six inches from the cathode. At its image focal point, three inches away, is located the focal point of a second, smaller quartz lens of

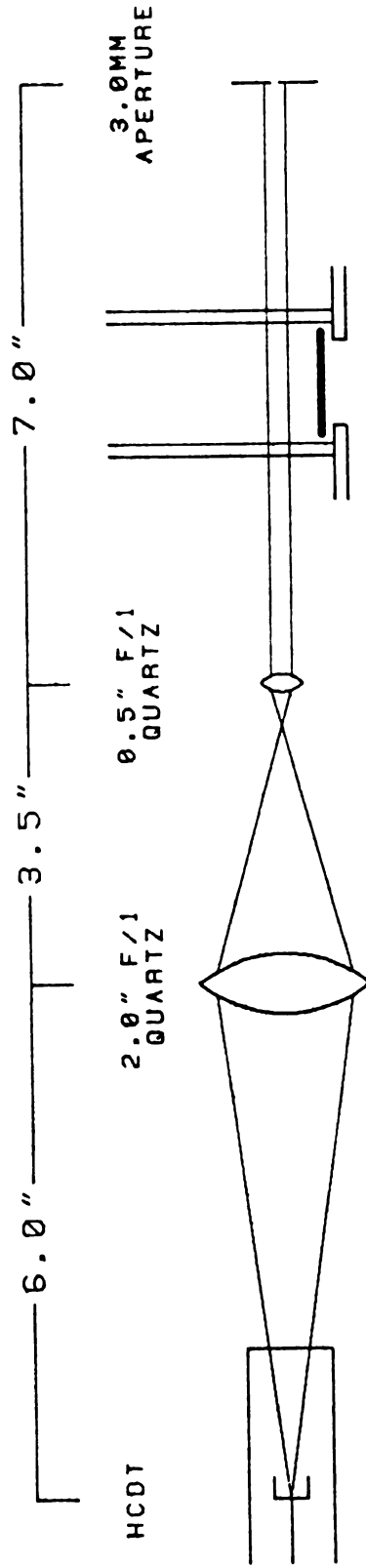


Figure 35. Optical system for the atomic absorption experiments.

diameter and focal length equal to one-half inch, which acts as a collimator. The collimated light beam passes through the chimney and cell to the entrance slit of the monochromator. There it is limited by an aperture which defines the vertical size of the region of space examined. The horizontal size is defined by the width of the slit. This combination of lenses gives an optical beam which has reasonably good intensity and which allows the use of manageable amplifier gain settings and photomultiplier voltages in spite of the limited field of view. It also permits the braid to be parallel to the optical axis without blocking the source light.

To be certain that the size of the space examined is accurately reflected by the aperture size and slit width, measurements were taken of the divergence of the beam after it passes the collimating lens. The optical system was prepared as shown, and a hollow cathode was used as a source. The collimated beam from the second lens was directed into the body of a single lens reflex 35 mm camera, and photographed at two different lens-to-camera distances. After film development and selection of representative exposures, the divergence of the beam was calculated from the difference in size of the spots at the two distances. The results showed about  $1^{\circ}30'$  divergence from the optical axis to the beam edge, or about  $3^{\circ}$  across the beam. These values are somewhat arbitrary, as they will change somewhat with wavelength due to effects

of chromatic aberration, but as a general estimate, they do confirm the fact that the beam collimation is of good quality, and that aperture and slit sizes may be regarded as fair estimates of the size of space examined in the cell.

Alignment or complete assembly of these optics is greatly facilitated through use of a low power continuous laser. The process is as follows. First, the laser is started and used to define the optical axis. Care is taken to assure that the laser beam is truly perpendicular to the plane of the entrance slit, and centered squarely on the slit itself. Next, the small lens is installed and so aligned to keep the diffused laser spot centered on the slit. Then the large lens is placed at its proper distance and aligned. Finally, the turret which holds the hollow cathodes is secured at its proper location.

### C. ATOMIC ABSORPTION INSTRUMENTATION

The remainder of the spectroscopic instrumentation is all of commercial origin and essentially unmodified. Hollow cathode lamps are powered by the Heath EU-703-70 Hollow Cathode Supply, and operated at the maximum recommended currents. The monochromator is the Heath EU-700 with accompanying wavelength controller. The photomultiplier is powered by the Heath EU-701-30 Photomultiplier Supply. Generally, for work done at wavelengths above 300 nm, the photomultiplier used is an RCA 1P28. Below

300 nm, a solar blind Hamamatsu R166 is used instead, because of its significantly greater spectral cathodic sensitivity. The output current from the photomultiplier undergoes current-to-voltage conversion with a Keithley 427 Current Amplifier, which provides adjustable gain, offset, and signal rise time. The output voltage from this amplifier is sent directly to the analog-to-digital converter of the data acquisition system, and is usually also monitored on an oscilloscope to facilitate the location of analytical lines and adjustment of the gain to provide a full 0 to +10 V output.

#### D. BRAID POWER SUPPLY AND CONTROLLER

The power supply used to heat the graphite braid is of original design and construction, but was in existence before the present work began.<sup>183</sup> The raw supply is a high current, 50 V, full-wave rectified DC supply. Power from it is switched into the braid on a regulated basis from a bank of parallel-wired, high current transistors mounted on water cooled heatsinks and driven by a multi-stage Darlington circuit. An instrument for regulating the heating was constructed by Mr. Pals; the reader is referred to his thesis for details of its operation. Simply put, it consists of a control operational amplifier which regulates the heating of the braid by comparing at its noninverting input the reference voltage supplied

from the digital-to-analog convertor and amplifier already described, with a feedback signal at its inverting input derived from the braid. The feedback signal may be derived from any one of four different sources, each of which has appropriate sensing and forming circuitry in the controller. First, the voltage dropped across the braid during heating may be used. Second, the current passed through the braid may be observed. Third, the power dissipated by the braid may be monitored by combining the voltage and current signals in an analog multiplier. Finally, the intensity of the blackbody emission from the braid as provided by the phototransistor mounted on the atomizer block may be followed. This final method is conceptually different from the first three techniques and has several attractive virtues which recommend it as a method of atomizer regulation; they are discussed in a later chapter.

#### E. OPERATING SOFTWARE

Certain sections of the controlling software written by Mr. Pals have already been described in the discussions of the instrumentation. These routines are part of a very extensive composite of software which supervises all aspects of available control over the system. A brief summary may be given here to clarify the manner in which the equipment is employed.

The software is written in Fortran IV, with assembly

language routines in Digital Equipment Corporation's assembler, RALF. The ability of Fortran IV to segment a complete package of software into overlaying sections has been of critical importance to this work, permitting the execution in a 16K computer environment of a software package that would require on the order of 28K of virtual storage. The central point of this software is a routine known as INPUT, which serves as a command interpreter for receiving instructions. All parameters of operation are under control of this routine. These include not only obvious quantities such as atomizer powers or positioner destinations, but also control variables such as whether or not to plot results as they are acquired, record them on a mass storage device, or wait for operator evaluation between successive runs. When the software is first started, INPUT "comes up" with a default set of values for all variables. The operator then modifies selectively those he desires in order to achieve the configuration pertinent to the work at hand. An extensive series of error checks is built into the software. For example, the computer checks to see that a reading of the dark current has been taken before allowing work to begin. The computer also flags improbable or unworkable values for variables, such as a call for a larger number of data points than there is room allotted in core for their storage.

Once all parameters are set and checked for legality,

execution of the task begins as ordered. Several major routines supervise the proper coordination of procedures, while others arrange for the sequencing of repetitive tasks, such as the systematic scanning of space by the positioner. A routine is also available if desired to plot the results of each sample on a high resolution CRT terminal. Perhaps most ingenious of all is the fact that the software contains provisions for including optional, user written routines that may be used to suspend the normal execution of the standard software to achieve unconventional functions from the instrumentation. For example, a subroutine may be included which suspends the normal method for the reduction of data in favor of the user's alternate approach. The software can even be configured in a batch mode to execute a predefined series of ordinary or non-standard tasks without need of operator intervention.

#### F. SUMMARY OF EVENTS FOR A SINGLE SAMPLE

To appreciate the discussions to follow, a summary may now be given of the general sequence of events occurring in the process of collecting the data from one single sample. The user is assumed to have prepared the instrumentation for use (such as selecting the proper hollow cathode), entered the desired values of all parameters to the input routine, and performed initializations consisting of resetting the positioner, initializing the sampler, and

taking a reading of the dark current.

When control is relinquished by the user to the system, the sampler begins to fill itself with the desired solution while the positioner sends the cell to location Horiz = 0.0 mm, Vert = 0.0 mm. A sample is deposited, and the braid gently heated to drive off the solvent. Next the cell is moved to the desired position of analysis, and upon arriving, 100 readings of 100%T are acquired and averaged. The braid is then successively heated to its ash and atomize levels. During atomization, data are acquired at the specified rate. After a brief delay to allow for cooling, the three step cycle of desolvate, ash, and atomize is repeated while data acquisition is taking place for the purpose of background correction. Upon conclusion of this second cycle, the cell is returned to the zero location to receive the next sample, while simultaneously the data from the sample just completed are processed and disbursed as requested.

This basic series of events continues in this manner for each successive sample (assuming the user has not modified the normal sequence) until the entire assigned task is completed, all without need for any intervention on the part of the user, after which the system returns control of itself to the user and awaits further instructions.

## G. CALCULATION OF ABSORBANCE

There are four types of readings acquired from the system. Nominally, they are the dark current, 100% T, sample data, and background data. If these are numbered one through four respectively, they can be written as four equations:

$$1 = I_d$$

$$2 = I_o + I_d$$

$$3 = I_s + I_b + I_d$$

$$4 = I_o + I_b + I_d$$

where  $I_d$  is the dark current,  $I_o$  is the 100% T level,  $I_s$  is the sample signal, and  $I_b$  is the background signal, these last two being variable with time during a given atomization. If these readings are combined algebraically according to the following relationship, they yield the correct definition for absorbance:

$$A = \log \frac{I_o}{I_s} = \log \frac{(2-1)}{(3-4) + (2-1)}$$

In the data reduction software, this calculation is performed on a point by point basis. The routine uses the average value for dark current, the average but

reacquired value for 100% T, and each associated pair of sample and background atomization data points. The point by point technique is better than the use of an averaged background reading, as the background level changes during the earlier portion of atomization while the braid is brought up to final temperature. The correction is however only useful for samples that possess a matrix which is either nonabsorbing or can be completely driven off prior to atomization. If such is not the case, and non-specific absorption is present, other correction techniques such as the use of a continuum lamp or analysis by standard additions would have to be employed.

Because the signal from the atomizer is a transient, the integrated absorbance of the sample is the ultimate readout value. In the present application, this is simply the sum of all the point by point absorbance readings. As a result, integrated absorbance is in itself not a meaningful parameter, as its value depends upon the rate of data acquisition. If the rate is known, it is trivial to scale values properly from different data sets. However, a more disturbing phenomenon exists which makes integrated absorbances even more nebulous, namely the fact that integrated absorbance depends on peak shape.

While working with the system it was noticed that increasing the rise time of the amplifier caused a decrease in integrated absorbance with no change in the

sample. For example, a series of atomizations of 2  $\mu\text{l}$  of 1 ppm silver were performed with rise times of 30 and 300 ms. For the former rise time, the integrated absorbance of five samples was  $10.84 \pm 0.33$ , whereas five samples with the latter time yielded a value of  $8.13 \pm 0.14$ . These data would seem at odds with the fact that a filter does not change the total area of a peak, though it does alter the shape. Indeed, if a signal generator and OA integrator are used to simulate transients, the rise time setting of the amplifier will, as expected, not affect the areas under the transient, given enough time for them to completely pass the filter. The explanation is that, in the present system, the area of the peaks is taken after the point by point conversion of the raw data to absorbance, which involves the nonlinear operation of taking logarithms. To illustrate, consider the idealized pair of peaks shown in Figure 36. Peak 1, with small rise time, penetrates to 10% T for one second. Its "integrated transmittance" or true area may be taken as 9.0, whereas with a sampling rate of 10 Hz, its integrated absorbance is 10.0. Peak 2, low and broad because of the effects of a filter, penetrates to 50% T for 1.8 seconds. The true area is still 9.0, but the integrated absorbance is only  $(18) \cdot (0.3)$  or 6.0. Thus peak shape is of great significance to integrated absorbance, which indicates that integrated absorbances from different systems or even different data sets may not be meaningfully comparable in

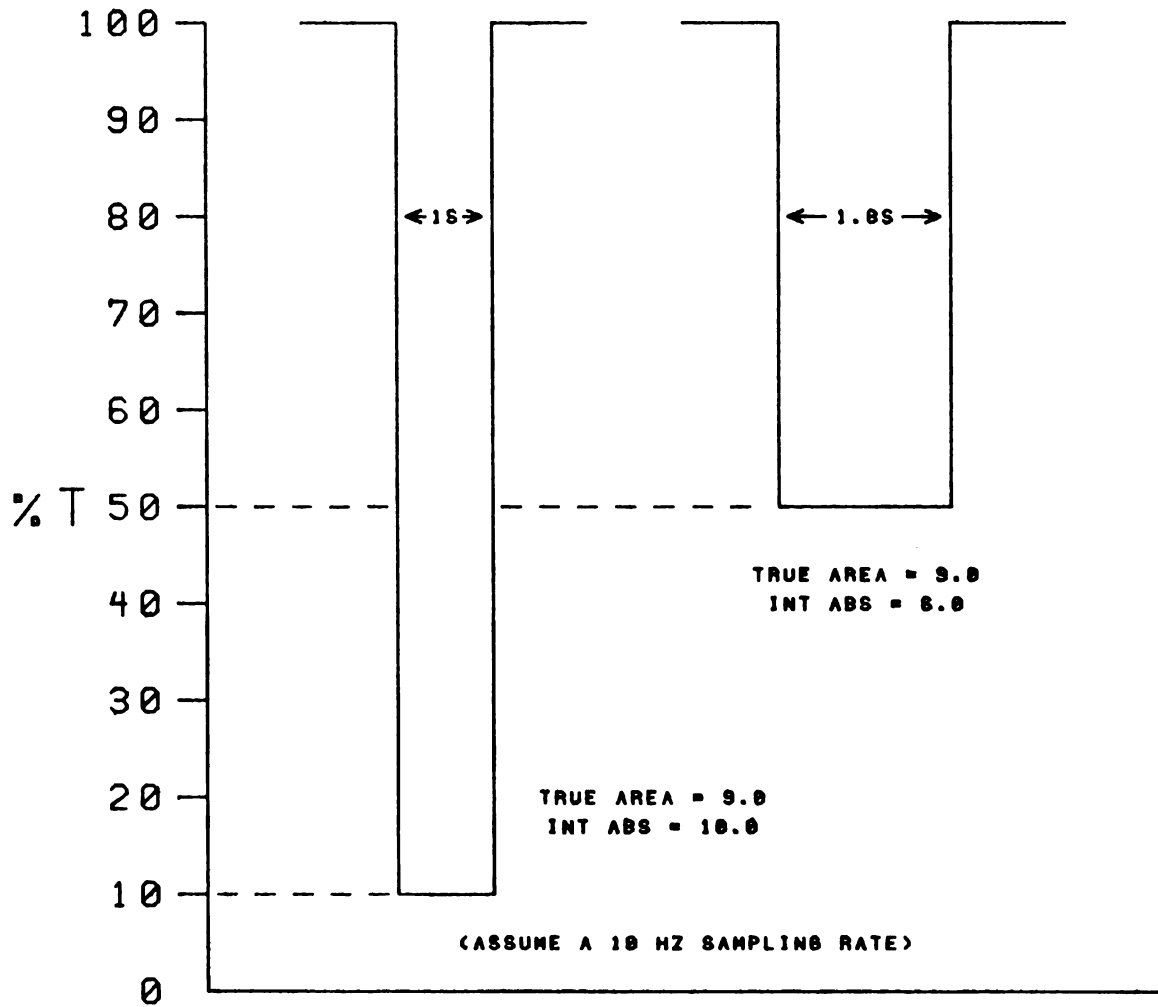


Figure 36. Illustration of the effect of readout time constants upon integrated absorbance.

the absence of peak shape knowledge, even though the samples are chemically identical.

#### H. PERPENDICULAR VERSUS PARALLEL BRAID ORIENTATION

The braid may be mounted either parallel with or perpendicular to the optical axis. When samples are placed onto a braid and soak into it, it might be expected that the parallel orientation would give greater sensitivity because of longer pathlength, and less contribution to background because the braid itself is not viewed as directly by the monochromator.

Some simple observations of the braid blackbody radiation at 650 nm indicate that turning the braid parallel to the axis reduces the observed braid emission intensity by about an order of magnitude. This fact can be significant for analyses of high boiling elements with resonance lines at longer wavelengths, such as calcium at 422.7 nm. Table 10 shows the improvement in integrated absorbance and precision realized for several elements when analyzed with the parallel as compared to the perpendicular geometry. The increase in integrated absorbance is rather small, generally only a factor of one to four, which indicates that longitudinal soaking of samples on the braid is not a very significant phenomenon. Precision is better in the parallel orientation as well, and again by roughly similar factors. This improvement may well be due to the

Table 10

Improvement of Signal and Precision for  
Parallel versus Perpendicular Braid Orientation

	Ag	Cd	Pb	Cu
$IA_{pa}/IA_{pn}^*$	1.5	3.7	2.8	1.8
Parallel	2.0%	3.1%	6.2%	8.4%
Perpendicular	7.3%	4.8%	20.0%	9.7%

\* Ratio of integrated absorbance in the parallel geometry to that in the perpendicular.

fact that with a perpendicular geometry, small inconsistencies in the exact point of sample deposition are far more critical than with a parallel orientation. The improvements do not show any clear cut trends; however, the consistent improvement as well as the reduced background level of emission do indicate that routine use of the parallel orientation is to be preferred.

#### I. EFFECT OF ENTRANCE SLIT GEOMETRY

Because of the high collimation of the source beam, the horizontal size of the space examined at any given cell location is determined by the monochromator slit width, which is typically only 200  $\mu\text{m}$ , fully an order of magnitude smaller than the diameter of the braid into which samples soak. An experiment was performed in which the monochromator was rotated through ninety degrees with the aid of a specially constructed platform. The purpose of this experiment was to see what changes might be observed if the 200  $\mu\text{m}$  dimension was used to limit the vertical size of the observation window rather than the horizontal. The results are given in Table 11, with several different apertures to define the other window dimension.

The two monochromator orientations appear to be rather similar. For all three apertures, the normal orientation gives slightly superior results, both in terms of integrated absorbance and precision, although the

Table 11

Effect of Monochromator Orientation Upon Results

	Traditional	Rotated 90
1 mm aperture	10.84 ± 0.29 2.7%	10.14 ± 0.29 2.9%
3 mm aperture	10.99 ± 0.20 1.8%	9.43 ± 0.31 3.3%
no aperture	10.29 ± 0.22 2.1%	9.04 ± 0.19 2.1%

Each data set consisted of 20 samples of 5 ppm cadmium.

precisions are inherently so close to the 2-3% limit of the sampling error that rigorous comparisons of them are probably not very meaningful. The integrated absorbance generally decreases consistently with aperture size; this is consistent with the fact that the larger apertures view a steadily increasing region of space which atomized samples, through diffusive and convective spreading, are not obliged to fill consistently. The behavior of these two orientations may well change with other elements requiring different atomization conditions than the humble ones necessary for cadmium, but at least it would appear that using the monochromator in the traditional orientation does not ignore an obvious means by which to improve the quality of results.

#### J. NATURE OF INSTRUMENTAL NOISE

Some brief investigations were performed to identify roughly the predominant sources of noise in the system, so that their effects might be recognized for possible future instrumental improvements.

The single most persistent source of noise in all of electrothermal atomic spectroscopy is what is generally referred to as the sampling error, which reflects the imprecision inherent in the delivery of sample volumes of only a few microliters, not only in the variation of the exact sample size, but also the variation in precisely

where it is deposited on the atomizer and where it might migrate to or soak into on the atomizer as the heating process begins. This source of noise is often the prime contributor to the total system noise of 1-2% at best, and can render a systematic study of other noise sources difficult or meaningless.

For the present work a computer program was written which would operate the data acquisition system at user specified rates and output the raw twelve-bit data conversions to the terminal or line printer along with the standard deviation of the set. With this program, data sets of one hundred conversions each could be taken over variable time periods.

The first item investigated was the amplifier and data acquisition system itself. With no input to the amplifier, and a large offset intentionally introduced to place the output at nearly the full-scale limit of the converter, one hundred data point sets were taken over courses of time ranging from one second to about one quarter hour. Amplifier gains ranging over the settings commonly used in spectroscopic work,  $10^6$  to  $10^{10}$  volts per ampere were used. This portion of the system was found to be essentially noise free. Regardless of the gain or time of measurement, the standard deviations of all data sets were significantly less than one LSB of the ADC. Thus, the noise level of the readout is below the resolution of the data acquisition system at least for single readings.

Virtually the same behavior was observed if the photomultiplier was connected as an input with its shutter closed. Only at the highest gain settings, such as  $10^9$  V/A and 800 V would the dark current noise seem to reach one converter LSB in magnitude. It was observed though that at such high amplifier gains, shaking the cable connecting photomultiplier and amplifier would introduce a very noticeable determinate noise in the output level. The use of special low noise cable for this connection, and perhaps a critical evaluation of the wiring of the photomultiplier base itself, might be of merit to guard against noise introduced from mechanical vibrations.

Of more interest were some observations taken using hollow cathode lamps as the sources of signals. Two lamps were studied. The first was a multielement lamp from which the silver resonance line at 328.1 nm was isolated. The second was a lead lamp examined at 283.3 nm. The lead lamp was more worn than the silver, and could not be used at as high a current rating, and thus required significantly more gain from the readout to get a solid output voltage. The settings used were: silver,  $10^8$  V/A and 700 V, and lead:  $10^9$  V/A and 610 V, both with a 200  $\mu\text{m}$  slit width. One hundred point data sets were taken of the output from either lamp over times ranging from one second to about one quarter hour. Figures 37 and 38 show plots of the data sets over the various time intervals. The ordinate values of the sets

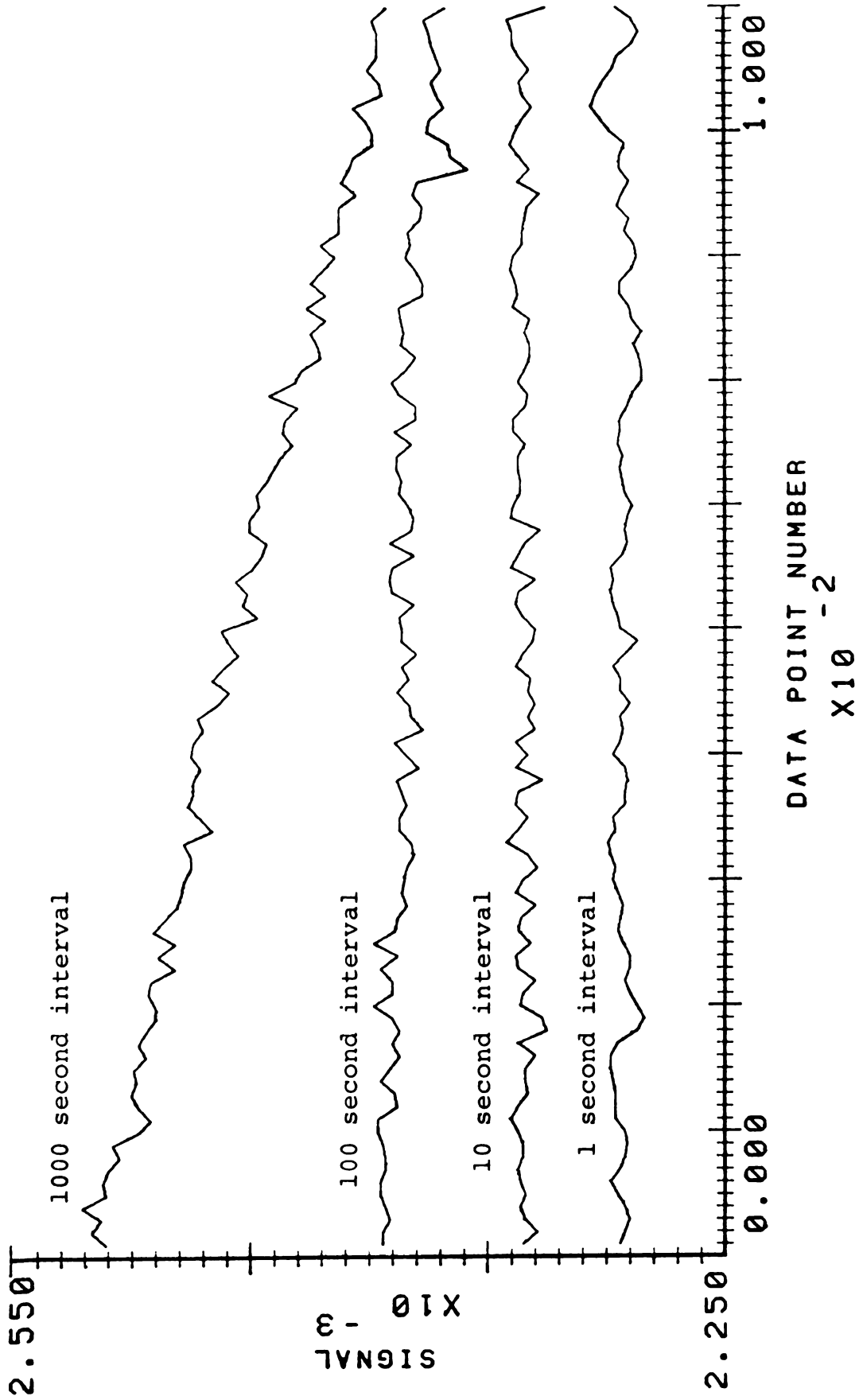


Figure 37. Noise characteristics of the instrumentation over various periods of observation: silver hollow cathode.

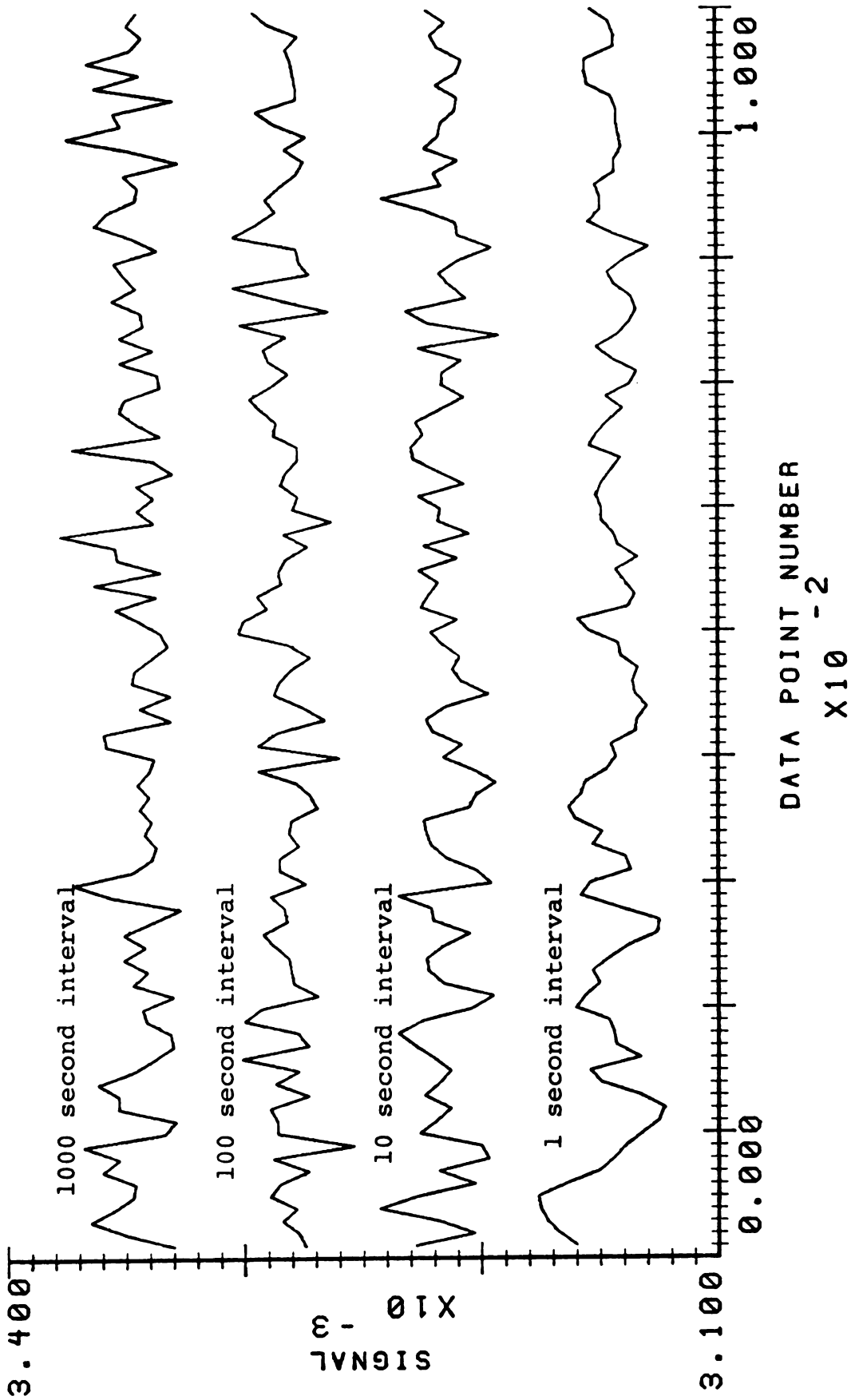


Figure 38. Noise characteristics of the instrumentation over various periods of observation: lead hollow cathode.

have been uniformly shifted where necessary to separate the sets.

In the case of the silver lamp, a long term drift effect is quite evident, in spite of the fact that both lamps were allowed to warm up for more than a half hour before any of this data was taken. The magnitude of the noise is greater for the lead lamp, reflecting the higher gain necessary to achieve good on-scale signals from it. The quickest data set, taken over one second of time, is comparable to the rate of data acquisition employed during normal spectroscopic analysis. For this set, the silver lamp shows a relative standard deviation of 0.17%, and the lead lamp 0.32%. To compare with these results, a similar set of observations was made with an ordinary tungsten lamp as the source, the same gain and photomultiplier settings as were used with the silver and lead lamps, and a change in the monochromator wavelength setting to get comparable signal intensities. The tungsten lamp yielded results so indistinguishable from the hollow cathodes that they need not be plotted. The one-second data set under the silver lamp conditions showed a standard deviation of 0.19% and that for lead conditions was 0.36%. The tungsten lamp also showed the same general susceptibility to long term drifts, and the same apparent randomness of short term fluctuations as did the hollow cathodes.

One would expect a tungsten lamp to have inherently superior short term stability compared to a hollow cathode.

Yet the very similar performance of the two sources in the above studies would seem to indicate that shot noise, and not source flicker is the principal contributor to the noise magnitude. This is not an unreasonable finding for a system like the present one in which light throughput is severely restricted to a small region of space. The drift of the hollow cathodes is not surprising. They are regulated by monitoring the current passed through the lamp. A superior method of regulation would be to do it optically, based on the intensity of the analytical line. This would not be trivial to implement, as unfortunately in atomic spectroscopy the sample cell precedes the monochromator. Optical regulation or compensation of the source would require a double beam geometry or a synchronously detected modulated source. Some sort of source stabilization might well be desirable however because of the time separated nature of the instrumental data. Readings of 100% T, sample atomization, and background correction all take place sequentially in time, with several seconds elapsing between each. Uncompensated drift of the source during such time could cause a significant contribution to the total imprecision of an analysis. For example, a decrease in source intensity by 0.2% T between the reading of 100% T and the sample atomization would make a contribution of 0.087 to the integrated absorbance observed during a one second atomization at a data acquisition

rate of 100 Hz. At this data rate, the transient signal seen from, say copper at 1 ppm, yields an integrated absorbance on the order of 16 or so. Consequently, the source drift would make a contribution of roughly 0.5% to the total imprecision of the analysis. This is not as much as that expected from the sampling error, but it is still a significant amount. It might also be pointed out that this analysis would not at all be close to the detection limit.

#### K. IMPORTANCE OF BACKGROUND CORRECTION

For several elements that can be analyzed with a parallel braid at relatively low temperatures, the contribution of the braid blackbody to the total photocurrent is quite tiny. For example, a direct measurement at the silver line of 328.1 nm of the blackbody intensity of a braid heated to 1700°K (very adequate to atomize silver) indicates that the blackbody contributes less than 0.01% to the total photocurrent, a negligible amount. An experiment was performed in which an alternate data reduction subroutine was used simultaneously with the usual one to eliminate taking into account the second, background burn of the braid. Four data sets of 20 samples each were atomized, the results of which are presented in Table 12. The first set compares the integrated absorbance seen

Table 12  
Significance of Background Correction

Data Set	With Back. Cor.	Without Back. Cor.
A	5.88 ± 0.55 9.3%	6.73 ± 0.57 8.4%
B	-0.048	0.56
C	-0.047	0.54
D	-0.003	0.02

A = 2  $\mu\ell$  1 ppm silver at vertical height 1.5 mm.

B = Baseline at vertical height 1.5 mm.

C = Baseline at vertical height 5.0 mm.

D = Baseline at vertical height 5.0 mm, braid not burned.

from samples of 2  $\mu\text{l}$  of 1 ppm silver. Without background correction, there is a slight improvement in precision, but the integrated absorbance is distinctly higher. Although the blackbody intensity is known to be negligible, it is interesting to note that the difference in integrated absorbance is opposite to that expected if the blackbody were significant. Set B compares baseline data between the two methods, burning the braid without sample. A noticeable absorbance without the correction is still present. It was suspected that perhaps this was due to the fact that observations were taking place very close to the braid (vertical height of 1.5 mm), and that during atomization, the braid was bowing upwards through thermal expansion into the source beam. Set C repeats this baseline data, but at a vertical height of 5 mm, sufficient to avoid the bowing effect. Although the uncorrected absorbance is reduced, it is still present. Finally in set D, comparisons are taken with the braid not burned at all. Here the integrated absorbances finally agree. It is evident that background in this system consists not merely of blackbody emission. Possible contributions from such sources as carbon specks lost from the braid or Schlieren effects from the heated sheath gas will also contribute to the total integrated absorbance, as well as to the precision of analysis. These effects would no doubt be quite difficult to quantify, as there is no simple means available to the present system by which to

detect them separately. Certainly a great deal of irreproducibility in these effects is to be expected. Worst of all is the fact that by turning the braid parallel to the optical axis to cut down on "background intensity", Schlieren effects and particulate losses are actually intensified, as they occur along the entire length of the braid, and would be observed by the system as such.

#### L. ALTERNATE METHODS OF DATA REDUCTION

One final test of performance was to investigate whether or not the precision of analysis could be improved by a data collection routine which would look for a peak, and confine the integration of absorbance to it only instead of the usual total summing of all points taken during the atomization time. The routine employed was configured to not begin accumulating absorbances for integration until at least five consecutive points were monotonically increasing and above a threshold absorbance arbitrarily set at 0.005. Integration would then continue until five points monotonically decreased or the absorbance fell below 0.01. Along with this modification, the routine also contained provisions to present the data in the usual mode of integrated absorbance, as well as in the form of what might be called the "integrated nontransmittance", namely:

$$IT = \frac{I_o - I}{I_o} = \frac{(4-3)}{(2-1)}$$

with the latter expression referring back to the numbered equations of the previous section. Again, these data were presented both with and without the peak seeking algorithm.

The results are shown in Table 13 for the analysis of three different concentrations of 2  $\mu$ l samples of silver. The average peak maximum absorbance is given with each data set to give a rough idea of the magnitude of the transient. It can first of all be seen that essentially no difference in precision is provided by using the peak seeking algorithm. Regardless of the peak height, the precision obtained in either the absorbance or transmittance mode of data representation is comparable with or without peak seeking. It is interesting however to compare the trend in precision between the absorbance and transmittance modes. For the concentrated solution of 1 ppm silver, the precision of the data set is about 1.58 times worse calculated as absorbance rather than transmittance. The intermediate solution value is 1.15, and the dilute solution gives a ratio of 1.04, or nearly comparable results. This effect is due again to the nonlinear nature of logarithms. The lower the percent transmittance, the greater the change in absorbance per unit change in transmittance. In the case of the concentrated solution then,

Table 13  
 Comparison of Calculation Algorithms

	1 ppm Ag	0.2 ppm Ag	0.04 ppm Ag
Int. Abs			
Normal	23.47 ± 0.88 3.8%	4.12 ± 0.29 7.0%	1.04 ± 0.15 14.2%
Peak Only	23.39 ± 0.89 3.8%	4.06 ± 0.29 7.2%	0.98 ± 0.15 14.8%
Int. Nontrans.			
Normal	29.68 ± 0.71 2.4%	8.26 ± 0.51 6.2%	2.25 ± 0.31 13.9%
Peak Only	29.66 ± 0.71 2.4%	8.24 ± 0.52 6.2%	2.23 ± 0.31 14.1%

the variations in data points from sample to sample near the peak maximum make abnormally large contributions to the imprecision in the total integrated absorbance. With more dilute solutions, in which the transmittance and absorbance functions have more similar slopes, the effect is gradually minimized. It is thus unfortunate that even if integrated absorbance is used as the readout parameter rather than the peak height, the peak height still can exert an influence with the type of imprecision that peak integration is hopefully intended to overcome.

## SCANNING ELECTRON MICROSCOPY

### STUDIES OF GRAPHITE BRAIDS

Graphite braids undergo some rather notable changes in physical appearance with time which depend on how they are used. In addition, the rather porous nature of the braid causes deposited samples to soak in during desolvation; their ultimate fate in undergoing desolvation to form dry salt particles is not well known. For these reasons, and for the sake of being able simply to take a closer look at the physical substance of the atomizer itself, scanning electron microscopic and x-ray fluorescence microprobe investigations were undertaken of typical graphite braids, both with and without samples. These studies were performed using instrumentation and photographic supplies provided by the BASF Corporation at their analytical research facilities in Wyandotte, Michigan. In this chapter, a discussion of the observations noted from selected photographs will be presented.

Scanning electron microscopy is an extremely powerful technique for the examination of samples requiring resolutions of as little as one hundred Angstroms or so.<sup>186,187</sup> The SEM can cover a very broad range of magnification, from the nearly molecular figure just quoted up to modest enlargements similar to those obtained with hand held magnifiers. The interpreted

electron image can be displayed on a phosphor or television screen with image contrasts and lighting effects which greatly imitate the appearance of illumination by natural light. Perhaps most significant of all is the fact that the SEM has a tremendous depth of field, which permits the examination of samples having considerable length along the electron axis with very little loss of focus. Accompanied by an x-ray microprobe, the SEM becomes a powerful analytical tool. The x-ray probe can be configured to scan the entire viewed area of sample, and yield an averaged readout of elemental composition, or it can be narrowed to a tiny, fixed spot only a few Angstroms wide, for a highly specific observation of a feature of particular interest. In this mode it can also be scanned across a specific location of the sample to produce a readout of elemental analysis versus sample location. This may be used to typify the chemical content of sample features. Analysis may be either of all recognizable elements simultaneously, or of just one specific element. Signal integration may be performed over long time periods as well for signal-to-noise ratio improvement.

Graphite braid is something of an ideal sample for SEM study. The carbon itself is of too small an atomic number to be detected by the x-ray microprobe (which was capable of elements of atomic number as low as sodium), and is also inherently electrically conducting, which

frees it of the accumulation of static charge that can white out an SEM image. This eliminates the pretreatment step, often needed for nonconducting samples, of the thermal vacuum deposition of a surface layer of platinum or gold. During transport to Wyandotte, sample braids were protected by enclosure in a piece of saran wrap. For analysis, a short section of braid (about one quarter inch long) was simply cut from the desired region of analysis, and affixed to a small aluminum stage with a conducting adhesive. The stage was then inserted into the sample port, and could be fully examined a few minutes later after establishment of the requisite high vacuum in the instrument.

Figure 39 illustrates virgin graphite braid at 50 diameters. This particular piece was taken straight off the supply roll and examined as such. Even physical handling of the braid was minimized. The braided nature of the material is well illustrated, as is the composition of braid bundles by individual graphite strands. The strands are quite small; each bundle may well contain a thousand or more of them. Also visible are small, randomly scattered specks in the braid, which may be the principal source of the initial impurities that are visibly ejected as smoke from a fresh braid when it is first heated. This idea is supported by the braid shown in Figure 40, which is a braid that has been subjected to one initial heating to remove the impurity smoke,



Figure 39. Virgin graphite braid at 50 diameters.

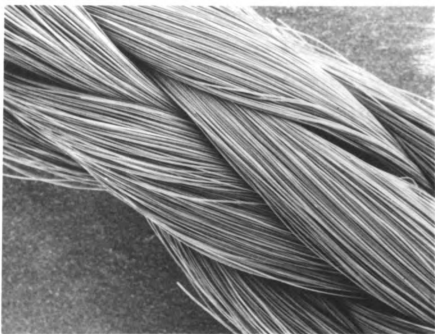


Figure 40. Degassed virgin braid at 50 diameters.

but which has been otherwise unused. The frequency of occurrence of the small particles seen in Figure 39 is quite markedly reduced.

Figure 41 shows virgin braid again, but at a magnification of 500 diameters. The open, porous nature of graphite braid is rather strikingly revealed in this image. Individual fibers are well collimated and uniform, but they are by no means very densely packed. It is obvious how easily deposited samples may soak into the fiber spaces during desolvation. Equally apparent is the fact that the potential total surface area of contact between atomizer and sample is quite large; this excellent contact undoubtedly plays a major role in promoting two of graphite braid's attractive features as an atomization device, namely its general freedom from memory effects, and its ability to perform complete atomizations on the subsecond time scale. Also notable from this photograph is the high consistency of interfiber dimensions. The diameter of any given fiber seems to be quite representative of them all, and individual fibers are apparently able to extend unbroken for considerable distances through the braid, if not damaged. Figure 42 shows one individual virgin fiber at 20,000 diameters. Again, the particulate matter visible on the fiber surface is suspected of being impurity deposits, as other photographs of fibers from braids that have been burned do not show them. From measurements of this photograph, the diameter of

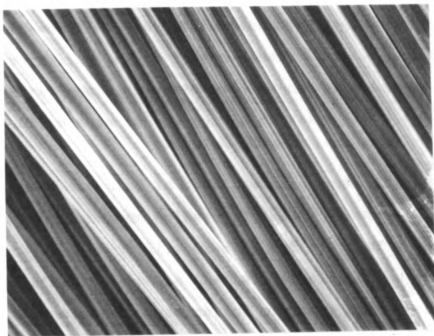


Figure 41. Virgin braid at 500 diameters.

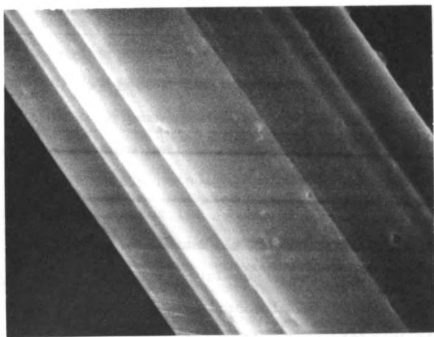
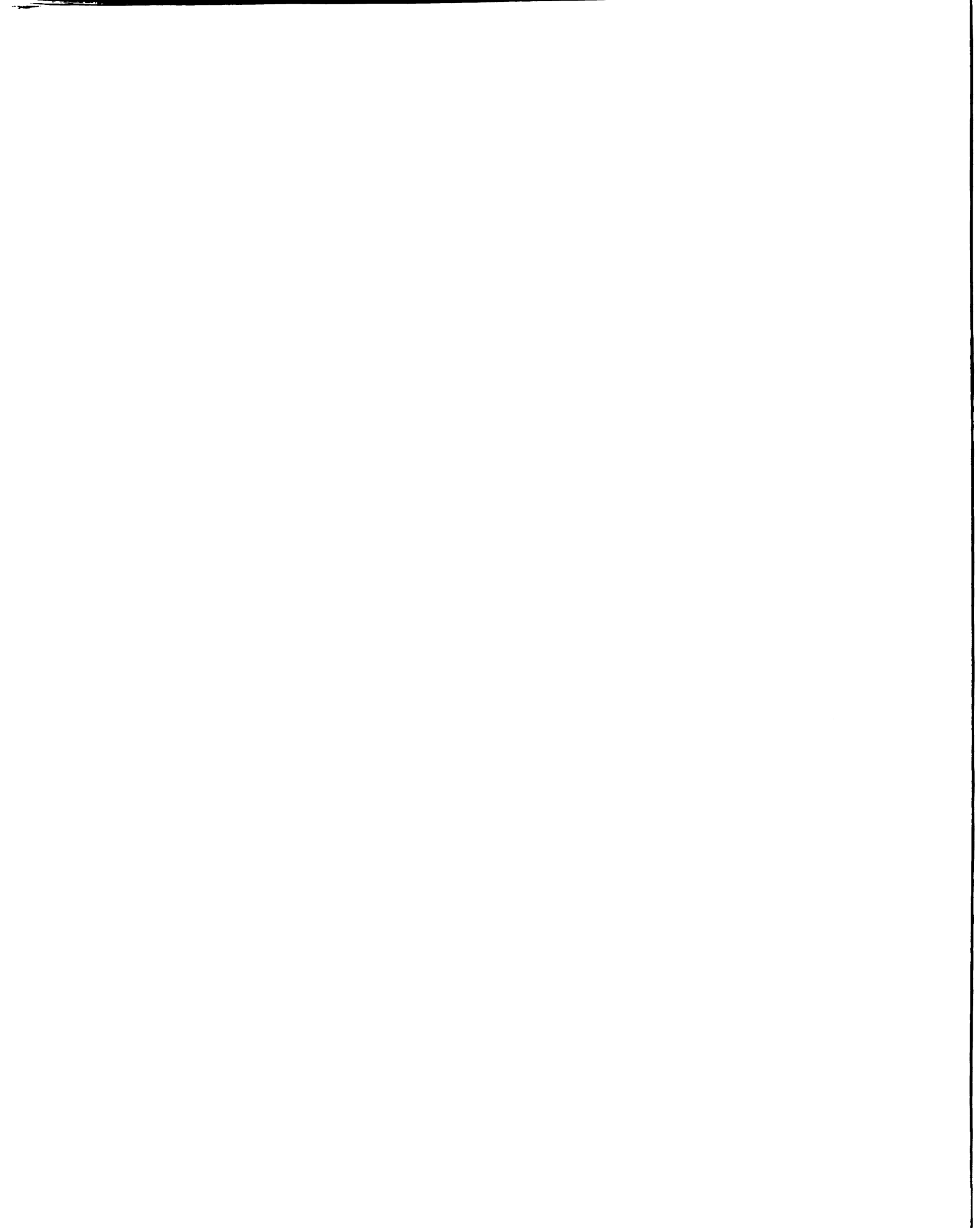


Figure 42. Individual fiber of braid at 20,000 diameters.

a fiber is about ten  $\mu\text{m}$ . Interestingly, there appear to be crystalline layers in the fibers which run along their entire length, as evidenced by the transitions in image brightness that occur in crossing the width of the fiber.

As braids are used in spectrometric work, the regions close to the electrode holders gradually become dull in appearance, and eventually develop hot spots of unusually high electrical resistance that ultimately become the sites of braid burnout. An examination of these dull areas in the next few figures is quite revealing with respect to the cause of this appearance.

Figure 43 shows a 20,000 diameter magnification of one individual fiber from the electrode holder region of a braid that had been in service sufficiently long to develop the dull appearance effect. It is plainly seen that the fiber has become pitted with numerous submicron size cavities, with perhaps slight evidence that these cavities tend to form near the boundaries of the crystalline layers previously noted. Their presence in the fibers accounts well for the visual observations listed above. As the fibers become pitted and scarred, light reflection from the fiber surface is cut down markedly, which leads to the dull appearance. In addition, the cavities, once formed, probably serve as sites of still further fiber destruction, which increases the fiber's electrical resistance and deterioration progressively



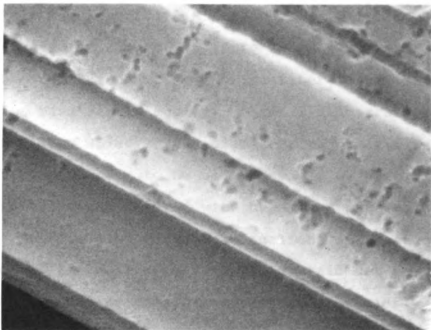


Figure 43. Individual fiber of a used braid at 20,000 diameters: electrode holder region.

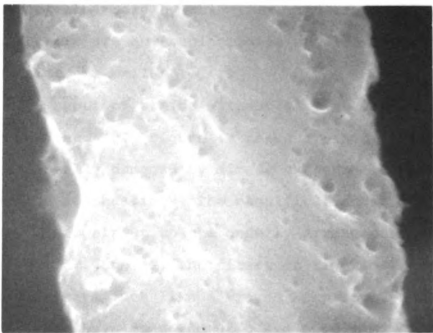


Figure 44. Individual fiber of a used braid at 20,000 diameters, with apparent extensive damage.

until the braid ruptures. A particularly battered fiber is illustrated in Figure 44. Here the pitting and scarring has progressed extensively, and the fiber is rapidly losing its mass and integrity. A final illustration is given in Figure 45 at 10,000 diameters. Here a fiber which does not appear to be badly damaged by pitting seems instead to be covered with deposited particulate matter. This is also reasonable in light of the fact that some of the dull appearance of a braid can be removed, and the shiny appearance restored, by simply rubbing a dull braid gently with one's finger. Finally, in Figure 46, a fiber is illustrated from the central, sample receiving portion of a braid that is very near to burnout. The dull appearance is beginning to extend into the center of the braid by this time, and expectedly, the fibers there are now beginning to show the pitted characteristics as well.

Two more types of braids without samples are shown in Figures 47 and 48. Figure 47 shows a braid that has been intentionally damaged by direct exposure to the atmosphere during heating. The magnification is 500 diameters. In contrast to the orderly arrangement of fibers seen in Figure 41, the fibers in Figure 47 are in great disarray, much like a frayed hemp rope, and large numbers of them have been ruptured and oxidized. Figure 48 shows a braid that has been in service at high temperatures, about 2200-2300° K, at a magnification of 100

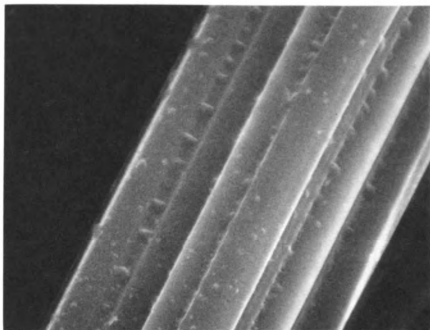


Figure 45. Individual fiber of a used braid at 10,000 diameters, with deposited particulates.

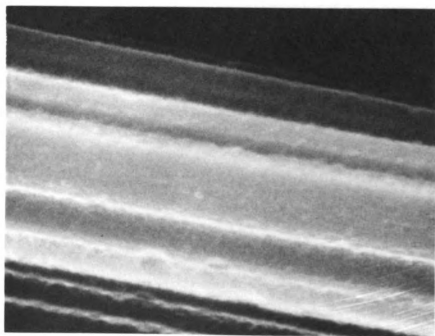


Figure 46. Individual fiber of an old braid at 20,000 diameters: central region.

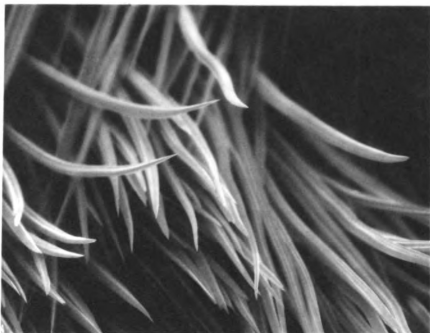


Figure 47. Braid intentionally damaged through atmospheric exposure, 500 diameters.

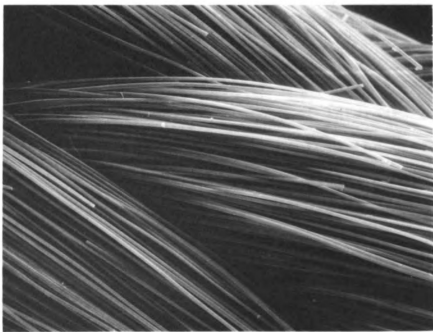


Figure 48. Braid used in high temperature work, 100 diameters.

diameters. Braids employed at the highest temperatures develop a shiny gray appearance in place of the usual black, and also seem to be perceptibly stiffer when handled. It was suspected that this was due to a marked change in fiber quality, such as the fusion of adjacent fibers together. However, Figure 48 shows that the braid is not greatly different in appearance from braids used at more conventional temperatures. Examinations at higher magnification show a similar lack of recognizable differences. Apparently, the alteration observed is one of the crystallinity of the graphite itself rather than a change in the surface structure.<sup>188</sup>

For the observation of desolvated samples on graphite braids, it was felt necessary to use sample solutions that were abnormally concentrated in order to assure that desolvated particles could be reliably found. The general procedure followed was to deposit a five microliter sample of a 1000 ppm solution of the element of interest, desolvate the sample, and then carefully package the braid at that point for transportation to Wyandotte. When these samples were subjected to analysis, it was found that even at such unrealistically high concentrations, authentic particles of desolvated sample were few and far between, and at times could not be located at all. This is somewhat surprising, as the volumes and concentrations of samples used should result in something like five to ten micrograms of salt crystals being desolvated. Some

possible explanations may be offered. First, the SEM can only observe the outermost fibers of the braid bundles. Considering that samples soak into the braid, it may well be that the great bulk of desolvation takes place in the braid interior, and that the population of salt particles is far denser within the depths of the fibers. Second, there is always the possibility of loss of the sample because of inevitable physical disturbances that occur when the loaded braid is stored for transport, or prepared for the microscope. With respect to the first problem, it might be suggested that an intentional spreading of the braid fibers before analysis to expose some of the interior regions might reveal an increased population of salt crystals. However, it is then equally obvious that any gains which might be realized through this procedure may be seriously offset by further disturbance of the braid, and consequent aggravation of the second mechanism. This is particularly so because unravelling of braid is not all that easy to do gently.

In spite of these problems, some authentic salt particles were located and identified with the x-ray microprobe, which was operated in the focussed spot mode. Figures 49 and 50 show, respectively, a copper nitrate and a nickel nitrate particle on braids examined at 10,000 diameters. (This is the magnification of all remaining pictures.) The copper particle measures about four  $\mu\text{m}$  long by three wide, whereas the nickel particle is

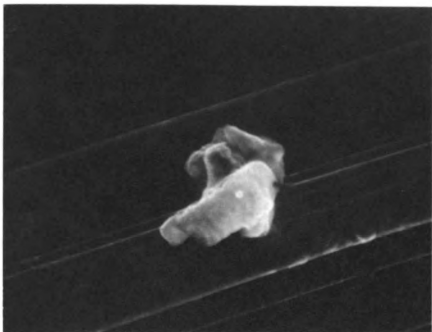


Figure 49. Copper nitrate salt particle on braid, 10,000 diameters.

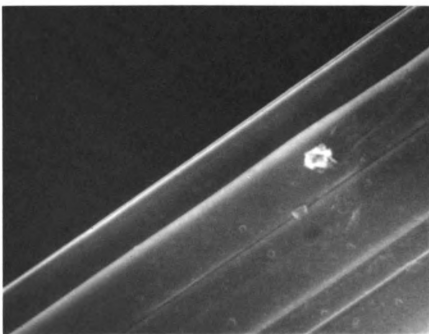


Figure 50. Nickel nitrate salt particle on braid, 10,000 diameters.

roughly spherical with a diameter of only 0.8  $\mu\text{m}$ . Such dimensions are rather typical of all particles located on the braids, which indicates that samples are desolvated as quite a few microcrystals of salt. This also attests to the braid's efficiency as an atomizer.

Figure 51 shows a phenomenon observed rather frequently with the braids, namely the presence of glass beads on the fibers. X-ray analysis shows a principal elemental composition of potassium, silicon, and calcium, with traces of iron, chromium, and titanium. Most of these elements are reported by Union Carbide to be present as trace impurities in braid.<sup>183</sup> The glass beads may well be formed from them upon heating and their common presence may stem from the fact that these braids were burned for only a few seconds to drive off the usual smoke before the sample was deposited. It may well be that if the braids had been used more extensively before being loaded with samples, many of the glass beads would have been volatilized away. In testimony to the sensitivity of the x-ray microprobe, it may also be mentioned that a fair number of particles found on these braids gave elemental compositions which strongly hinted that the particles were airborne chalk dust. (Calcium and sulfur peaks were quite prominent.)

Figure 52 shows a particle about two microns in diameter that was desolvated from a sample solution 500 ppm each in cadmium and zinc. X-ray microprobe analysis

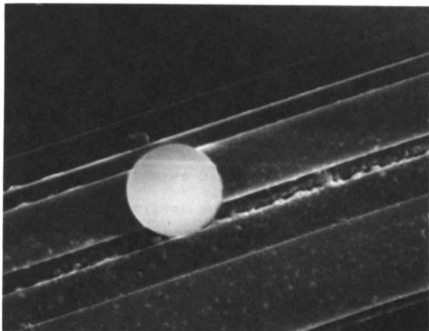


Figure 51. Glass bead on braid, 10,000 diameters.

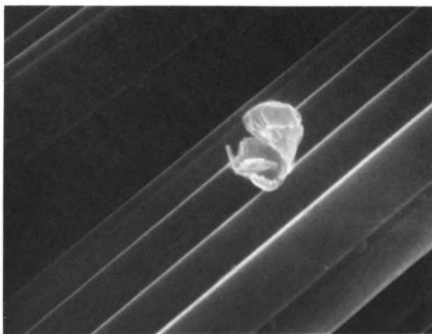


Figure 52. Combined cadmium and zinc nitrate salt particle on braid, 10,000 diameters.

revealed that this particle contained a mixture of salts of both elements. That they should have desolvated together is perhaps not too unusual, as both elements were in solution as the nitrates, and both occupy the same group in the periodic table. In contrast to this are the particles shown in Figures 53 and 54, which are, respectively, nitrates of silver and copper. Here the two were again present together in solution at a level of 500 ppm each, but desolvation seems to have occurred separately. (Another particle was located in which both were combined.) Here it may be that a separation occurred because, although both elements are again from the same periodic group, the copper ion has twice the charge of the silver ion. This may lead to sufficiently different crystallizing tendencies to promote separate growth. Most interesting is the observation that the silver particle appears to have exploded. It is quite likely that it originally desolvated as a crust of salt which surrounded a still liquid center. When the enclosed solution boiled to final dryness, it caused a violent and widespread rupturing of the outer salt shell. Such occurrences could constitute a source of imprecision in electrothermal atomic spectrometry if they are a common desolvation phenomenon because of a loss of analyte from the atomizer. The effect could be most severe in devices such as the more traditional filaments, which do not have the braid's soaking-in capabilities.

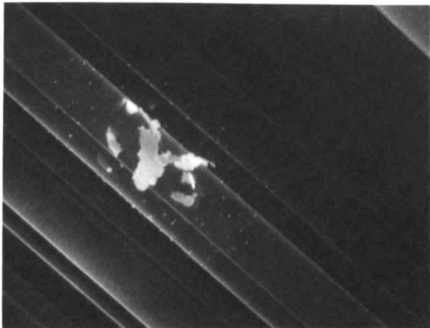


Figure 53. Exploded silver nitrate salt particle on braid, 10,000 diameters.

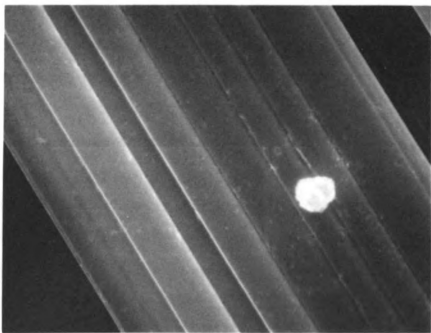


Figure 54. Copper nitrate salt particle on braid, 10,000 diameters.

In future applications of these studies it might be of interest to compare the physical appearance and performance of graphite braid to commercially produced graphite devices, or to some of the other types of filament atomizers such as metal foils and wires. Such devices should be equally easy to examine, as the electrical conductivity of the medium would still exist, and the lack of sample soaking would keep all of a desolvated sample in plain view on top of the atomizer for observation. In the cases of the metallic atomizers, there might be interesting trends in the progression of oxidation of the atomizer surface, with different chemical compositions at different depths. Different chemical deterioration with sample variety and sample matrix may occur as well. Electron microscopy would also permit a firsthand look at atomizer changes which occur as a result of lifetime enhancement techniques, such as the use of traces of methane in the sheath gas flow.

The greatest disappointment in the present work is the scarcity of salt particles seen even with enormously concentrated sample solutions. Reasons for this and the problems likely to be encountered in doing anything about them have already been touched upon. Perhaps one technique which might offer some assistance would be to unravel a braid prior to sample deposition, and then mount and deposit the sample upon only one bundle of fibers. This would in effect act like a miniature braid. With a

th  
wi  
pc  
re  
ex  
di

thin device such as this, and fewer fibers to contend with, it may be possible to locate and observe a dense population of salt particles, yet still have them be reasonably representative of the behavior likely to be experienced within the interior of an atomizer of full diameter.

AN EVALUATION OF THE RADIATION METHOD  
FOR ATOMIZER TEMPERATURE CONTROL

A. INTRODUCTION

One of the most important variables in atomic spectroscopy is the regulation of the temperature of the atomization device. In flame methods the atomization temperature is adjusted roughly by selection of the particular fuel and oxidant combination and finally through adjustment of the fuel-to-oxidant ratio. The hottest flame occurs at the stoichiometric mixture. Moreover, the regulation of temperature in the flame methods is largely self controlling. The flame is a dynamic medium, continually refreshed by new volumes of fuel and oxidant. A natural steady state condition is established between heat gained from further combustion and heat lost from convective and radiative dispersions. Given a high quality, reproducible gas flow controller and a well designed burner head, an extremely stable and well-behaved flame can be routinely produced. In electrochemical methods, the temperature is adjusted by the amount of power delivered to the atomizer from its supply, which gives the advantage of nearly continuous electrical selection of temperature up to the upper limit of the device in question. But the regulation of this temperature is a significant problem. The same atomizer must

be used repeatedly throughout a long lifetime. This can give rise to temperature drifts as the device ages, particularly since it must be driven from room temperature up to atomization temperature in the process of vaporizing samples. A flame burns steadily at the desired temperature, whether sample is present or not.

It was previously mentioned that there are (at present) four possible ways in which to regulate the heating of the graphite braid. These are the voltage developed across the braid, the current passing through it, the power dissipated by it, or the blackbody radiation emitted from it. The last method, regulation by monitoring of the blackbody emission intensity, is rather different from the others. Philosophically speaking, this is so because, of the four techniques, the first three are observing in one way or another a physical input to the braid, whereas the blackbody emission method, hereafter known as radiation programming, functions on the basis of a physical output from the braid. Radiation programming can, therefore, be free from the effects of some system parameters or errors which can greatly affect regulation performed with the other three methods.

## B. QUALITATIVE COMPARISON OF THE TECHNIQUES

The differences between radiation programming and the other methods are to an extent visible to the user when graphite braids are heated. A braid for which the electrical power dissipated, hereafter known as power programming, is the means of regulation can be observed to heat up to its final temperature with a sort of ramp function. A braid heated under radiation programming seems to flash up to the final temperature very quickly. This effect can be seen in the plots of Figure 55, which are oscilloscope photographs of signals from two different observation points in the braid power supply. The top two tracings show the voltage developed across the supply current sensing resistor for the two programming methods. In power programming (on the left), the current starts and remains at a more or less constant level, being changed only slightly as required by the power regulation. In radiation programming, however, the current begins with a near square wave rise to a very high value, follows this with a continued high level in which some fluctuation is observed as the supply recovers from the heavy drain, and then suddenly settles down to a low, quite constant level. The explanation is relatively simple. In radiation programming, blackbody emission must be developed from the braid to establish the regulated heating level. However, when power is first applied,

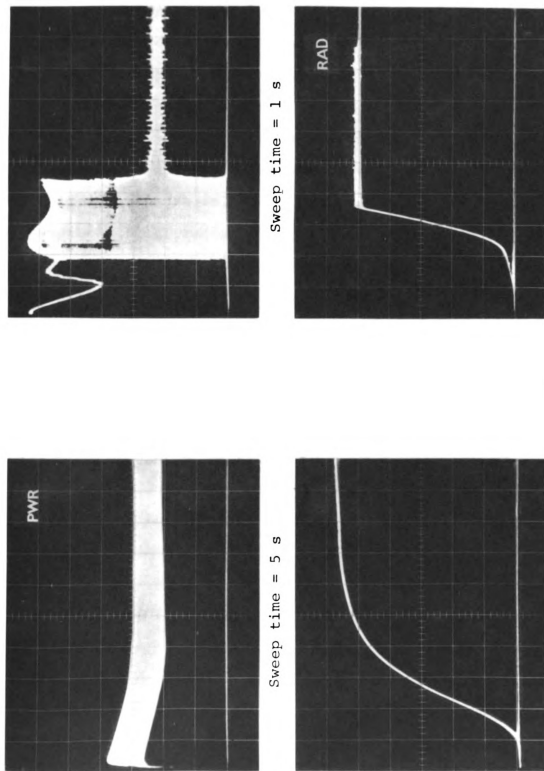


Figure 55. Oscilloscope photographs of power supply responses under radiation and power programming.

the braid is not incandescent, so the supply turns on very hard in an attempt to establish emission and stays on hard until emission is seen. As a consequence, the heating rate is very rapid compared to the power method. The bottom traces in Figure 55 show the signal developed from the braid-observing phototransistor under the same conditions. With the power method, the emission, and hence the braid temperature, rises smoothly but slowly to an asymptotic final value. In radiation programming, the temperature rises very quickly to the final value, reaches it with no appreciable overshoot, and then holds that level precisely for the remainder of the burn.

### C. TEMPERATURE CALIBRATION OF THE GRAPHITE BRAID

Blackbody emission from an object is described by the well known Stefan-Boltzmann expression, in which the total electromagnetic radiation emitted from a source is proportional to the fourth power of the absolute temperature of that source. As a consequence, radiation programming of an electrothermal atomizer carries with it the inherent possibility of accurate temperature calibration of the atomizer and a convenient way to monitor temperature in the output signal from the phototransistor. Such a temperature calibration was performed for the graphite braid.

At first it was proposed that the calibration be

done by burning the braid under radiation programming at a series of reference voltage and output operational amplifier switch settings and observing the blackbody emission at each with an optical pyrometer. A computer program was written which would burn the braid at user specified levels and times, allow delays for cooling of the braid between burns and sighting of the pyrometer. The pyrometrically determined temperatures would be entered by the user for statistical evaluation. After some preliminary work with the pyrometer however, it was decided that a complete pyrometric calibration would not be practical for two reasons. First, the graphite braid is not nearly as uniform in temperature as the pyrometer is intended to expect. The bundled, braided nature of the fibers gives rise to a fair amount of thermal texture in the atomizer, which is easily observable through a dark red filter. As a result, a consistently objective assessment of an average temperature against which to match the pyrometer filament is extremely difficult to make. The pyrometer setting may be easily shifted by fifty degrees and still give a filament color which could conceivably be taken as a reasonable average of the entire atomizer. Second, to get a reliable reading with the pyrometer, it is necessary to repeat the observation five or six times at each temperature, burning the braid about six seconds per observation. Under such conditions, an individual braid will not survive long enough to

complete an extensive calibration before burning out or aging beyond the point of reliability.

To overcome such difficulties, an alternate means of observing the blackbody was developed. A graphite braid was mounted, and one particular temperature was accurately determined with the pyrometer. The braid was then turned perpendicular to the optical axis and again heated to the same level. The blackbody emission was recorded by the spectroscopic instrumentation on a chart recorder with the monochromator set to 650 nm; the wavelength of the pyrometer. The braid was then burned at a regular series of additional levels. The intensity of each burn was recorded on the chart. Simultaneously with the acquisition of this data, a second chart recorder was used to record the corresponding phototransistor output signals.

Interpretation of the data was performed with the Planck equation for the spectral emission from a blackbody. According to this equation, the emission  $E$  of a blackbody at a wavelength  $\lambda$  and temperature  $T$  is given by:

$$E = \frac{\epsilon c_1 \lambda^{-5}}{(e^{c_2/T} - 1)}$$

where  $\epsilon$  is the emissivity (1 for a blackbody) and  $c_1$  and  $c_2$  are composite fundamental constants. This equation was solved for  $E$  at the braid temperature which

was determined with the optical pyrometer. The deflection obtained on the chart recorder for this temperature then served as a reference for all other temperatures examined. To determine any other temperature, it was merely necessary to multiply the reference emission value by the ratio of the chart deflections observed for the new and reference temperatures, and then reverse the Planck equation with the new emission value to yield the new temperature. For example, let us suppose that a temperature of 1500°K was determined for a braid with the pyrometer and that at this temperature, the chart recorder shows an arbitrary deflection of 200 mV. To determine the temperature which causes a 500 mV deflection, one first solves for the blackbody emission at 1500°K, with a result of  $0.4 \times 10^{-4} \text{ wsr}^{-1} \text{ cm}^{-2} \text{ nm}^{-1}$ . This value is then multiplied by the ratio of the two deflections, which yields  $1.0 \times 10^{-4} \text{ wsr}^{-1} \text{ cm}^{-2} \text{ nm}^{-1}$ . Finally, by reversing the Planck equation for this emission value, a temperature of 1599°K is obtained.

Fortunately, the assumption inherent in this process, that the braid is a perfect blackbody, does not influence the results. Strictly speaking, if the emission of a blackbody at a temperature  $T$  is  $E$ , then that of graphite at the same temperature will be  $\epsilon E$ , with  $\epsilon$  typically about 0.85 to 0.9 (89). After multiplication by the ratio of the chart deflections one obtains a new value  $\epsilon E'$  for the emission of graphite at the new temperature  $T'$ . To correct

this value back to that of a blackbody at  $T'$ , one must divide by the value of  $\epsilon$  for graphite. Thus, the emissivity cancels out, and the braid may be assumed to be a blackbody for purposes of the calculations.

With this method of observation, the braid needed to be burned only once at each setting to get an accurate reading, and the burn itself could be shortened to only a few seconds. This permitted not only completion of a calibration run on one braid, but even two complete repetitions of the entire run on the same braid for statistical evaluation. In addition, the chart deflections obtained are somewhat representative of the average temperature of the braid. The work was done with the monochromator slit open fully to 2 mm. Even with such a wide slit, the limited acceptance angle of the monochromator probably confines the region of the braid viewed to the central few millimeters. However, as this is the point at which samples are deposited, it may be argued that this region is the one for which a temperature calibration has most meaning.

Shown in Figure 56 is a family of curves giving the absolute temperature of the braid as a function of the reference voltage supplied from the DAC for a series of OA switch settings. The pyrometric reference temperature was obtained with a 5.00 volt DAC output on OA switch setting 1, for which the pyrometer gave a temperature of  $1571 \pm 7^\circ\text{K}$  from six averaged readings. (This particular

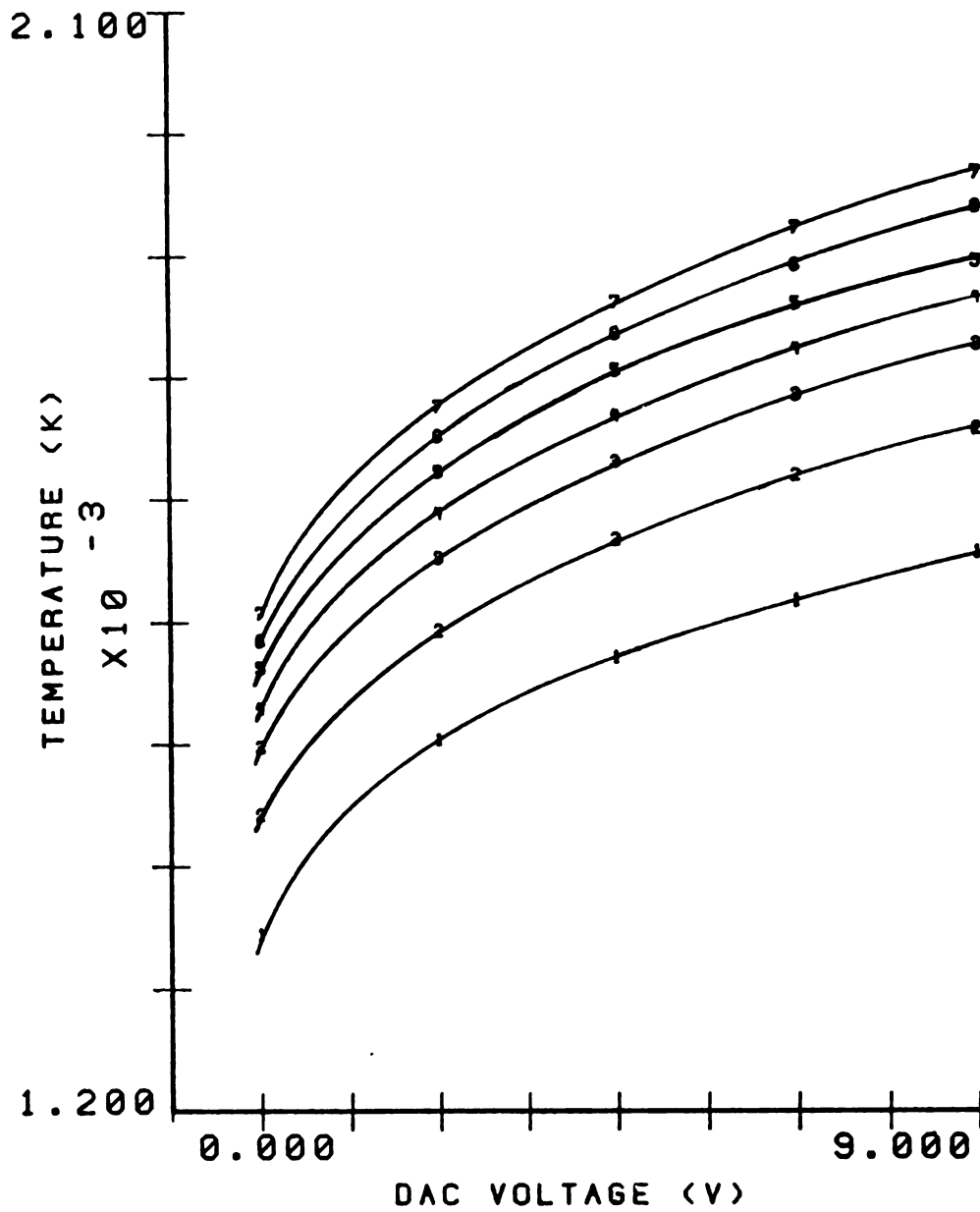


Figure 56. Temperature calibration of graphite braid with respect to reference voltage: low temperature region.

level was selected as being convenient to observe on the pyrometer.) The data points in Figure 56 are the average of three complete calibrations, which agree with each other at all points to within five or ten degrees. Agreement among different braids is on the order of ten to twenty degrees, which is only a factor of two or so above the statistical validity of the pyrometer. Some slight variation is to be expected among braids, because the exact orientation of given braids with respect to the phototransistor can vary and cause local minor inconsistencies in the distribution of temperature.

Calibration at temperatures higher than those shown here was not at first possible, as the phototransistor becomes saturated by directly observing temperatures above 2000°K. This causes the braid power supply to go out of regulation. To calibrate the upper temperature range, it was necessary to attenuate the light reaching the phototransistor. This was accomplished by inserting a small neutral density filter made from several glued layers of fogged spectrographic glass plate film in front of the transistor. Figure 57 shows a similar family of curves obtained with this filter for the high temperature range. With the filter, it is possible to drive the braid to the highest temperature attainable, about 2600°K. To get beyond this point, a different power supply would be required. At a level of 2600°K the present supply is dumping current continuously at 22-24 A, which closely

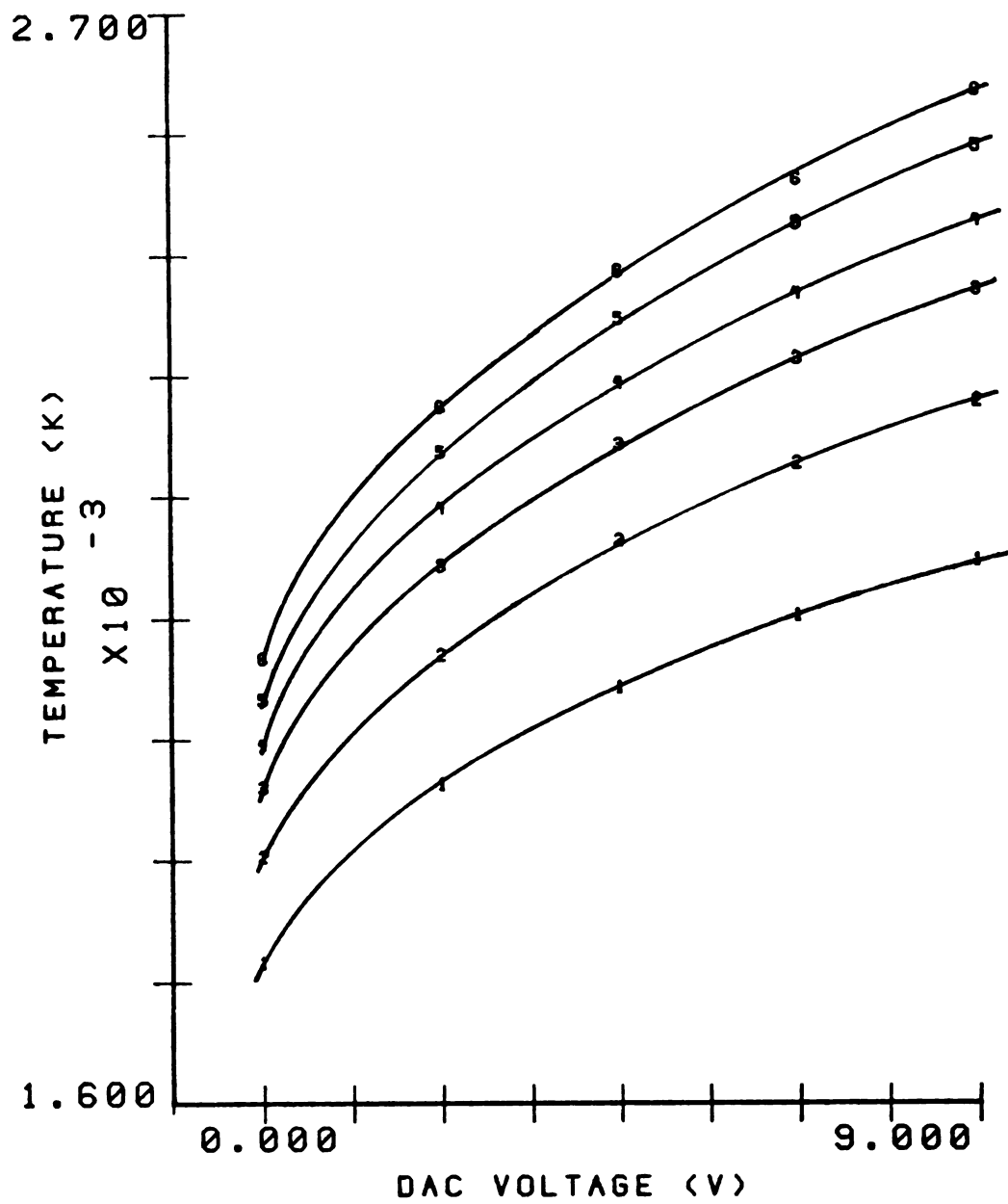


Figure 57. Temperature calibration of graphite braid with respect to reference voltage: high temperature region.

matches the maximum predicted current for a 50 V supply presented with approximately a  $2 \Omega$  load. Higher temperatures are probably not practical, however, as the braid suffers rapid and severe damage at such levels. Indeed, although the data of Figure 57 is again the average of three complete runs on the same braid, it was necessary to correct these runs for the damage suffered at the highest temperatures by reobserving the reference temperature level frequently throughout the data collection process. Because of this damage, the range previously quoted of ten to twenty degree accuracy for the drawn loci probably degrades to perhaps twice as much for the upper temperature end of Figure 57.

As a check on the accuracy of this method of calibration, the pyrometer was used to examine some of the calibrated temperatures. The results are shown in Table 14. Agreement between the two techniques is rather good.

The maximum temperature attainable is dictated by the limitations of the power supply. The minimum attainable is the lowest temperature at which the braid has sufficient incandescence to provide light to the phototransistor. For the present system, that limit occurs at about  $1100^{\circ}\text{K}$ . This limit could be extended downward if desired by use of a photosensor with better spectral response in the near infrared than the present device.

As previously mentioned, along with the blackbody emission data, a second chart recorder was simultaneously

Table 14. Comparison of Pyrometrically Observed Temperatures with the Present Method.

Present	Pyrometric
1345°K	1353 ± 6°K
1571	1563 ± 8
1608	1595 ± 6
1777	1779 ± 7
1861	1851 ± 12
1923	1919 ± 11
1968	1966 ± 5

run which observed the phototransistor output for each temperature level. These readings were highly reproducible, as they ultimately are compared directly to the reference voltage at the power supply control OA. Figures 58 and 59 show plots of the phototransistor output versus temperature for the low and high temperature ranges respectively. On these plots, of course, the data from all seven (six) curves overlay each other into one smooth locus. With the data of Figures 56-59 available, it is possible to select and monitor braid temperatures reliably if the braid in question is not excessively aged or otherwise damaged.

#### D. LONG TERM TEMPERATURE DRIFTS

Aging is inevitable in electrothermal atomizers. Regardless of the device employed, with constant use it will eventually deteriorate to the point where its performance is no longer acceptable. The principal variable to preserve during an atomizer's lifetime is again the temperature. The radiation programming method, because it monitors a quantity sensitively dependent on temperature, is a superior means of sustaining constant temperatures throughout the useful life of an atomizer.

The upper locus of Figure 60 shows a plot of the decay in intensity of the blackbody radiation typically observed throughout the lifetime of a graphite braid that is heated repeatedly under radiation programming to about 1500°K. The ordinate is scaled in arbitrary units of

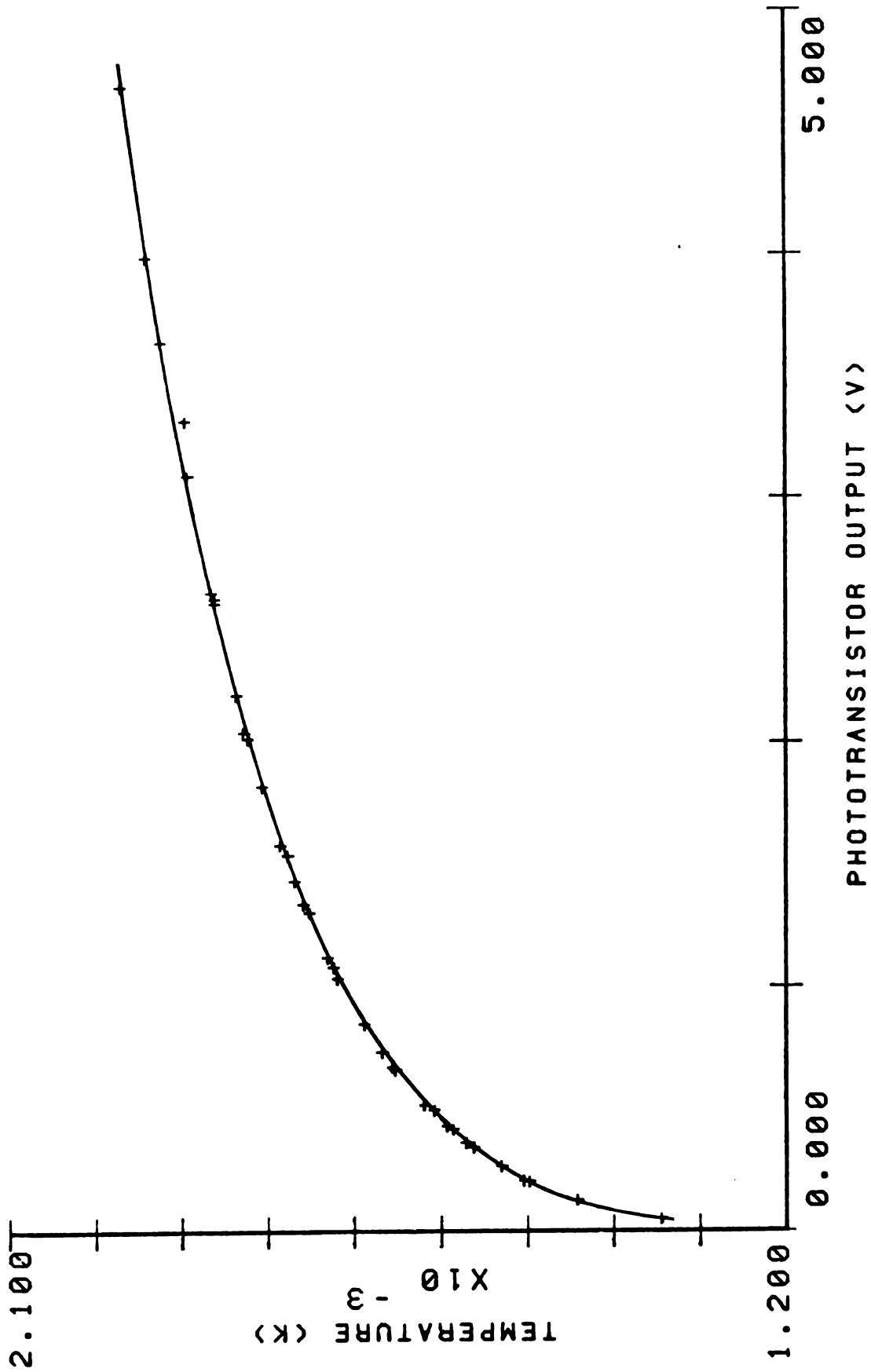


Figure 58. Temperature calibration of graphite braid with respect to photo-transistor output: low temperature region.

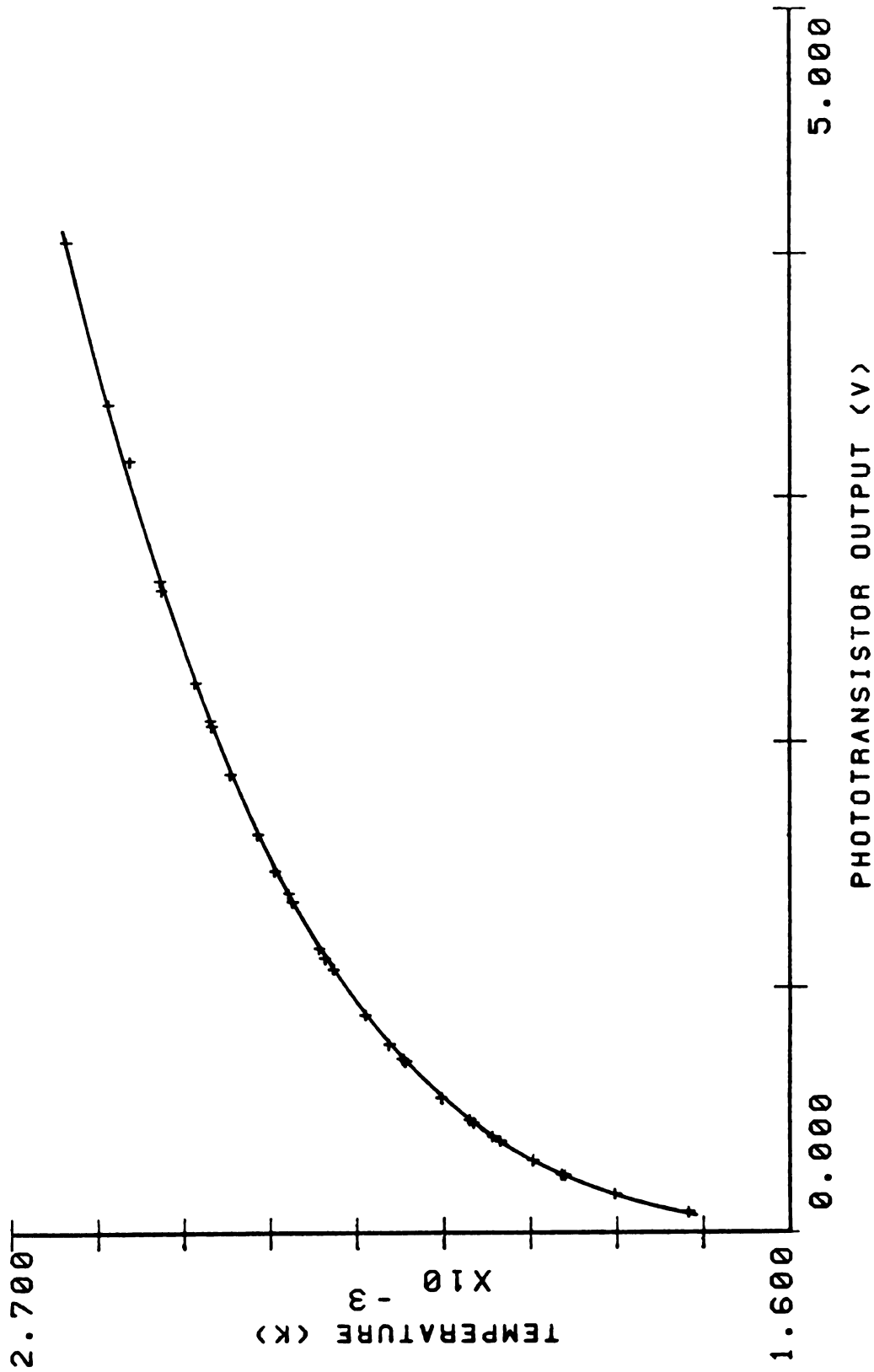


Figure 59. Temperature calibration of graphite braid with respect to phototransistor output: high temperature region.

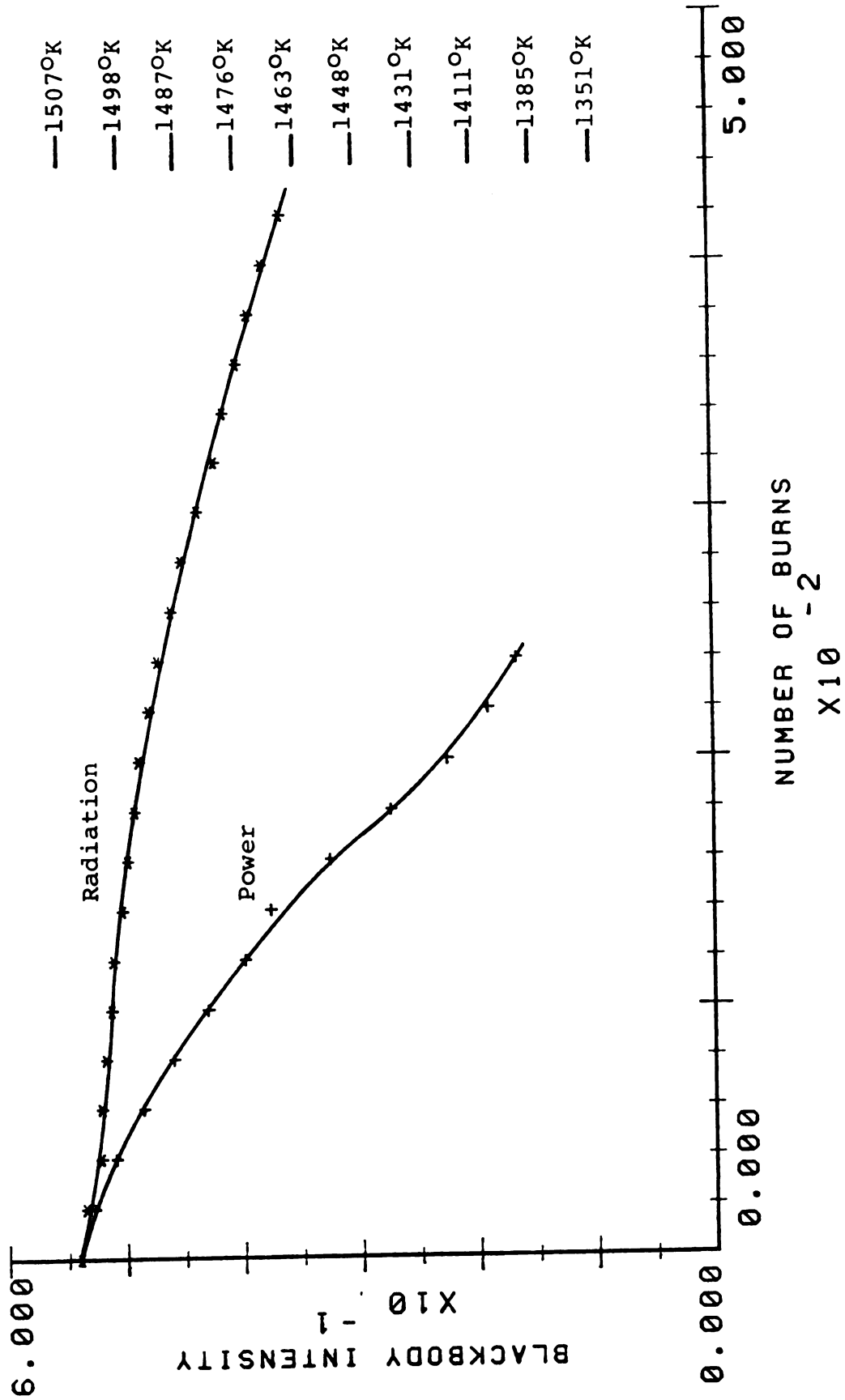


Figure 60. Temperature decay of graphite braid under radiation and power programming: low temperature.

blackbody intensity at 650 nm, as observed on a chart recorder, whereas the abscissa is scaled in number of burns, with each burn having a duration of three seconds. Along the right hand side of the plot are some temperatures appropriate to the decay observed. Throughout the total lifetime of the braid, the decay in temperature with radiation programming amounts to about  $50^{\circ}$ , or roughly three percent. Such a decay can be accounted for by observing visibly what happens to a braid as it ages at this temperature. With continued heating, damage begins to set in at the vicinity of the brass electrodes. This leads to a catastrophic mechanism of failure in which the damaged areas begin to dissipate abnormally large fractions of the total electrical power, which causes them to become hotter, and to experience yet greater damage. Several possible explanations might be offered for why the spots develop specifically at the electrodes. Because of the proximity to the chimney wall, this is the region of the least effective flow of sheath gas. In addition, the quality of the contact between individual fibers may be lessened by the mashing of the braid in the electrode grip. Finally, the bending of the braid at the electrodes in order to secure them may cause strains that rupture fibers under heating. Whatever the cause, the phototransistor which regulates the heating observes the braid at about a  $45^{\circ}$  angle, whereas the intensity data in Figure 60 were observed by the monochromator with the field of view confined

to the central few millimeters of the braid. Thus, as the hot spots develop, the phototransistor observes at least one of them directly, but the monochromator does not. The transistor is thus unduly influenced by the hot spots, and steadily cools the braid down.

The second locus shown in Figure 60 gives the analogous performance of a braid heated under power programming. The level of heating is that which eventually achieves the same final temperature as the corresponding level under radiation programming. The two loci have been normalized to the same initial value. Before discussing the second locus, a brief comment may be given on the comparison of the methods in this manner. It is not possible to compare the radiation and power methods fairly by simply having the times of heating in each burn be identical. As the photo tracings at the start of this chapter illustrated, radiation programming reaches the final temperature much faster than power programming. A fair comparison must account for this difference. When the data for the power locus of Figure 60 were taken, the burns were increased to six seconds each as an estimate of the required correction. At a later time, a more exact comparison was made in which an electronic integrator was used to sum the total area of the blackbody emission from single burns by the two methods. From these experiments it was found that one burn for three seconds at  $1500^{\circ}\text{K}$  under radiation

programming was equivalent to 0.98 burn for six seconds which approaches 1500 K under power programming. The original data for the power locus has thus been adjusted in Figure 60 to account for this slight correction, by lengthening the abscissa in the amount of 1.02. The superior performance of the radiation method for preserving constant temperature is obvious. The power locus decays about 115°K in temperature over a range in which radiation decays only about 15°K. This is a direct consequence of regulating with a temperature sensitive probe.

The same comparison of methods at the significantly higher temperature of about 1920°K is illustrated in Figure 61. The lengths of the original burns here were three seconds for radiation and four seconds for power. Integration of the blackbody as before yielded an equivalent of one radiation burn for every 1.1 power burns. The same general effect is seen, with the braid lifetimes generally reduced because of the higher temperature. The decay of the power locus is, however, even more severe than the radiation, with a loss of fully 300°K over a range in which the radiation method loses at most only 30°K. Such a large loss under power programming could easily upset analyses through several mechanisms. As the cooling progresses, the braid might lose its ability to atomize samples completely, or free them from stubborn matrices. Also, the atomic plume from a cool braid would be lowered and broadened with respect to that from a hot one, and

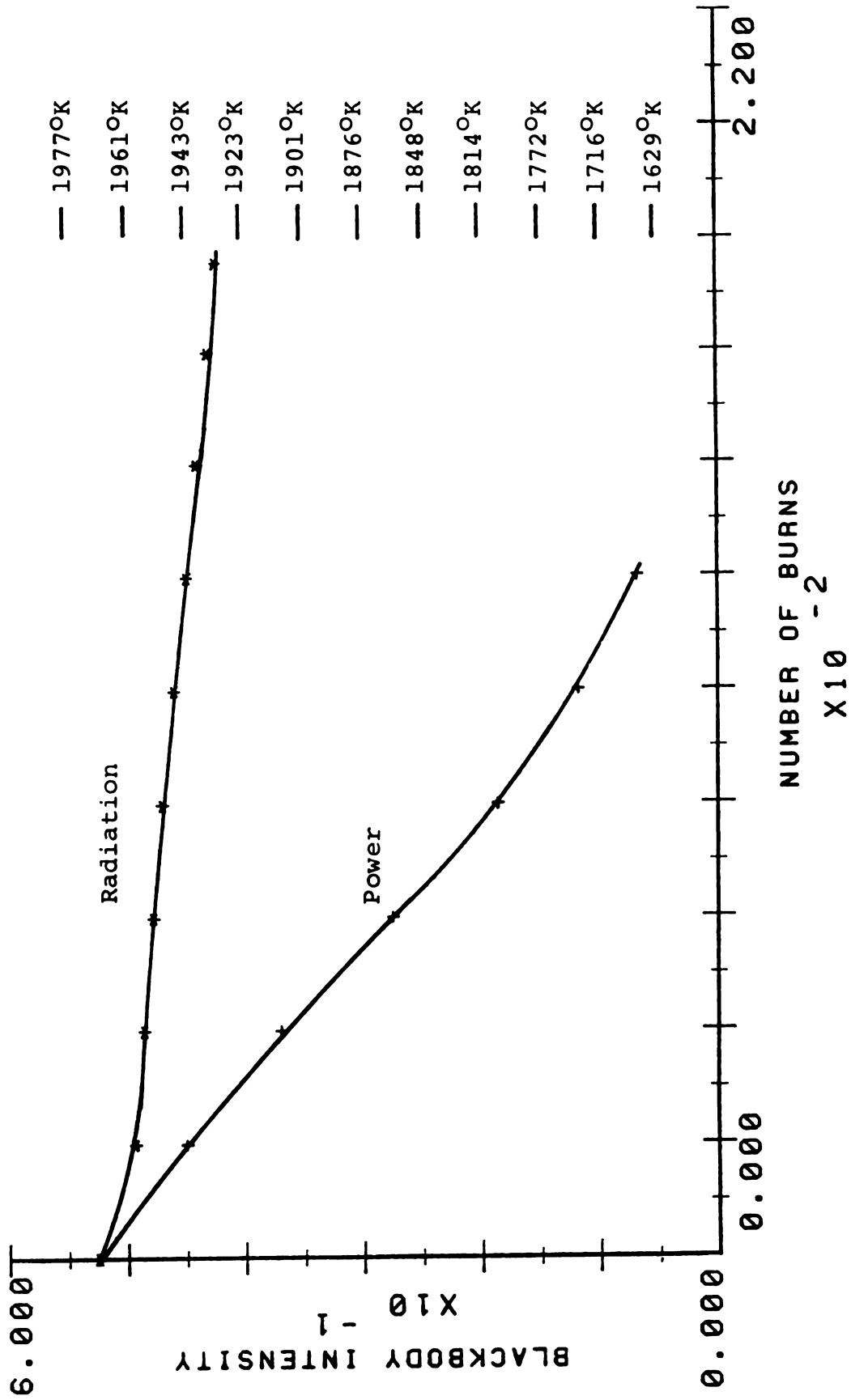


Figure 61. Temperature decay of graphite braid under radiation and power programming: moderate temperature.

differences in peak shape have already been shown to have great effect upon integrated absorbances.

One additional set of such temperature decay comparisons was also performed for a high temperature of about 2300°K. Some results of the study are presented in Figure 62. However, the examples shown are not totally representative. In contrast to Figures 60 and 61, in which a progressive loss in temperature is seen for both methods, the observations at the highest temperature were rather erratic. Under both radiation and power programming, the fluctuation in temperature throughout the braid lifetime was rather small, only a few tens of degrees, but it does not progress in a smooth decay. Instead, a region of decay might be observed at first, but later this might well be followed by a region of temperature gain. Such rather random alteration between gain and decay would continue down to the final burnout of the atomizer. This would generally occur after approximately 100-120 three second radiation burns or their power equivalent. A clue to an explanation for this altered behavior might be the change in appearance of braids with repeated heating at high levels. Hot spots do not seem to form as readily near the electrodes. In fact, the braid will almost always burn out somewhere in the middle section. The lack of the electrode hot spots may account considerably for the more nearly constant temperature-time curve under radiation programming. Perhaps, at high temperatures, the electrodes

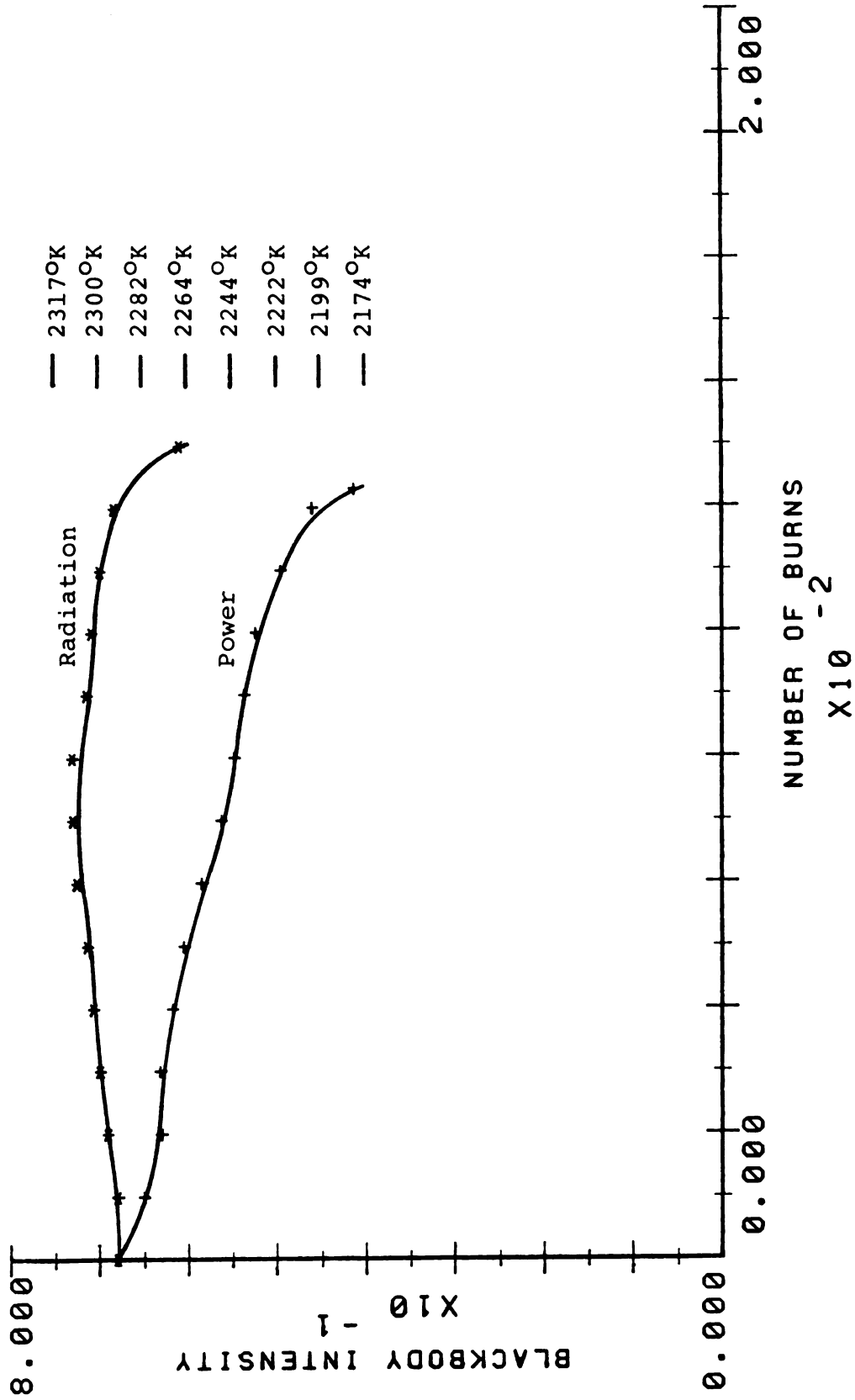


Figure 62. Temperature decay of graphite braid under radiation and power programming: high temperature.

function to conduct potentially damaging heat away from the braid ends.

#### E. SHEATH GAS FLOW AND CONTACT RESISTANCE EFFECTS

Two additional variables to which radiation programming of temperature should be immune are the rate of sheath gas flow and the possible presence of atomizer-electrode contact resistance. Comparisons of both radiation and power programming were performed for these variables. The effects of the sheath gas flow upon temperature were largely negligible. Theoretically, under power programming, the slower the flow of sheath gas, the less effective its contribution to the removal of heat from the atomizer, and thus the hotter the atomizer itself. It was found, however, that in varying the sheath flow from one to five liters per minute, no appreciable effect upon the braid emission intensity could be observed. Instead, the successive burns of the braid merely continued to reflect the usual slow decay of temperature with time similar to Figures 60 and 61, regardless of what the sheath flow did. The same behavior was of course observed for radiation programming. One curious and unexpected phenomenon was observed though. If the flow rate of the sheath gas were allowed to fall below about 1.25 liters per minute for either method of programming, the regulation of braid temperature seemed to be lost. In place of the usual smoothly rising

curves of emission intensity with time, the emission from the braid fluctuated wildly and randomly under power programming, and similarly although less severely under radiation programming. Furthermore, after restoration of more traditional flow rates, the emission intensity, and hence the braid temperature, was seen to have jumped significantly higher under either method of regulation. The explanation was revealed by a physical inspection of the braid. After being heated even only once or twice at the very low sheath gas flow rate, the braid became noticeably thinner and more worn in appearance, evidence of atmospheric damage. (Exposure of the braid directly to the atmosphere without any sheath will cause its destruction with only a few burns at even low temperatures.) Apparently with excessively low sheath flow rates, the feeble movement of sheath gas can be very easily upset by the convective currents produced by the hot braid. As a result, atmospheric oxygen from the top of the chimney can be caught in these currents and swept down to the braid itself. The fact that the temperature of the damaged braid is higher after restoration of normal sheath gas flow can be explained in light of this damage. In power programming, the braid will have lost some of its original mass, and obviously goes to higher temperatures if still controlled to dissipate the same amount of power. In radiation programming, the regulating phototransistor still demands the same amount of light flux to establish the proper output

signal. Thus, a smaller braid of decreased size, and consequent decreased apparent light-emitting surface area, must go to higher temperatures to supply the required light. This illustrates well the fact that even radiation programming is not the ultimate temperature regulating technique for electrothermal atomic spectroscopy. Even though black-body intensity depends only upon temperature, any real system which uses radiation programming will still have optical and physical variables associated with it which can affect both the means and amount of observation of atomizer emission.

The presence of contact resistance between the atomizer and electrodes was simulated by introducing a  $0.27 \Omega$  resistor in series with the braid. The results were as expected. With radiation programming, the phototransistor simply calls for more power from the supply to preserve the required level of emission intensity. With power programming, a large reduction in temperature is observed as the resistor dissipates a significant fraction of the allotted power. The practical meaning of these observations was brought to light with some experiments on how the temperature of the braid varies with the technique employed to mount braids in the electrodes. Comparisons were taken of the emission from four mountings. The first was normal. The second was somewhat loose, in the sense that the braid was slightly long and curved upward in the middle. A third was tightly stretched between the electrodes, and

the fourth was normal, but with the grip of one electrode poorly secured. For both regulation methods, the first three types of mounts gave very comparable emission levels. Some slight differences were seen, but they did not follow any regular trend, and amounted to temperature changes of only a few degrees. This is reassuring in the sense that it is not essential to have an exceptionally rigorous or reproducible technique to follow when mounting braids. If reasonable care is taken, any temperature differences caused by variations in operator mounting technique are quite negligible. The last variant mentioned above (a poorly secured holder) did, however, show an adverse effect on results. Essentially, it created a contact resistance, which under power programming caused a severe drop in temperature. Even though radiation programming acts to correct this problem, it is to be avoided, because the offending electrode is subjected to severe overheating as it dissipates the excess power.

#### F. PERFORMANCE OF METHODS DURING ATOMIZATIONS

After investigating the physical parameters of performance for the two programming methods, they were compared chemically as well by performing atomizations of selected elements at different temperatures. For each element in question, a recommended analysis wavelength was selected with the monochromator, and the photomultiplier

and amplifier gains were adjusted to yield a full-scale, 100%T level of nearly ten volts at the A/D converter, with the appropriate hollow cathode lamp operated at its maximum recommended current. The solutions analyzed were prepared from deionized water stocks of the pure salts and were intentionally selected to be of significant concentration so as to obtain strong, relatively noise-free signals. Five elements were investigated. They were cadmium, lead, silver, copper and nickel, listed here in order of increasing temperature required for atomization. The various system parameters for each of these elements are given in Table 15. For each element, a number of equivalent atomizations was done at each of a series of temperatures under radiation programming. The normal output of peak absorbance, time of peak absorbance, and integrated absorbance was logged by the line printer. A second set of data was then taken in which five atomizations were done at each temperature, and the point by point absorbance readings along each transient were stored on floppy disc. At a later time, another computer routine read and averaged these five stored peaks into one composite, representative peak, and printed the averaged readings on the line printer.

An identical procedure was followed as well for atomizations performed under power programming. In each case, the heating level chosen for a group of power programmed atomizations was carefully selected so as to yield ultimately the same final temperature of the braid as the

Table 15. Instrumental Parameters for the Comparison of Radiation and Power Programming.

Element	Conc.	Matrix	Temp.	Wavelength HCDT	PM Volt	Amp Gain
Cd	5ppm	CdCl <sub>2</sub>	1280°K	326.1nm	720V	10 <sup>7</sup> V/A
			1440			
			1600			
			1760			
Pb	1ppm	Pb(NO <sub>3</sub> ) <sub>2</sub>	1280°K	283.3nm	640V	10 <sup>9</sup> V/A
			1440			
			1600			
			1760			
Ag	1ppm	AgNO <sub>3</sub>	1280°K	328.1nm	760V	10 <sup>8</sup> V/A
			1405			
			1535			
			1695			
Cu	1ppm	Cu(NO <sub>3</sub> ) <sub>2</sub>	1775°K	324.7nm	820V	10 <sup>7</sup> V/A
			1865			
			1975			
			2115			
Ni	2ppm	Ni(Cl) <sub>2</sub>	2200°K	232.0nm	700V*	10 <sup>9</sup> V/A
			2330			
			2450			

\* Solar blind tube.

Constants: Sample size: 2 ul; Slit width: 200 um; Position of cell: Horizontal - 0.0mm, Vertical - 3.0mm; Sheath Gas flow: 3 liter/minute; Amplifier rise time: 30 ms.

corresponding data under radiation programming.

Shown in Figure 63 is a plot of absorbance versus time peak shapes for cadmium samples atomized under radiation programming at four temperatures. (The data for the three highest temperatures are essentially superimposable.) All of the peaks are well shaped Gaussians, which rise to a peak absorbance about 0.14 second after the onset of atomization, and return to baseline in 0.50 second. In contrast to this are the corresponding plots done under power programming illustrated in Figure 64. Here the four peaks are well separated. The times required for atomization are significantly longer, even for the highest temperatures. Furthermore, the peak absorbances obtained are much lower than those observed with radiation programming. These facts are well brought out by the superimposed radiation programmed peak repeated from Figure 63 with the dotted line.

Figures 65-72 illustrate the analogous data obtained for the other four elements. Consistently, the radiation method of programming gives rise to atomizations that are accomplished in less time and with higher peak absorbances than the power method. In fact, at the highest radiation programmed temperature for all elements studied, the transients assume a rather good Gaussian shape. With all elements available for comparison, some additional conclusions may be drawn from details of the plots.

The cadmium and lead data are extremely similar to

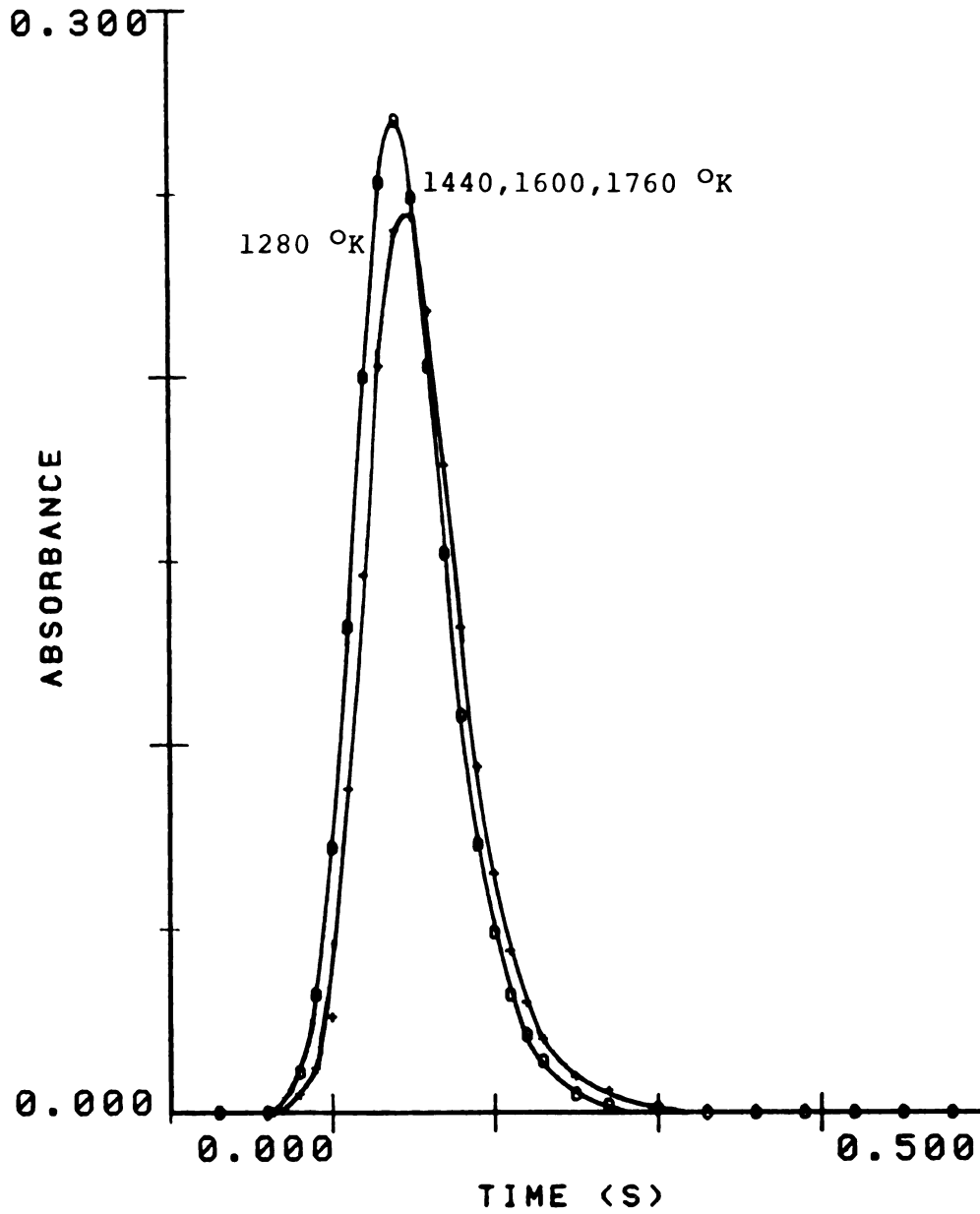


Figure 63. Cadmium transients under radiation programming.

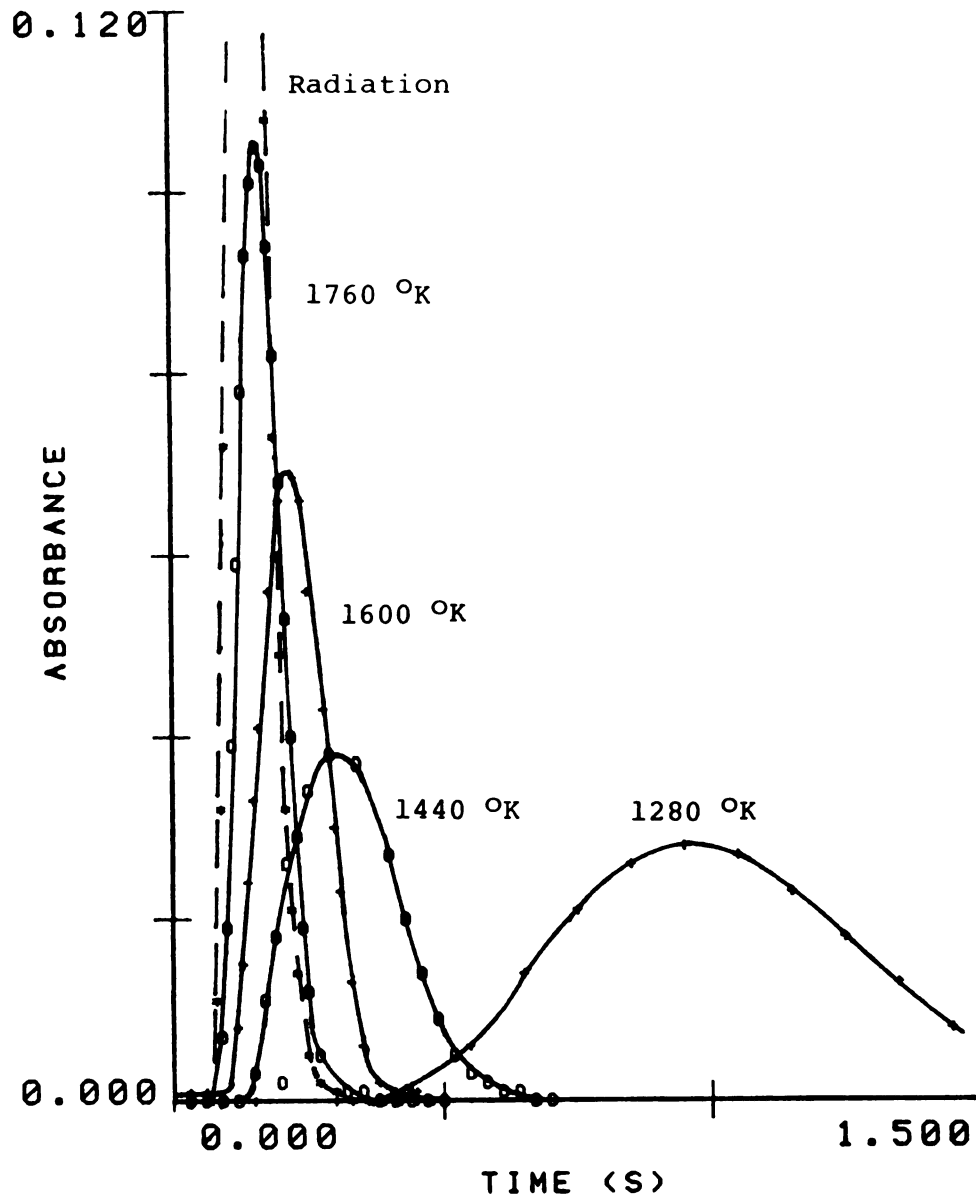


Figure 64. Cadmium transients under power programming.

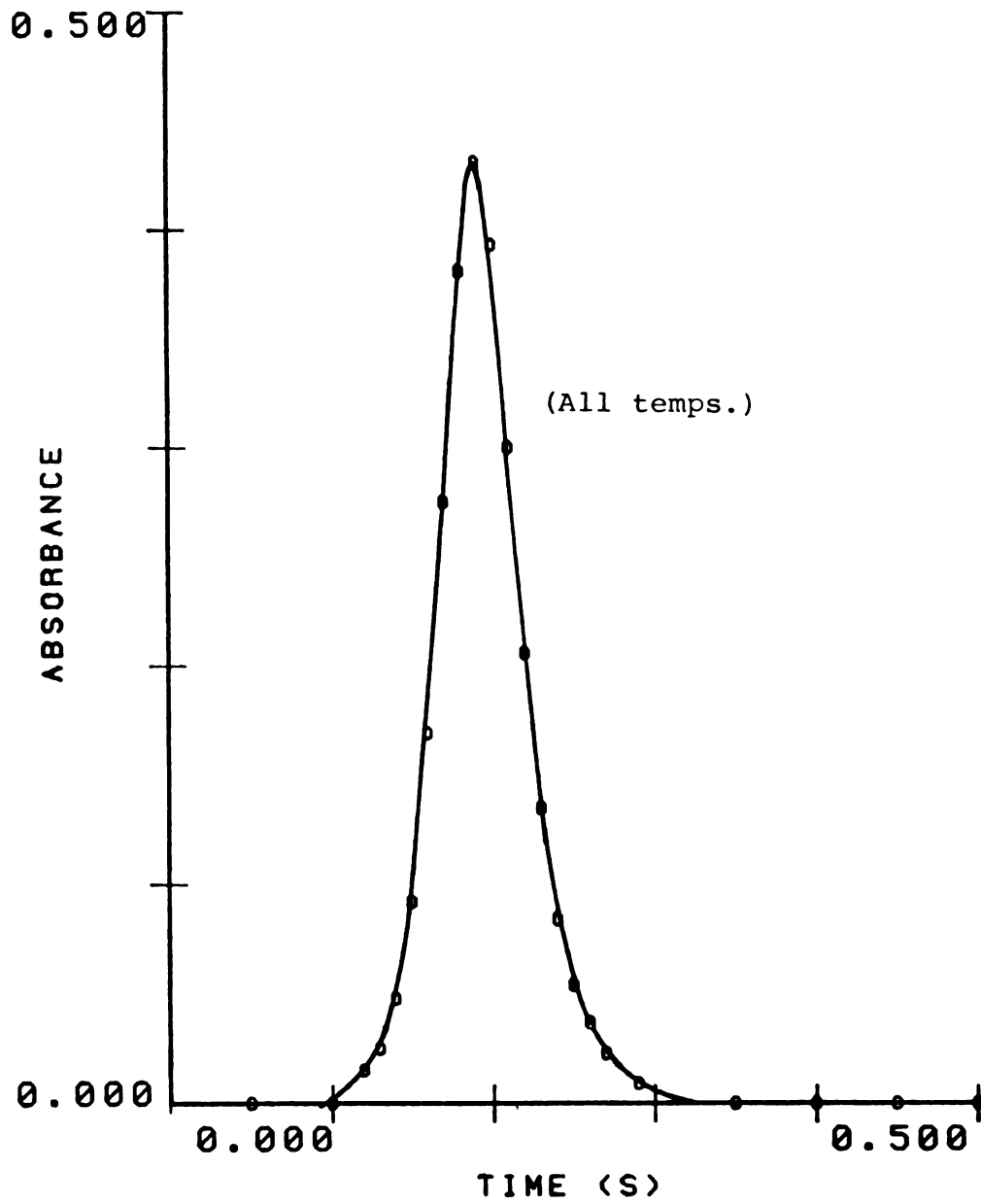


Figure 65. Lead transients under radiation programming.

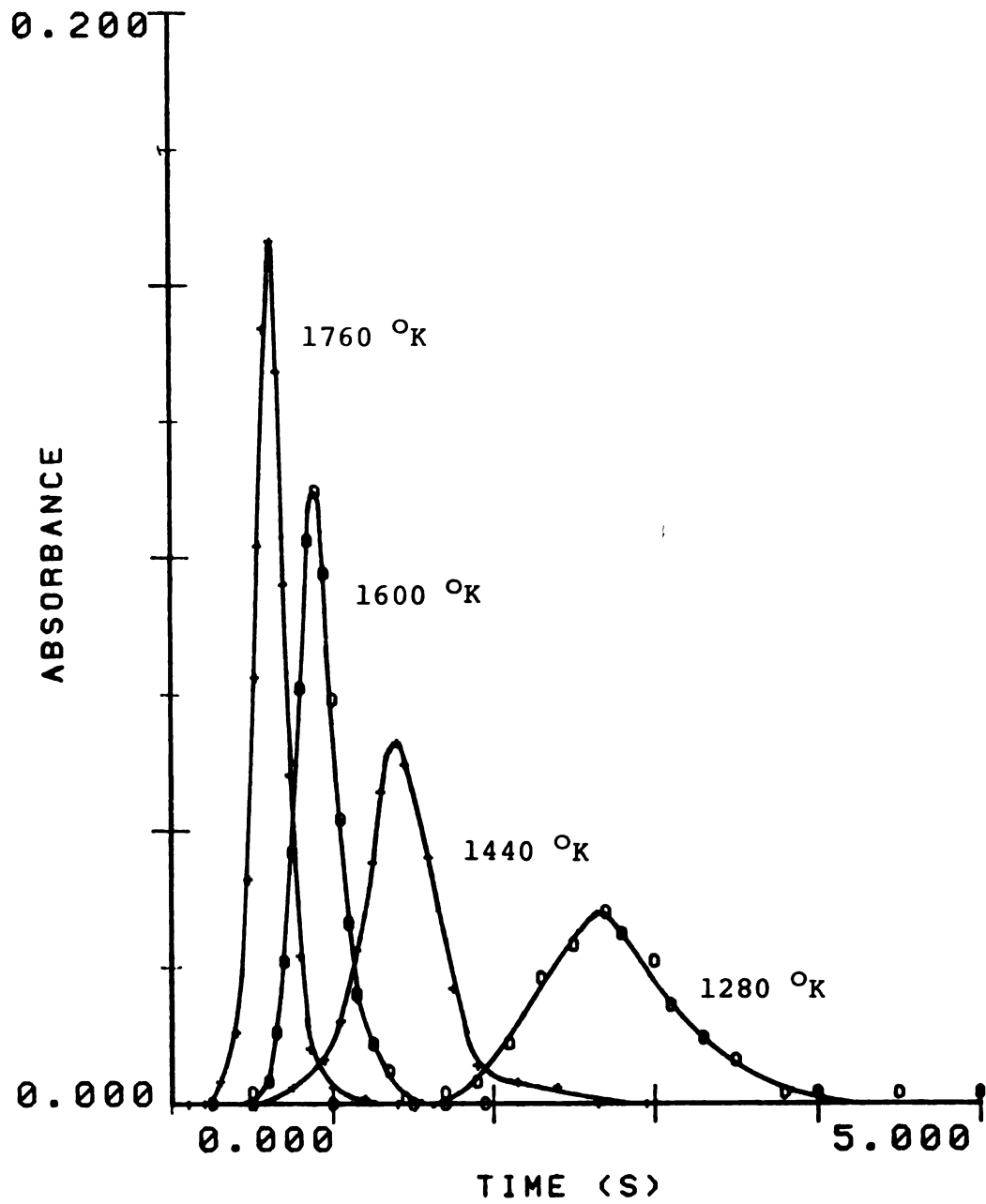


Figure 66. Lead transients under power programming.

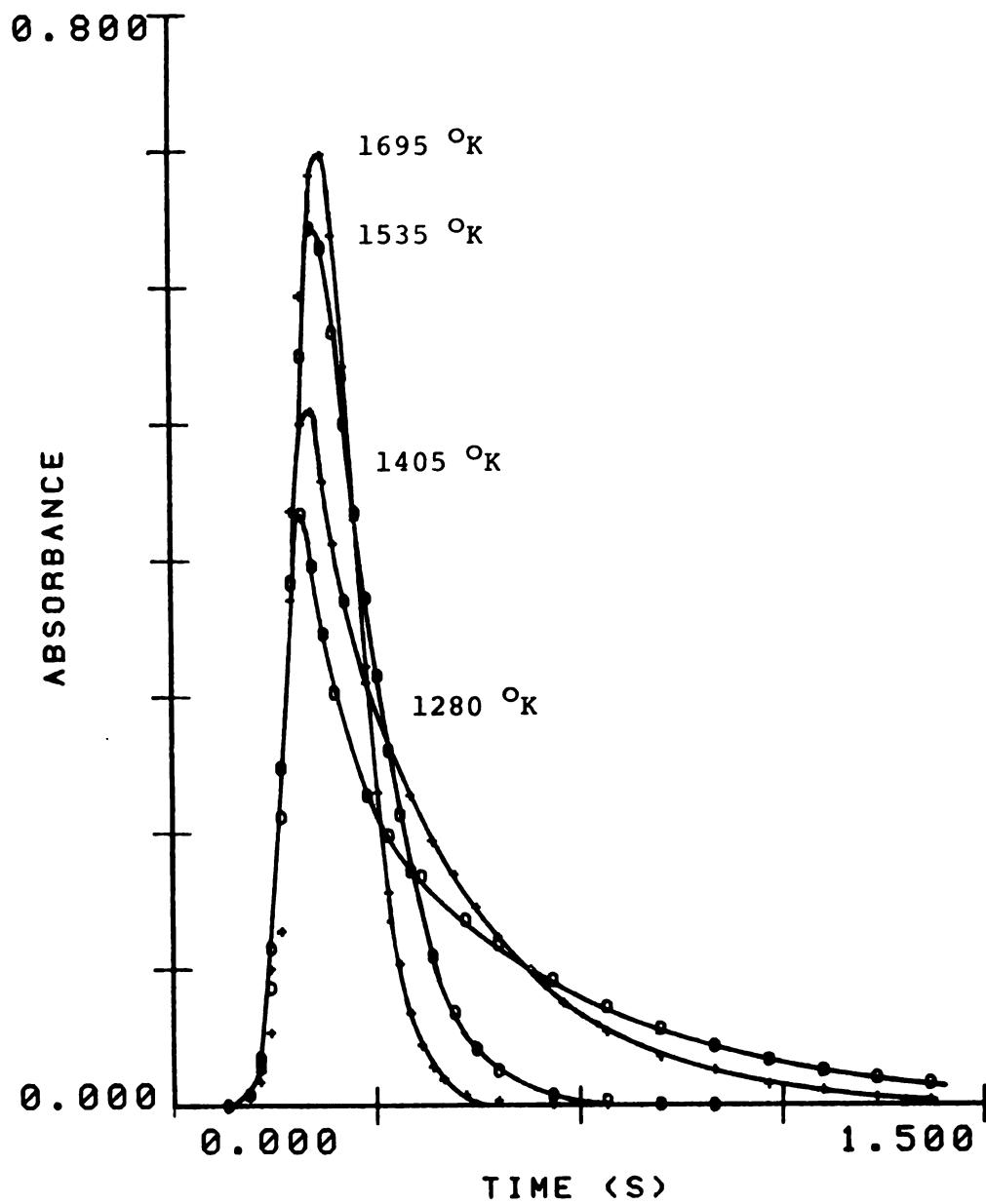


Figure 67. Silver transients under radiation programming.

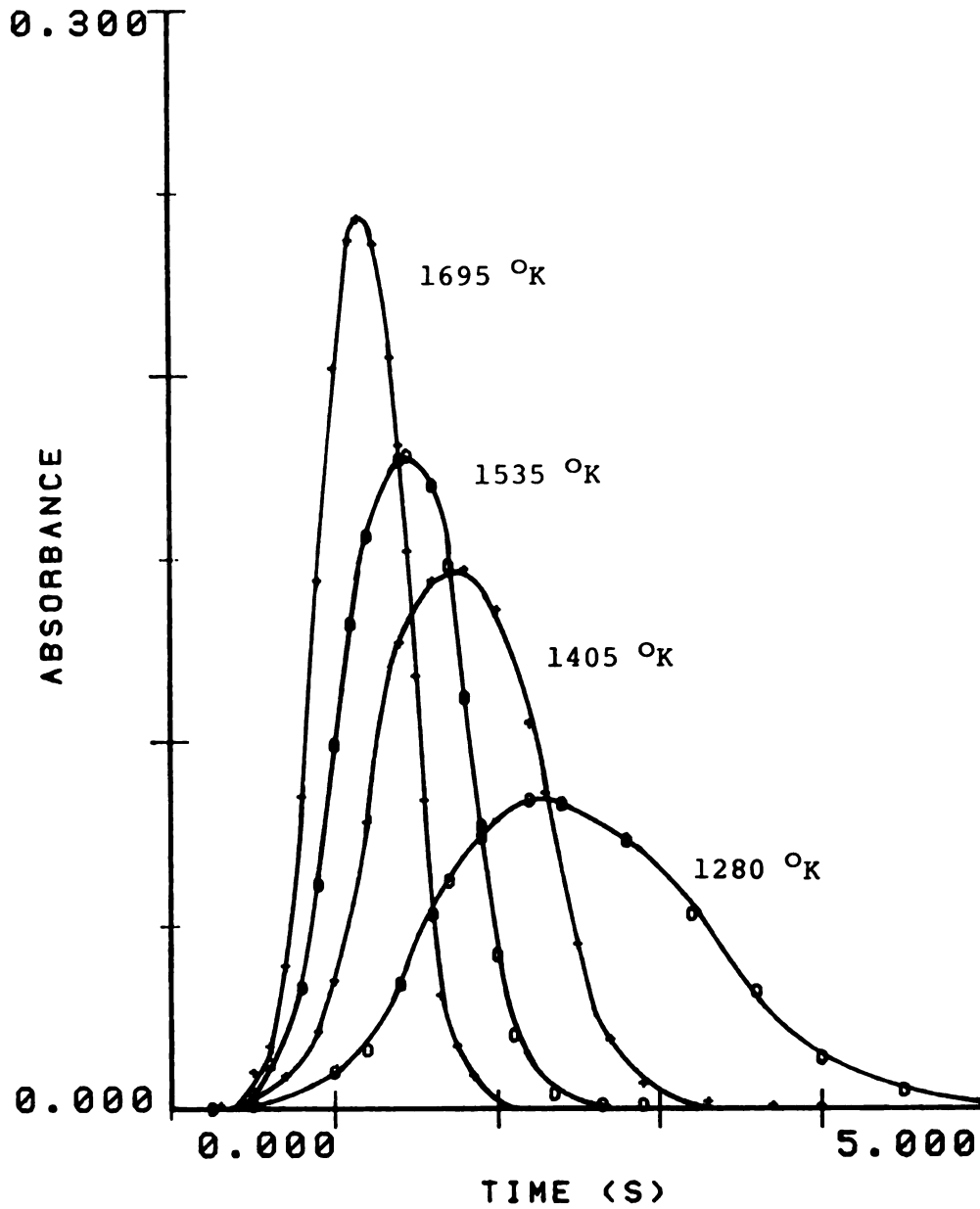


Figure 68. Silver transients under power programming.

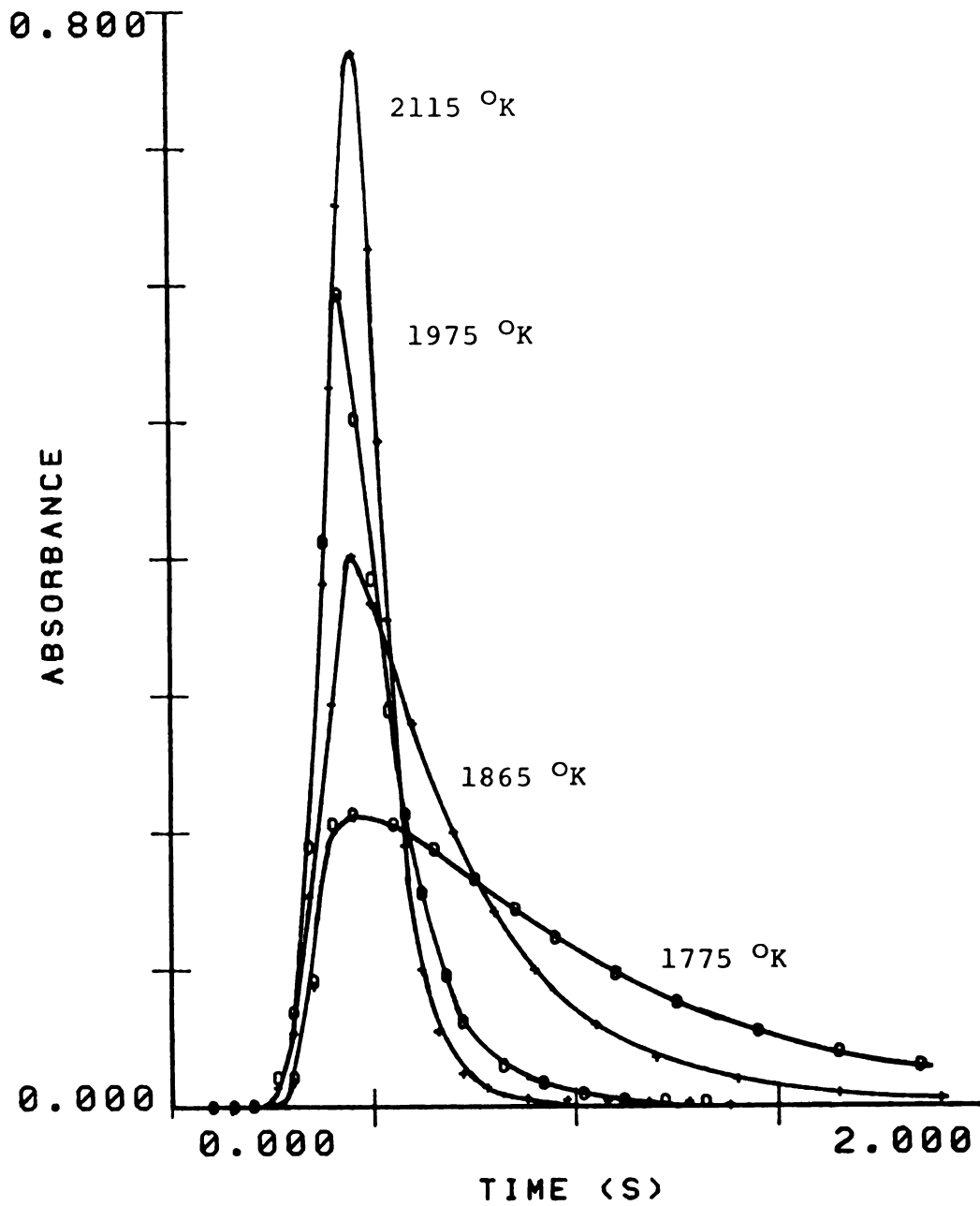


Figure 69. Copper transients under radiation programming.

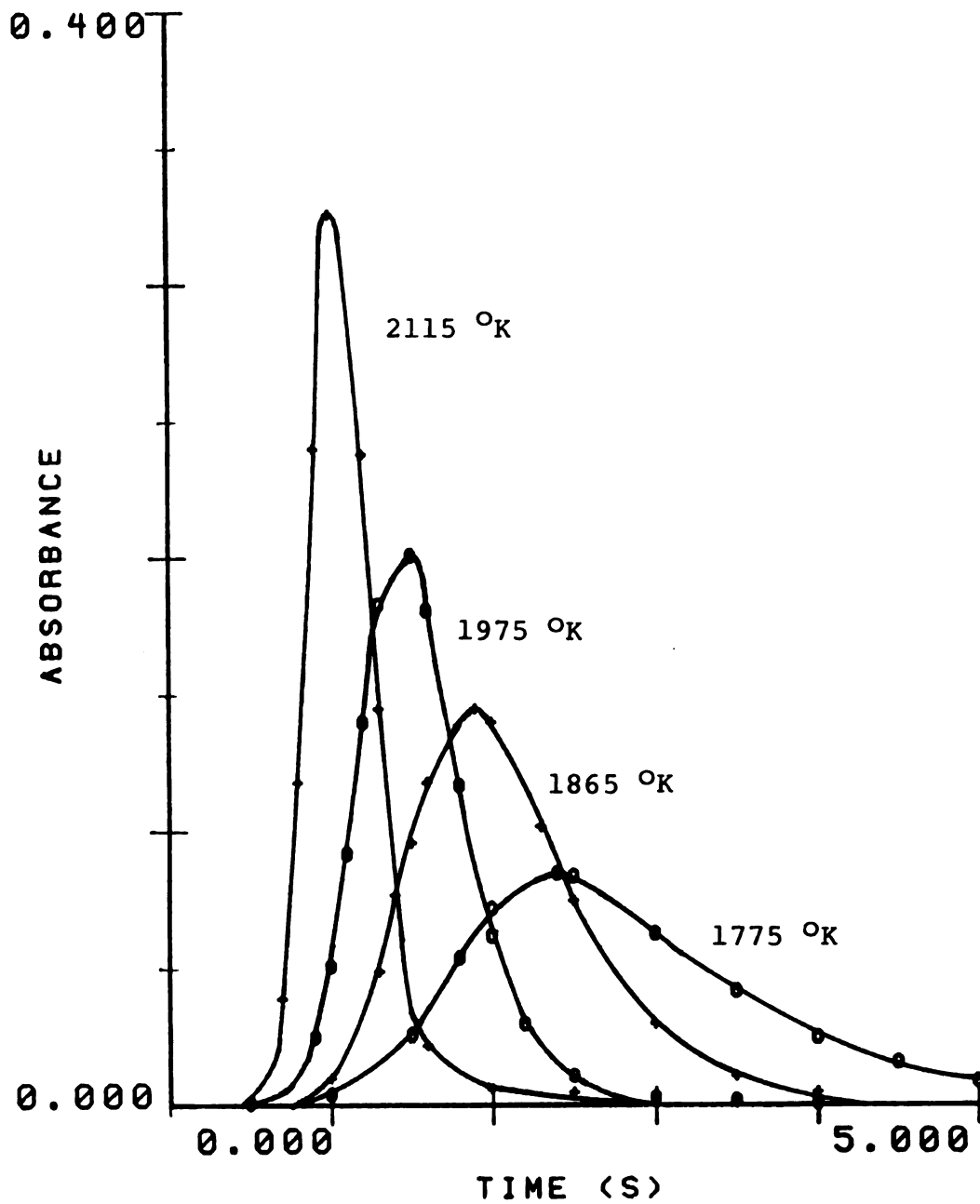


Figure 70. Copper transients under power programming.

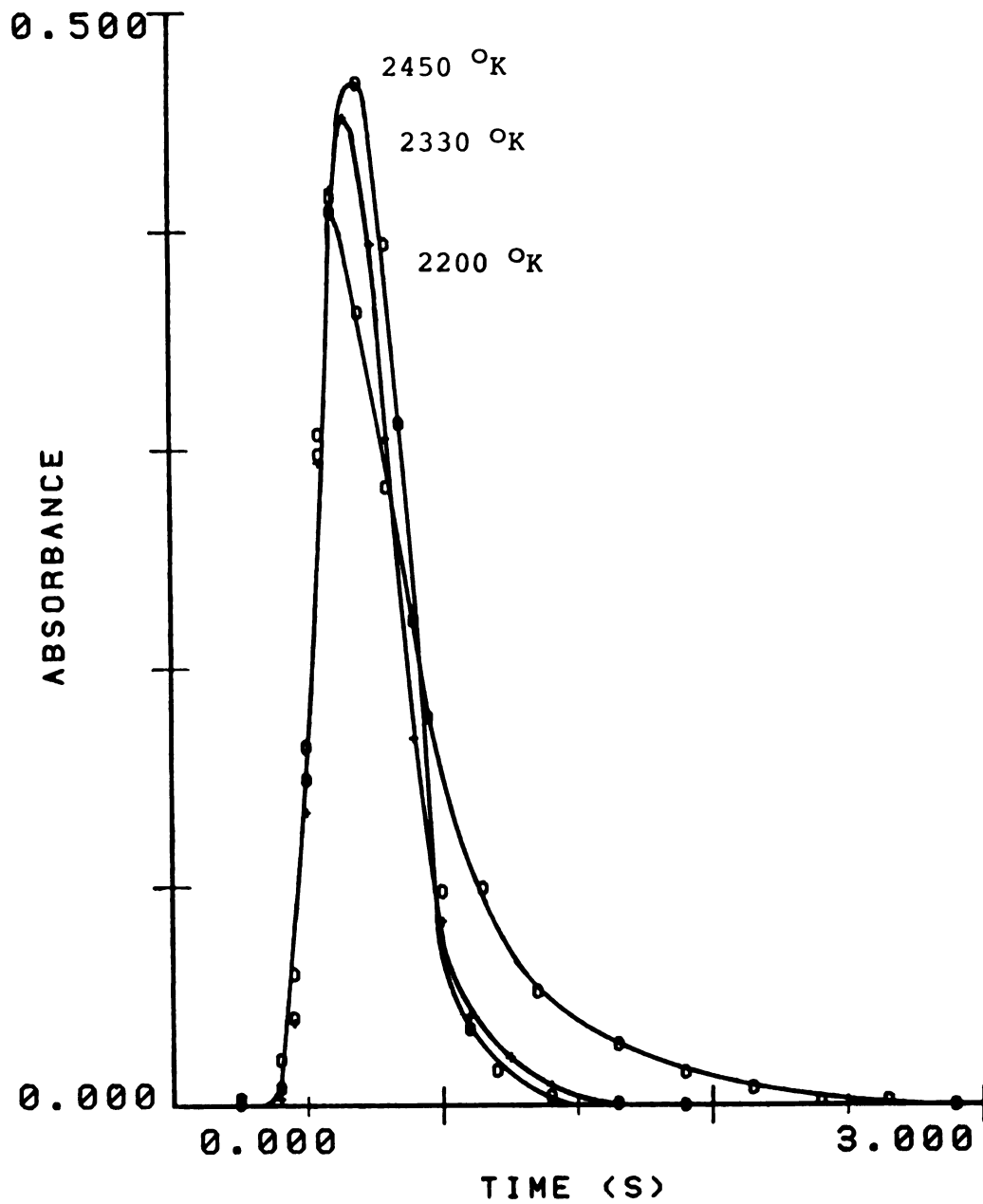


Figure 71. Nickel transients under radiation programming.

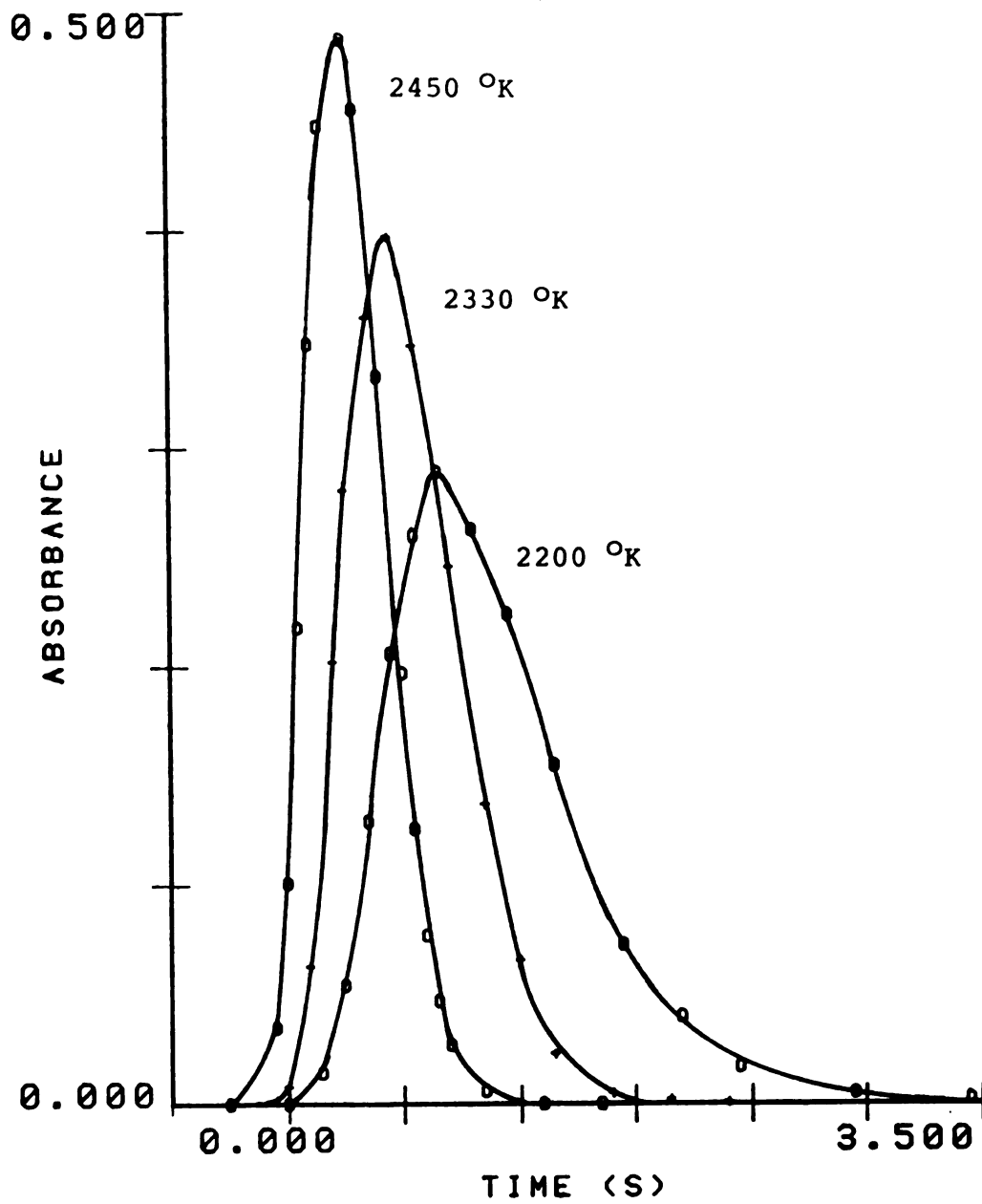


Figure 72. Nickel transients under power programming.

each other, as is expected from their similar volatility. It can now be seen that the plots for these elements overlay each other under radiation programming because even the lowest temperature investigated for them is significantly in excess of the minimum required to atomize effectively. The Gaussian peak shape merely reflects the kinetic process of getting all of the sample out of the braid. In fact, the minimum attainable temperature with radiation programming is probably sufficient to atomize cadmium and lead. In the case of silver it is possible to see the effect of temperature in the radiation mode. The peaks begin low, broad, and asymmetric, and gradually lose these qualities as they become Gaussian. The power mode peaks for silver do not show the asymmetry that radiation does, which reflects the slower rise time of temperature under power programming. These effects are even more pronounced for copper. In fact, the copper peaks under radiation programming resemble somewhat the appearance of a Gaussian peak affected by a low pass filter of varying time constants. Finally, the nickel results begin to de-emphasize the differences between radiation and power programming. The radiation method is still at an advantage, but because the power supply for the braid is now approaching the upper limit of its capabilities, the advantage of radiation programming is beginning to level off.

One consequence of the use of radiation programming is seen in Figure 73, namely, the effect of readout time

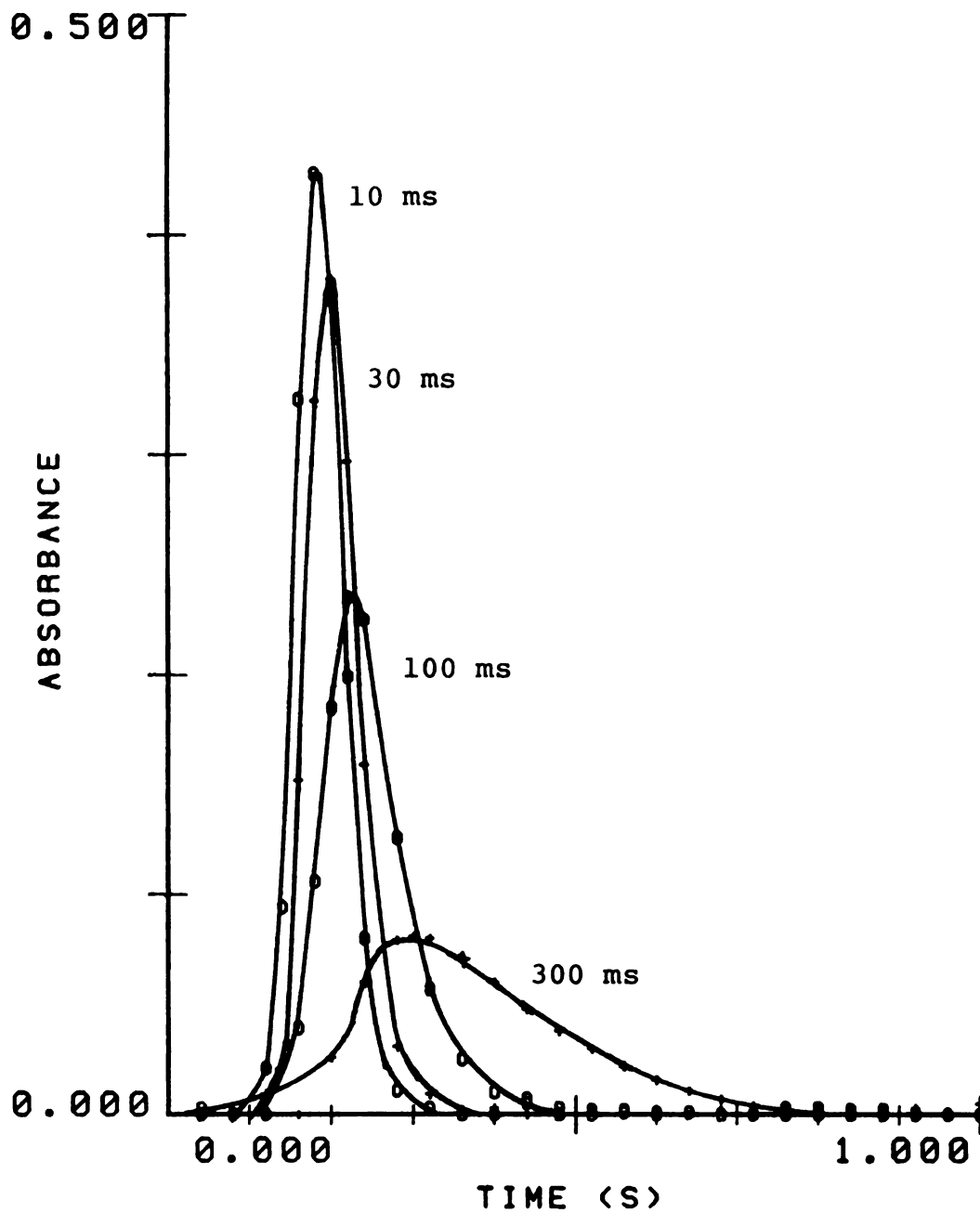


Figure 73. Distortion of transients under radiation programming by readout time constants.

constants upon the data. From the peak shapes for lead illustrated, a small but noticeable improvement in the true peak shape still occurs in going from an amplifier rise time of 30 ms, as was used for Figures 63-72, to one of only 10 ms. This would seem to indicate that use of radiation programming almost necessitates an all electronic readout; mechanical systems, even with fast response chart recorders, might not be quick enough to present properly the fast transients obtained for volatile elements on a radiation programmed instrument.

An area of possible future interest with these studies is the opportunity of "dematrixing" a complex sample. With the rapid heating and precise temperature control afforded by radiation programming, a multistep atomization sequence might often be beneficial in providing sequential volatilization of several components in a single sample. Multielement analysis is not presently possible at all with the current system of instrumentation; however, a crude simulation of this concept was attempted. Three solutions were prepared in deionized water: 5 ppm cadmium, 1 ppm copper, and a mixture of both 5 ppm cadmium and 1 ppm copper. The cadmium solution was analyzed under conditions appropriate to a good, radiation-programmed cadmium atomization, and the mixture was analyzed in the same manner. The nonatomized copper was driven off by forced heating between samples. Next, the copper solution was analyzed appropriately, and then the mixture, with both cadmium

and copper driven off by the single burn. Table 16 gives a comparison of the integrated absorbances observed. Although the match is not perfect, the basic concept of sequential volatilization seems workable. The cadmium in the mixture is easily driven off without interference from copper, and with no change in parameters from those used for pure cadmium solution. A similar disregard of cadmium by the copper atomizations is observed. Admittedly these elements differ greatly in volatility, and had roughly comparable concentrations in the mixture. However, in certain favorable cases, it may be possible to put this technique to use in suppressing some of the interelement effects often seen in real samples.

#### G. SUMMARY AND CONCLUSIONS

To summarize, perhaps the most significant conclusion to draw from this comparison is that the maintenance of strict and reliable control over the atomization temperature in electrothermal atomic spectroscopy is a concern of paramount importance. Compared to electrical means of atomizer temperature control such as the power dissipated, the method of radiation programming can offer significant advantages in achieving this goal. This method is far superior in preserving constant temperature throughout the useful life of an atomizer, and can actually extend an atomizer's life, because the rapid rise of

Table 16. Analysis of the Cadmium-Copper Mixture.

Solution	Analyte	Integrated Absorbance
5ppm Cd	Cd	8.06 ± 0.20
1ppm Cu	Cu	22.94 ± 1.50
Mixture	Cd	8.00 ± 0.19
Mixture	Cu	24.97 ± 0.75

temperature to the final level permits significant reductions in the total atomization time. Atomic transients come off the atomizer with greater peak height, which makes them easier to detect above baseline. In addition, the ability to calibrate atomizer temperature, and monitor it as well, would be of great importance in thermodynamic or kinetic studies of atomization mechanisms. At the same time, the use of radiation programming obligates the user to make companion improvements in his or her atomic spectroscopic system. These consist principally of a fast response readout that can accurately represent the quick transients that radiation programming produces, as well as an atomizer power supply with sufficient voltage and current reserve to take full advantage of the benefits provided by the rapid, near step function atomizer heating. Also, although the monitoring of temperature is excellent and free from interference by several variables, radiation programming is still not the ultimate means of regulation, as it is subject to optical variations in the observation of the atomizer.

Perhaps the best means of programming would be the direct sensing of temperature in the atomizer by a thermocouple. Such a facility might be rather difficult to implement with the graphite braid, not only because of its small size, but because most attempts in this writer's experience to undo or modify the braided bundles (as would be necessary to install a thermocouple) usually damages

the braid beyond use. In a more massive and rigid device such as a furnace, however, a thermocouple implant might be very beneficial indeed, and offer an excellent means of holding a constant atomizer temperature even beyond the precision with which radiation programming functions.

# ATOMIC CONCENTRATION PROFILES OVER GRAPHITE BRAIDS

## A. INTRODUCTION

Although the full array of computer-controlled instrumentation has played essential parts in the atomic spectrometric experiments that have been discussed thus far, the benefits and powers of the broad computer control are best appreciated and most fully exercised in the examination of atomic concentration profiles. To get some understanding of why this is true, consider briefly what is involved in obtaining concentration profile data with both flame and filament electrothermal instruments.

For concentration studies in a flame, the flame would be ignited, and sample would be aspirated continuously from a suitable reservoir. By analogy to the present instrumentation, the burner would then be systematically moved with respect to the optical axis as data is gathered. Because of the continuous sample aspiration, the distribution of free atoms in the flame would be in the steady state. This means that data could be acquired as fast as the burner is translated, or perhaps even continuously as it is translated. A high quality log amplifier could be used to present the readout in an absorbance mode, and extensive advantage could be taken of phase locked

detection and signal averaging techniques for improved signal-to-noise ratios. A thorough examination in two dimensions could be concluded within minutes.

In a filament electrothermal system, the situation is somewhat altered. The sample is not continuously atomized, but is rather deposited on the atomizer as a discrete aliquot. The atomization cell is then displaced to the proper position of analysis, and the regular sequence of heating intervals must be performed. The analytical signal will be a transient, and must be treated as such although the point by point data acquisition process does provide valuable information about each sample, such as time relationships of the signal shape and signal peak, or the ability to integrate the total signal derived for each sample. Finally, the cell must be returned to its initial position so that it may receive the next sample, after allowing a few seconds for cooling of the atomizer. All of this work results in one solitary data point for one single position in space. Several more samples must undoubtedly be repeated at the same position to get a reasonable statistical picture of their validity, and then the entire process must be repeated for the next atomizer cell position. This continues until the full region of space has been examined, with the entire procedure consuming some hours of time, and with no change in instrumental or sample parameters save the position of the cell.

Such is the case for the present system. Typically, it takes about 75 seconds for the instrumentation to execute an entire cycle of sampling, atomizing, and data processing for one sample. Four samples are usually done at each cell location. A typical scan would be to examine atomic populations at intervals of 3 mm from 0 to 24 mm vertical height above the braid. This is a total of thirty six samples, and requires about 45 minutes to perform. Additional such vertical columns at other fixed horizontal locations would also take 45 minutes each. Hours of on line computer time can easily be consumed, and yet the sample is constant throughout. Changing a parameter to see what effect it might have upon results implies further hours of repetitive work. During all of this time, the atomizer is aging and undergoing subtle but progressive changes. Were it not for computer control and the use of automated instruments, these studies would be so tedious and prone to error that it would be nearly impractical to do them. With automated computer control, a fixed though lengthy task can be defined, and the computer and instruments can see to its execution without the need for operator intervention. Such is the manner in which these studies have been done.

To do concentration profile work, a constant sample of the analyte of interest is repetitively delivered in a fixed amount to the atomizer. The concentration of the analyte is intentionally selected to give transients of

significant peak absorbance, in order to assure that they may be easily detected above baseline noise as far away from the atomizer as possible. Radiation programming is used for all the work, and the other conditions of atomization such as heating times and levels are usually adjusted to produce the analyte transient as a quick, sharp signal, as was seen in the previous chapter. This also enhances the detectability of signals, and extends the lifetime of an atomizer as much as possible. Table 17 lists most of the common instrumental parameters for the various elements involved in these studies.

As data points are acquired, the records of cell positions, integrated absorbances, peak absorbances, and times of the peak absorbances are simultaneously printed by the line printer and stored on a floppy disc. At a later time, a separate computer routine is used to pick up the magnetically stored data, average the results of each cell location, and print out these averages as well as their standard deviations.

#### B. VERTICAL APPEARANCE OF CONCENTRATION PROFILES

The shapes of concentration profiles can be intuitively predicted. A plot of integrated absorbance versus vertical height above the atomizer should resemble some sort of decay curve. The concentration of free atoms will be greatest at the atomizer, and progressively less above

Table 17. Common Instrumental Parameters for Atomic Concentration Profile Work.

Element	Conc.	Matrix	Temp.	Wavlenth.	HCDT
Cd	5 ppm, 100 ppb	Cl <sup>-</sup> , NO <sub>3</sub> <sup>-</sup> , SO <sub>4</sub> <sup>2-</sup>	1440°K	326.1 nm	10 mA
Pb <sup>a</sup>	1 ppm	NO <sub>3</sub> <sup>-</sup>	1440°K	283.3 nm <sup>b</sup>	8 mA
Ag	1 ppm	NO <sub>3</sub> <sup>-</sup>	1695°K	328.1 nm	15 mA
Cu	1 ppm	NO <sub>3</sub> <sup>-</sup>	2115°K	324.7 nm	15 mA
Zn	100 ppb	NO <sub>3</sub> <sup>-</sup>	1440°K	213.8 nm <sup>b</sup>	15 mA
Mg	1 ppm	NO <sub>3</sub> <sup>-</sup>	2115°K	285.2 nm <sup>b</sup>	15 mA
Hg <sup>a</sup>	10 ppm	NO <sub>3</sub> <sup>-</sup>	1440°K	253.6 nm <sup>b</sup>	15 mA
Tl	1 ppm	NO <sub>3</sub> <sup>-</sup>	1440°K	276.8 nm <sup>b</sup>	10 mA

## Constants:

Sample Size: 2 ul      Amplifier Gain: 10<sup>8</sup> V/A<sup>c</sup>

Slit Width: 200 um      Amp Rise Time: 30 ms

Sheath Flow: 3 l/min

<sup>a</sup>Solution 0.5% in H<sub>2</sub>O<sub>2</sub><sup>b</sup>Solar blind PM<sup>c</sup>10<sup>7</sup> V/A for Mg

it as diffusive, convective, and chemical mechanisms all combine to diminish the available atomic population. A plot versus horizontal displacement will be akin to a symmetrical distribution curve, with the greatest atomic concentration directly over the atomizer, and lesser concentrations to either side. The higher the vertical height for such a horizontal examination, the lower and broader the concentration curve should become. Generally, this is what was observed in the present work.

Shown in Figures 74, 75, and 76 are some concentration profiles with vertical height for a series of elements. The concentration axis is in integrated absorbance, but the readings have all been normalized so that all plots begin with an arbitrary value of 10.0 at grazing incidence, to allow for intercomparisons on a fair basis. The various elements display a wide variation in free atom lifetimes. The best ability to survive in the free atomic state is shown by zinc, which retains fully 50% of its original population as far as almost one inch away from the atomizer. One inch above the atomizer is quite far removed from the atomizer heat, particularly at the low temperature sufficient to atomize zinc efficiently. The temperature of gases at that point is probably very nearly back to room temperature again. The worst survival is shown by thallium, which is lost completely by a height of 12 mm.

An interesting effect is seen for those elements

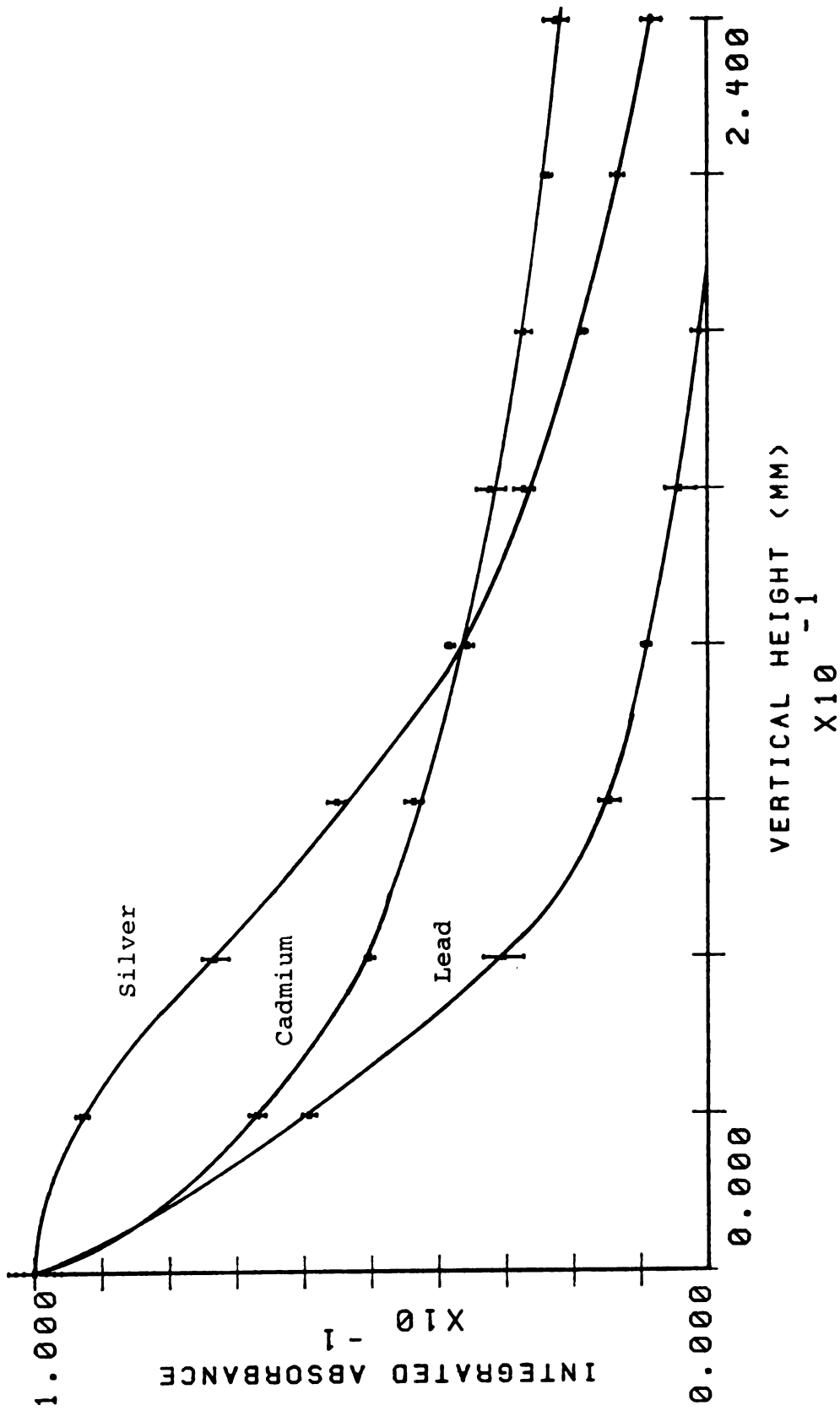


Figure 74. Normalized concentration profiles with vertical height for silver, cadmium, and lead.

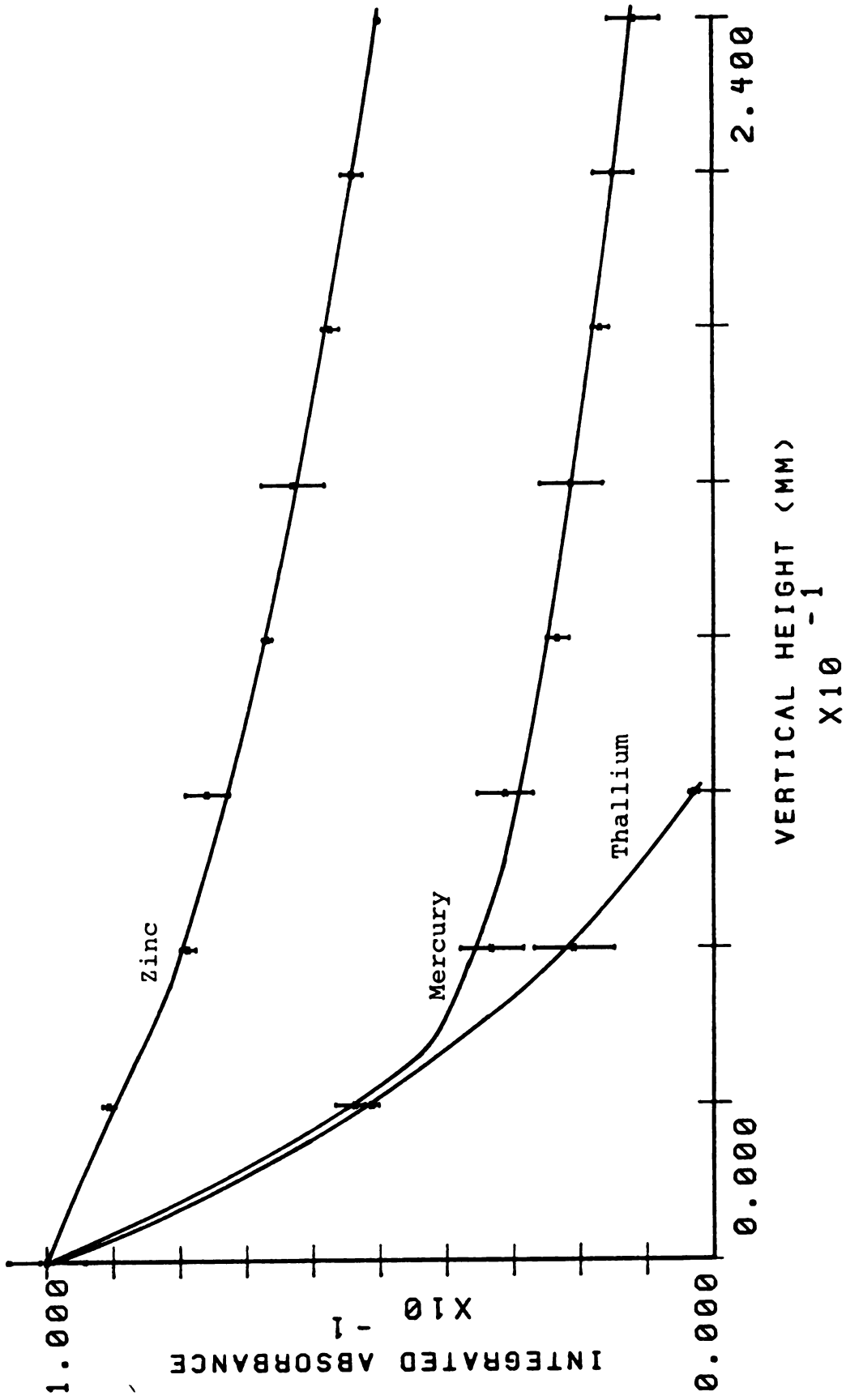


Figure 75. Normalized concentration profiles with vertical height for zinc, mercury, and thallium.

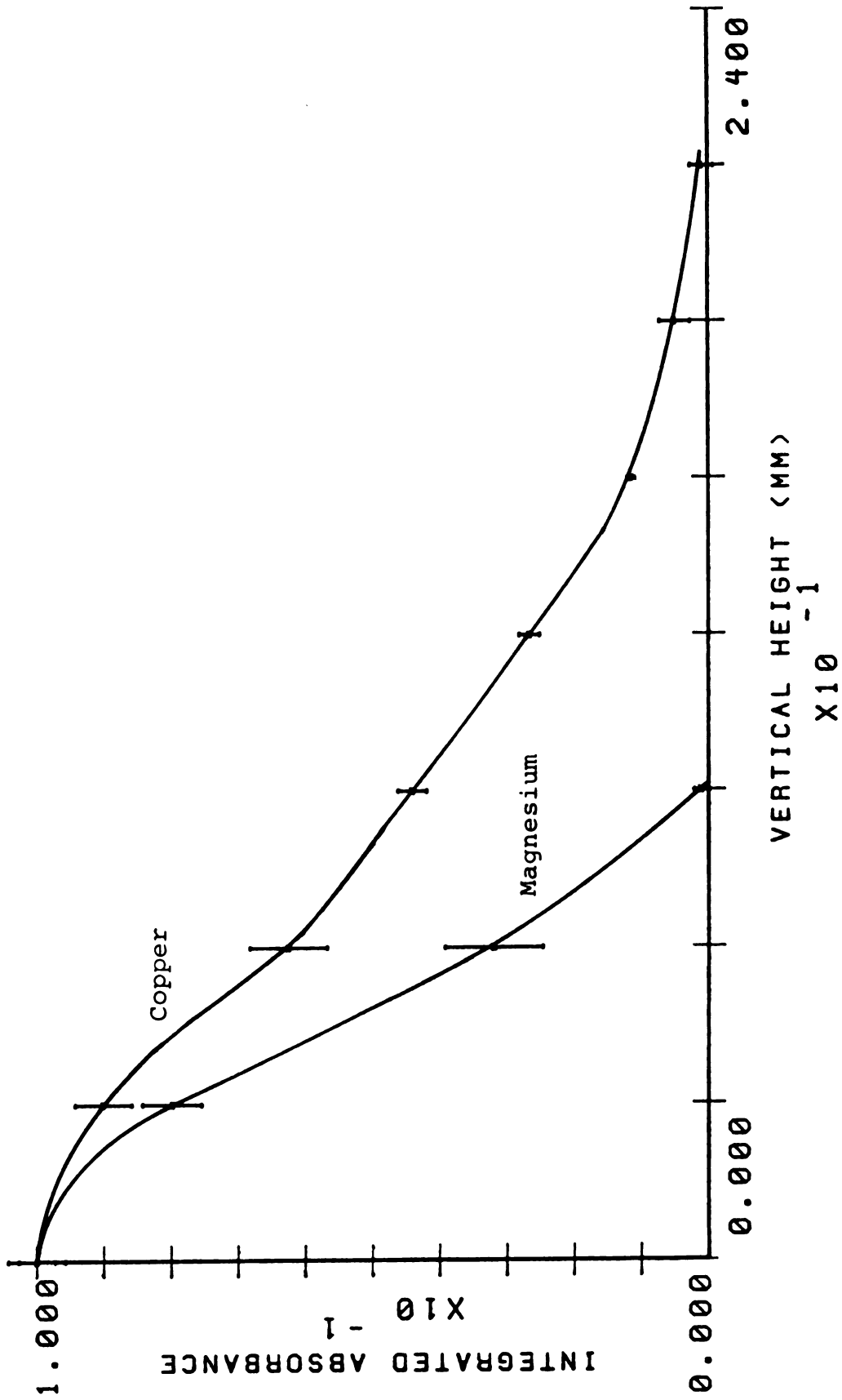


Figure 76. Normalized concentration profiles with vertical height for copper and magnesium.

which require the highest levels of heating, namely silver, copper, and magnesium. In each of these cases, the decay curve begins with a region of convex rather than concave curvature, with an inflection point occurring a few millimeters above the atomizer. This may possibly be an illustration of the benefits provided by hot sheath gas in preserving free atoms. With the atomizer heated strongly to drive off the analyte, the sheath gas immediately above its surface is also hotter than usual, and may help to retard chemical condensation mechanisms which begin to scavenge free atoms almost immediately for the elements that atomize well with less heat.

The rates at which the various elements' populations decay do not correlate well with any single physical property which is likely to explain them. If plots are made, for example, of estimates of the rate of decay of the atomic populations against such likely thermodynamic quantities as the heat of vaporization of the element, or the heat of formation of the common elemental oxide, there is no clearly defined locus. The plots are instead quite scattered and random. This is unfortunate, because if such a correlation could be established, it would provide an excellent theoretical basis from which to design and interpret further experimentation. At the same time, however, it is perhaps not unexpected that no such correlation exists. Thermodynamic or kinetic data depend critically upon temperature, and any experiments which

hope to receive a rigorous thermodynamic or kinetic explanation must either have a constant temperature or be able to predict and account for a changing temperature in an orderly fashion. In filament atomic spectrometry, however, the desolvated samples are subjected to temperature rises of hundreds of degrees as they are atomized, after which the free atomic vapor experiences an equally rapid temperature drop of comparable amount as it is carried away for analysis. There is little chance for even an approximation to equilibrium. The decay of a population is thus most likely a rather nondescript combination of both physical and chemical mechanisms which do not readily admit to a systematic interpretation, and which probably shift in relative importance from element to element, or even within the course of events for a single sample.<sup>173,174</sup> Not surprisingly, studies done to date on thermodynamic or kinetic processes in electrothermal atomizers are most often performed with furnace devices, in which the sample continues to be exposed to high temperatures for some time after atomization.<sup>190</sup>

### C. HORIZONTAL APPEARANCE OF CONCENTRATION PROFILES

The horizontal distribution of atomic populations for three typical elements is shown in Figures 77 and 78

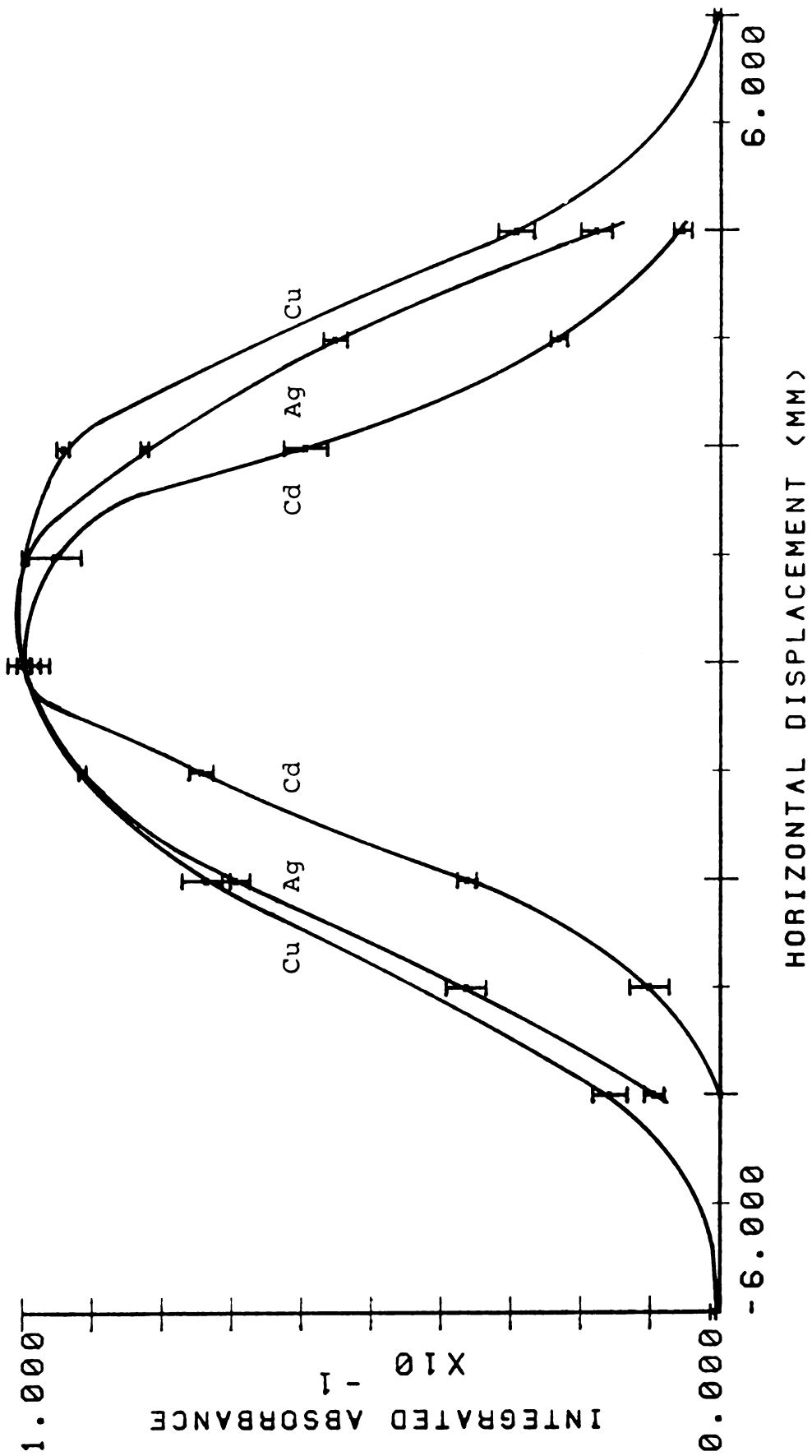


Figure 77. Normalized concentration profiles with horizontal displacement at a vertical height of 0 mm.

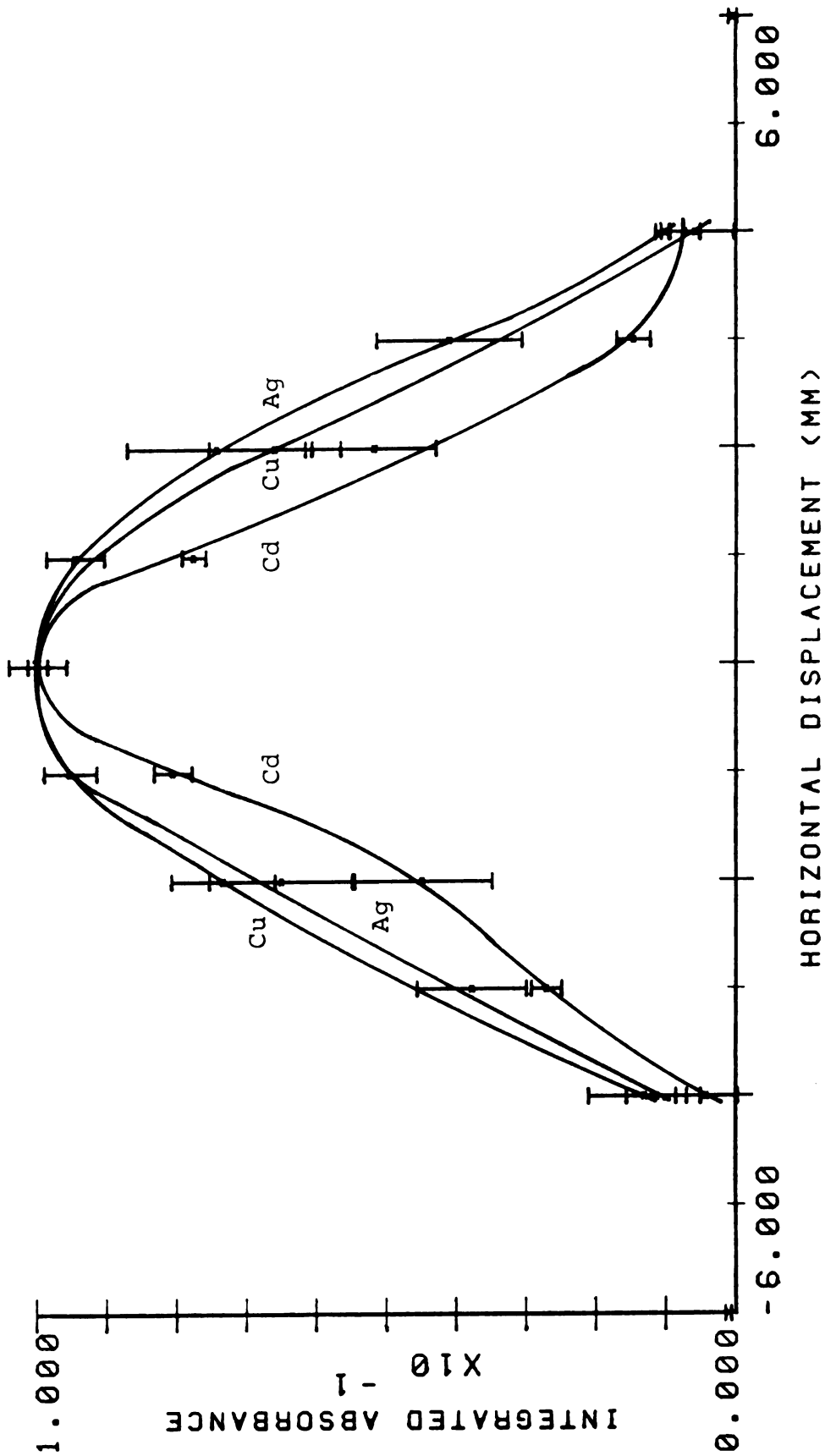


Figure 78. Normalized concentration profiles with horizontal displacement at a vertical height of 6 mm.

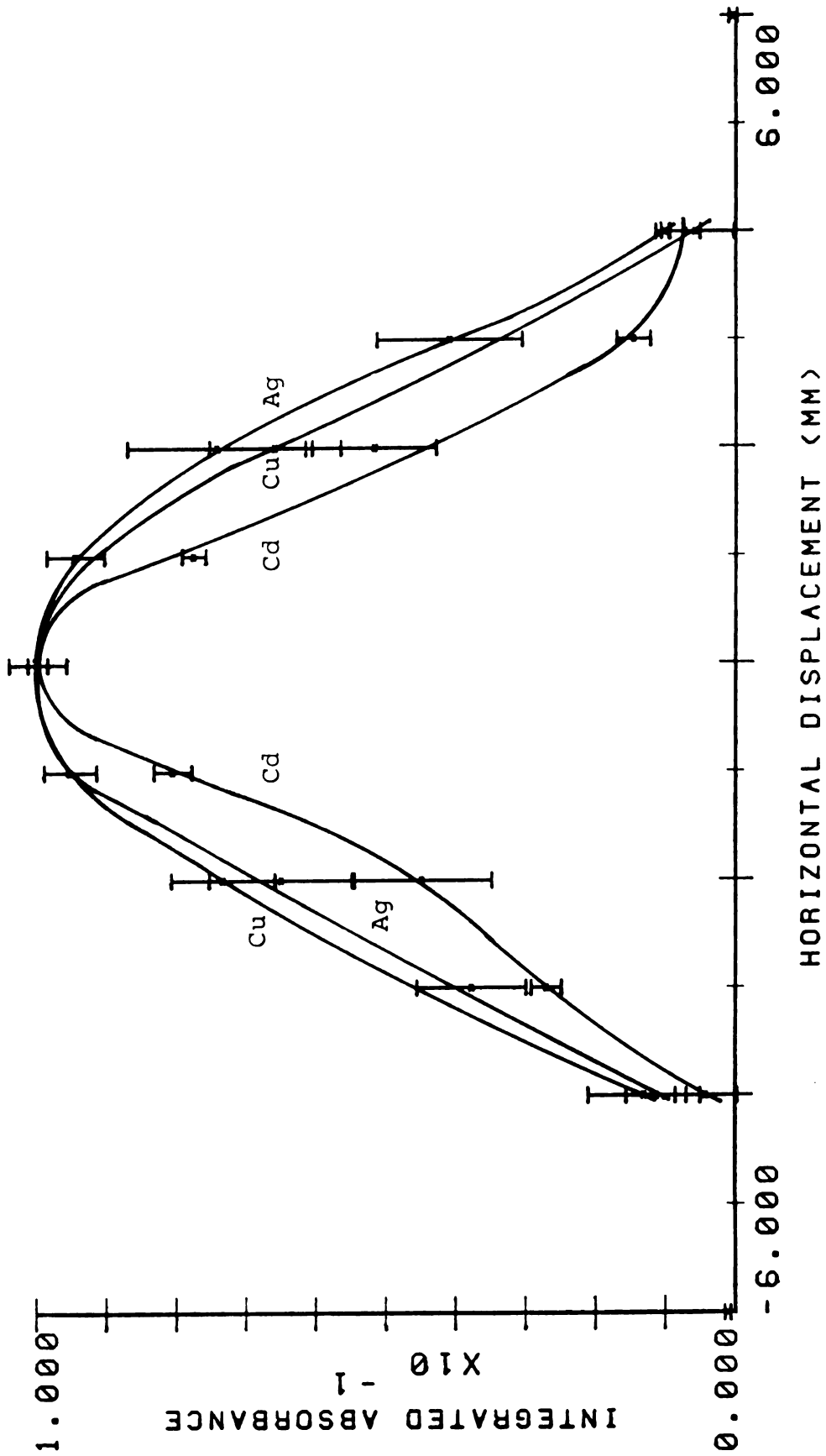


Figure 78. Normalized concentration profiles with horizontal displacement at a vertical height of 6 mm.

for vertical heights of 0 and 6 mm. The elements selected, cadmium, silver, and copper, cover a reasonably representative range of atomizer temperatures. The distance over which the atomic populations are scattered is not very great. (The braid itself is about two millimeters in diameter.) A significant amount of the sample is present a short distance away from the atomizer, however, even at grazing incidence. This is undoubtedly a direct consequence of the fact that samples soak into the braid when they are deposited, and distribute themselves more or less throughout the entire braid cross section. At the time of atomization, portions of the sample will be located at the sides of the braid, or perhaps even the bottom, and will thus find that exit from the sides or bottom is most probable. Such exit would be further assisted by convective forces created by the hot atomizer itself. The width of the plots increases steadily in the order cadmium, silver, copper. This coincides directly with the temperatures required for atomization, and indicates, reasonably so, that the violence and strength with which samples are atomized depends on how strongly the atomizer is heated.

At 6 mm height, the plots retain their same general shape. The precision of the data points is, however, noticeably worse, particularly along the sides of the curves. These regions represent the points at which

the streamer of warm sheath gas which is carrying the sample is coming into conflict with cooler gases that are rising through the remaining bulk of the atomization cell. This could lead to some local turbulence in the sheath flow. In addition, if some wavering in the sheath flow patterns were present, individual samples examined at these cell locations might by chance happen to intersect the optical axis well in some instances, and poorly in others. These effects would combine to cause the imprecision seen.

At still greater heights, these trends simply continue. Eventually, the magnitude of the imprecision becomes so comparable to the size of the signal itself that the plots lose much of their meaning. Throughout the entire 24 mm of examinable height however, the horizontal distributions of free atoms stay remarkably compact. The width of the plots does not change much at all from the initial width created at grazing incidence. This can be seen somewhat in the illustration of Figure 79, which shows the distribution of silver at three heights without the clutter of the error bars. This lack of spreading into the wings is probably due somewhat to the fact that the transit time for free atoms from grazing incidence to full cell height is usually only a few tens of milliseconds. Diffusion simply does not have much time to occur. Nevertheless, it is also an additional testimony to the quality of the sheath gas flow. A turbulent

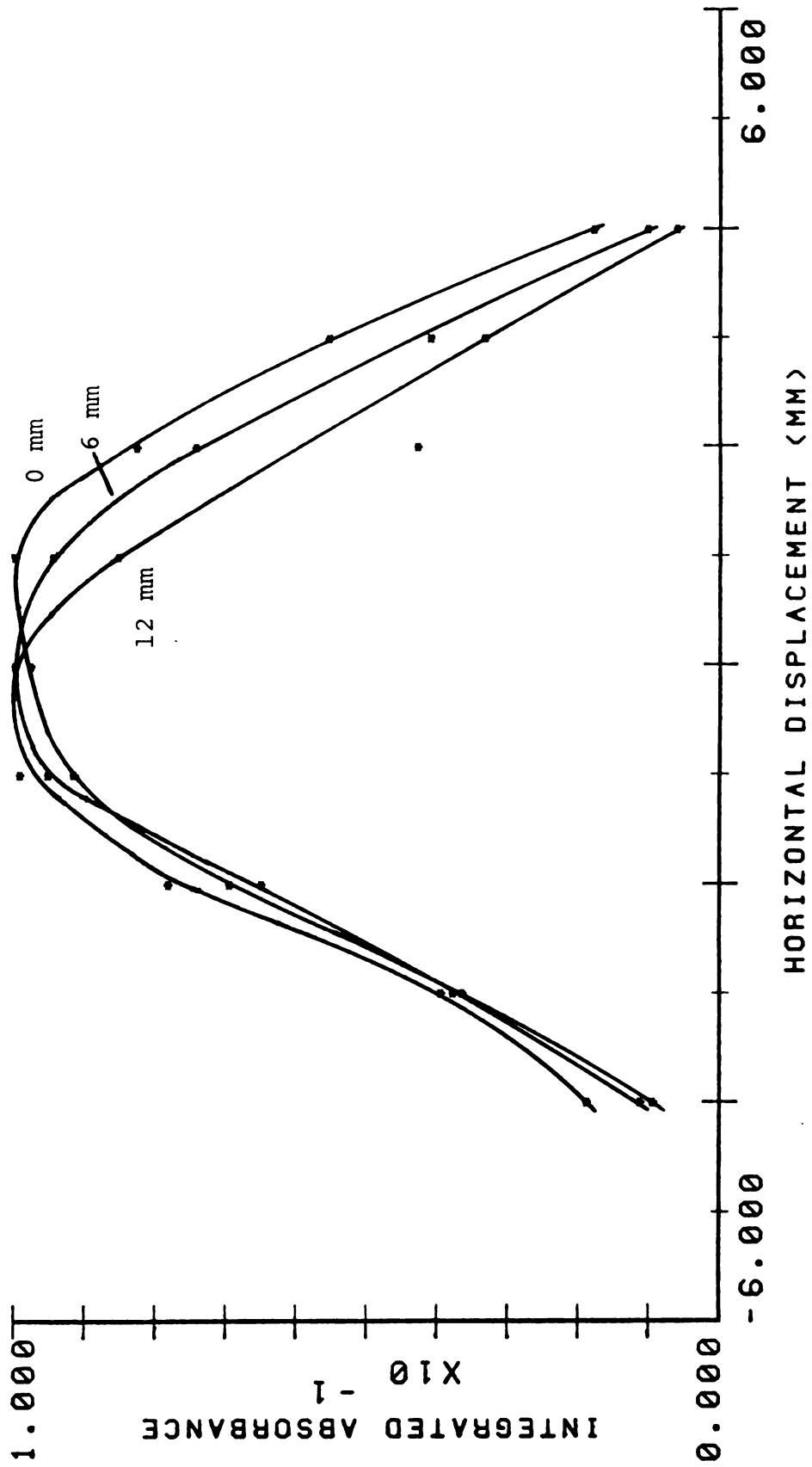


Figure 79. Normalized concentration profiles with horizontal displacement for silver at various vertical heights.

flow would certainly widen the free atom distribution as the gas formed spirals and vortices. A final curiosity observed for all elements, and just starting to be visible in Figure 79, is the invariable shifting of the atomic cloud towards regions of negative displacement. By the time an atomized sample reaches the full 24 mm height, the peak concentration is usually found in the range of -1 to -2 mm horizontally. It is conceivable that this effect could be imaginary, and caused by a slight lack of parallel alignment in the two faces of the chimney through which the optical beam passes. However, if a laser is targeted on a distant surface, and the chimney is then placed in the beam path, no appreciable displacement of the target spot is seen at all. This shifting effect is therefore real, and perhaps results from the influence exerted on the sheath gas flow pattern by the prevailing laboratory air currents in the region of the atomization cell.

Another interesting insight into the nature of horizontal concentration profiles is provided by an examination of their behavior on braids that have been turned perpendicular to the optical axis. Shown in Figures 80, 81, and 82 are plots of the three test elements at respective vertical heights of 0, 6, and 12 mm.

Although the profiles are very similar in general shape to those observed with a normal, parallel braid, they are somewhat wider because of the ease of soaking of the

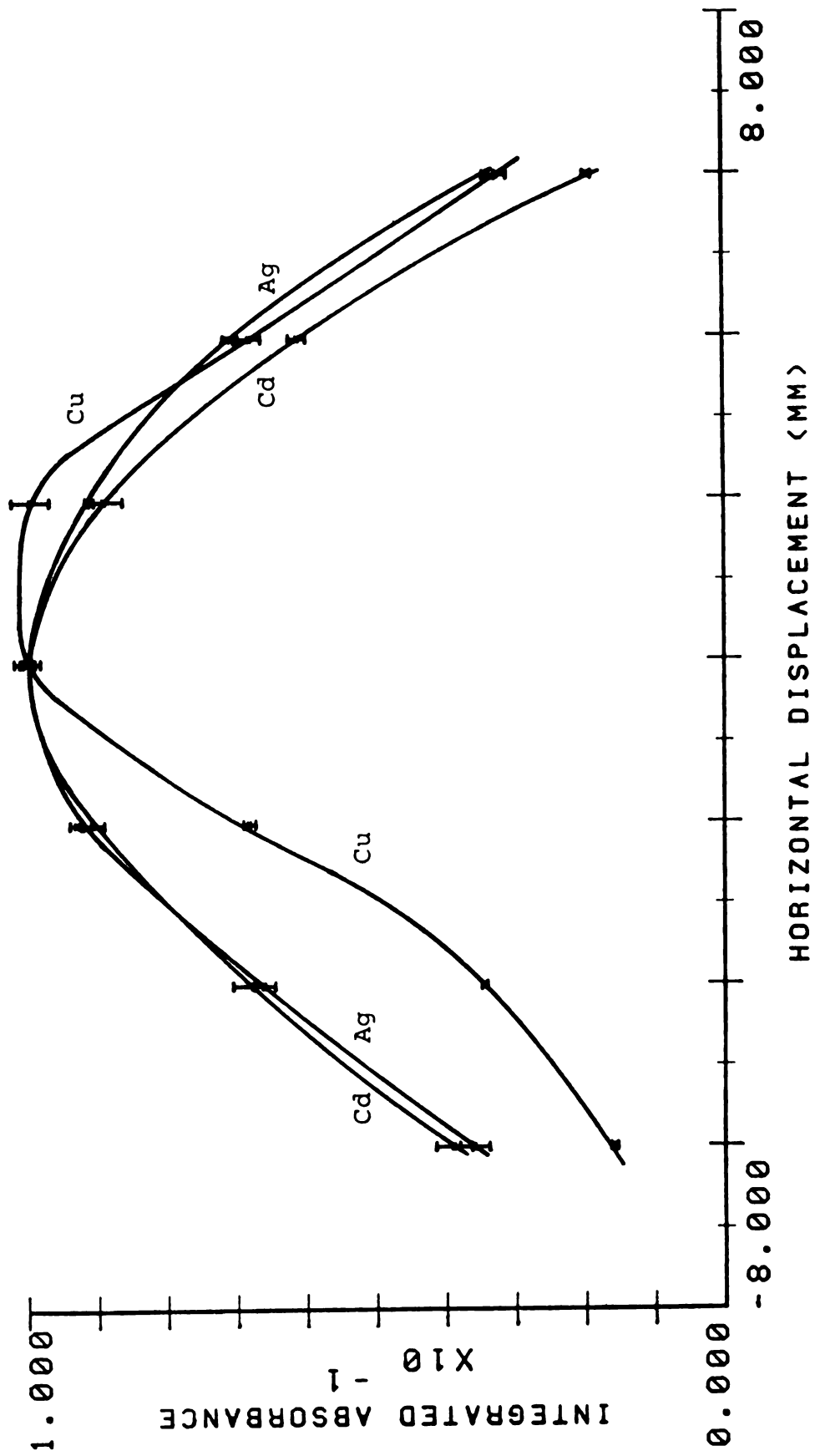


Figure 80. Normalized concentration profiles with horizontal displacement at a vertical height of 0 mm and a perpendicular braid.

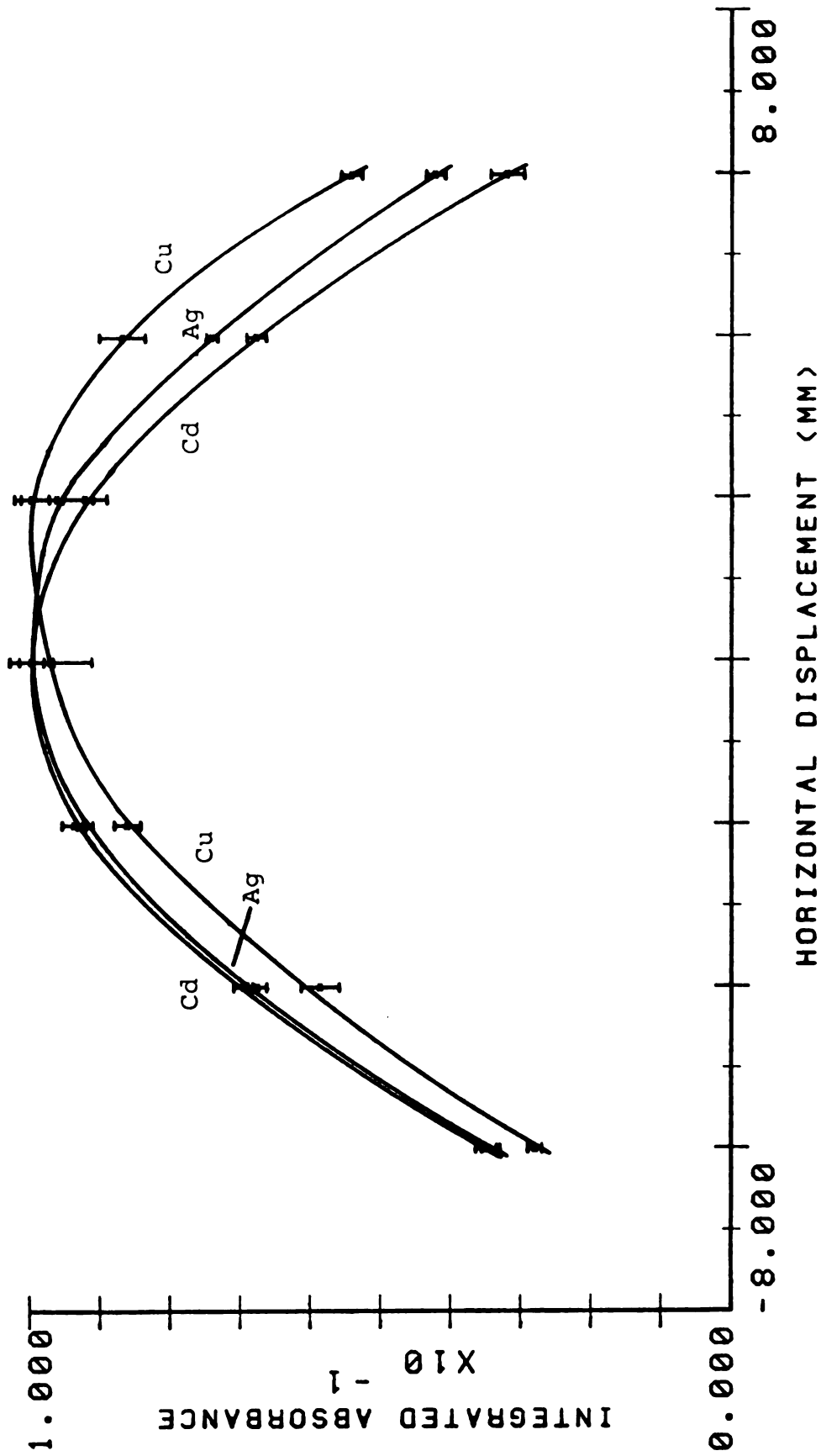


Figure 81. Normalized concentration profiles with horizontal displacement at a vertical height of 6 mm and a perpendicular braid.

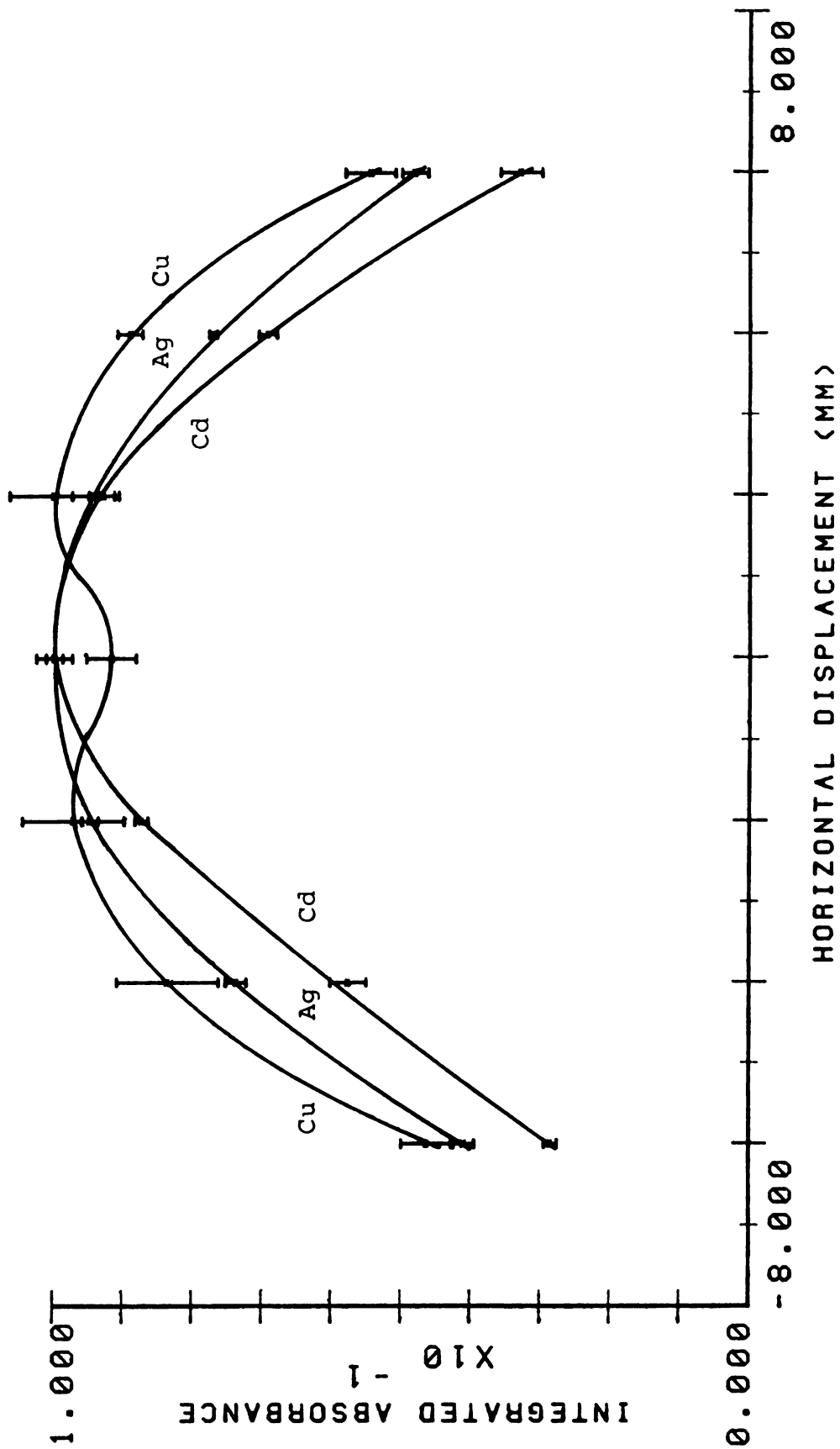


Figure 82. Normalized concentration profiles with horizontal displacement at a vertical height of 12 mm and a perpendicular braid.

sample along the length of the braid. The increase in width is not excessive, however, which indicates that desolvation to dry salt takes place quickly, before the sample can spread too far. In contrast to the parallel braid data, there is a small tendency for the profiles to broaden with height, (more easily visible if the plots can be overlaid) and there is not as severe a loss in precision in the profile wings. It is felt that this is due to the lack of severe thermal gradients along the width of these profiles. Horizontal spreading above parallel braids must cross a large thermal and convective gradient, whereas comparable spreading above a perpendicular braid more or less fans out into regions of comparable thermal and convective influence. Similar reasoning may well account for the lack of a clear relationship between profile width and atomizer temperature, as was seen with the parallel braid data.

#### D. EFFECT OF TEMPERATURE UPON SILVER

##### INTEGRATED ABSORBANCE

It was illustrated in a previous chapter that the shape of an atomic transient has great influence upon the integrated absorbance, because of the nonlinearity introduced through the point by point computation of logarithms. The general effect observed was that for two otherwise identical transients, the transient which is narrow and

tall will yield a larger integrated absorbance than the one which is broad and short. In addition, as the atomizer temperature is increased, it is observed that atomic transients become narrower and taller. One might logically expect, therefore, that the integrated absorbance of transients will increase as temperature increases.

In practice, some elements do not show much change in integrated absorbance with temperature at all. Cadmium and lead fall in this category. But this is not unexpected, as cadmium and lead are quite volatile, and under radiation programming produce transients which have essentially the same shape no matter what temperature is used. A most significant change is seen for silver, however, and it is opposite to the trend predicted above. This is illustrated by the data of Table 18, which shows how the integrated absorbance of silver transients falls more than 50% over the range of temperature covered, in spite of the fact that the transient shape is becoming narrow and tall.

There is a twofold explanation for the effect. Part of the reason is the general observation, previously discussed, that as the atomizer temperature increases, the width of the free atomic plume increases as well. This is seen for silver in the plots of Figure 83, which show integrated absorbance as a function of horizontal displacement for the family of temperatures. Only one side of the cell is plotted, and the error bars are left out

Table 18. Change in Integrated Absorbance of Silver Samples with Temperature.

Vertical Height	1280°K	1405°K	1565°K	1695°K
0 mm	35.05	29.69	15.72	12.91
33 mm	28.11	25.33	15.85	13.43
6 mm	21.86	20.09	13.71	11.96
9 mm	17.85	16.98	11.86	10.50
12 mm	14.99	13.34	10.13	9.02
15 mm	12.92	10.70	7.25	6.95

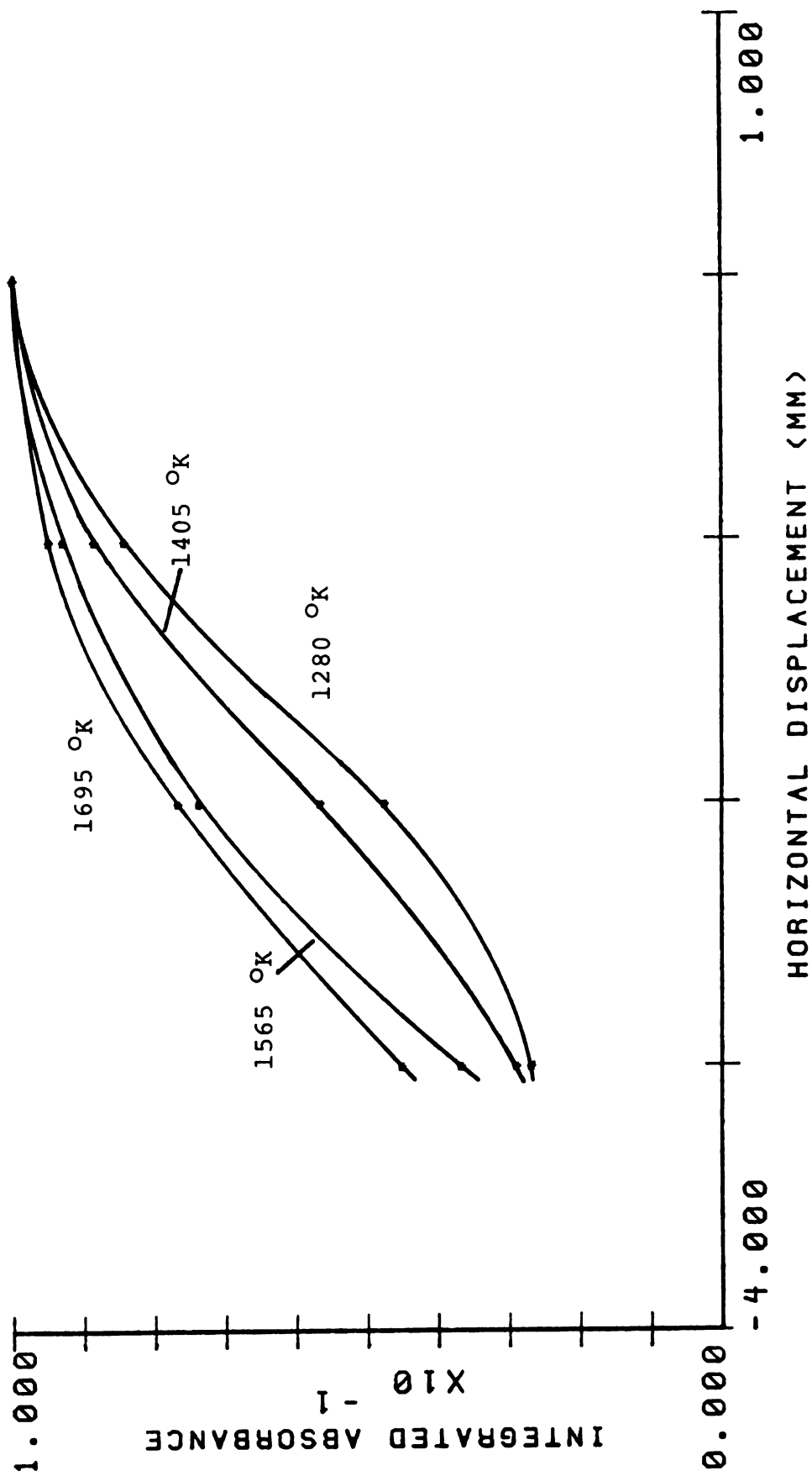


Figure 83. Normalized concentration profiles with horizontal displacement for silver at various atomizer temperatures.

for clarity. Clearly, as the temperature is increased, there is a net reduction in the absolute quantity of absorbing atoms within the observation window of the spectrometer at any given time. This will tend to lower integrated absorbance with atomizer temperature.

The second contributor to the phenomenon is the effect that the hot atomizer has upon the flow rate of the sheath gas. Table 19 lists the time elapsed from the start of atomization until the occurrence of the peak maximum absorbance for silver transients examined at vertical heights of 0 and 12 mm. The differences between these sets of times represent the time required for the transient to cover the 12 mm distance up the chimney. It can be seen that this time drops steadily, with the exception of the highest temperature. This effect almost certainly results from the expansion of sheath gas by the presence of the hot atomizer. The laminar flow of the sheath may further assist this process by permitting the hot gas to "stream" rapidly up from the atomizer without much hindrance. As a result, as atomizer temperature increases, the cloud of free atoms is carried through the observation window at any point at a growing velocity. For a fixed rate of data acquisition, this leads to steadily less and less observation of the sample as it passes, and again, a lowered integrated absorbance.

Why the transit time should rise again for the final temperature is not conclusively known. Perhaps at that

Table 19. Transit Times for Silver Samples at Different Temperatures.

	Peak A Time: 0 mm	Peak A Time 12 mm	Difference
1280°K	222 ms	265 ms	43 ms
1405°K	240 ms	277 ms	37 ms
1565°K	270 ms	300 ms	30 ms
1965°K	272 ms	312 ms	40 ms

temperature some slight turbulence is being set up which interrupts a smooth gas flow. The integrated absorbance still goes down in spite of this fact. Apparently the continued widening of the atomic cloud is enough to keep the net atomic concentration declining. The peak shape effect is no longer of much importance at that temperature, as is apparent from the very slight difference in shapes between the 1565 and 1695°K plots of Figure 83.

Some brief tests were performed with cadmium as the analyte to investigate the effect that the flow rate of the sheath gas in general has upon results. Vertical profiles of concentration were performed for cadmium, with rotometer flow rate settings of 2, 3, and 4 liters per minute of argon. The results are given in Table 20. There is no appreciable drop in the transit time for the peak absorbance maxima with increase in flow rate, but a small drop in the integrated absorbance. The effect is very minor, however. In light of these results, it was concluded that, given a reasonable bulk flow rate of sheath gas to carry the sample, any alterations in the instrumental performance which arise from perturbations upon the sheath gas flow can be ascribed to the presence of the hot atomizer. The basic flow of the sheath itself is a parameter of only slight influence.

Table 20. Effect of Sheath Flow Rate upon Cadmium Spatial Data.

	Integrated A	Time of Peak A
2 l/min:		
0 mm	12.68 ± .18	113 ms
12 mm	4.89 ± .22	165 ms
24 mm	3.05 ± .60	201 ms
3 l/min:		
0 mm	12.56 ± .10	114 ms
12 mm	4.55 ± .37	168 ms
24 mm	2.85 ± .38	203 ms
4 l/min:		
0 mm	12.27 ± .14	112 ms
12 mm	4.48 ± .16	166 ms
24 mm	2.82 ± .16	201 ms

E. A DISCUSSION OF SOME PROBLEMS  
OF INTERPRETATION

At this point it might be well to pause briefly and consider how complex explanations of atomic spectrometric phenomena can be. The susceptibility of results to changes in the flow of sheath gas caused by the atomizer has just been illustrated. With so many different atomizers in use, each of which as often as not has its own particular sheath gas delivery system, it can be appreciated how effects observed for one given system are not of importance in another. If the sheath gas flow in this instrument were turbulent, for example, the changes in integrated absorbance with temperature for silver might not be serious, because the sheath would more effectively resist the alterations to which it is actually susceptible at present. Contradictory behavior can be seen even within the limits of the present system. Copper, for example, also shows an effect of decreased integrated absorbance with temperature, though not as severe as that of silver. Yet in the case of copper, the transit times (between 0 and 12 mm) for the atomic cloud rise steadily with temperature from a minimum of 10 to a maximum of 25 ms. Thus both this effect and the peak shape effect should resist the trend in integrated absorbance observed. If plots are compared of the horizontal displacement of integrated absorbance for these temperatures, the changes in width vary somewhat

from temperature to temperature, but in not nearly as regular a manner as was seen for silver. This raises the possibility of chemical differences in the mechanism of atomization which influence the population of free atoms.

Another illustration of the complexities involved in this work is given by the vertical height decay behavior shown by zinc, cadmium, and mercury in Figures 74 and 75. The elements are listed in the order of their longevity. Seemingly contradictory to this is the fact that they are also listed in the order of decreasing reactivity for other chemical systems, such as the standard electrochemical potentials. Some insight into the problem is possibly suggested by an examination of the times at which the peak absorbance occurs at a given vertical height. At grazing incidence, for example, the times of peak absorbance are as follows: zinc, 160 ms into atomization, cadmium, 120 ms, and mercury, 70 ms. These distinct separations in time might explain the longevity trend. Zinc does not leave the atomizer until well into the burn. Decomposition products from its salt or any other trace sources have already been expelled into the sheath. When the zinc finally comes off, the atomizer is somewhat hotter, and the hot gas helps to preserve the free zinc atoms. Mercury, on the other hand, is very volatile, and leaves the atomizer extremely early. There is not much benefit to be gained from hot sheath gas, and the mercury atoms are expelled along with their matrix. For mercury, this may be

unusually severe because of the necessity of using peroxide to prevent mercury losses prior to atomization. Interestingly enough, once the mercury atoms are a few millimeters away from the atomizer, the severe loss in population is strongly arrested, and further decay occurs at a rate no more severe than that of zinc. Cadmium, being intermediate in atomization time, is also intermediate in these effects. This is all speculative, but it does illustrate how very complex the activities within an atomic spectrometric cell are, and how many explanations can often arise to decipher unusual behavior.

#### F. EFFECT OF OXYGEN UPON FREE ATOM POPULATIONS

In an attempt to learn somewhat more about the ability of free atoms to survive as they leave the hot atomizer, experiments were done in which oxygen was intentionally included in the sheath gas. The normal flow of 3 liters per minute of argon was retained, but it was supplemented by a flow of 0.2 liters per minute of oxygen. The effect upon the graphite braid was devastating. After only five or six burns in such an atmosphere, the braid was severely damaged, and an equal amount of additional burns would bring the braid close to burnout, in spite of the use of very low temperatures. Because of this fact, only elements of high volatility were examined, and even for them it was possible to get only one single data point

per cell location. Shown in Figures 84, 85, and 86 are the results obtained for cadmium, zinc, and lead. The lack of repetitive data makes it tenuous to draw conclusions, but it is apparent that the presence of the oxygen does not automatically mean the total and rapid scavenging of all free atoms produced. The plots for the oxygen data all begin at a disadvantage with respect to the normal data. This is particularly true for zinc, which perhaps reflects zinc's greater tendency to form an oxide than cadmium or lead. Most of the damage is done near the braid, however. Once away from the braid into cooler regions of the sheath, the data taken in oxygen do not decay rapidly. In all three plots, in fact, the loci tend to converge. It seems that if a troublesome matrix or scavenger is present in a sample, it will do its damage in the vicinity of the atomizer, where the generally higher prevailing temperatures will better promote the energetics and kinetics of such reactions as the formation of oxides. At greater distances from the atomizer, the prevailing temperatures around a sample are cool, and free atom-scavenging mechanisms may lack the necessary energy to remain functioning. Some additional support for this concept is provided by the distinct lessening in slope that many of the vertical decay curves of Figures 74-76 show in the region of 4-6 mm vertical height.

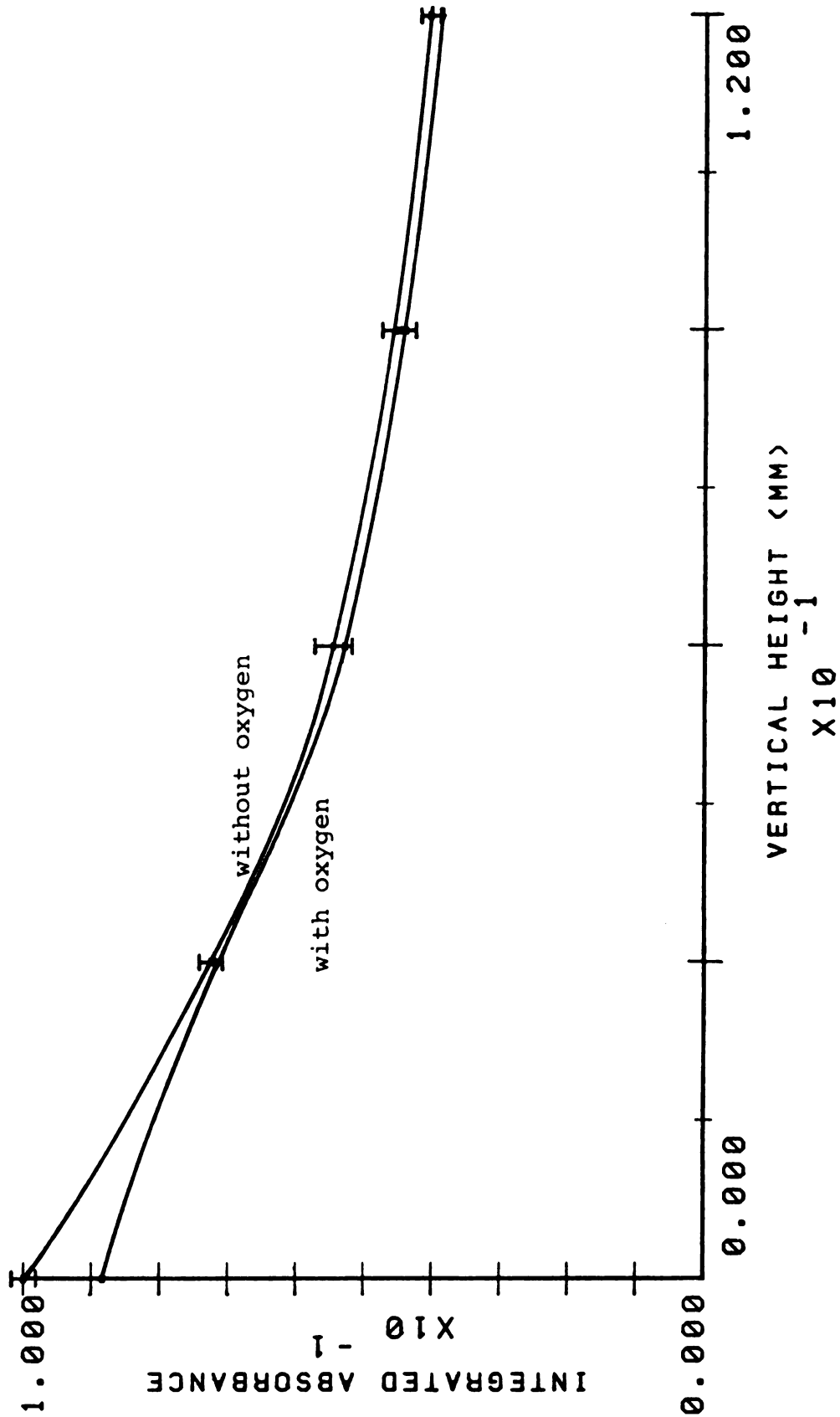


Figure 84. Effect of oxygen upon the vertical concentration profile of cadmium.

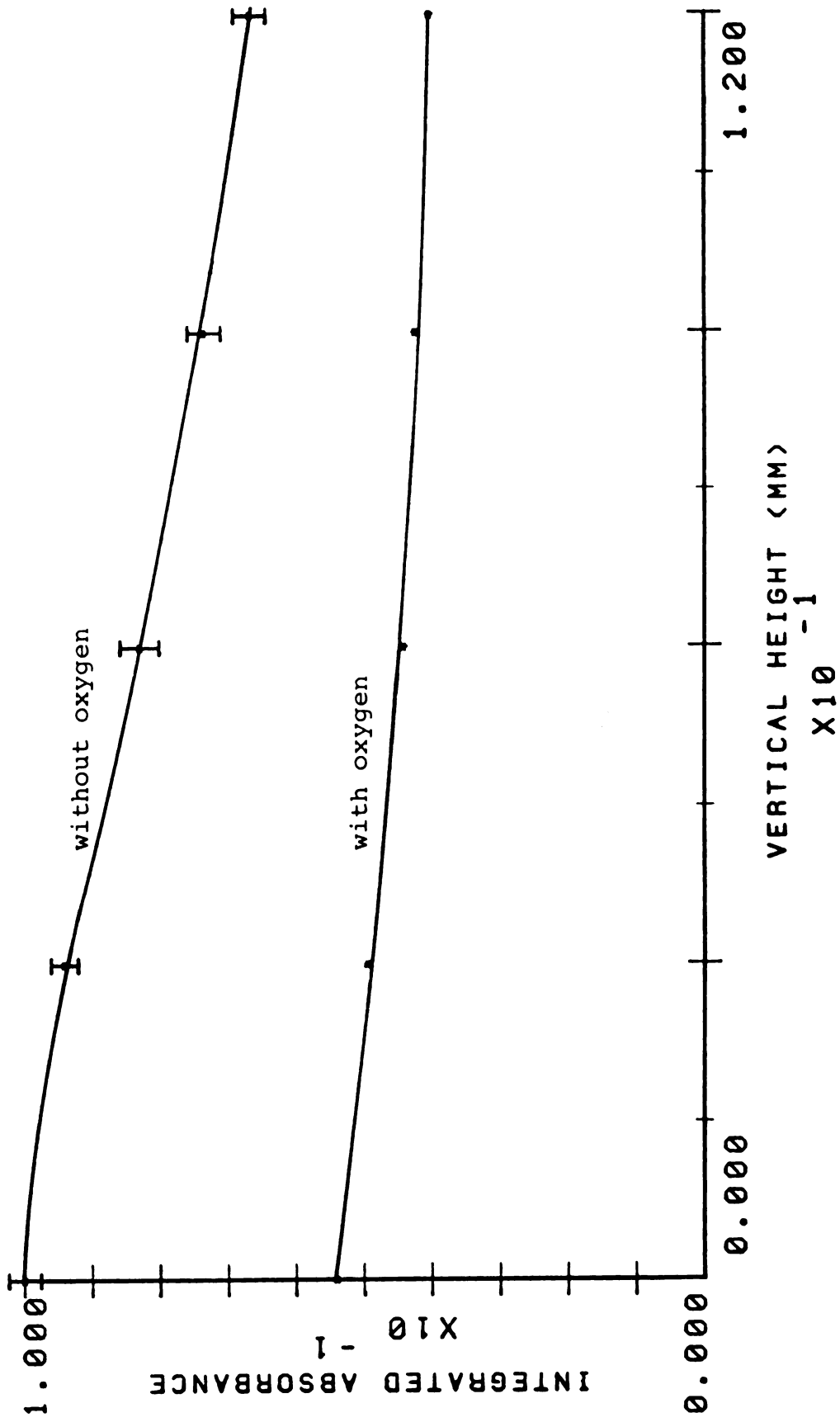


Figure 85. Effect of oxygen upon the vertical concentration profile of zinc.

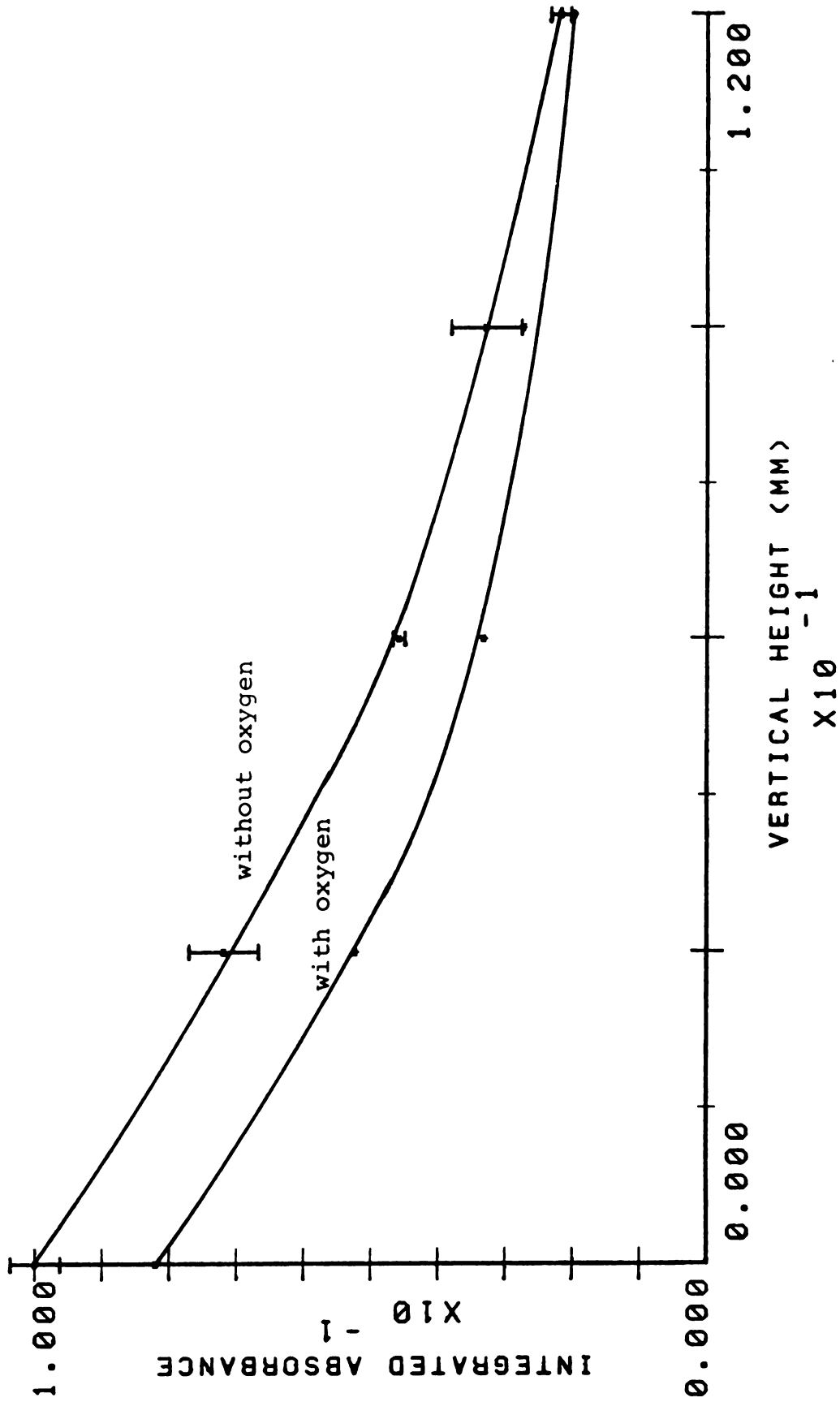


Figure 86. Effect of oxygen upon the vertical concentration profile of lead.

#### G. EFFECTS OF MATRICES UPON CONCENTRATION PROFILES

A final field of investigation of concentration profiles was that of some matrix effects. A large percentage of current analytical problems involves the performing of analyses for substances that are familiar in themselves, but which are contained in an unusual or stubborn matrix. Atomic spectrometry is no exception, and the ability to do a spatial analysis of an electrothermal atomization cell can provide a means for gaining further knowledge about matrix effects and using this knowledge to eliminate or minimize such effects.

Some preliminary work was done using cadmium as the analyte and solutions of the common mineral acids as the matrix. The concept was to begin these studies with a matrix that should be relatively gentle and easily volatilized. Solutions of 5 ppm cadmium made from stock cadmium chloride, nitrate, and sulfate were supplemented by additional amounts of standardized hydrochloric, nitric, and sulfuric acids to produce solutions of different concentrations of the respective anion, up to a maximum of 250 ppm. It was found that the presence of these acids, even up to the highest concentration level, had very little effect upon the integrated absorbance of cadmium solutions compared to that obtained from solutions which lacked the acids. An example of some of this data is shown in Table 21, for additions of sulfuric acid. With

Table 21. Effect of Sulfate Ion from Sulfuric Acid Upon Integrated Absorbance of Cadmium

Height	0 ppm $\text{SO}_4^{2-}$	50 ppm $\text{SO}_4^{2-}$	250 ppm $\text{SO}_4^{2-}$
0 mm	10.00 ± .78	9.23 ± .24	8.84 ± .21
3 mm	6.48 ± .20	6.44 ± .14	6.37 ± .04
6 mm	5.03 ± .15	4.90 ± .13	4.94 ± .06
9 mm	4.13 ± .13	4.09 ± .14	4.10 ± .43
12 mm	3.45 ± .11	3.72 ± .24	3.43 ± .17
15 mm	3.00 ± .17	3.01 ± .32	3.05 ± .19
18 mm	2.58 ± .37	2.59 ± .43	2.72 ± .31
21 mm	2.25 ± .32	2.35 ± .39	2.28 ± .44
24 mm	2.09 ± .45	1.91 ± .41	2.25 ± .23

the possible exception of grazing incidence, there is virtually no significant difference between the data sets. The same can be said for the data of hydrochloric and nitric acids as well.

This is not very unusual. All three acids are rather volatile. Hydrochloric acid would be completely evaporated at desolvation temperatures. Nitric acid would be effectively decomposed. Only sulfuric acid could survive desolvation, but it too would be removed from the braid before cadmium and, being a liquid, would not effectively remove cadmium salts prematurely because of entrainment.

As a next step in worsening the matrix, the studies on cadmium with added chloride, nitrate, and sulfate were repeated, but with the ammonium salts as the anion sources. The reasoning was that ammonium salts should retain the matrix as a solid, and survive desolvation conditions better than the mineral acids, but still present a matrix which can be quite readily decomposed by heat.

Shown in Figure 87 are the results for cadmium in the presence of ammonium chloride. Here a consistent matrix effect is seen, beginning with even small concentrations of the added salt. Ammonium nitrate and sulfate did not show any such consistent trends, but left the cadmium absorbance largely unaffected. The effects of increased temperature upon these matrices can explain the behavior seen. Ammonium nitrate decomposes at low temperatures into nitrous oxide and water, and ammonium

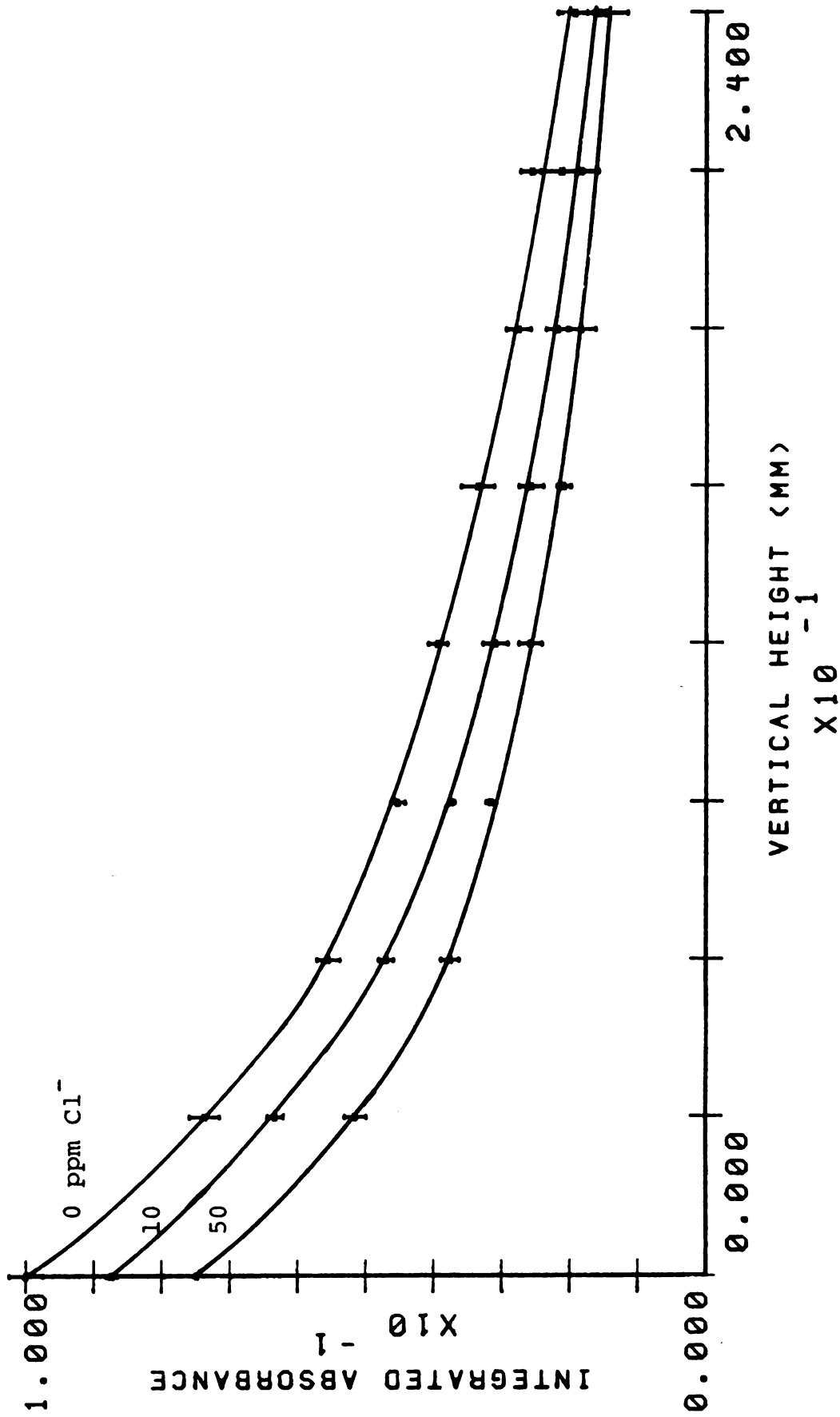


Figure 87. Effect of added chloride ion as ammonium chloride upon the vertical concentration profile of cadmium.

sulfate decomposes at 235°C. Ammonium chloride, however, remains intact at higher temperatures, though it does sublime at 340°C.<sup>191</sup> It is possible that in the present instance, the sulfate and nitrate are destroyed prior to atomization of cadmium, but that the chloride, or at least some of it, survives long enough to be atomized with the cadmium where it can exert a depopulating influence. It may be noted that the slopes of the decay curves are quite similar, with or without the matrix present. This indicates that the matrix does its damage directly at the site of atomization and ceases to have any influence upon the population once it is in the sheath gas.

As a last step in the progression of difficulty of the matrices, the anion studies of cadmium were repeated a third time, with potassium salts as the source of the matrix. In these cases, the survival of the matrix through the desolvation step is assured. All three salts are sufficiently involatile to be present during cadmium atomization. Indeed, to assure that excess matrix salt did not build up on the braid, atomization was performed at 1760°K rather than the usual 1440°K.

As was the case with the ammonium salts, only potassium chloride showed a significant matrix effect. Both the nitrate and sulfate did not yield any clear cut trends. In the case of potassium chloride, for the first time, the matrix contributed significantly to the total absorbance observed. Indeed, at a concentration of 250 ppm added  $\text{Cl}^-$ ,

the ejection of the matrix from the braid was faintly, but perceptibly visible as a brief white smoke. Some results are listed in Table 22. A small, but noticeable effect is seen upon addition of only a slight amount of KCl. At high KCl levels, however, there seems to be an increase in the absorbance again, even after correcting the raw data for the absorbance by the matrix itself. An exact reason for this apparent reversal of events is not known, but it does illustrate one of the instrumental limitations of the present system. The atomic absorption spectrometer of these studies is only a single beam instrument. To correct for nonspecific absorbance by matrices, it is necessary to run the matrix alone as a separate sample at some later time, and apply corrections. Aside from the excessive waste of time involved in running such sample matrices without analyte, the possibility remains that this is not truly an exact means for achieving the necessary correction.

To conclude the cadmium studies, an investigation was done in a 50 ppm  $\text{Cl}^-$  matrix of KCl, in which a small aperture of diameter only 0.5 mm was used at the monochromator in place of the traditional 3.0 mm aperture. The decay of a cadmium population in 0.5 mm increments away from the braid, both with and without added KCl, is shown in Figure 88. In spite of the greatly improved vertical resolution, it can still be seen that the cadmium populations in the presence of the matrix are reduced

Table 22. Effect of Chloride Ion from Potassium Chloride upon Integrated Absorbance of Cadmium.

Height	0 ppm Cl <sup>-</sup>	10 ppm Cl <sup>-</sup>	250 ppm Cl <sup>-</sup>
0 mm	10.00 ± .32	8.62 ± .10	9.09 ± .52
3 mm	6.49 ± .16	6.19 ± .33	6.66 ± .08
6 mm	4.94 ± .11	4.52 ± .11	5.35 ± .13
9 mm	4.02 ± .10	3.86 ± .10	4.63 ± .20
12 mm	3.47 ± .25	2.97 ± .56	3.65 ± .35
15 mm	3.05 ± .30	2.59 ± .34	3.16 ± .18
18 mm	2.73 ± .21	2.23 ± .15	2.86 ± .43
21 mm	2.53 ± .19	2.22 ± .20	2.03 ± .17
24 mm	2.25 ± .43	1.89 ± .29	1.85 ± .62

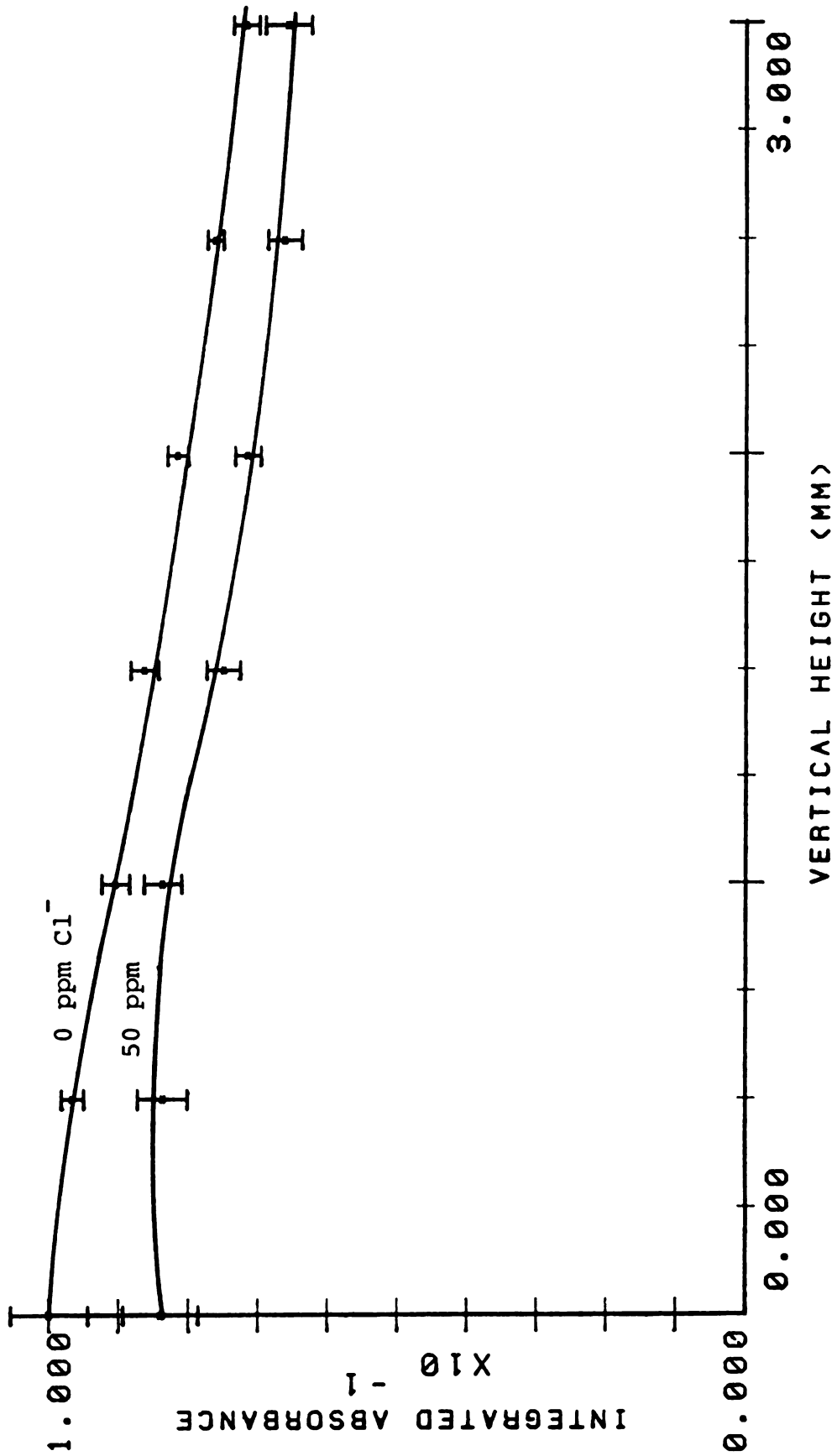


Figure 88. Effect of added chloride ion as potassium chloride upon the high resolution vertical concentration profile of cadmium.

right from the edge of the braid; the matrix curve is separate from the nonmatrix curve at grazing incidence instead of meeting it. Again, the matrix effect would appear to be one of interference in the primary atomization process. The exact cause can arise from several mechanisms. During atomization, potassium chloride may provide a ready population of effective free cadmium scavengers. Chemical affinities during desolvation may cause the cadmium to be well occluded in KCl crystals, so that it is ejected in the KCl salt smoke, or otherwise prevented from atomizing effectively. Once away from the braid, the population decays both with and without a matrix are quite similar, as was observed for ammonium chloride.

If other elements are investigated for matrix effects, it is found that each individual element seems to have its own particular behavior. A few examples may be given here in order to illustrate some of the other tendencies and effects that may play a role in matrix interferences.

One of the most simple is that the severity of a matrix effect may depend on the absolute quantities of sample and matrix. This is illustrated by some observations with zinc and cadmium. Most of the work done in these studies with cadmium was at the triplet resonance line at 326.1 nm. The reason for this was that the sensitivity of cadmium at the singlet line, 228.8 nm, is so high that severe and vexing problems exist with automated

delivery of trace cadmium levels. At the triplet line, sensitivity is sufficiently lowered so that more concentrated solutions could be used. Zinc is equally as sensitive at its singlet line as cadmium, but a similar procedure was not possible for zinc because its triplet line at 307.6 nm is a very weak absorber. Zinc studies thus had to be done at the singlet line, 213.8 nm, with zinc concentrations of only 100 ppb, and matrix concentrations of up to 5 ppm. This gives the same maximum 50:1 matrix to analyte ratio as was used for 5 ppm cadmium and up to 250 ppm matrix. Zinc matrices, however, were not all that serious. Table 23 shows the integrated absorbances obtained for zinc solutions, and for zinc solutions made with ammonium and potassium chloride matrices, such as were effective with cadmium. The differences are rather slight. For a comparison with this data, cadmium solutions were also analyzed at 100 ppb levels with 5 ppm of matrix, using the cadmium singlet resonance at 228.8 nm. The results are also shown in the same table, and they too show an insensitivity to the presence of the matrix. This indicates that the analyte to matrix ratio is not always of sole importance in predicting the possible existence of a matrix effect. The absolute quantity of material can play a role as well. With more salt on the atomizer, it is possible that analyte may be entrapped within matrix salt crystals of large size, and prevented from atomizing as effectively as it would with less total

Table 23. Matrix Effects of Zinc and Cadmium at Lowered Total Salt Concentrations.

	No Matrix		5 ppm Cl <sup>-</sup> (KCl)		5 ppm Cl <sup>-</sup> (NH <sub>4</sub> Cl)	
Zinc	12.09	.14	12.21	.29	12.36	.20
Cadmium	13.72	.28	13.94	.11	13.74	.48

Zinc, cadmium concentration = 100 ppb.

material present.

Results for copper are of interest to illustrate how the effectiveness of a given substance as a matrix interferent can change for different elements and atomization conditions. Shown in Table 24 are some results observed for matrices of various salts. In contrast to cadmium, copper is not severely interfered with by potassium chloride, but is significantly affected by potassium nitrate and sulfate. Figure 89 shows the vertical profile of the sulfate interference. The initial loss in integrated absorbance is still seen, as with cadmium, but so too is an increase in the decay rate of free copper population in the presence of the matrix. These results give further clues to the importance of analyte and matrix volatilities. The ammonium salts have little effect on copper, which reinforces the concept that these matrices are decomposed and ejected prior to the atomization of the analyte. Similar reasoning can be proposed for the

Table 24. Effects of Matrices upon Integrated Absorbance for Copper and Magnesium.

Matrix	Copper	Magnesium
None	15.40 ± .29	21.03 ± .53
KF	10.27 ± ±.33	0.42 ± .05
KCl	13.79 ± .20	7.65 ± .84
KBr	12.96 ± .24	13.28 ± 1.3
KI	10.49 ± .38	8.78 ± .65
	9.71 ± .15	
	9.56 ± .24	
KNO <sub>3</sub>	8.01 ± .29	1.96 ± .11
K <sub>2</sub> SO <sub>4</sub>	6.59 ± .15	2.09 ± .15
NH <sub>4</sub> NO <sub>3</sub>	15.73 ± .09	20.81 ± .67
NH <sub>4</sub> Cl	15.67 ± .60	18.91 ± 1.0
(NH <sub>4</sub> ) <sub>2</sub> SO <sub>4</sub>	15.47 ± .26	19.57 ± 2.3

Copper, Magnesium concentration = 1 ppm.

Matrix concentration = 250 ppm in the anion.

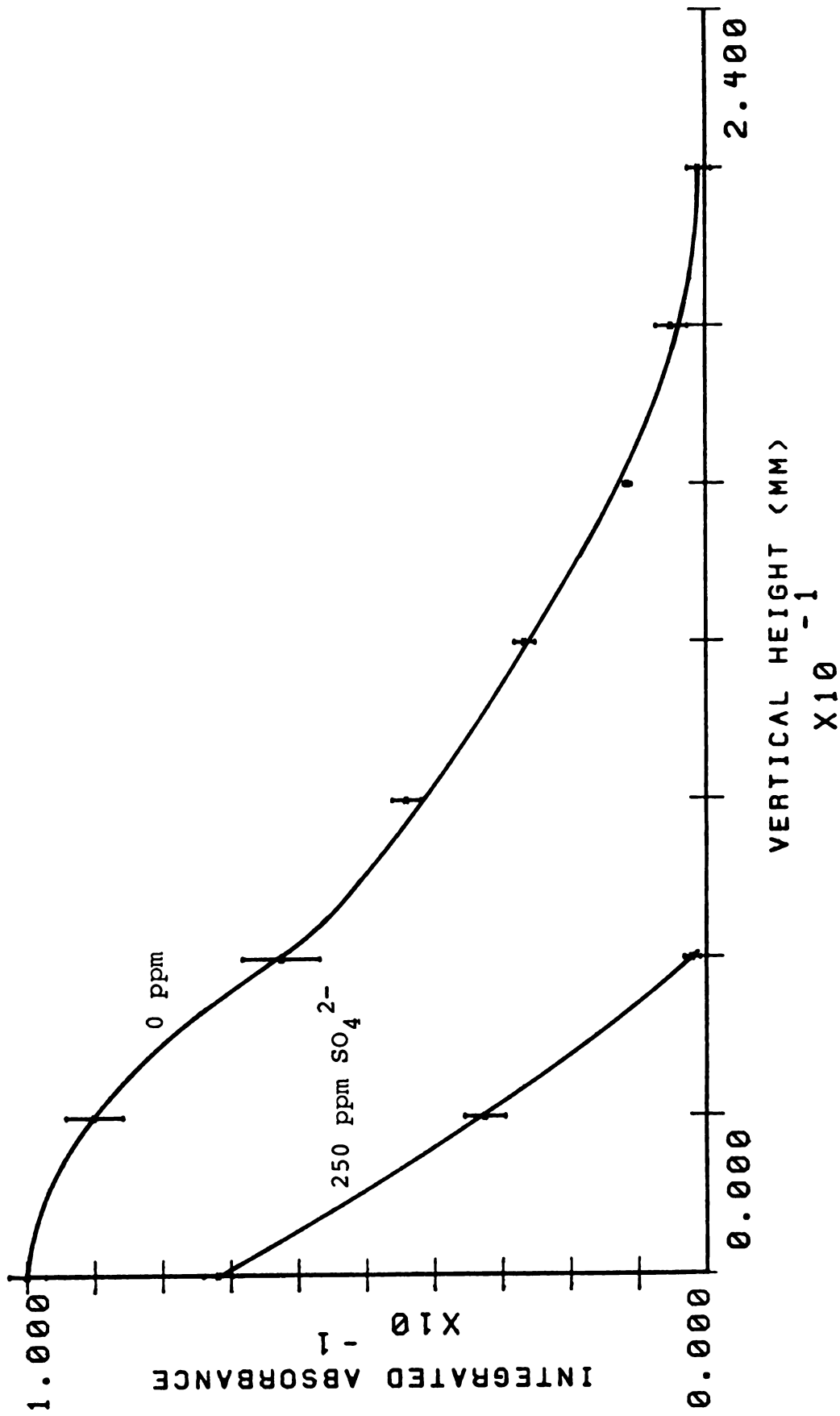
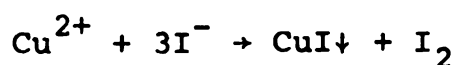


Figure 89. Effect of sulfate ion as potassium sulfate upon the vertical concentration profile of copper.

matrix effectiveness of potassium nitrate and sulfate. Copper requires much more heat to atomize than cadmium does. In the cases of copper and the potassium nitrate or sulfate matrices, the analyte and matrix may be volatilized essentially simultaneously, which provides the opportunity for the matrix to exert a depopulating influence. For cadmium and these matrices, the two may volatilize sufficiently separate in time to avoid much interaction. Unfortunately, neither potassium nitrate nor sulfate show any appreciable nonspecific absorption at the copper wavelength and the 250 ppm concentration level, so it is not possible to compare directly the times of maximum absorbance for samples of copper with and without these matrices, to see if the simultaneous volatility concept is true.

Another interesting effect is shown by the matrix of potassium iodide upon copper. In the presence of iodide, copper II ion undergoes the reaction:



Notice how the integrated absorbance averages for the copper-potassium iodide mixture decrease with time. No visible precipitation was present in solution at this trace copper level, and even if precipitate were present, it should still be delivered from the autosampler to the atomizer. The drop in integrated absorbance suggests

that insoluble CuI is adsorbed or otherwise retained upon the surfaces of the autosampler syringe parts, thereby reducing the total copper concentration delivered to the atomizer in each successive sample. Similar processes might also explain matrix effects that are observed in, for example, supernatants drawn off from suspensions such as effluent samples. Many of the investigations performed for lead in the present work were extremely confusing until the use of hydrogen peroxide in lead solutions was adopted to prevent the take up of lead by glass surfaces such as the autosampler syringe barrel.

A final illustration which emphasizes the contribution of chemical affinities to matrix effects is afforded by a comparison of effects between magnesium and copper. Both elements were studied at the same levels of analyte and matrix concentration, and under the same conditions of atomization as well. Yet magnesium suffers far worse in the presence of the matrices than does copper. Only for the ammonium salts does magnesium seem to be relatively matrix immune. This is again consistent with the volatility concepts of these salts. The increased susceptibility of magnesium to other matrices in general can be ascribed to its greater inherent chemical reactivity than copper.

The concentration dependence of the severe fluoride matrix with magnesium is illustrated in Figure 90, and a high resolution examination close to the braid is presented in Figure 91, with the assistance of the small

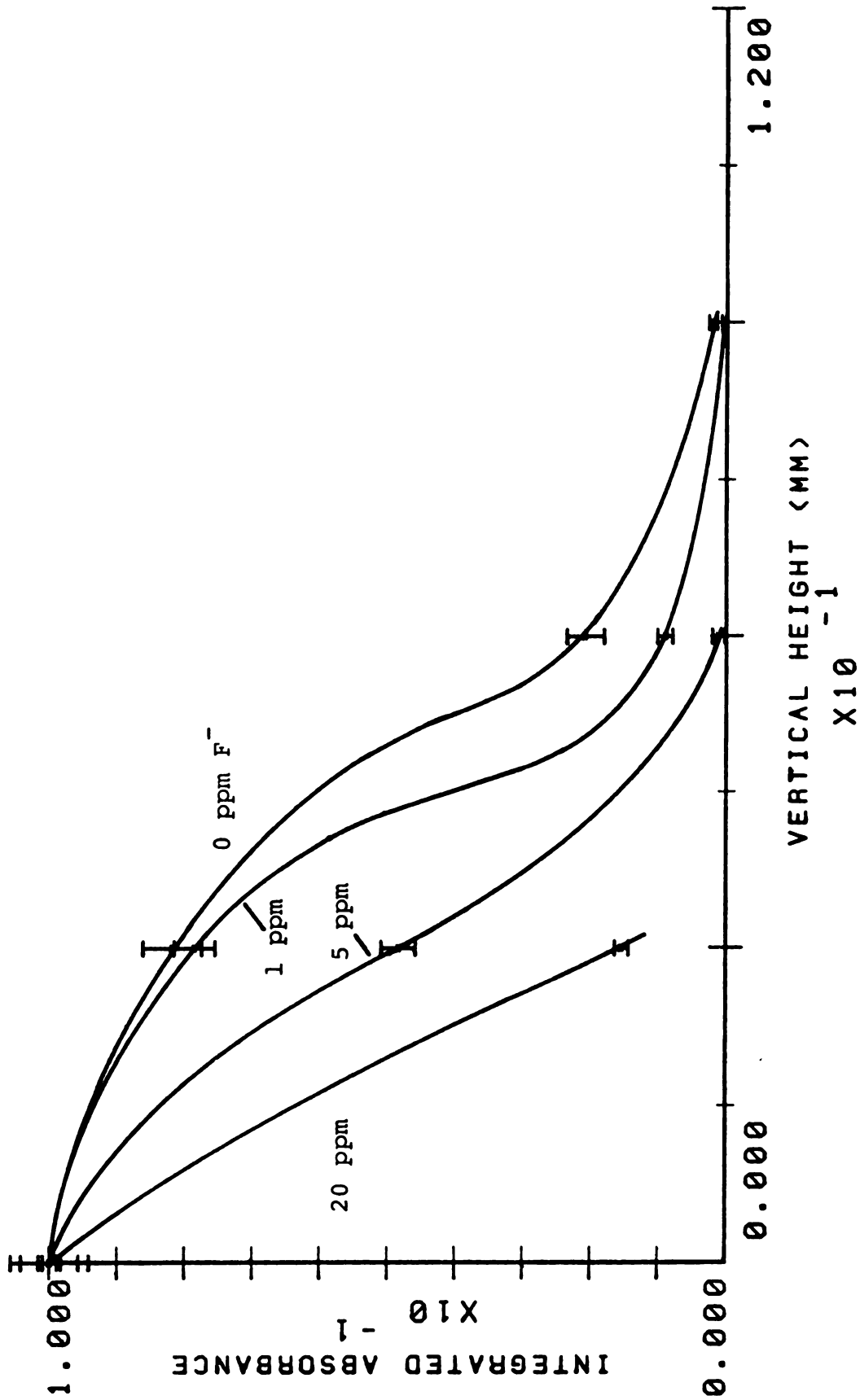


Figure 90. Concentration dependence of the effect of added fluoride ion upon the vertical concentration profile of magnesium.

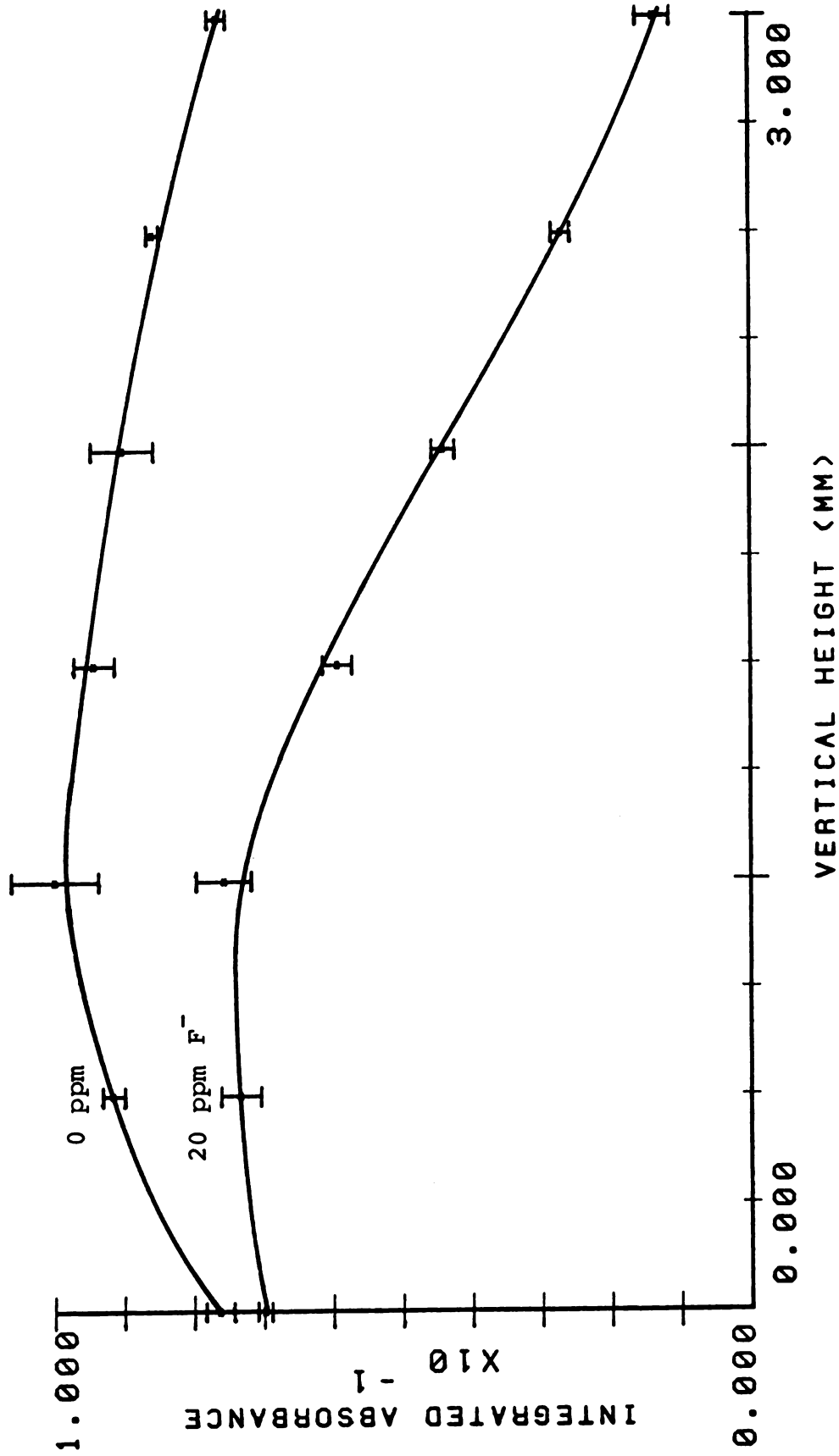


Figure 91. Effect of added fluoride ion upon the high resolution vertical concentration profile of magnesium.

aperture. The former figure is drawn with all data origins normalized to 10.00. The raw data shows some variability in the absorbance at grazing incidence regardless of fluoride content. It is a problem at times to get reproducible atomizations at given locations in space with elements that decay as rapidly as magnesium does. The flexibility of the braid, and the expansions it undergoes in heating give rise to small perturbations in the exact location of grazing incidence with time that can cause noticeable alterations in the integrated absorbances observed for such elements. The latter figure shows the familiar pattern that, in the presence of the matrix, the free atom population is reduced from the outset. The noticeable rise in integrated absorbance, with or without the matrix, for the first short distance of vertical travel, is something new, and indicates that for magnesium at least, mechanisms favorable to free atom production are still in effect away from the atomizer surface.

## SUMMARY AND CONCLUSIONS

The goal of this work was to characterize aspects of the performance of a filament electrothermal atomizer through the use of powerful instrumentation and automated computer control. Insofar as these studies were carried, this goal has been achieved. Experiments that require a great deal of time, as well as considerable attention to the control of a variety of instrumental links have been executed with thoroughness and consistency.

The two major instruments constructed, the positioner and autosampler, have many additional potential applications. The positioner can continue to provide the spatial control over the instrumentation that concentration profile studies require. But, there is little about the positioner that ties it specifically to its present application alone. If viewed as a separate instrument, it is really a dual channel, digital positioning device. The two motors can be connected to any sort of mechanical instrumentation that requires spatial variation under computer control. The autosampler is more directly tied to filament atomic spectrometric work, but it should have a long future of service in that area. Regardless of the exact mechanical configuration of the device, it has been the experience in this laboratory that an autosampler can consistently outperform a manual, hand-held syringe in terms of the precision of sample delivery.

This holds true for both the size of the sample itself, and its consistent placement on the atomizer. The present device is not perfect, and changes such as those outlined previously should be made. Its continued active use is, however, of certain benefit to further atomic spectrometric work.

The largest single shortcoming of the present instrumentation is that it is single channel. Additional work should be accompanied by refinements to correct this problem. At the least, a simple background corrector formed from a continuum lamp and beamsplitter could be coupled with a lamp pulsing circuit and phase-locked detector to accomplish this goal. The necessary lamp and optics are already available for such an addition. Alternate techniques are equally possible, such as the wavelength modulation method of O'Haver,<sup>192</sup> or the use of a true, multichannel device such as a diode array. The incorporation of such a device would imply extensive changes in the data collection electronics and interface. Microprocessor applications to this problem would be numerous.

The advantages of radiation programming for atomizer heating have been well illustrated. The use of a power supply of higher base voltage would permit further improvements in the characteristics of radiation programming. Investigations should also be done with photosensors which have improved infrared response to allow a lowering of

the regulation threshold. Comparative studies on other atomizers would assist in assessing the method for electrothermal atomic spectrometric work in general. With some of the more massive and rigid atomizers, the opportunity to do direct temperature regulation with a thermocouple also exists.

The microscopy studies should be carried on with an emphasis on methods by which to locate the principal salt crystal population. The scarcity of authentic salt particles located, even with inordinately concentrated samples, tends to remove these studies somewhat from truly reflecting atomizer conditions during real analyses. If undoing of the braid fibers should prove impractical, the examination of alternate atomizers which do not allow sample soaking could be substituted. The ability to examine a dried sample directly, and take its x-ray fluorescence spectrum, would be of great benefit in evaluating hypotheses about matrix effects.

The spatial examination of a filament atomization cell is a field of inquiry that is almost without bound. If time permits, much additional work could be done, not only for a wide range of matrix effects, but also for other phenomena which were not addressed in this work, such as interelement effects, the behavior of the sheath gas in the presence of the hot atomizer, or the nature of the hydrogen diffusion flame.

Finally, beyond the extensions of these topics listed

above, the graphite braid in general is deserving of further work to investigate its potentials as a general purpose atomizer, particularly for elements of low to moderate volatility. The soon anticipated construction of a tunable dye laser in this research group will offer a powerful instrumental tool for such work, particularly in the field of electrothermal atomic fluorescence, which has not as yet been the subject of much study on either the braid or many other devices.

## **APPENDICES**

APPENDIX A

SIMPLE HARDWARE CONTROL APPROACH  
FOR SEQUENCING CHEMICAL INSTRUMENTATION

by

S.R. Crouch\*, D.N. Baxter, E.H. Pals and E.R. Johnson<sup>†</sup>

Department of Chemistry  
Michigan State University  
East Lansing, Michigan 48824

\* Author to whom reprint requests should be sent

<sup>†</sup> Present address: Varian MAT  
25 Hanover Road  
Florham Park, NJ 07932

In modern analytical instrumentation, digital controllers have become more and more complex and flexible in recent years as instruments have become more highly automated. The controller directs the sequencing of various instrument functions. For example, in a modern, automated gas chromatography system, the controller might be required to send signals to an automatic sampler for introduction of the sample into the column, to control the oven temperature and its temperature program, to control the sensitivity of the detection system, and to control the detection and integration of the various chromatographic bands as they elute from the column. Such controllers may be simple fixed order sequencers, or may require branching to skip certain functions if certain instrument conditions are set by the user (i.e., unless the temperature program button and rate have been set, the controller would skip this part of its sequence).

In modern instruments, controllers take the form of hardwired logic systems, minicomputers or microprocessors. The microprocessor is certain to become the controller of choice in the future for many control operations, because the program (sequence) can be altered without changes in hardware. Also, even the most complex control operations, with multiple and nested branches can be readily carried out under the supervision of a microprocessor. However, the microprocessor requires the instrument designer to be re-educated in terms of software and processor capabilities. This education process may require months to years in order

to get working systems into the laboratory with microprocessors as "intelligent" instrument controllers.

A few years ago our research group became heavily involved in controllers when we decided to undertake a project which involves the spatial profiling of atomic concentrations above a filament-type electrothermal atomizer using atomic absorption spectrometry. We desired to automate fully the operations of sample introduction to the filament, movement of the filament in both x and y directions away from the AA optical axis to predetermined destinations, temperature programming of the filament, data acquisition of background corrected peak area, and automatic return to position "zero" for pickup of a new sample. The filament position controller was intended to move the atomization cell freely over a total displacement of one inch in either of two dimensions, through the use of stepper motor driven micrometer translation stages. The controller was required to function in either a "local" mode, in which the desired filament position could be set by the user via front panel BCD switches, or in an "on line" mode in which the controller received binary information from a minicomputer and functioned as a hardware slave to the processor. In addition, we required the controller to convert BCD position code to binary code in the local mode, to use position instead of displacement as the input (i.e., to remember where it is and to determine the direction to move and how far to go), and to be capable of a hardware reset to an optically defined

reference position. Finally, we required the controller to correct for play in the leadscrews of the translation stages in that if a requested movement was in the positive direction (i.e., away from the optical reference), the controller would intentionally move the cell to a known distance beyond the desired destination, and then reverse direction and return to the true destination, in contrast to movement in the negative direction, which would proceed directly to the destination without such overshoot. In this manner, no matter whether the net movement was positive or negative, the cell would be moved last in the negative direction, thus leaving the leadscrews tightly meshed in that direction of movement.

Because our group had no microprocessor experience at that time, we decided on the simple hardware approach described in this paper. Although the complexity of our application is such that we might at this time have chosen to use a microprocessor, there are many more simple control functions for which the approach described is highly suitable. Even for our complex application, this systems-level approach to controller design enabled us to design in about 3 hours a unit requiring over 50 IC's per motor controller. Construction and debugging of the position controller required additional time of course. The speed of our design was made possible by the use of a method originally described by Richards<sup>179</sup>, which allows all the complex sequential operations to be treated by using only a simple flow chart

at the beginning, and by implementing the flow chart with 2-3 MSI IC's.

To understand the approach, we present in the first section of this paper the general concepts and principles of the "state" of a controller and the simple implementation which results from the Richards<sup>179</sup> approach. We then present a chemical example of a "fall through" sequencer which controls an automatic fraction collector used in elution chromatography. In the last section we describe a branching sequencer and illustrate its use as an electro-thermal atomizer position controller.

#### A. THE CONCEPT OF THE STATE

In all but the most trivial control applications, a series or sequence of functions must be controlled. For such applications there are many approaches, but as the number of functions and the complexity increases, solutions can become exceedingly complicated. The systematic approach advocated in this paper allows even the most complex control applications to be handled with ease.

To help understand this approach several terms must be defined. This can be done most conveniently with the aid of an example. Consider the controller for the thermostat on a temperature bath. Using the method described by Richards<sup>179</sup>, it can be considered to have three states: State 0 = thermostat off - heater off; State 1 = heater on; and

State 2 = heater off. In State zero the thermostat controller waits for the condition of the thermostat power switch to be on. The on condition of the switch then is referred to as a transfer condition. When the transfer condition for state zero is true, i.e., the switch is on, the controller advances to state one. The process of this advance causes a transfer function to occur. The heater is turned on. The second state (state one) tests to see if the bath temperature exceeds the limit set on the thermostat. When the bath temperature does exceed the limit, the controller steps to state two, causing another transfer function to occur. The heater is turned off. The transfer condition for state two is a bath temperature below the thermostat limit. When this condition is met, no transfer function is required except to return to state zero and repeat the cycle.

Viewing such a trivial example in terms of states, transfer conditions, and transfer functions may seem overly complicated, but it is useful for two reasons. First, the method is also applicable to much more complex control applications. Second, by using this approach, the circuit design is greatly simplified by use of a standard circuit for the heart of the controller.

The application of this approach involves first converting the states, transfer conditions and transfer functions into a standard flowchart format. The two basic flowchart units for each state are shown in Figure A1. The unit which is used depends on what is to occur at that particular state.

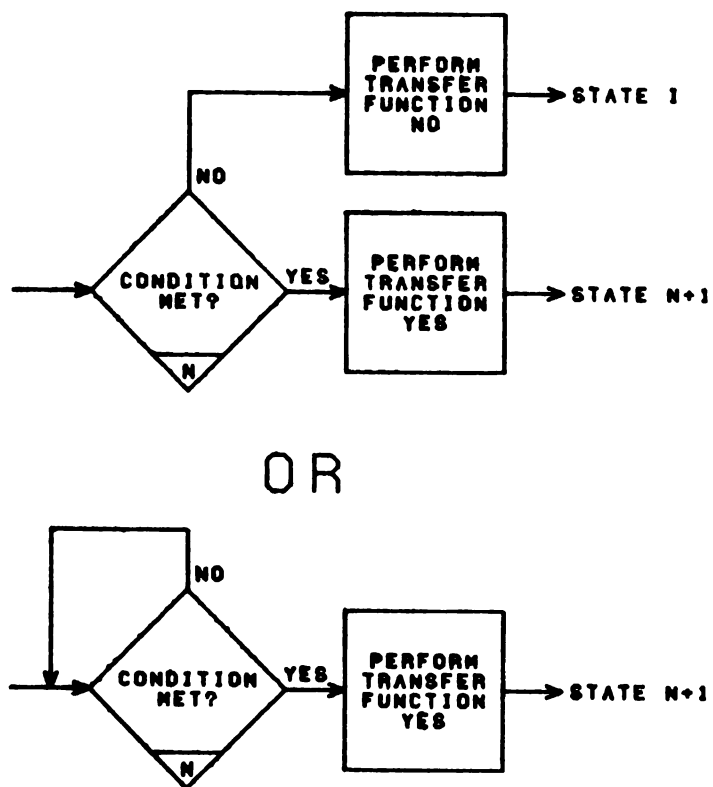


Figure A1. Basic flowchart units for transfer conditions and transfer functions.

Either unit contains a diamond shaped box which represents the state and contains the transfer condition. Depending on the application, the basic unit will also contain one or two rectangles which represent the transfer functions which occur depending on whether the transfer conditions are met or not. In this method the transfer function on the "no" leg is available only if the transfer condition not being met causes a move to a state I other than the present state. This transfer function, if it is used, is called a secondary transfer function as opposed to the primary transfer function on the "yes" leg. Figure A2 shows the flow chart for the bath thermostat example. No secondary transfer functions are required for this application and the controller is therefore an example of a fall through sequencer (no conditional branches).

Once the flowchart for the particular application has been constructed, the circuitry required for the "heart" of the controller can be chosen. The heart of a controller constructed using this method consists of a k-bit counter, an n-bit multiplexer and one or two n-bit decoders (the number of decoders depends on whether the application requires secondary transfer functions), where the number of states is n and  $n \leq 2^k$ .

Schematically, the heart of the controller is shown in Figure A3. The output of the counter indicates the present state of the controller. Using these outputs the multiplexer supplies the transfer condition appropriate to that state

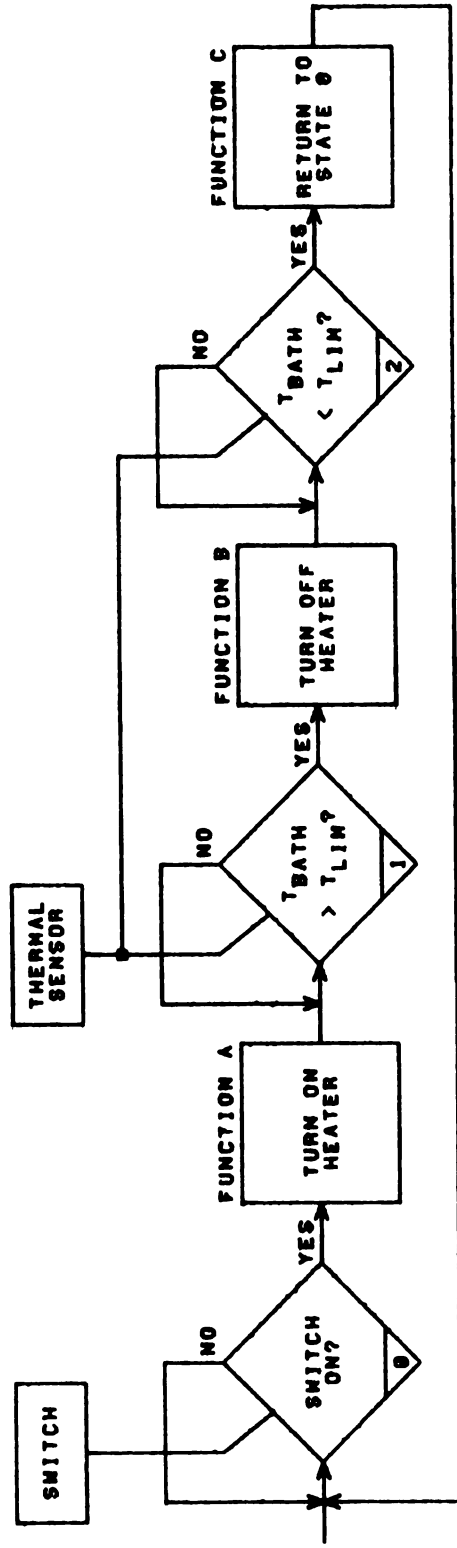


Figure A2. Sequencer flowchart for the example of a bath thermostat.

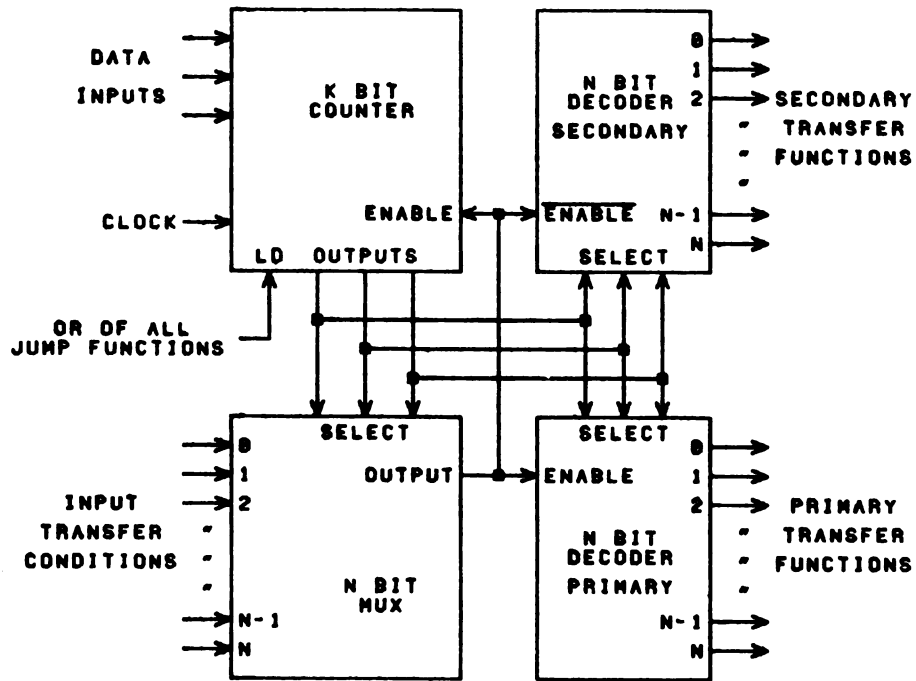


Figure A3. General schematic diagram of a controller.

to the state counter and to the decoder(s). If the transfer condition is true, then the clock on the state counter is allowed to increment to the next state. The presence of a true transfer condition also causes the associated primary transfer function from the decoder to go true, but this is only a pulse since the next clock pulse will step the state counter to the next state. If the transfer condition is false either a secondary transfer function may be generated if the controller is to go to a new state or the state counter may wait for the transfer function to become true.

Implementing this circuit for an eight state sequencer requires a 74163 counter, a 74151 multiplexer, and one or two 7442 decoders. At current single unit quantity prices they can be obtained for just over three dollars.

#### B. THE FALL-THROUGH SEQUENCER

The fall-through sequencer is the simplest type of sequencer. In this sequencer the only type of decision to be made is whether to remain in the present state or proceed to the next state. In a closed-loop operation this decision is based on receiving an "all done" signal (flag) from a previously actuated circuit. In an open-loop operation the change of state may be immediate or may occur upon receiving a signal that a time delay has elapsed.

A chemical example of a fall-through sequencer is a controller for an automatic fraction collector used in elution chromatography. Typically, the fraction collector has a rotatable tray which contains vials that are sequentially rotated beneath the column outlet valve. When a vial is directly beneath the outlet valve, the valve is opened for a preset time, then closed, and the next vial rotated into the receiving position. These motions are then repeated until the desired number of fractions have been collected.

In Figure A4 the decisions and actions involved in controlling this apparatus are represented in flow diagram form, along with the inputs used by the decisions in functioning. Assume that the operator has initialized the apparatus by rotating the first vial into position beneath the valve and loaded the number of fractions desired into a counter register. Also assume that the controller is initially in State  $\emptyset$ . Condition A is satisfied since the counter is non zero, so the controller generates Function A, which is to open the delivery valve and to start the delay timer. Now the controller moves to state 1 and repeatedly queries the delay timer until it signals that enough solution has been delivered (Condition B). When Condition B has been satisfied the controller closes the valve and starts the vial tray moving (Function B). Now the controller moves to State 2 and waits for a position indicator microswitch beneath the

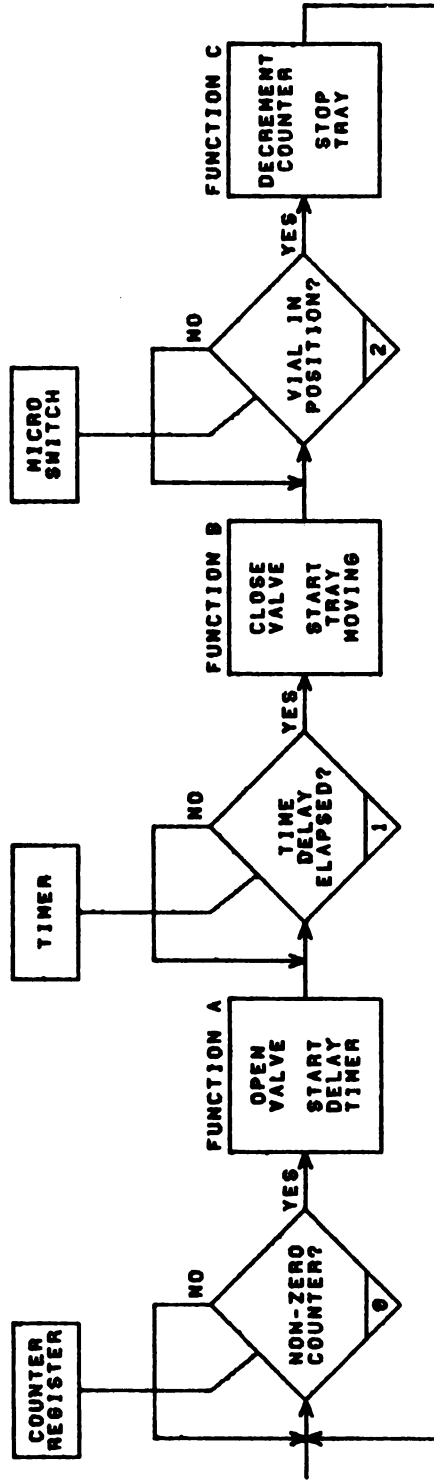


Figure A4. Sequencer flowchart for the example of an automatic fraction collector.

outlet valve to be tripped (Condition C). When Condition C is met the controller must decrement the fraction counter register, stop the tray, and effect a jump back to controller state  $\emptyset$  (Function C). This sequence is then repeated until the fraction counter register is decremented to zero. When this happens condition A can never be met, so the apparatus halts since it becomes hung up in State  $\emptyset$ .

This controller can be quite easily implemented using a sequencer composed of three IC's: a 74163 counter, a 74151 multiplexer, and a 7442 decoder. Of course additional packages may be necessary for such things as delay timing but these three IC's handle the generation of all the signals necessary to initiate the actions at the appropriate times. Figure A5 shows how these IC's are interconnected and also shows the input and output signals that are required in this particular application. When power is turned on, an initialize pulse is required to clear the fraction counter register and to assert the clear input of the state counter. This forces the counter to zero, which is State  $\emptyset$ . The QA, QB, and QC outputs of the state counter are all LO, which sets the multiplexer's Y output LO. This LO signal is fed to the state counter's ENABLE P input, which inhibits the counter from counting clock pulses at its CLOCK input. Thus it remains in State  $\emptyset$ . The multiplexer's complementary output W is directed to the decoder's D input. Output W is HI, and examination of the truth table

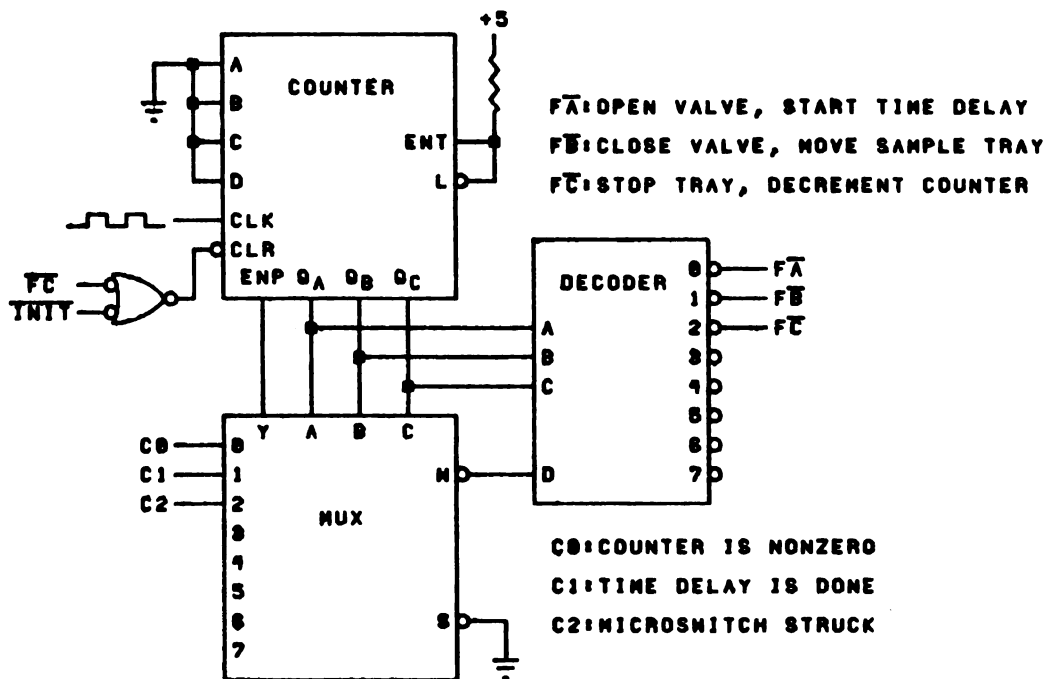


Figure A5. Schematic diagram of the controller for the example of the automatic fraction collector.

for the decoder indicates that the 0 through 7 decoder outputs must be HI when D is HI (Negative logic is used at these outputs so that a function is generated only when the output goes LO). This means that initially none of the functions are being asserted. When the operator gives the "GO" command, the number of fractions desired is loaded into the fraction counter register, and Condition A is satisfied. Now the multiplexer's W output goes LO, and the decoder now points to a decimal 0, which asserts the Function A signal.

Function A triggers external circuitry to open the delivery valve and start a time delay circuit. In addition, the multiplexer Y output is HI, so that the state counter's ENABLE P input is asserted, and on the first clock pulse the counter is incremented once (State 1). Now the multiplexer shifts from selecting data channel 0 (Condition A) to data channel 1 (Condition B). Assuming that the required time delay has not yet elapsed, Condition B is not yet satisfied so that the multiplexer Y output falls, locking the state counter in State 1, and the W output goes high, concluding function A and inhibiting the decoder from generating any functions.

When the required time delay has elapsed, Condition B is satisfied and a similar sequence occurs in the state counter, multiplexer and decoder. The multiplexer's W output enables the decoder, and its A, B, C and D inputs point to decimal 1. Thus, output 1 (Function B) is asserted. This triggers the valve to close and starts the tray moving. The

multiplexer Y output goes high allowing the counter to count one pulse and move to State 2. Now the state counter requests the multiplexer to address the status of Condition C.

When the new sample vial reaches the position beneath the outlet valve, a microswitch is tripped and Condition C is satisfied. Again this activates the decoder, and Function C is asserted. Function C stops the tray and decrements the fraction counter register. Also, since this is the last function in the sequence, it is used to assert the CLEAR input of the state counter and return the controller to State  $\emptyset$ .

Unless this was the last fraction to be collected, the fraction counter register will be non-zero when the state counter enters State  $\emptyset$  so that Condition A is immediately satisfied. Thus, as soon as the Function C pulse has cleared the state counter to State  $\emptyset$ , Function A will be generated and on the next clock pulse State 1 will be achieved. This entire delivery sequence will continue until the fraction counter register reaches zero, which prevents Condition A from being satisfied. Then the apparatus will halt because the controller becomes hung up in State  $\emptyset$  until the operator intervenes to start a new collection sequence.

## C. THE BRANCHING SEQUENCER

In many cases it is desirable to have a sequencer capable of branching; that is, one in which sections of the basic state sequence may be skipped, repeated, or otherwise altered as requested by the instrumentation under control. An example of such a sequencer is the electro-thermal atomizer position controller mentioned previously.

The flow diagram of its sequence is shown in Figure A6. The system waits in State  $\emptyset$  until data representing a new location are received, and a command to move is given. Upon receipt of this command, the overflow flag is cleared, and the system determines if it is being operated under local or computer control. If control is local, the desired destination has been entered in BCD format from front panel thumb-wheel switches, which requires a BCD to binary conversion. A check is made to see if the system is free of overflow, and if so, another check is made to see if BCD to binary conversion is complete. If conversion is not complete, the registers are clocked, and the checks for overflow and complete conversion are repeated. If an overflow should occur, the sequence will abort to State  $\emptyset$  with the overflow flag set. (Overflow results from entering a destination outside the defined limits of the system.) If no overflow occurs, then upon completion of the conversion, the stepper motor direction is determined, and the stage begins to move.



If control is from the computer, the BCD to binary conversion is unnecessary. Thus, this section of the sequence is omitted.

The stage moves until the destination is reached. At this point the system checks to see if the direction of movement was positive. If so, the stage continues to move ten additional increments positive, and when finished, reverses direction and comes back ten increments negative. If movement was originally negative, the sequence is concluded immediately. In this manner gear play is removed from the mechanism by assuring that movement always occurs last in the negative direction.

To implement a branching sequencer such as this, it is necessary to add only one additional decoder IC to the basic controller circuit. The actual wiring is shown in Figure A7. The actions of this controller are identical to the simpler three chip system previously discussed as long as the basic, non-branching sequence is followed. If a branch is called for, however, (if the selected data channel of the multiplexer is low when a potentially branchable state is reached), the following events occur. The LO state of output Y from the multiplexer causes the function pulse to be generated by the second decoder instead of the first decoder. This function pulse is used by the instrument to perform tasks in the same manner as any function pulse from the first decoder. In addition, this pulse is also fed back to the state counter where it serves

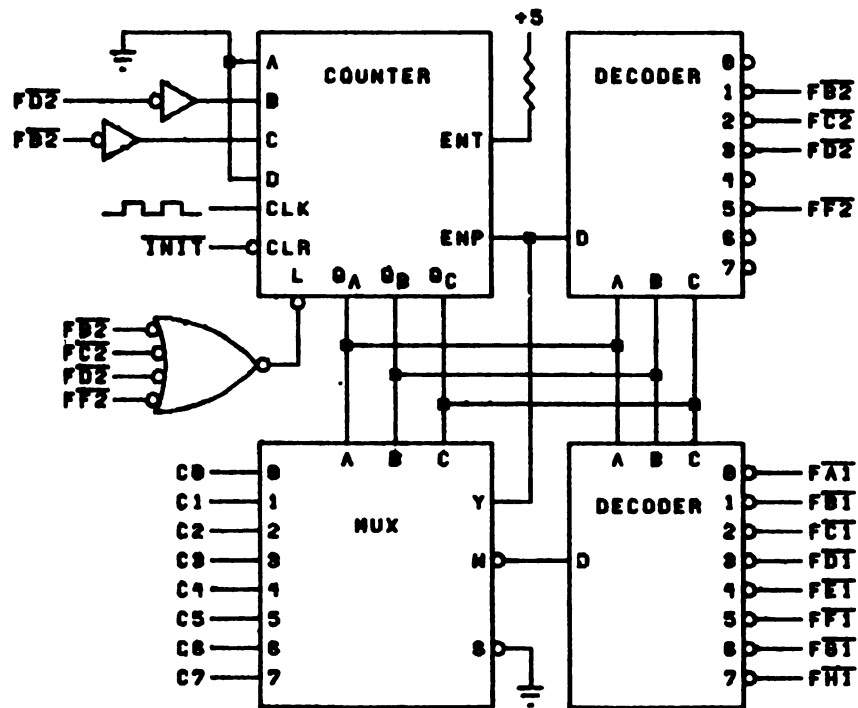


Figure A7. Schematic diagram of the controller for the filament positioning instrument.

simultaneously to provide binary data representing the state to which to branch as well as to load those data into the state counter. For example, in the positioner sequence, if the system is under computer control when state 1 is entered, the L0 level at the data channel 1 of the multiplexer disables the first decoder, but causes the second decoder to generate function B2. Function B2 is used in the circuitry to update the direction of movement and start the motor, just as function D1 of the first decoder does under local control. But, it is also present at the C and Load inputs of the state counter, so that as it occurs, the state counter is forced to skip directly to state 4 through parallel loading. All additional functions which are part of other such branches are similarly directed back to the Load and appropriate data inputs of the state counter, using simple gates as shown to OR them together as required.

By adding additional multiplexer and decoder chips to the controller, it is possible to produce sequencers of even greater complexity in which the branches consist not only of single function pulses, but also of additional states or even complete subsequences reminiscent of nested computer subroutines<sup>179</sup>. Similarly, it is also possible to substitute basic chips different from those employed here to produce sequences of more than eight basic states. However, such systems can quickly become unwieldy in their complexity and might very well be better performed using

microprocessor-managed controllers even if the user has no previous experience with such devices<sup>192-195</sup>.

#### D. CONCLUSIONS

We have described in this paper a hardware approach for designing instrument sequencers, which we feel greatly reduces design time, yet allows complex sequences to be readily implemented. The increasing education of chemists as to the potential, the software, and the interfacing of microprocessors will certainly lead to a level of controller complexity at which a microprocessor is the sequencer of choice. Even so, the concepts presented here should enable simple controllers to be designed and implemented readily by chemists unfamiliar with microprocessors or for applications in which it is undesirable to "tie up" the processor in simple, unchanging control tasks. In our own laboratories, the cross-over point between using hardwired-logic and microprocessor controllers has continuously declined as our knowledge of microprocessor technology has improved. At present, in our case, a controller requiring >30 IC's would probably be implemented with microprocessors. For electronics designers, the crossover point is undoubtedly fewer IC's than our figure. Nonetheless, the simplicity of the approach presented here, should prove valuable to

other chemists involved in the automation of chemical instruments.

#### ACKNOWLEDGMENTS

We are grateful to Dr. T.V. Atkinson for his assistance in the use of a computerized graphics facility for the production of our figures. D.N.B. acknowledges both a summer and a full year ACS Analytical Fellowship under the sponsorship of the Procter and Gamble Company of Cincinnati, Ohio.

## APPENDIX B

### SOURCES OF COMMERCIAL INSTRUMENTATION

#### Computer:

Model 8/e - Digital Equipment, Maynard, MA

#### Internal Bus Options:

8K core memory

8K random access memory

Extended arithmetic element

Real-time clock

Positive I/O bus interface

#### External Bus Options:

RK8E hard disc

Dual floppy disc (Model 7200, Sykes Datatronics,  
Rochester, NY)

Graphics terminal (Consul-980, Applied Digital  
Data Systems, Hauppauge, NY)

LA-30 Decwriter

Computer Interface Buffer (Heath, Benton Harbor, MI)

#### Spectrometer Components: GCA McPherson, Acton, MA

HCDT Supply: Model EU-703-70

Monochromator: Model EU-700

Photomultiplier: Model EU-701-30

#### Spectrometer Accessories:

**Hollow Cathode Lamps:**

Jarrell-Ash, Fisher Scientific, Livonia, MI

Westinghouse, Elmira, NY

Flowmeters: Type 13 Roger Gilmont Instruments, Great  
Neck, NY

Lenses, chimney plates: Grade S1-UV quartz, Esco  
Optics, Oak Ridge, NY

Photocurrent Amplifier: Model 427, Keithley Instruments,  
Cleveland, OH

Laser: Model LS-32, Electro-Nuclear Labs, Waltham, MA

**Positioner:**

Translation Stages: Model 420-S1, Newport Research,  
Fountain Valley, CA

Circuit Boards: Type 11-DE-S, Douglas Electronics,  
San Leandro, CA

Motors: Model 23D6102A, Computer Devices, Santa Fe  
Springs, CA

**Autosampler:**

Syringe: Model S1100, Roger Gilmont Instruments,  
Great Neck, NY

Motors: Models 23D6102A (rotor) and 23D6306A (vertical),  
Computer Devices, Santa Fe Springs, CA

Models 202215D200-F1.6 (syringe) and 10-2013D40-F75  
(turret), Sigma Instruments, Braintree, MA

**Data Acquisition and Other:****Converters:**

D/A: Type DACHY12BC, Datel, Canton, MA

A/D: Type ADCHY12BC, Datel, Canton, MA (no longer available)

Power Supplies:

HD5-12/OVP (+5 volts) and HBAA-40W ( $\pm 15$  volts),

Power One, Camarillo, CA

Card Rack: Model SR-20105, Bud Radio,

Willoughby, OH

## REFERENCES

## REFERENCES

1. Hieftje, G. M., Copeland, T. R., and deOlivares, D. R., *Anal. Chem.*, 48, 142R (1976).
2. Winefordner, J. D., and Vickers, T. J., *Anal. Chem.*, 46, 192R (1974).
3. Woodward, C., "Annual Reports on Analytical Atomic Spectroscopy, 1973", Vol. 3, Society for Analytical Chemistry, London, 1974.
4. Woodward, C., "Annual Reports on Analytical Atomic Spectroscopy, 1974", Vol. 4, Society for Analytical Chemistry, London, 1974.
5. Kirchhoff, G., and Bunsen, R., *Fresenius Z. Anal. Chem.*, 1, 1 (1862).
6. Mika, J., and Torok, T., "Analytical Emission Spectroscopy", Crane and Russek, New York, 1974.
7. Ahrens, L. H., and Taylor, S. R., "Spectrochemical Analysis", Addison-Wesley, Reading, Massachusetts, 1961.
8. Slavin, M., "Emission Spectrochemical Analysis", Wiley-Interscience, New York, 1971.
9. Barnes, R. M., *Syst. Mater. Anal.*, 3, 23 (1974).
10. Butler, L. R. P., Human, H. G. C., and Scott, R. H., *Handb. Spectrosc.*, 1, 816 (1974).
11. Skogerboe, R. K., *ibid.*, 1, 845 (1974).
12. Mitchell, A. C. G., and Zemansky, M. W., "Resonance Radiation and Excited Atoms", Cambridge University Press, New York, 1961.
13. Walsh, A., *Anal. Chem.*, 46, 698A (1974).
14. Walsh, A., *Spectrochim. Acta*, 7, 108 (1955).
15. Russell, B. J., Shelton, J. P., and Walsh, A., *Spectrochim. Acta*, 8, 317 (1958).
16. Gaydon, A. G., "The Spectroscopy of Flames", 2nd. ed., Halsted, New York, 1974.

17. Kirkbright, G. F., and Sargent, M., "Atomic Absorption and Fluorescence Spectroscopy", Academic Press, New York, 1974.
18. Wood, R. W., *Phil. Mag.*, 10, 513 (1905).
19. Nichols, E. L., and Howes, H. L., *Phys. Rev.*, 23, 472 (1924).
20. Alkemade, C. Th. J., *Proc. Colloq. Spectrs. Internat.*, Spartan Books, Washington, D.C., 1963.
21. Winefordner, J. D., and Vickers, T. J., *Anal. Chem.*, 36, 161 (1964).
22. Browner, R. F., *Analyst*, 99, 617 (1974).
23. West, T. S., *Analyst*, 99, 886 (1974).
24. Kirkbright, G. F., *Analyst*, 96, 609 (1971).
25. Denton, M. B., and Malmstadt, H. V., *Anal. Chem.*, 41, 241 (1972).
26. Syty, A., *Crit. Rev. Anal. Chem.*, 4, 155 (1974).
27. King, A. S., *Astrophys. J.*, 56, 318 (1922).
28. King, A. S., and King, R. B., *ibid.*, 82, 377 (1935).
29. King, R. B., and Stockbarger, D. C., *ibid.*, 91, 488 (1940).
30. Lvov, B. V., *Spectrochim. Acta*, 17, 761 (1961).
31. Lvov, B. V., and Lebedev, G. G., *Zh. Prikl. Spektrosk.*, 7, 264 (1967).
32. Lvov, B. V., *Spectrochim. Acta*, 24B, 53 (1969).
33. Woodruff, R., and Ramelow, G., *Spectrochim. Acta*, 23B, 665 (1968).
34. Woodruff, R., Stone, R. W., and Held, A. M., *Appl. Spec.*, 22, 408 (1968).
35. Woodruff, R., and Stone, R., *Appl. Optics*, 7, 1337 (1968).
36. Woodruff, R., Culver, B. R., and Olsen, K. W., *Appl. Spec.*, 24, 530 (1970).

37. Woodriff, R., and Shrader, D., *Anal. Chem.*, 43, 1918 (1971).
38. Pagenkopf, G. K., Neuman, D. R., and Woodriff, R., *Anal. Chem.*, 44, 2248 (1972).
39. Woodriff, R., Culver, B. R., Shrader, D., and Super, A. B., *Anal. Chem.*, 45, 230 (1973).
40. Massmann, H., *Spectrochim. Acta*, 23B, 215 (1968).
41. Massmann, H., in "Flame Emission and Atomic Absorption Spectrometry", Vol. 2, Dean, J. A., and Rains, T. C., Eds., Marcel Dekker, New York, 1971.
42. Perkin-Elmer Corporation, *Instrument News*, 21, 4 (1970).
43. Kahn, H. L., and Slavin, S., *A. A. Newsletter*, 10, 125 (1971).
44. Perkin-Elmer Corporation, "Analytical Methods for Atomic Absorption Spectroscopy using the HGA Graphite Furnace", Norwalk, Conn., March, 1973.
45. Winefordner, J. D., *Pure Appl. Chem.*, 23, 35 (1970).
46. Christian, C. M., and Robinson, J. W., *Anal. Chim. Acta*, 56, 466 (1971).
47. Robinson, J. W., and Slevin, P. J., *Amer. Lab.*, August, 1972, pp. 10.
48. Robinson, J. W., Slevin, P. J., Hindman, G. C., and Wolcott, D. C., *Anal. Chim. Acta*, 61, 431 (1972).
49. Robinson, J. W., Wolcott, D. K., Slevin, P. J., and Hindman, G. D., *Anal. Chim. Acta*, 66, 13 (1973).
50. Headridge, J. B., and Smith, D. R., *Talanta*, 18, 247 (1971).
51. Langmyhr, F. J., and Thomassen, Y., *Z. Anal. Chem.*, 264, 122 (1973).
52. Murphy, M. K., Clyburn, S. A., and Veillon, C., *Anal. Chem.*, 45, 1468 (1973).
53. Black, M. S., Glenn, T. H., Bratzel, M. P., and Winefordner, J. D., *Anal. Chem.*, 43, 1769 (1971).
54. Molnar, C. J., and Winefordner, J. D., *Anal. Chem.*, 46, 1419 (1974).

55. Chapman, J. F., Dale, L. S., and Kelly, J. W., *Anal. Chim. Acta*, 69, 207 (1974).
56. Robinson, J. W., and Wolcott, D. K., *Anal. Chim. Acta*, 74, 43 (1975).
57. Robinson, J. W., Wolcott, D. K., and Rhodes, L., *Anal. Chim. Acta*, 78, 285 (1975).
58. Church, D. A., Hadeishi, T., Leong, L. McLaughlin, R. D., and Aak, B. D., *Anal. Chem.*, 46, 1352 (1974).
59. Kantor, T., Clyburn, S., and Veillon, C., *Anal. Chem.*, 46, 2205 (1974).
60. Clyburn, S. A., Kantor, T., and Veillon, C., *Anal. Chem.*, 46, 2213 (1974).
61. Molnar, C. J., and Winefordner, J. D., *Anal. Chem.*, 46, 1807 (1974).
62. Sturgeon, R. E., and Chakrabarti, C. L., *Anal. Chem.*, 49, 90 (1977).
63. Runnels, J. H., Merryfield, R., and Fisher, H. B., *Anal. Chem.*, 47, 1258 (1975).
64. Fuller, C. W., and Thompson, I., 102, 141 (1977).
65. Thomassen, Y., Larsen, B., Langmyhr, F., and Lund, W., *Anal. Chim. Acta*, 83, 103 (1976).
66. Ottaway, J. M., and Shaw, F., *Analyst*, 100, 438 (1975).
67. DeGalan, L., *Anal. Chim. Acta*, 87, 259 (1976).
68. Fuchs, C., Brasche, M., Paschen, K., Nordbech, H., and Quellhorst, E., *Clin. Chem. Acta*, 52, 71 (1974).
69. Perry, E. F., Koirtyohann, S. R., and Perry, H. M. Jr., *Clin. Chem.*, 21, 626 (1975).
70. Pekarek, R. S., Hauer, E. C., Wannemacher, R. W., Jr., and Beisel, W. R., *Anal. Biochem.*, 59, 283 (1974).
71. Kamel, H., Brown, D. H., Ottaway, J. M., and Smith, W. E., *Analyst*, 101, 790 (1976).
72. Fernandez, F. J., *Clin. Chem.*, 21, 558 (1975).
73. Toffaletti, J., and Savory, J., *Anal. Chem.*, 47, 2091 (1975).

74. Ebert, J., and Jungmann, H. Z. Anal. Chem., 272, 287 (1974).
75. Chao, S. S., Kanabrocki, E. L., Moore, C. E., Oester, Y. T., Greco, J., and vonSmolinski, A., Appl. Spec., 30, 155 (1976).
76. Ihnat, M., Anal. Chim. Acta, 82, 293 (1976).
77. Gong, H., and Suhr, N. H., 81, 297 (1976).
78. Langmyhr, F. J., Stubergh, J. R., Thomassen, Y., Hanssen, J. E., and Dolezal, J., Anal. Chim. Acta, 71, 35 (1974).
79. Siemer, D., and Woodriff, R., Spectrochim. Acta, 29B, 269 (1974).
80. Frech, W., and Cedergren, A., Anal. Chim. Acta. 88, 57 (1977).
81. Henn, E. L., Anal. Chem., 47, 428 (1975).
82. Lord, D. A., McLaren, J. W., and Wheeler, R. C., Anal. Chem., 49, 257 (1977).
83. Hageman, L., Torma, L., Ginther, B. E., J. Assoc. Off. Anal. Chem., 58, 990 (1975).
84. Persson, J. A., Frech, W., and Cedergren, A., Anal. Chim. Acta, 89, 119 (1977).
85. Medina, R., Z. Anal. Chem., 271, 346 (1974).
86. Kragsten, J., and Reynaert, A. P., Talanta, 21, 618 (1974).
87. Marks, J. Y., Welcher, G. G., and Spellman, R. J., Appl. Spec., 31, 9 (1977).
88. West, T. S., and Williams, X. K., Anal. Chim. Acta. 57, 281 (1969).
89. Anderson, R. G., Maines, I. S., and West, T. S., Anal. Chim. Acta, 51, 355 (1970).
90. Alder, J. F., and West, T. S., Anal. Chim. Acta, 51, 365 (1970).
91. Jackson, K. W., West, T. S., and Balchin, L., Anal. 45, 249 (1973).

92. Belyaev, Uy. I., Pchelintsev, A. M., Zvereva, N. F., and Kostin, B. I., *Zh. Anal. Khim.*, 26, 492 (1971).
93. Belyaev, Uy. I., Karyakin, A. V., and Pchelintsev, A. M., *Zh. Anal. Khim.*, 25, 852 (1970).
94. Belyaev, Uy. I., Koveshnikova, T. A., and Kostin, B. I., *Zh. Anal. Khim.*, 28, 2111 (1973).
95. Belyaev, Uy. I., Pchelintsev, A. M., and Zvereva, N. F., *Zh. Anal. Khim.*, 26, 1295 (1971).
96. Amos, M. D., Bennett, P. A., Brodie, K. G., Lung, P. W. L., and Matousek, J. P., *Anal. Chem.*, 43, 211 (1971).
97. Amos, M. D. and Matousek, J. P., 23rd Pittsburgh Conf. Anal. Chem. Appl. Spectrosc., Cleveland, Ohio, March 1972.
98. Dipierro, S., and Tessari, G., *Talanta*, 18, 707 (1971).
99. Montaser, A., Goode, S. R., and Crouch, S. R., *Anal. Chem.*, 46, 599 (1974).
100. Montaser, A., and Crouch, S. R., *Anal. Chem.*, 46, 1817 (1974).
101. Montaser, A., and Crouch, S. R., *Anal. Chem.*, 47, 38 (1975).
102. Molnar, C. J., Reeves, R. D., Winefordner, J. D., Glenn, M. T., Ahlstrom, J. R., and Savory, J., *Appl. Spec.*, 26, 606 (1972).
103. Donega, H. M., and Burgess, T. E., *Anal. Chem.*, 42, 1521 (1970).
104. Hwang, J. Y. Ullucci, P. A., and Smith, S. B., *Amer. Lab.* August 1971, pp. 41.
105. Takeuchi, T., Yanagisawa, M., and Suzuki, M., *Talanta*, 19, 465 (1972).
106. Maruta, T., and Takeuchi, T., *Anal. Chim. Acta*, 62, 253 (1973).
107. Cantle, J. E., and West, T. S., *Talanta*, 20, 459 (1973).
108. Winefordner, J. D., *Pure Appl. Chem.*, 23, 35 (1970).

109. Bratzel, M. P., Dagnall, R. M., and Winefordner, J. D., *Appl. Spec.*, 24, 518 (1970).
110. Bratzel, M. P., Dagnall, R. M., and Winefordner, J. D., *Anal. Chim. Acta*, 48, 197 (1969).
111. Goode, S. R., Montaser, A., and Crouch, S. R., *Appl. Spec.*, 27, 355 (1973).
112. Williams, M. and Piepmeier, E. H., *Anal. Chem.*, 44, 1342 (1972).
113. Chauvin, J. V., Newton, M. P., and Davis, D. G., *Anal. Chim. Acta*, 65, 291 (1973).
114. McCullough, M. R., and Vickers, J. J., *Anal. Chem.*, 48, 1006 (1976).
115. Ohta, K., and Suzuki, M., *Talanta*, 22, 465 (1975).
116. McIntyre, N. S., Cook, M. G., and Boase, D. G., *Anal. Chem.*, 46, 1983 (1974).
117. Newton, M. P., and Davis, P. G., *Anal. Chem.*, 47, 2003 (1975).
118. Koliheva, D., Sychra, V., *Chem. Listy*, 68, 1091 (1974).
119. Evenson, M. A., and Warren, B. L., *Clin. Chem.*, 21, 537 (1975).
120. Stafford, D. T., and Saharovici, F., *Spectrochim. Acta*, 29B, 277 (1974).
121. Henkin, R. I., Mueller, C. W., and Wolf, R. O., *J. Lab. Clin. Med.*, 86, 175 (1975).
122. Blood, E. R., and Grant, G. C., *Anal. Chem.*, 47, 1438 (1975).
123. Ratcliffe, D. G., Byford, C. S., and Osman, P. B., *Anal. Chim. Acta*, 75, 457 (1975).
124. Mullen, J. D., *Talanta*, 23, 846 (1976).
125. Nikolaev, G. I., Podgornaya, V. I., Kalinin, S. K., and Zakharenko, V. M., *J. Anal. Chem. USSR*, 29, 124 (1975).
126. Ohta, K., and Suzuki, M., *Anal. Chim. Acta*, 77, 288 (1975).

127. Tam, K. C., Environ. Sci. Technol. 8, 734 (1974).
128. Janouskova, J., Sulcek, Z., and Sychra, V., Chem. Listy, 68, 969 (1974).
129. Shigematsu, T., Matsui, M., Fujino, O., and Kinoshita, K., Anal. Chim. Acta, 76, 329 (1975).
130. Janssens, M. and Dams, R., Anal. Chim. Acta, 70, 25 (1974).
131. Brady, D. V., Nantalov, J. G., Jr., Glowacki, G., and Pisciotta, A., Anal. Chim. Acta, 70, 448 (1974).
132. Riandey, C., Linhares, P., and Pinta, M., Analisis, 3, 202 (1975).
133. Osborne, A. C., and West, T. S., Proc. Soc. Anal. Chem., 9, 198 (1972).
134. Chuang, F. S., and Winefordner, J. D., Appl. Spec., 28, 215 (1974).
135. Dittrich, K., and Mothes, W., Talanta, 22, 318 (1975).
136. Goleb, J. A., and Midkiff, C. R., Appl. Spec., 29, 44 (1975).
137. Henn, E. L., Anal. Chim. Acta, 73, 273 (1974).
138. Huffman, H. L., Jr., and Caruso, J. A., J. Agric. Food Chem., 22, 824 (1974).
139. Alger, D., Anderson, R. G., Maines, I. S., and West, T. S., Anal. Chim. Acta, 57, 271 (1971).
140. Reeves, R. D., Patel, B. M., Molnar, C. J., and Winefordner, J. D., Anal. Chem., 45, 246 (1973).
141. Prudnikov, E. D., Zh. Prikl. Spektrosk., 14, 145 (1971).
142. Prudnikov, E. D., Zh. Anal. Khim., 27, 2327 (1972).
143. Prudnikov, E. D., and Shapkina, U. C., Zh. Anal. Khim., 28, 1055 (1973).
144. Kahn, H. L., Peterson, G. E., and Schallis, J. E., A. A. Newsletter, 7, 35 (1968).
145. Ringhardt, I., and Welz, B., Z. Anal. Chem., 243, 190 (1968).

146. Hauser, T. R., Hinners, T. A., and Kent, J. L., *Anal. Chem.*, 44, 1819 (1972).
147. Curry, A. J., Read, J. F., and Knott, A. R., *Analyst*, 94, 744 (1969).
148. Delves, H. T., *Analyst*, 95, 431 (1970).
149. Ediger, R. D., and Coleman, R. L., *A. A. Newsletter*, 11, 33 (1972).
150. Joselow, M. M., and Bogden, J. D., *A. A. Newsletter*, 11, 99 (1972).
151. Rose, G. A., and Willden, E. G., *Analyst*, 98, 243 (1973).
152. Barthel, W. F., Smrek, A. L., Angel, G. P., Liddle, J. A., Landrigan, P. J., Gehlbach, S. H., and Chisolm, J. J., *J. Assoc. Offic. Anal. Chem.* 56, 1252 (1973).
153. Clark, D., Dagnall, R. M., and West, T. S., *Anal. Chim. Acta*, 60, 219 (1972).
154. Lieberman, K. W., *Clin. Chem. Acta*, 46, 219 (1973).
155. Heinemann, G., *Z. Klin. Chem. Klin. Biochem.*, 11, 197 (1973).
156. Henn, E. L., *A. A. Newsletter*, 12, 109 (1973).
157. Holak, W. *Anal. Chem.*, 41, 1712 (1969).
158. Lichte, F. E., and Skogerboe, R. K., *Anal. Chem.*, 44, 1480 (1972).
159. Chu, R. C., Barron, G. P., and Baumgartner, P. A. W., *Anal. Chem.* 44, 1476 (1972).
160. Vijan, P. N., and Wood, G. R., *A. A. Newsletter*, 13, 33 (1974).
161. Schmidt, F. J., and Royer, J. L., *Anal. Lett.*, 6, 17 (1973).
162. Pollock, E. N., and West, S. J., *A. A. Newsletter*, 11, 104 (1972).
163. Fernandez, F. J., *A. A. Newsletter*, 12, 93 (1973).
164. Poluektov, N. S., Vitkun, R. A., and Zelyukova, Uy. V., *Ah. Anal. Khim.*, 19, 937 (1964).

165. Agemian, H., and Chan, A. S. Y., *Anal. Chim. Acta*, 75, 297 (1975).
166. Dessani, S. D., McClellan, B. E., and Gordon, M., *J. Agric. Food Chem.*, 23, 671 (1975).
167. Teeny, F. M., *J. Agric. Food Chem.*, 23, 668 (1975).
168. Knauer, H. E., and Milliman, G. E., *Anal. Chem.*, 47, 1263 (1975).
169. Hawley, J. E., and Ingle, J. D., Jr., *Anal. Chem.*, 47, 719 (1975).
170. Lundgren, G., Lundmark, L., and Johansson, G., *Anal. Chem.*, 46, 1028 (1974).
171. Patel, B. M., Reeves, R. D., Browner, R. F., Molnar, C. J., and Winefordner, J. D., *Appl. Spec.*, 27, 171 (1973).
172. Reeves, R. D., Patel, B. M., Molnar, C. J., and Winefordner, J. D., *Anal. Chem.*, 45, 246 (1973).
173. Aggett, J., and West, T. S., *Anal. Chim. Acta*, 55, 359 (1971).
174. Aggett, J., and West, T. S., *Anal. Chim. Acta*, 55, 349 (1971).
175. Ebdon, L., Kirkbright, G. F., and West, T. S., *Anal. Chim. Acta*, 59, 187 (1972).
176. Johnson, D. J., West, T. S., and Dagnall, R. M., *Anal. Chim. Acta*, 66, 171 (1973).
177. Torsi, G., and Tessari, G., *Anal. Chem.*, 45, 1812 (1973).
178. Denton, M. B., Routh, M. W., Mack, J. D., and Swartz, D. B., *Amer. Lab.*, 8 (2), 69 (1976).
179. Richards, C. L., in "Circuit Designer's Casebook", (Electronics Magazine, eds.), McGraw-Hill, New York, pp. 88-94.
180. Crouch, S. R., Baxter, D. N., Pals, E. H., and Johnson, E. R., submitted to *Anal. Chem.*
181. "Sigma Stepping Motor Handbook", (Sigma Instruments, eds.), Braintree, Mass, 1972, pp. 23.

182. Malmstadt, H. V., Enke, C. G., and Crouch, S. R., "Digital and Analog Data Conversions", Benjamin, New York, 1973.
183. Montaser, A., Ph.D. Thesis, Michigan State University, East Lansing, Michigan, 1974.
184. Crouch, S. R., Montaser, A., Goode, S. R., in "Information Chemistry: Computer Assisted Chemical Research Design", (S. Fujiwara and H. B. Mark, Jr., eds.), University of Tokyo Press, Tokyo, 1975, pp. 107-124.
185. "Designing with TTL Integrated Circuits", (R. L. Morris and J. R. Miller, Eds.), McGraw-Hill, New York, 1971, pp. 177, 241.
186. Beer, M., Anal. Chem., 48, 93R (1976).
187. Beer, M., Anal. Chem., 46, 428R (1974).
188. Ubbelohde, A. R., and Lewis, F. A., "Graphite and Its Crystal Compounds", Clarendon Press, Oxford, 1970.
189. "C. R. C. Handbook of Chemistry and Physics", (R. C. Weast, ed.), The Chemical Rubber Company, Cleveland, 1969-1970, pp. E-237.
190. R. E. Sturgeon, C. L. Chakrabarti, and C. H. Langford, Anal. Chem. 48, 1792 (1976).
191. "C. R. C. Handbook of Chemistry and Physics", (R. C. Weast, ed.), The Chemical Rubber Company, Cleveland, 1969-1970, pp. B-174 to B-177.
192. A. T. Zander, T. C. O'Haver, and P. N. Keliher, Anal. Chem. 48, 1166 (1976).
193. T. R. Blakeslee, "Digital Design with Standard MSI and LSI", Wiley-Interscience, NY, 1975.
194. D. R. McGlynn, "Microprocessors", Wiley-Interscience, NY, 1976.
195. B. Soucek, "Microprocessors and Microcomputers", Wiley-Interscience, NY, 1976.
196. A. Barna and D. I. Porat, "Introduction to Microcomputers and Microprocessors", Wiley-Interscience, NY, 1976.